AN ASSESSMENT OF COASTAL HEADLAND ALONG NEGERI SEMBILAN COASTLINE IN MALAYSIA FOR TIDAL ENERGY EXTRACTION

GOH HOOI BEIN

FACULTY OF ENGINEERING
UNIVERSITY OF MALAYA
KUALA LUMPUR

2021

AN ASSESSMENT OF COASTAL HEADLAND ALONG NEGERI SEMBILAN COASTLINE IN MALAYSIA FOR TIDAL ENERGY EXTRACTION

GOH HOOI BEIN

THESIS SUBMITTED IN FULFILMENT OF THE REQUIREMENTS FOR THE DEGREE OF DOCTOR OF PHILOSOPHY

FACULTY OF ENGINEERING
UNIVERSITY OF MALAYA
KUALA LUMPUR

2021

UNIVERSITY OF MALAYA

ORIGINAL LITERARY WORK DECLARATION

Name of Candidate: Goh Hooi Bein

Matric No: 17035157/1

Name of Degree: Ph.D.

Title of Project Paper/Research Report/Dissertation/Thesis ("this Work"):

An assessment of coastal headland for tidal energy extraction along Negeri Sembilan coastline

Field of Study: Water Resources Engineering (Civil Engineering)

I do solemnly and sincerely declare that:

(1) I am the sole author/writer of this Work;
(2) This Work is original;
(3) Any use of any work in which copyright exists was done by way of fair dealing and for permitted purposes and any excerpt or extract from, or reference to or reproduction of any copyright work has been disclosed expressly and sufficiently and the title of the Work and its authorship have been acknowledged in this Work;
(4) I do not have any actual knowledge nor do I ought reasonably to know that the making of this work constitutes an infringement of any copyright work;
(5) I hereby assign all and every rights in the copyright to this Work to the University of Malaya ("UM"), who henceforth shall be owner of the copyright in this Work and that any reproduction or use in any form or by any means whatsoever is prohibited without the written consent of UM having been first had and obtained;
(6) I am fully aware that if in the course of making this Work I have infringed any copyright whether intentionally or otherwise, I may be subject to legal action or any other action as may be determined by UM.

Candidate's Signature Date: 11.11.2021

Subscribed and solemnly declared before,

Witness's Signature Date:

Name:

Designation:

AN ASSESSMENT OF COASTAL HEADLAND ALONG NEGERI SEMBILAN COASTLINE IN MALAYSIA FOR TIDAL ENERGY EXTRACTION

ABSTRACT

Large tidal currents usually can be observed around coastal headlands due to their geometrical effects. This coastal feature may become attractive tidal energy extraction site for electricity generation. Straits of Malacca consists of some recognized tidal stream energy sites in the world, but their detailed characteristics were previously unknown. This thesis focuses on the exploration of tidal stream energy along Negeri Sembilan coastline. The main objectives of this study is to achieve tidal current turbine deployment with maximum tidal energy extraction exploitability with minimal environmental impact. Resource assessment was done at multiple headlands along Negeri Sembilan coastline in the first stage of the study using a detail hydrodynamic numerical model. The model was then refined at a key site, the Tg Tuan Headland, the most promising tidal stream site among the four selected headlands. The country can save about RM 13.4 million (~ USD 3.2 million) of natural gas per year as a total amount of 185 GWh or 660 TJ of natural gas can be replaced every year with tidal current turbine installation at Tg Tuan Headland. Artificial energy extraction was parameterised at the sub-grid-scale via porous plate in the developed numerical model. This study was set to measure the energy production potential and to gauge the effects of tidal energy extraction in different configurations: depth, array in different numbers of row, and single and cumulative tidal arrays on the coastal environment. The result on depth effect assessment showed that depth of deployment is not significant in changing the current speed and extractable electrical

power. The difference is less than 0.002 m/s and 0.02 MW compared D1 (highest) and D8 (lowest) mean current speed and electrical power extraction for about 7 m difference. For array effect assessment, diminishing returns on the power generation was obtained, where peak power production from L6 (9.2 MW) was 97% of its total electrical power capacity, less than the corresponding values for each row of the smaller array, even though considerably low extraction was made with considerably large gap 10D was assumed in between each turbine. Comprehensive numerical models were developed to investigate the interaction risk of single and cumulative tidal array (1.5 km x 1.5 km) effect along the Negeri Sembilan Coastline, where, the sites are with combination of higher and lower peak velocities. Several aspects have been studied that included hydrodynamic mechanisms, bed shear stress, sediment transport and monsoonal variation in the assessment. For cumulative impact assessment, the analysis results showed positive exploitability for implementing sites with combination of higher and lower peak velocities with close proximity (~ 10 km), where the interference to each tidal array is less than 10% to each other. The results from this study can be used as basis to provide spatial and temporal information for further assessment of tidal energy extraction impacts to the environment. The outcomes yielded from this study would be a good source of reference to the authorities in decision making related to deployment of tidal turbine near Tg Tuan Headland.

Keywords: Headland; Energy feasibility; Tidal energy extraction effect; Depth effect; Single and cumulative effect

KAJIAN PENGEKSTRAKAN TENAGA ARUS LAUT UNTUK GARIS PANTAI NEGERI SEMBILAN MALAYSIA

ABSTRAK

Arus pasang surut yang kuat biasanya diperhatikan di sekitar kawasan tanjung pantai kesan daripada keadaan geometrinya. Ini merupakan satu kriteria pendorong untuk penerokaan tenaga arus laut bagi kegunaan penjanaan tenaga elektrik. Selat Melaka telah dikenalpasti oleh kajian lain yang amat berpotensi untuk pengekstrakan tenaga arus. Namun, ciri terperinci dari segi hidrodinamik di tapak tersebut masih kurang diketahui. Objektif utama kajian ini adalah untuk mencapai pengekstrakan tenaga arus elektrik yang maksimum tanpa mengakibat kesan yang ketara terhadap alam sekitar. Kajian sumber tenaga telah dijalankan di sepanjang tanjung Negeri Sembilan melalui model numerik hidrodinamik pada tahap pertama. Seterusnya, Tg Tuan dipilih untuk kajian sumber tenaga di tahap kedua memandangkan keupayaan penjanaan tenaga arus untuk tanjung ini adalah paling menjanjikan di antara empat tanjong dikaji. Dijangka penjimatan sebanyak ~ RM 13.4 million (~ USD 3.2 million) setiap tahun setimpal dengan penggunaan gas natural berjumlah 185 GWh atau 660 TJ dengan penggantian aplikasi teknologi turbin arus laut di kawasan Tg Tuan. Perlaksanaan kajian pengekstrakan tenaga daripada turbin arus laut melalui sekatan permukaan tegak berliang telah dimasukkan secara skala sub-grid dalam kerja permodelan. Penilaian potensi dan kesan pengabstrakan tenaga arus pasang surut telah dijalankan untuk pelbagai konfigurasi termasuk kedalaman air dan bilangan barisan turbin arus laut. Hasil permodelan perubahan kelajuan arus air menunjukkan bahawa pemasangan alat turbin arus laut di kawasan yang lebih cetek

menyumbang perubahan yang lebih ketara berbanding dengan kawasan lebih dalam. Namun demikian, kesan kedalaman air adalah tidak ketara dalam mempengaruhi arus laut dan penghasilan kuasa elektrik, dimana perubahannya adalah kurang daripada 0.002 m/s dan 0.02MW bagi perbandingan antara D1 and D6 (perbezaan kedalaman laut = 7 m). Manakala penilaian kesan aturan turbin laut L6 menunjukkan bahawa penghasilan penjanaan tenaga elektrik menurun, iaitu 97% berbanding dengan aturan berasingan walaupun jurang yang besar (10D) di antara setiap turbin disimulasikan. Simulasi model numerik yang komprehensif telah dibangunkan untuk mengkaji risiko intetraksi untuk pemasangan turbin secara individu dan kumulatif (1.5 km x 1.5 km) di sepanjang garis pantai Negeri Sembilan. Beberapa aspek penilaian yang meliputi hidrodinamik, tekanan ricih dasar laut, pengangkutan sedimen dan variasi musim telah telah dijalankan. Hasil simulasi pengabstrakan tenaga arus laut menunjukkan bahawa pengaruh pemasangan turbin di tanjung secara individu dan kumulatif memberikan kesan hidrodinamik yang minimum kepada tanjung di sekelilingnya. Hasil kajian impak persekitaran mendapati bahawa kesan interaksi antara tanjung terhad (perubahan arus laut < 10%) walaupun empat tanjung kajian adalah berdekatan antara satu sama lain (~ 10 km). Hasil daripada kajian ini boleh digunapakai sebagai asas bagi maklumat spasial dan temporal untuk penilaian lebih lanjut mengenai kesan pengabstrakan tenaga arus laut kepada alam sekitar. Ia juga boleh digunapakai sebagai sumber rujukan yang amat berguna kepada pihak berkuasa berkaitan dengan perancangan pemasangan turbin arus laut di kawasan laut Tg Tuan.

Keywords: tanjong; tenaga berkemungkinan; kesan pengekstrakan tenaga arus; kesan kedalaman; kesan individu dan kumulatif

ACKNOWLEDGEMENTS

I would like to thank Associate Prof. Dr. Lai Sai Hin and Prof. Mohammed Jameel for their support, advice, and great supervision throughout my Doctorate of Philosophy. They have given me a lot of freedom in developing ideas and interest of research. I would like to thank the unconditional support and love from my family and friends while I worked in this research work, and making my study time in University of Malaya so rewarding.

TABLE OF CONTENTS

LIST OF FIGURES

LIST OF TABLES

LIST OF SYMBOLS AND ABBREVIATIONS

SYMBOLS

α	:	ratio of total force from regulated force to unregulated force
α_4	:	wake flow velocity of tidal current turbine
A	:	cross-sectional area of moving fluid flow
A_c	:	cross-sectional area of a channel
A_j	:	amplitude of the constituent
A_s	:	structure exposed area
A_T	:	swept area of the turbine blades
β	:	power feedback control parameter
β_4	:	bypass flow velocity coefficient
C_{2D}^2	:	2D-Chezy coefficient
$c_b^{(\ell)}$	:	average sediment concentration in the near bottom computational layer
C_D	:	drag coefficient
c_{loss}	:	loss coefficient
c_{loss-u}	:	quadratic friction coefficient in u-direction
$c_{loss-\mathrm{v}}$	:	quadratic friction coefficient in v-direction
C_p	:	power coefficient
C_p'	:	fixed-pitch power coefficient

C_T : thrust coefficient

C_s : support structure drag coefficient

$\Delta\xi$: cell size for ξ-component

$\Delta\eta$: cell size for η-component

δ_j : frequency of the constituent

d : local water depth

D : diameter of the tidal current turbine

$D^{(\ell)}$: deposition flux

Δt : time step

E_k : kinetic energy

$E^{(\ell)}$: erosion flux

$\emptyset$: tidal current turbine axial direction

f : coriolis parameter

f_ξ : horizontal Reynolds stresses

$F_{D,total}$: total drag force

F_ξ : retarding force on the fluid

F_T : fluid dynamic efficiency dissipation force

F_s : turbine support structure dissipation force

g : gravity

h : cell depth

$h(t)$: height of the tide at time t

H	:	the total water depth
H(t)	:	sun's mean longitude
j	:	individual constituent
K_n	:	neap/spring factor
K_s	:	velocity shape factor
λ_d	:	First-order decay process
L	:	mean lunar time
μ	:	kinematic water viscosity of water
$\dot{m}$	:	moving fluid mass
M	:	chosen harmonic constituent number
$M^{(\ell)}$	:	user-defined erosion parameter
M_ξ	:	momentum sinks in ξ-component
M_η	:	momentum sinks in η-component
n	:	Manning coefficient
N'(t)	:	mean ascending's node longitude in negative direction
Oi	:	measured parameter
ρ	:	fluid density
ρ_o	:	reference density
ρ'	:	anomaly density
P	:	power
P_{ex}	:	power density

P_i	:	simulated parameter
P_{mean}	:	mean available power
P_ξ	:	pressure gradients for ξ-component
P_η	:	pressure gradients for η-component
P'(t)	:	mean longitude of the solar perigee
P(t)	:	lunar perigee's mean longitude
P_ξ	:	energy extraction
θ	:	tidal current velocity direction
Q	:	intensity of mass sources per unit area
r	:	coefficients of determination
r	:	Froude number
R	:	source term
σ	:	Root-mean square of the turbulent current velocity fluctuation
S(t)	:	moon's mean longitude
$\tau_{cr,e}^{(\ell)}$	:	user-defined critical erosion shear stress
$\tau_{cr,d}^{(\ell)}$	:	user-defined critical deposition shear stress
$\tau_{s\xi}$	:	ξ-components of the wind stress acting on the sea surface
$\tau_{s\eta}$	:	η-components of the wind stress acting on the sea surface
$\tau_{b\xi}$	:	shear stress in ξ-components at the bottom
$\tau_{b\eta}$	:	shear stress in η-components at the bottom
θ	:	angle between wind stress vector and local grid direction

θ_j : constituent phase

TI : turbulence intensity

u : free-stream current speed of the fluid

U : vertically integrated eastward components of the velocity

$|\vec{U}|$: depth-averaged horizontal current velocity magnitude

U_{ax} : tidal stream velocity in the turbine axial direction

U_d : velocity deficit

U_{in} : cut-in speed

U_N : tidal current velocity at a particular number of time-step

U_o : Initial velocity

U_{out} : cut-out speed

U_ξ : tidal velocity for ξ-component

u_{peak} : maximum spring velocity

U_r : rated speed

U_{tip} : tip of tidal current turbine blade

U_w : wake velocity

v : fluid velocity

υ_h : kinematic horizontal eddy viscosity

V : vertically integrated northward components of the velocity

ω : kinematic conditions

$\omega_s^{(\ell)}$: fall velocity

v_V : vertical eddy viscosity coefficient

Ω : rotational speed of tidal current turbine

ζ : free-surface elevation above reference plane

Common variables

2D : Two-dimensional

2DH : Two-dimensional Hydrodynamic

3D : Three-Dimensional

ADCP : Acoustic Doppler Current Profiler

CD : Chart Datum

CFL : Courant-Friedrichs-Lewy number

EIA : Environmental Impact Assessment

GEBCO : General Bathymetric Chart of the Oceans

ISMP : Integrated Shoreline Management Plan

MCT : Marine Current Turbine

MSL : Mean Sea Level

OTIS : OSU Tidal Inversion Software

RMSE : Root Mean Square Error

RPM : Revolutions per minute

SIF : Significant Impact Factor'

TNB : Tenaga National Berhad

TSR : Tip speed ratio

TSS : Total Suspended Solid

1 INTRODUCTION

1.1 The Development of Tidal Stream Energy

There are six types of ocean energy resources that are commonly explored; these are ocean wave, tidal range, tidal current, ocean current, ocean thermal energy, and salinity gradient (Melo, 2014). Among which, tidal energy, wave energy and thermal energy have drawn the most interest among researchers and policy makers due to the cost consideration (Davide Magagna, 2014; González-Gorbeña et al., 2015; Hammons, 1993; Melo, 2014; Turner & Owen, 2007; Uihlein & Magagna, 2016; Westwood, 2004, 2007). An annual report by Marine Energy showed that cumulative energy contributed from tidal stream and wave sources increased drastically from less than 5GWh in Year 2009 to 45GWh in Year 2019 (Marine Energy, 2020). For tidal energy, it has better advantage over other resources due to its predictability and power quality (Lewis et al., 2019).

Tidal current energy turbines could be used to exploit the kinetic energy for areas in fast moving tidal currents. Strong tidal currents can be normally observed in estuaries, narrow straits, islands, and around headlands (Draper et al., 2013; Finkl & Charlier, 2009). According to Robins et al. (2015), a tidal farm consisting of low rated turbines built over an unbounded sea space area potentially produces more electricity than that built within a confined space with the turbines of higher rates (Robins et al., 2015). Thus, in comparison to tidal channels, the unbounded tidal stream around islands and coastal headlands possesses higher potential for tidal current extraction (Rourke et al., 2010).

Numerous tidal resource studies, particularly tidal current enhancement by various coastal features – islands and headlands, have been performed all over the world. The examples of tidal current enhancement by islands are Pentland Firth (Martin-Short et al.,

2015), Zhoushan and Zhaitang Island (Chen et al., 2015), Kinmen Island (Chen et al., 2015) and Hulu Island (Gao et al., 2015). Whereas, the examples of tidal current enhancement by headlands are Admiralty Head of Puget Sound (Thyng & Riley, 2010), Portland Bill (Batten et al., 2007) and Alderney Race (Neill et al., 2012). Due to their geometrical effects, these locations become advantageous sites for deployment of tidal current turbines.

The statistic published by Suruhanjaya Tenaga indicated that Malaysia is one of the highest energy-using countries in terms of consumption and intensity of energy per capita in Asia with 6% annual growth rate for a 20 years period (Rahman et al., 2019). Realizing that, the government is keen to explore this renewable ocean energy to meet the country's growing demand in electricity resources (Faez Hassan et al., 2012). The implementation of this ocean renewable energy intervention is highly recommended as it is able to reduce carbon levels and fossil fuel dependency as well as to achieve sustainable national development in Malaysia; also, this is in compliance with the signatory to the United Nations Framework Convention on Climate Change (Hannan et al., 2018).

The coastline of Malaysia, which is bounded by South China Sea and Straits of Malacca, offers abundance of tidal stream energy for exploration and exploitation (Faez Hassan et al., 2012; Lim et al., 2015; Mohamed, 2015; Sakmani et al., 2013). There are numerous-headlands and islands that may be the potential sites for tidal energy extraction within the strait. However, the detailed characteristics of some recognized tidal stream energy sites within the Straits of Malacca were previously unknown. This thesis emphases the investigation of tidal stream energy along Negeri Sembilan coastline.

1.2 Background of the Problem

The spatial model result described in the studies of Sakmani et al. (2013) and Lim & Koh (2010) indicated high current velocity (> 1 m/s) at the Negeri Sembilan area. Similarly, a more recent study by Bonar et al. (2018) also showed that Port Dickson has high potential due to its geometrical condition that allows larger area for energy extraction. By adopting the findings from previous studies, Negeri Sembilan, which was recognized as one of the high potential coastal area for resources exploitation is selected to be further explored with a better resolution numerical model owing to its high complexity of local coastline and geomorphology condition.

Coastal water numerical modelling was introduced since the year 1960/70s. Since then, it has constantly evolved in terms of complexity and precision. Whilst numerical models differ in their working processes and parameters involved, they serve the analogous objective: to numerically simulate dynamic complex system and predict probable changes to the system, e.g., predicting the effect of tidal energy extraction. Often, computational cost is a vital consideration in numerical modelling. In order to achieve economic viability for developing a hydrodynamic model, computational cost optimization must be achieved. Generally, computational cost can be defined by its computational time required. Therefore, minimizing the computational time will subsequently lower the computational cost. Nevertheless, integration of more parameters (e.g., morphological parameters, wind, wave and, etc.) into the model will increase the complexity of the model and subsequently increases the computational time and cost. Previous studies by Bonar et al. (2018), Sakmani et al. (2013) and Lee & Seng (2009) have adopted low spatial resolution hydrodynamic model that covered the Straits of Malacca domain with considerably large grid spacings significantly reduced the computational costs. These studies indicated that Port Dickson within the Negeri Sembilan coastline is most suitable site for energy exploration with high current velocity and larger space for exploration. However, the

detailed characteristics at the Negeri Sembilan coastline as potential site was not well described. Therefore, a solution to this problem may be establishment of an optimum spatial resolution numerical model along the Negeri Sembilan coastline that can serve the purpose right.

The collection of temporal and spatial scale data is crucial in producing a high-quality numerical model for tidal current resource assessment. The parameters essential to evaluate the quantitative relationship through field measurement are not yet established from any studies by previous researchers. This is mainly due to limited finding available from previous studies. In addition, there would be considerable engineering risk and challenges to conduct survey at such complicated tidal current areas. The model developed by Lee & Seng (2009) and Bonar et al. (2018) for Malaysian sea was calibrated only with the predicted tide data. The current velocity, which is the main parameter for resource assessment was not calibrated. Calibrated numerical tool can precisely simulate the hydrodynamic in both space and time by using field measurement data, and that can be a very accommodating tool for assessment of resource and resulting hydro-environmental effects of tidal energy. In order to fill this gap, the reliability of the Negeri Sembilan hydrodynamic model can be further enhanced by incorporating site measurement data into the model.

The effect of tidal current energy extraction on the current velocity, bed shear stress and sediment transport can be simulated via added porous plate loss. The parameterization of the turbine included into the hydrodynamic model can be varied for different types of devices. To date, there are still limited measurements available for tidal stream turbine commercialized in the market. Hence, an analytical method based on published characteristics of a common type of tidal current turbine, i.e., horizontal-axis turbine needs to be developed and validated to reflect the non-linear dynamics of the tidal current

turbine operation. This is necessary as validated tidal current turbine representation parameters will be further implemented in the tidal array impact assessment.

Many important economic and social activities are now taking place in coastal areas. The consequences of changes to the coast can be a serious concern not only to the relevant government agencies, but also to all users of this vast, diverse and productive region. Any coastal changes due to deployment of the tidal turbine technology and implementation of the coastal management strategies would potentially pose impacts to economic and social activities of the coastal populations. The effect of influence of tidal energy extraction is governed by combination of different factors. Most of the site selection performance assessment in the previous studies only focused on the exploitability of tidal stream energy. In fact, a good tidal energy production site shall be gauged by two main considerations: exploitability and effects they pose to the coastal environment as the operation of tidal energy extraction causes flow alteration around the turbine and deviation of tidal current circulations from their original paths (Pacheco & Ferreira, 2016; Robins et al., 2015; Wang & Yang, 2017). A comprehensive numerical model to accurately simulate the problem by resolving the secondary flows for single tidal current turbine and array in (1) quantifying potential energy yields for assessing the resource performance and (2) interference of tidal energy extraction in different configurations is highly desired. The results yielded from these studies would be a good reference to policy makers and potential investors on tidal energy exploitation in Malaysia.

A study on potential site for tidal energy extraction at Gulf of California demonstrated that regions with less energetic tidal currents but in deeper waters can be chosen due to large tidal energy resource to be explored (Mejia-Olivares et al., 2018). Other than that, with the advancement of turbine technology and the plant design enhancement, the tapping of the marine energy at areas of lower current velocities is still feasible. Hence

the risk of interaction to sites geographically close to each other will grow when intermediary sites are developed (Haverson et al., 2017). Considering the environmental risk due to the large-scale deployment, it is important that the intermediary effects of single and multiple tidal farm deployment within the higher potential tidal energy extractable area in proximity of the headland within the coast of Negeri Sembilan need to be looked into in detailed.

1.3 Aims and Objectives

The main aim of this research was the establishment of a suitable numerical model for optimizing the location and configurations of tidal turbine deployment relative to both extractable energy and environmental impacts assessment. In achieving the aim, a number of objectives were to be fulfilled:

- Establish field campaign specification for primary data collection.
- Establish a hydrodynamic model capable of quantifying the electrical power resource for a tidal stream energy potential site.
- Develop a methodology for parameterizing within a numerical model, the energy extraction associated with a representative array of tidal current turbine.
- Investigate the interactions between the tidal kinetic energy dissipation and the environment in response to power take-off of tidal stream energy for a representative configuration of tidal current turbines.
- To investigate the potential risk of interaction to sites geographically close to each other when intermediary sites are developed within the coast of Negeri Sembilan

1.4 Scope of Works

This research started with literature review to understand the ocean power exploration and justification for selection of tidal stream energy for Malaysian Sea. For utilizing the tidal energy from the sea, the tides and tidal currents in the sea were appreciated in detail. The mechanism of various tidal energy extraction technologies, i.e., tidal barrage and tidal current energy was deliberated in detail to rationalize the suitability of its application in Malaysian sea. The background of the Study Area that includes tidal level, tidal current flow, wind and wave, and geomorphological condition was reviewed thoroughly to understand the hydrodynamic and morphodynamical conditions at the study area. Previous studies on tidal current energy resource and effect assessment were reviewed. The approaches applied in the previous studies were compared and deliberated. As current research involved two main aspects: exploitability performance and environmental impact assessment, previous studies of similar nature were thoroughly reviewed. The approach and outcome of previous studies had been carefully reviewed to ensure that the present research is novel and able to fill in the gaps of previous studies.

Numerical modelling is the main approach applied for this research and field-measured data is an essential input required to establish a high-definition numerical model. The present research involve in the determination of potential site area and energy exploration focusing mainly at Negeri Sembilan coastline. This coastline is selected based upon the findings from the previous studies, as discussed earlier in Section 1.2. The field data specified for this study was collected by surveyor at the study area. The data included bathymetry, tidal level, tidal current, bed grab sampling and Total Suspended Solid (TSS). Followed by that, field data check analysis was carried out to ensure that the quality input data is attained.

Using the field-measured data, the Negeri Sembilan hydrodynamic model was developed using Delft3D-FLOW module. The model was calibrated for two locations along the Negeri Sembilan coastline for two main hydrodynamic parameters: tidal level and tidal current. With the calibrated and validated model, water sampling and TSS were adopted to establish the sediment transport modelling using Delft3D-SED module. The established model was further used for various subsequent scenarios modelling.

Novel analytical method based on published characteristics of most commonly applied tidal current turbine, i.e., Horizontal Axis Turbine (HAT) was developed as Tidal Energy Converter (TEC) device. The parameterization of regulated and un-regulated HAT was compared to show the significance for tidal current force regulation. Considering the axis misalignment at the actual site, the effect of axial direction (0-70°) was assessed in this study.

The derived turbine parameterization was further employed to quantify the power produced from a tidal current turbine, or array as well as to examine both the resulting effects of individual turbine and the interaction between tidal array of multiple headlands. This study has been set to measure the energy production potential and to gauge the effects of tidal energy extraction in different configurations: depth and array in different numbers of row, single and cumulative tidal array, that may pose to the coastal environment. In order to understand the interaction and cumulative risk for single and cumulative headland deployment, the assessment on current flow, water level, bed shear stress and sediment transport were conducted along the Negeri Sembilan. The monsoonal effect, i.e., pure tide, Northeast and Southwest monsoon was also evaluated.

1.5 Significance of the Study

The main novel contribution of this research is the development of a comprehensive numerical model for detailed resource assessment of Negeri Sembilan coastline, in which potential deployment sites are identified based on a developed sophisticated assessment approach. The developed model is capable for potential site assessment by quantifying the power resources and through impact assessment. The potential site selection was conducted along Negeri Sembilan coastline which consists of multiple headlands and followed by zone selection assessment surrounding of a selected headland.

Another contribution is the development of tidal current turbine optimization algorithm of single and array tidal current turbine. This algorithm is able to carry out optimization of array configurations by considering the performance through power extraction and the impact through changes on current velocity. Optimization was particularly focused on the Tg Tuan Headland at turbine scale model. This research is novel as the combined influence of depth and array number on tidal turbine deployment at headland is first ever studied and quantified. The effect of added drag on the surrounding flow field was plotted and the hydrodynamic change through the combined effect at the headland site was quantified. The findings of this study can be used as a more comprehensive guidance for selection of tidal turbine deployment in terms of depth and array number for coastal zone based on two main criteria – exploitable energy and impact of deployment.

The favoured site that located in the Straits of Malaysia is rich of mangrove habitat. The hydro morpho dynamic characteristics of coastal zone in the Straits of Malacca are complicated and thus the sensitivity assessment of the tidal flats towards the tidal extraction energy is crucial. To date, limited number of researches have considered the resulting effect of tidal turbine deployment on bed shear stress and sediment transport.

The third novel contribution is the comprehensive impact assessment of single and cumulative headland deployment considering that intermediary sites at multiple headlands are potentially to be deployed with tidal array using suitable device. The assessment includes of several important aspects of environmental impact assessment, i.e., hydrodynamic, sediment transport, bed shear stress and monsoonal variation effect. The simulation was reliable as the sediment transport model was setup by using the TSS and bed grab sampling data collected at the study area. The result of the assessment for both before and after the operation can be used for identification of suitable recommendations for an effective monitoring implementation. By this way the mangrove forest at the intertidal zone can be strictly secured and safe to the highest degree. Other than that, the spatial and temporal results of current velocity, bed shear stress and sediment transport changes can be further employed by marine biologist for benthic and marine habitat assessment.

In overall, the findings from this study will form a good basis for further study on the development of innovative and suitable tidal energy technologies as well as prototyping of the selected technology by exploring the deployment configurations influencing at a potential headland site. More detail of the study site will be deliberated in the following sections.

1.6 Thesis Layout and Content

The thesis layout and content of this thesis are as follows:

Chapter 2 deliberated a literature review of relevant studies of recourse assessment and effect of inclusion of tidal stream using numerical modelling. Various methodologies applied in previous studies to quantify the tidal stream resources are discussed. The

discussion involves conventional approaches to tidal stream resource assessment, by including the parameters, which influence the precision of the formulation of the available tidal stream power production equation. Different methodologies of numerical simulation of tidal stream energy extraction, which emphasized on turbine representation are discussed. This is mainly to elaborate the development of the tidal stream energy extraction model. Followed by that, a review of the hydro-environmental impact of tidal turbines is carried out with a view to including an 'impact limitation' in the model optimization. The hydrodynamic impacts assessment of both single tidal turbine and arrays are deliberated. Followed by that, relevant environmental impacts in relation to the hydrodynamic changes are reviewed. The environmental impacts and summary of published literature relating to these impacts are presented. The novelty of present research is then outlined based on the findings of the literature review.

In Chapter 3, the approaches of the field measurement works conducted to acquire the primary data at the site are presented. The primary data collected in this study included bathymetry, Acoustic Doppler Current Profiler (ADCP), Total Suspended Sediment (TSS) and Bed Grab Sampling. The bathymetry data acquired is used to represent the bed level of the study site in this research. The extent of the bathymetry is determined based on the preliminary assessment from previous studies. Two points of ADCP taken at different locations at the study site for 16 days in 10-minute interval were used for numerical hydrodynamic model calibration and validation purposes. The TSS and Bed Grab Sampling were conducted at various locations at the study site to determine the bed material and suspended material in the water column. The second subsection of Chapter 3 discussed the methodology of numerical modelling carried out this study. The concept and theory behind the 2D numerical model, Delft3D-FLOW model, was discussed. The governing differential equations of the numerical model and its formulations are outlined and deliberated. Further of that, the model solution is further outlined and discussed. The

numerical model deliberated the model grid structure, boundary conditions and bathymetry interpolation of the model. The theory of sediment transport is presented as the use of morphological changes as a proxy for environmental impact assessment of tidal stream energy extraction during the research.

Chapter 4 discussed the site suitability assessment for Tidal Energy Converter (TEC) for efficient power extraction. The numerical model was established for Negeri Sembilan Coastline with multiple headlands to examine the potential of extractability at each headland. The findings from the first model were used to further refine the research where a detailed assessment was then established on the selected case study site – Tg Tuan Headland. More detailed resource assessment at the selected site is discussed. The calibration and validation of both developed hydrodynamic models to measured water level and current velocity are also presented. The finding from this chapter was further utilized in Chapter 6 for tidal current energy extraction study.

Chapter 5 discussed the development of realistic tidal stream operation. The parametrization of tidal current turbine, which was conducted in a series of model tests are elaborated. The effect of anisotropic and non-linearity in current speed to the tidal current turbine is discussed. The turbine parameterization derived from this chapter was further employed for scenarios and discussed in Chapter 6.

Chapter 6 discussed the development of the tidal energy extraction simulation, which involved the modification of governing equations as deliberated in Chapter 5. Tidal energy resource extraction assessment is carried out on the case study sites – the Negeri Sembilan Coastline. A study into the impact of single and array configuration on power generation and kinetic energy dissipation was discussed. The last section of Chapter 6 discussed the examination on the effect of multiple intermediary headland tidal array deployment along one coastline in vicinity. The resulting hydro-environmental impacts

due to power take-off from tidal stream energy focused on the current velocities, bed shear stress and sediment transport. The effect of monsoon to the extraction was also investigated. This research provides valuable information on the dynamics of combination of cohesive and non-cohesive sediments in presence of tidal current turbine at multiple headlands, and enhance the understanding of the complex hydro-morphodynamics of headland coast which enable regulators, planners, project developers, marine researchers to conduct accurate environmental assessment and design proper

Chapter 7 includes a summary of the results presented in the thesis, draws overall conclusions, and provides some recommendations for future research.

2 LITERATURE REVIEW

2.1 Introduction

Literature review in this chapter began with review on the exploitability of marine renewable energy from the ocean resource, as described in Section 2.2. Based on the review elaborated in Section 2.2, tidal stream energy is one of the most viable technology to be applied in Malaysian sea. Henceforth in Section 2.3, the review has further focused on tidal current background to understand the characteristics of tidal level and tidal current energy. Section 2.4 elaborated two main types of technologies available for tidal flow energy extraction, which are tidal range extraction and tidal current extraction devices. The review on tidal current energy exploitation potential in Malaysia sea is given in Section 2.5. A detail review on the hydrodynamics and morphodynamic condition at the Straits of Malacca is given in Section 2.6. This is followed by a review of methodologies to tidal current energy resource assessment, which includes of resource assessment methodologies, accurateness with resource assessment methodologies and vitality to include impact assessment of tidal current turbine placement into a resource assessment. It is then leading to a summary review of published laboratory and numerical studies, which studied on impact assessment of tidal turbine placement, for both single and array configurations. The comments and summary based on the literature review is discussed in the last section in this chapter.

2.2 Review of Ocean Power Exploration

The oceans are a gigantic and powerful source of energy. It could be harnessed to provide more than adequate amount of energy to fulfil the demand for electricity

internationally (Pelc & Fujita, 2002). Ocean energy can be extracted in different forms, e.g., wind, heat, tides, waves and currents as marine renewable energy. It can be subdivided into four major energies:

a. Offshore wind energy
b. Ocean thermal energy
c. Tidal energy (tidal barrage/tidal stream energy)
d. Wave energy

The exploration of marine renewable energies has great advantages over land-based renewable energies. The oceans can be exploited on a very large scale without causing land-based issue for renewable energies. It is highly recommended for Malaysia to venture into marine renewable energy, as some states of the country are facing limited land area issue. Hence the complication over planning consent, land use, social impact and noise impacts can be avoided.

Wave energy is more suitable to be utilised at areas where there are strong waves. However, wave density of Malaysia is not adequate for electricity generation commercially. The average wave power at the west of Peninsular of Malaysia is in only within 0.5 to 2.0kW/m (Azman et al., 2011). This range is slightly lower for wave power generation. While for application of the thermal energy from the sea, it is more feasible if the thermal difference is larger than 20 degrees Celsius across the water column of the sea. However, the temperature gradient in Malaysia is usually less than 20 degree Celsius as the water depth at most of Malaysia's seawater is not more than 1000 m. Hence this form of energy may not be commercially viable in Malaysia, especially in Peninsular of Malaysia.

The preliminary study from Marine Renewable Energy Research Group of the University of Malaya showed that the Strait of Malacca, which has plentiful of tidal

stream energy resources is feasible to convert the tidal stream energy into commercial use (Sakmani et al., 2013). The tidal energy's consistency of supply is its major advantage over other renewable energies. The tidal constituents of the marine water are mainly driven by the predictable forces that are produced by the sun and moon.

2.3 Tidal Currents in the Sea

The tides in the sea refer to the rise and fall of water level periodically attributed by the gravitational force between the sun, moon and earth. The tidal current in the sea is referring to the horizontal movement resulting from the tides. Referring to **Figure 2.1**, the surface water on the earth is attracted and pulled towards the moon by its gravitational force. The gravitational force is stronger at the source of the gravitational field on the earth side nearest to the moon, creating a bulge in the surface water of the ocean, called lunar tide on the nearest side of the earth and greater than that on the opposite side. Both moon and earth are rotating around the center of mass of the earth-moon system and hence it creates a second bulge of surface water of the ocean on the far side of the earth (Thompson, 2007). Sun is another gravitational force for tide generating force. Although the sun is much larger than moon in mass, it has a much greater distance away from the earth and hence the effect on tidal variations in the earth's sea surface water, solar tide is much lesser than moon's lunar tide (refer to **Figure 2.2**).

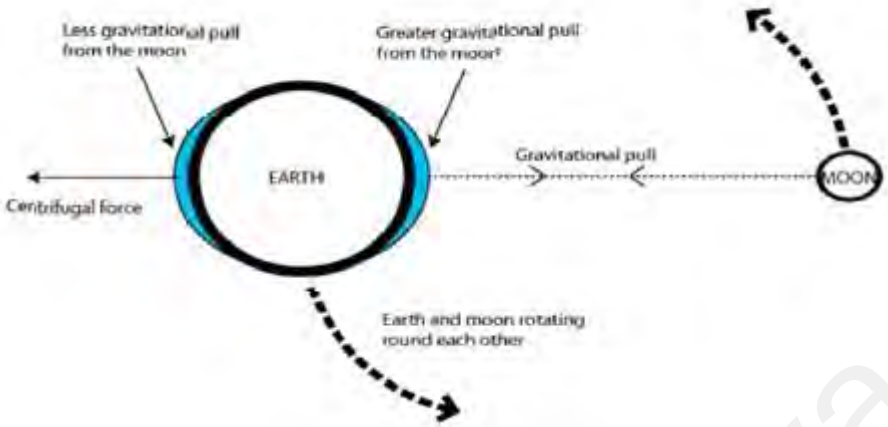

Figure 2.1: Illustration of tides generation (Fallon, 2012)

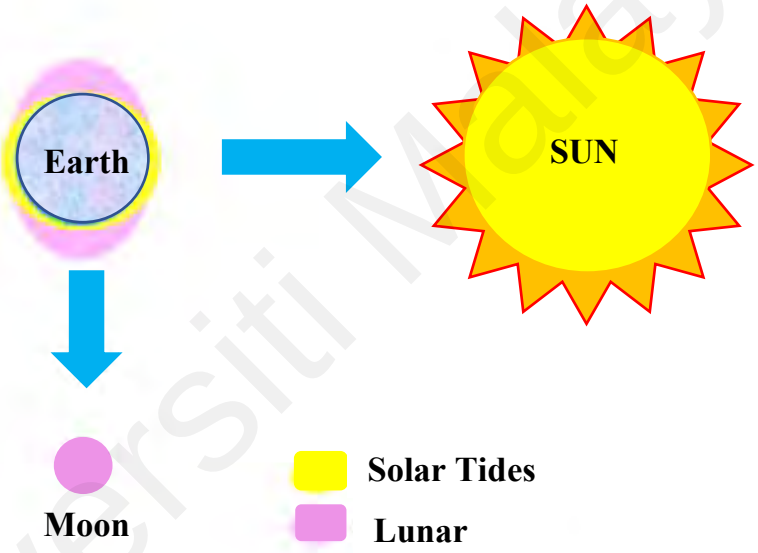

Figure 2.2: Illustration of influence of solar and lunar gravitational force to tides (Thompson, 2007)

Generally, the earth is experiencing two tidal oscillations in daily basis. The tide rises to a peak level, known as high tide (high water) and then begins to fall to a lowest level, known as low tide (low water) (**Figure 2.3**). The water level difference between the peak and lowest points of a tide is referred to as the tidal range. The tidal range varies for different locations and time (Hicks, 2006).

The tidal condition in any location is decided by the tide generating forces, where its sinusoidal oscillations are the major factors for the distribution of forces. A lunar day is

referring to the period between times when the moon is overhead the matching point on the earth, which is equivalent to a period of 24 hours and 50 minutes (Thompson, 2007). For a single lunar day, the primary force is due to lunar attractions which produces a sinusoidal tide (two high and two low tides) occurring in a lunar day, termed as semi-diurnal tide. There is another type of tide characterized as diurnal tide, in which only one tidal cycle (one high and one low tide) occurs over one lunar day.

Tidal changes can be observed over longer time periods, covering spring-neap tide cycle, which repeats about every 14 days due to the orbital movement of earth around the moon. The occurrence of spring and neap tide is due to combined lunar-solar forces. Spring tide occurs during new, or full moon as the gravitational pull of the moon and sun are aligned (in the same direction), and therefore generating tidal ranges greater than average monthly range (Hicks, 2006). The lunar and solar force are misaligned during the first and last quarters throughout the lunar phase and thus generating smaller tidal range during neap tide in comparison to average tidal range (**Figure 2.4**).

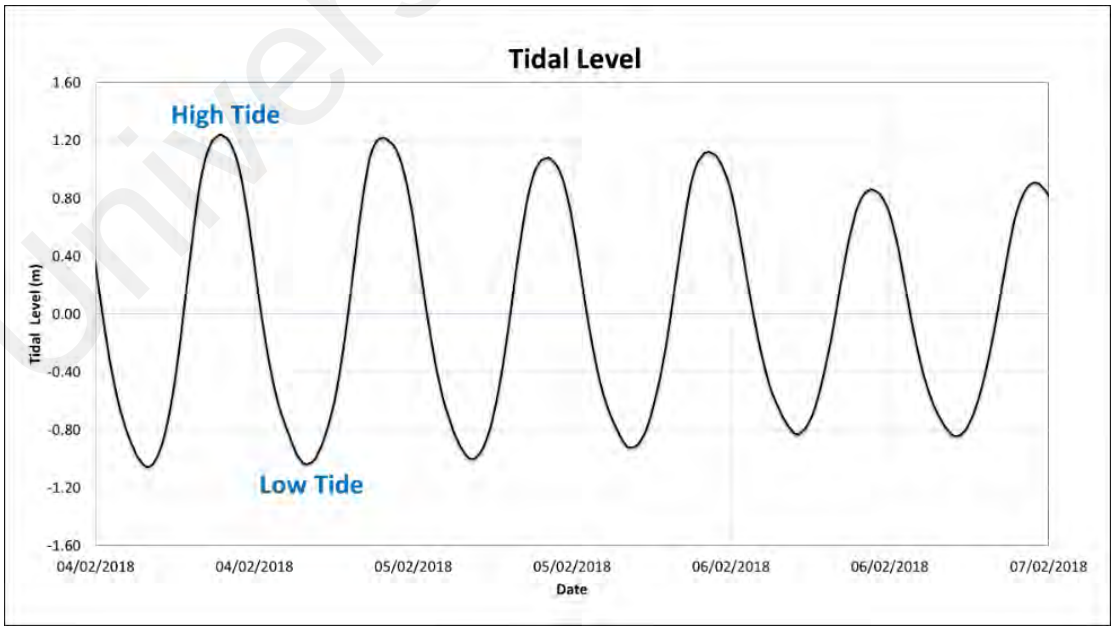

Figure 2.3: Illustration of high and low tides for flood and ebb tide

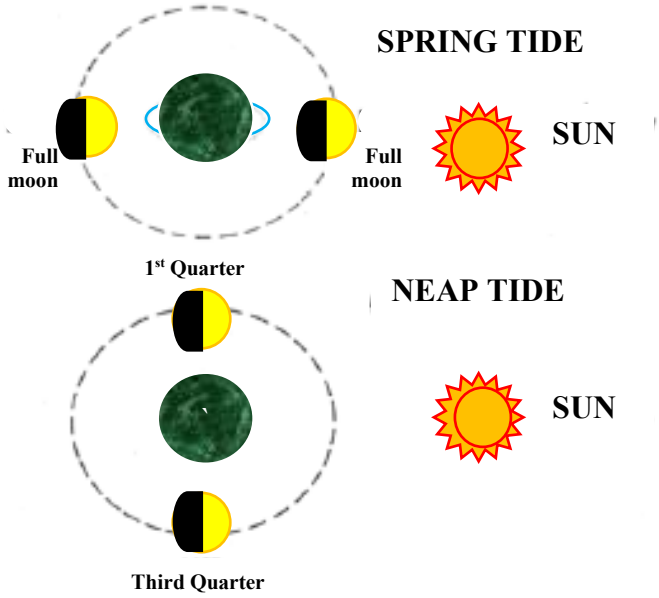

Figure 2.4: Illustration of spring tide (during new or full moon) and neap tide (during first and last quarters)

Currents in the sea are the movement of seawater in horizontal direction and are characterized as either 'tidal' or 'non-tidal' flow. Tidal flow currents are the horizontal water flow with periodic rise and fall of tide. Non-tidal flow current is due to non-tidal factors, i.e., Coriolis forces, seabed changes (bathymetry), salinity, freshwater inflows, temperature and density (Fallon, 2012).

2.4 Tidal Energy Extraction Technologies

The extraction of tidal energy can be sub-divided into tidal range and tidal current technologies; this will be discussed in following subsections.

2.4.1 Tidal Barrages

It is an expensive scheme to apply tidal barrage for power generation. Tidal barrage is normally constructed across the bay or estuary. This technology is equipped with sluices gates and turbines. Tidal barrage mechanism works in the similar approach to

hydroelectric schemes. Tidal barrage retained water at high tide within the barrages, using sluices and when tides on the other plane of the barrage start to drop down to a certain level, a substantial water head is created between two planes of the barrage. Subsequently the water is being released through low head turbines for power generation. To date, the largest tidal barrage in the world is located at La Rance in Brittany, France. This tidal barrage system has commenced operating in the 1960's with a capacity of 240 MW (Frau, 1993).

The electricity of tidal barrage is produced based on the work operation as follows:

i. Flood tide: The electricity is produced on a flooding tide as the basin fills up. The basin fills up throughout the flooding tide period with the sluice gates open.

ii. Ebb tide: The electricity is produced through the turbines as the tide begins to subside/ebb. This tidal condition provides the two highest energy for a day, which takes place for about 3 hours following flood tide and it occurs for 4-6 hours (Hammons, 1993).

iii. Two-way production: it combines an ebb and flood generating system, whereby the energy can be produced on both the flood and ebb tides. The power output for this system is generally less than pure ebb generation. Nevertheless, it increases the frequency of supply. Commercial application is only be economically viable in high tidal range regions (Frau, 1993) seeing that the construction cost for tidal barrage would be much more costly.

The drawback of tidal barrage is the construction cost. The construction of the tidal barrage requires huge capital investment and long construction period. Besides that, this structure may cause a lot of adverse environmental and ecological impacts. Tidal barrage sites are usually sited in estuaries, which consists of substantial region of mud-flats

exposed at low tide (Boyle, 2004). Hence the tidal barrage can take away mudflats that consist of precious mangrove habitat, which provides shelter to birds and also can act as a barrier to the passage of migratory fish (Ball, 2002). The development of tidal barrages therefore is limited. So far, no tidal barrage had been constructed in Malaysia.

2.4.2 Tidal Current Energy

Due to the limitation of tidal barrage, another technology being developed is the tidal current energy. Tidal current energy takes advantage of the kinetic energy generated by the tidal flow. Energy can be extracted using single or multiple turbines to be installed in an array or tidal farm, which extends through a waterway. So far, this technology is not fully implemented yet. Only prototypes are being installed and tested in the sea (Bahaj, 2011).

The fundamental for tidal current energy converter mechanism is considerably similar to harnessing wind energy. Hence several tidal current energy converters resemble wind turbines, which are called tidal current turbines. Tidal current energy converters are able to capture the kinetic energy from moving water. In comparison to tidal barrage, tidal current technology is more advantageous as it leads to lesser ecological and environmental impact. It is also better than other land-based renewable energy resources as the tidal current energy converter can be deployed on a large array in the sea by eliminating the constraints of complication over land-use (Fraenkel, 2002). Tidal current energy converter is studied in this thesis.

During early stage, tidal turbine designs worked in a similar manner to horizontal axis wind turbines albeit. The design of vertical axis marine current energy converter was also inspired from early vertical axis wind turbines. It is believed that the application of this

technology is able to reduce the environmental impacts and huge capital cost associated with tidal barrages. The application of this technology is generally only viable and cost-effective at certain locations where tidal flow velocities have been enhanced by confined topography (Fraenkel, 2002). The next critical stage of development will be seen when farms or large scale of turbines being installed. These required varieties of research to be carried out. Acknowledging that, this study is conducted to assess and quantify the impact from the large-scale turbine deployment. Optimization of the tidal turbine array configurations are also conducted in this study.

Generally, there are four types of tidal turbine, which are horizontal axis turbines, vertical axis turbines, variable foil systems, and venturi system. These will be discussed in the following subsections. The European Marine Energy Centre (2015) have identified another two innovative tidal energy converter devices, which are Archimedes screw and tidal kite (EMEC, 2020).

A. Horizontal axis turbines

For horizontal axis turbines (Figure **2.5**), its rotational axis is parallel to the incoming direction of the tidal flow (Bryden, 2006). The operating mechanism of this device is replicate on wind turbines. The deployment of this system can be either mounted at seabed or attached from bottom of the floating blocks (Buigues et al., 1998). The electricity is produced by transferring the hydrodynamic force component normal to the blade rotation plane along a shaft to drive the generator. The horizontal tidal turbine has been installed in the Bristol Channel between England and Wales.

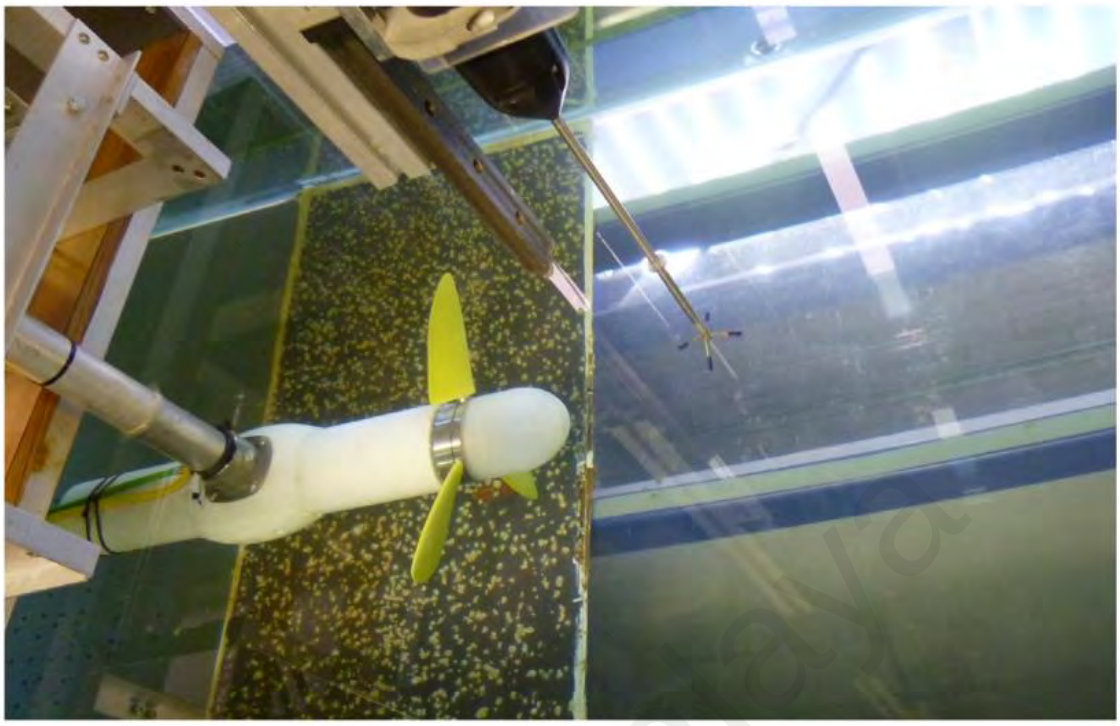

Figure 2.5: An example of horizontal axis turbine prototype mounted in the flume in Cardiff University's hydraulics laboratory (Ouro et al., 2017)

B. Vertical axis turbines

For this type of turbine, the flow is perpendicular to the rotational axis (Buigues et al., 1998). This turbine is designed to work with the crossing flow (Mason, 2005), where the rotor transmission shaft and blades' components are parallel with each other and these components are perpendicular to the incoming flow (**Figure 2.6**). The design of vertical axis turbine enables the rotor to rotate in the same direction without considering the incoming current flow direction (Mason, 2005). Two main sets of vertical axis tidal turbine are categorized based on their blade shapes which are helicoidal-blade and rectilinear-blade turbines. An example of the first mentioned device is the Kobold Turbine. Another example of the latter is the Gorlov helical turbine rotor, which was installed in Korea. The key advantage of the rectilinear blade turbine is that the power extraction of the shaft is perpendicular to incoming current flow, which enables it to have a drive train neither in a surface vessel nor on the mounted sea bed (Fraenkel, 2002). However, the

main disadvantage of rectilinear blade is that it is highly unstable and has a high tendency to rupture due to vibrations (Buigues et al., 1998). Using helicoids turbines, the vibration problem is resolved and hence the rupture problem is solved as well. Another advantage of the helicoids Gorlov turbine is the quantity of the energy extraction from the tidal current (35%) in comparison to 23% from the rectilinear turbine and 20% from the conventional horizontal axis turbines (Buigues et al., 1998).

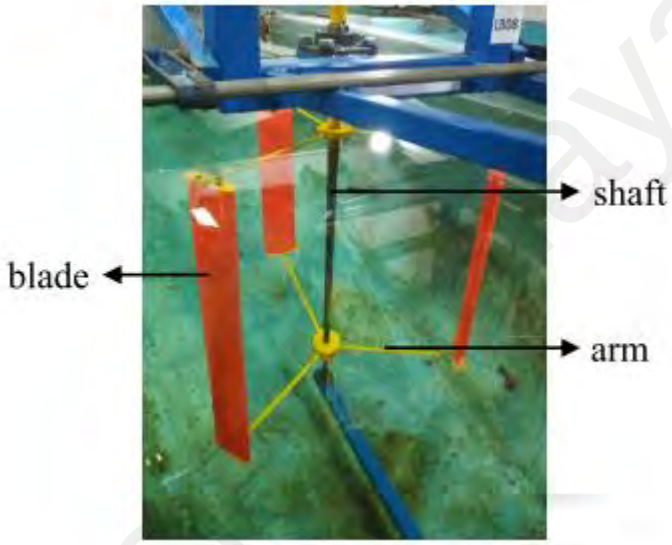

Figure 2.6: An example of vertical-axis turbine experimental model (Satrio & Utama, 2021)

C. Variable foil systems

This type of tidal turbine is not as widely applied as the horizontal and vertical axis types. One of the most commonly applied Variable Foil System is the 'Stingray' turbine (Department of Trade and Industry DTI, 2003). This device is developed for 150 kW generation of electricity utilising the power of tidal currents. So far, the prototype units had been undergoing testing in Yell Sound in Shetland (Bryden, 2006; Department of Trade and Industry DTI, 2002).

'Stingray' differs from other tidal turbine devices as it uses an oscillating motion to harness the tidal energy. The 'Stingray' is varied by its simple mechanism of turbine, which consists of a hydroplane where its attack direction is relative to the incoming current flow direction as shown in **Figure 2.7** (Engineering Business Ltd, 2003). The 'Stingray' arms oscillate up and down due to the drag and lift force of the tidal current flow. Its arm is attached with a hydraulic cylinder which can alternately extends and retracts due to the tidal current force and produces high pressure oil to deliver the hydraulic motor for driving the generator for electricity production (Department of Trade and Industry DTI, 2003). The whole system is fully submerged and rigidly fixed to the seabed. The specialty of this type of turbine is mainly of its large wing-like hydroplane that is able to be pitch-controlled, oscillating up and down for oil compression to convert the hydraulic power (Buigues et al., 1998).

Figure 2.7: An example of flapping hydrofoils (Wang et al., 2016)

D. Venturi based systems

The principle of this system of tidal current energy converter is that it uses pressure difference in contracting the flow to force the secondary extraction (I.G. Bryden & S.J. Couch, 2006). Two most common system found that using such principle are the GENTEC venturi (by Greenheat Systems Ltd) and the Rochester venturi (by HydroVenturi), both in the UK. This is the most suitable type of turbine to be applied in

Malaysia Sea with current velocity less than 1 m/s. According to Sakmani et al. (2013), the application of funnel/venturi (**Figure 2.8**) can be modified to suit the low current flow condition in Straits of Malacca for power generation.

Figure 2.8: An example of venture based system (Roshanmanesh et al., 2020)

E. Archimedes screw

This device is in helical corkscrew shape. It is designed in such shape in order to allow current to flow up and go through the spiral, and subsequently allows the rotation of the turbines and hence to generate energy (**Figure 2.9**)

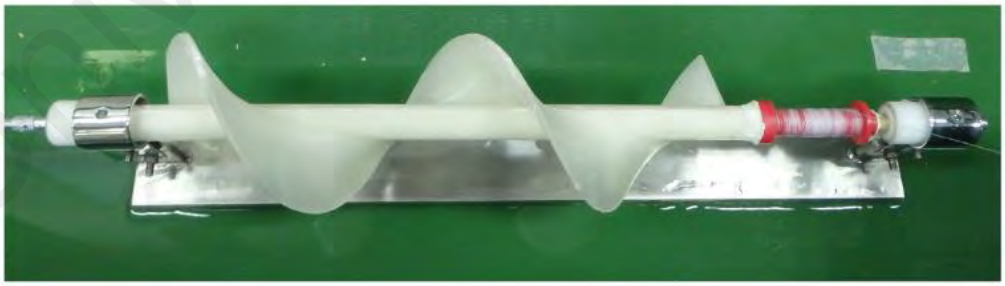

Figure 2.9: An example of Archimedes screw turbine (Zitti et al., 2020)

F. Tidal Kite

The turbine of this device is within the wing of the kite. The kite is tied to the seabed. The energy is generated by current flow acceleration through the kite's looping motion. The kite is flying in a numbered-eight shape above its anchor point.

To date, the most commonly applied tidal energy converter device is horizontal axis turbine. The world's first open sea horizontal axis turbine implementation was the Marine Current Turbine (MCT) installation in Year 2003. Verdant Power's Roosevelt Island Tidal Energy (RITE) has successfully deployed the world's first grid connected tidal turbine array comprising six numbers of 5-meter diameter horizontal axis turbines. Followed by that, commercialization of tidal turbine has begun with the world's first commercial scale tidal stream turbine deployment – MCT's 1.2 MW 'SeaGen', which consists of two numbers of 16 m horizontal axis rotor turbine. From then onwards, many other commercial turbine developers (e.g. OpenHydro, Atlantis Resources, Andritz Hydro Hammerfest, Scotrenewables) ventured and successfully made deployments of full-scale, or near to full scale horizontal axis turbines (Phoenix, 2017).

Considering the forefront of the horizontal axis turbine in the tidal stream energy sector, this research is therefore focused on simulation of potential and enviro-impact of horizontal axis turbines, and any further elaboration on tidal turbines in this thesis is implying on horizontal axis turbines.

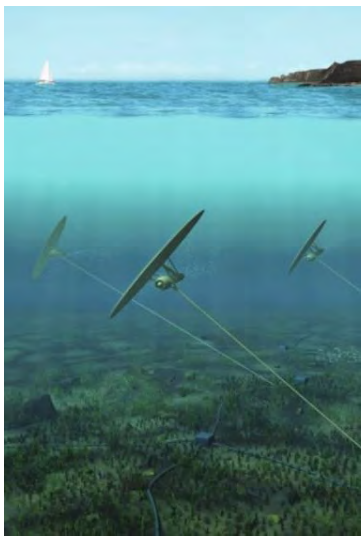

Figure 2.10: An example of tidal kite (Neill & Hashemi, 2018)

2.5 Potential Tidal Current Energy Exploitation in Malaysia

Malaysia has great prospective to utilise the tidal energy as a renewable energy resource due to abundance of ocean resource circumstancing the country shoreline. The electricidal power estimation analysis for tidal current energy extraction conducted by (Lim & Koh, 2010) showed that the highest potential locations (Pulau Jambongan, Kota Belud, and Sibu) is approximately 14.5 GWh/year. Lim & Koh (2010) study showed that the estimated electrical power of tidal stream energy from was significantly much higher than the estimated electrical power of Photovoltaic System (PV solar system) in 2010. Hence, Malaysian government or Tenaga National Berhad (TNB) Malaysia can reduce the cost of approximately RM 1.1 billion of natural gas and reduce the greenhouse emission of approximately 4,552,512 tonnes/year through the application of tidal stream energy system. The cost of the system is able to be recovered after 10 years of full operation and positive income can be achieved followed by then.

Another study (Yusoff et al., 2015) using the tides table Malaysia 2014 by National Hydrographic Centre to look for potential tidal energy harnessing site found that Port

Klang (Selangor) has the highest potential location of harnessing tidal energy compared to other locations. The tidal level for this region ranges between 0.4 meters and 5.3 meters. However, this analysis only depended on one parameter, which is tidal range and thus the result from this research is not sufficient to be used as a good reference for the author to select the potential tidal current extraction site in Malaysia.

It is important to determine a suitable site for tidal current energy exploitation. There are several criteria in tidal stream site selection. A site with tidal current speeds of more than 2 m/s is strongly recommended for implementation for its intensive renewable energy fluxes in comparison to other conventional renewable energies, such as solar and wind energies (**Table 2.1**).

Table 2.1: Relative power density of marine currents with wind and solar resources (Fraenkel, 2004)

Energy Source	**Tidal Currents**					**Wind**	**Solar**
Velocity (m/s)	1	1.5	2.0	2.5	3.0	13	Peak at noon
Power Density (kW/m^2)	0.52	1.74	4.12	8.05	13.91	1.37	~ 1.0
**Note: the maximum power can be achieved by wind turbine at velocity 13 m/s*							

In addition to the velocity criteria requirement for tidal current energy extraction, a potential tide site shall also need to meet water depth requirement to be effective for tidal current energy utilization. Water depth is crucial for tidal current energy converters, installation and it directly decides the size of tidal current energy devices. The ideal water depth needs to be a minimum of 15 m at low tide, and at that depth the smallest rotor, which can be accommodated is about 10 m diameter. Ideally, the maximum water depth at high tide probably is not more than 40 or 50 m, but the upper limit is according to the type of tidal current energy converters and the installation methods to be applied. A suggested criterion for rotor diameters of a tidal current turbine in horizontal axis, according to a range of seawater depths, is shown in **Table 2.2**.

Table 2.2: Influence of water depth on maximum permitted turbine size (Buigues et al., 1998)

Water depth (m)	Rotor diameter (m)
20-25	5
25-40	10
>40	20

A general rule used in practice is by applying a rotor diameter to be half of the depth of the water and the center of rotor must be at the midwater depth. In addition, a spacious seabed is needed to allow a large enough array of tidal current devices to be installed, that makes the overall project cost-effective. A relatively flat seabed also has advantage in reducing ambient turbulence as well as the loss of tidal current velocity near the seabed. Sites should also be close to shore-based grid connections. Other factors associated with tide sites selection have also been discussed by Fraenkel (2002) & Buigues et al. (1998).

The preliminary study from Marine Renewable Energy Research Group of the University of Malaya showed that Strait of Malacca has abundant of tidal stream energy resources and thus it has great potential to exploit the tidal energy in the condition of an appropriate water depth at the deployment site (Sakmani et al., 2013). Tidal current speeds to exceeding 2 m/s is required for viability of commercial development (Fraenkel, 2004). Regional model of previous study showed the highest current speed is discovered in the mid of the strait, especially at region between Pulau Rupat and Negeri Sembilan coastline (in red lined circle) as shown in **Figure 2.11.** However, as the resolution of the previous model is not sufficient and fine enough to provide an in-depth information of the extractable energy at this area. Therefore, a high-resolution model specifically focused at the Negeri Sembilan coastline has been initiated in this study to assess the energy extraction potential along multiple headlands of this coastline. For some areas where the current magnitude in Malacca Strait may not be sufficient to utilise full capacity

of the turbine's blade, a research conducted by Sakmani et al. (2013) concluded that low speed turbine which requiring lesser current speed for area with low current speed can be applied. They have suggested modifying the typical tidal stream energy with the application of funnel/venturi shaped turbine to bring in the current flow into the turbine in order for better blades rotation.

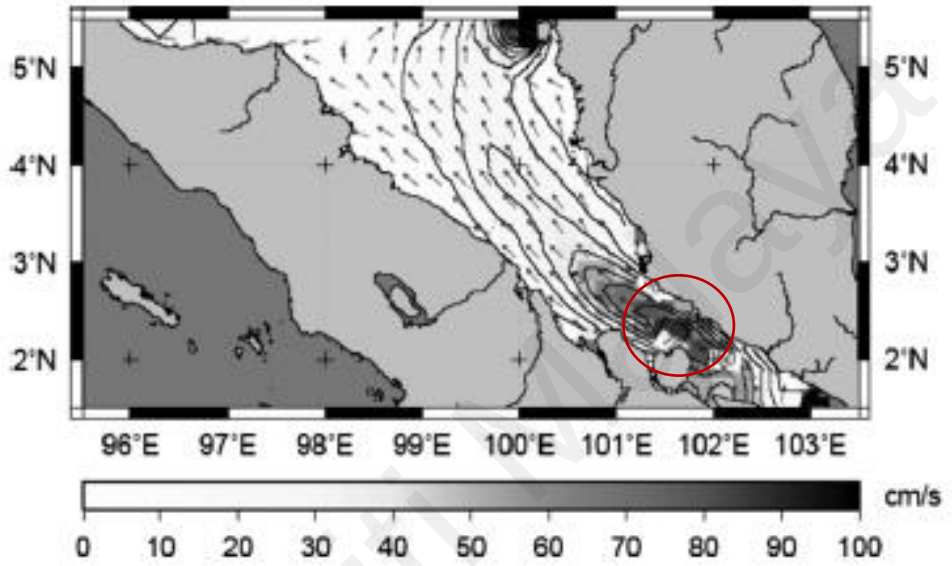

Figure 2.11: The surface current velocity during February in Straits of Malacca

2.6 Background of Study Area

Proposing the tidal energy extraction within coastal region may possibly lead to erosion problems and long-term changes on the shoreline. The erosion problem will be worsening due to poor design installation and lack of maintenance as well as if the impacts to the neighbouring shores are not cautiously assessed. Thus, understanding the hydrodynamic and morphodynamical conditions at the proposed site is essential for assessing the impact due to the tidal energy extraction. A review on the study area is elaborated in the next subsections.

2.6.1 Geographical Location of Straits of Malacca

The Straits of Malacca is situated between Sumatera Island and Peninsular of Malaysia. The length of the Strait is approximately 800 km with an average depth of approximately 25 m. It is the longest route for navigation in the course of a strait, which joined between the Indian Ocean through the north of Straits of Malacca with the South China Sea to the south through the Johor Strait (Chua et al., 2000). This strait is an important waterway as it caters shipping route between the East and West of the world. Besides function as the main shipping route, this large water body is the habitat for the fisheries, coral reefs and mangrove forest. The mangrove forest is ecologically important habitat that links the marine and terrestrial environments and provides habitat for both marine and terrestrial organisms, including several threatened species. A mangrove ecosystem is vital to the biological productivity and food webs of coastal waters and provides critical nursery areas for many fish and crustaceans, including commercially and recreationally important species.

The mangrove forest is found along the coastline of west Peninsular Malaysia within the Straits of Malacca (Kanniah et al., 2015) as shown in **Figure 2.12**. There are 641,886 ha of mangrove forests in Malaysia, of which 57% are found along the coastline of Sabah and 26% in Sarawak and the remaining 17% in Peninsular Malaysia. Mangroves on the west coast of Peninsula Malaysia are widespread along the coast. Approximately 91 000 ha of mangroves are found along the west coast (Shaharudin et al., 2001). The mangrove forest distribution map is shown in **Figure 2.12**.

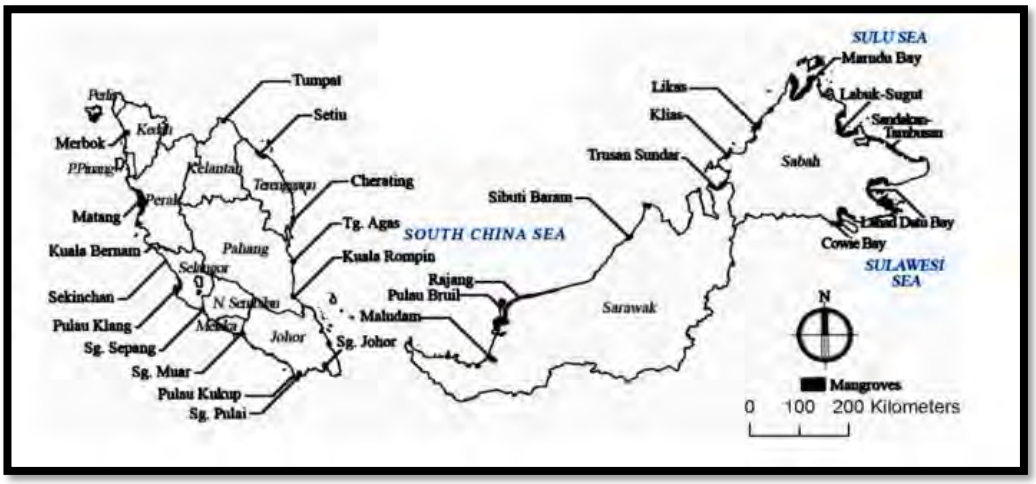

Figure 2.12: Mangrove forest distribution map in Malaysia (Kanniah et al., 2015)

2.6.2 Tidal Condition

The tides are a periodic phenomenon. The periodic nature of the reaction varies depending on the interaction between the gravitational effects and movement between the moon and the sun, as well as their unique geography. There are three main characteristics of tides phenomenona in Malaysia, which consists of diurnal, semidiurnal, and mixed tides as shown in **Figure 2.13**. Diurnal tides are the one sort of tides with its period relates to a complete transformation of the moon with respect to the earth for about 24 hour and 50 minutes (Gorlov, 2001). Such a tide has one high tide every day.

Semi-diurnal tides are liable to varieties emerging from the hub of revolution of the earth being slanted to the planes of the circle of the moon around the earth and the earth around the sun (Rourke et al., 2010). Semi-diurnal tides was described (Draper et al., 2014) as one kind of tides having a period that matches the key time of the moon for 12 hours and 25 minutes. Any seas with such tides are having two high and two low tides every day. The tides, amplitude changes according to the lunar month, whereby tidal extent is most prominent during full/new moon (spring tides) when the sun, moon, and earth are adjusted (Gorji-bandpy, 2013).

Reverberation phenomena in connection to the period of 12 hours 25 minutes portray tidal reach. Mixed tides are the combination between the two characters of semi-diurnal and diurnal tides. They might likewise show month to month and bimonthly variety. When the semi-diurnal is dominant in mixed tides, the highest tidal current takes place during spring tides and the lowest tidal current takes place during the neap tides (**Figure 2.13**). If the diurnal is dominating in mixed tides, the largest current occurs at the highest declination of the moon and the lowest current occurs when declination is zero (Lee & Seng, 2009).

Figure 2.14 shows that Malaysia consists of semidiurnal, mixed tides with dominant semidiurnal and mixed tides with dominant diurnal. There is no diurnal tides in Malaysia (Lim & Koh, 2010). North and West of the Peninsula have been spearheaded by the semidiurnal tides. Among these are Kedah, Perak, Penang and Selangor. While the area South and East of the Peninsula have been spearheaded by mixed tides with dominant semidiurnal. Among these are Johor, Pahang, Kelantan, and one-third of the state Terengganu, Sabah and Sarawak. The rest of area for Malaysia, spearheaded by mixed tides with dominant diurnal.

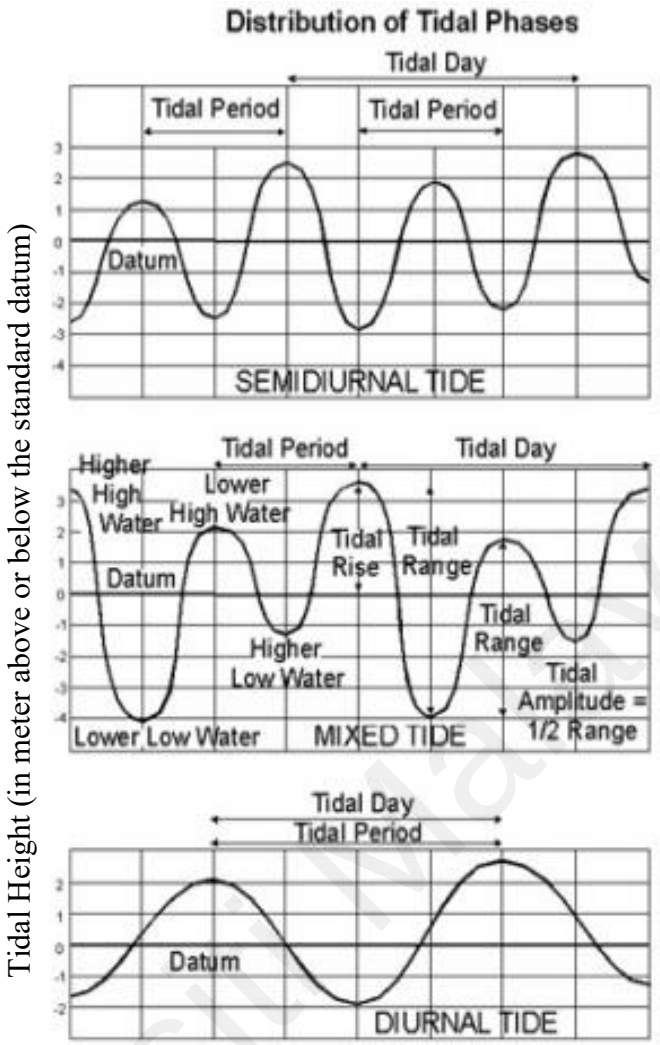

Figure 2.13: Types of tides: (a) semidiurnal Tide; (b) Mixed Tide; (c) Diurnal Tide (Araquistain, 2006)

The tide level for some of the standard ports along the coast at Peninsular Malaysia is shown **Figure 2.15** in referring to the Tide Tables of Malaysia published by Royal Malaysian Navy (2015). The tidal constituents with the combination of M2, S2, K1, O1, N2 and K2 tides components drive the tidal flow into this region, whereby M2 tide is the component that dominantly drives the flow.

Figure 2.14: Types of tides available in Malaysia (Lee & Seng, 2009)

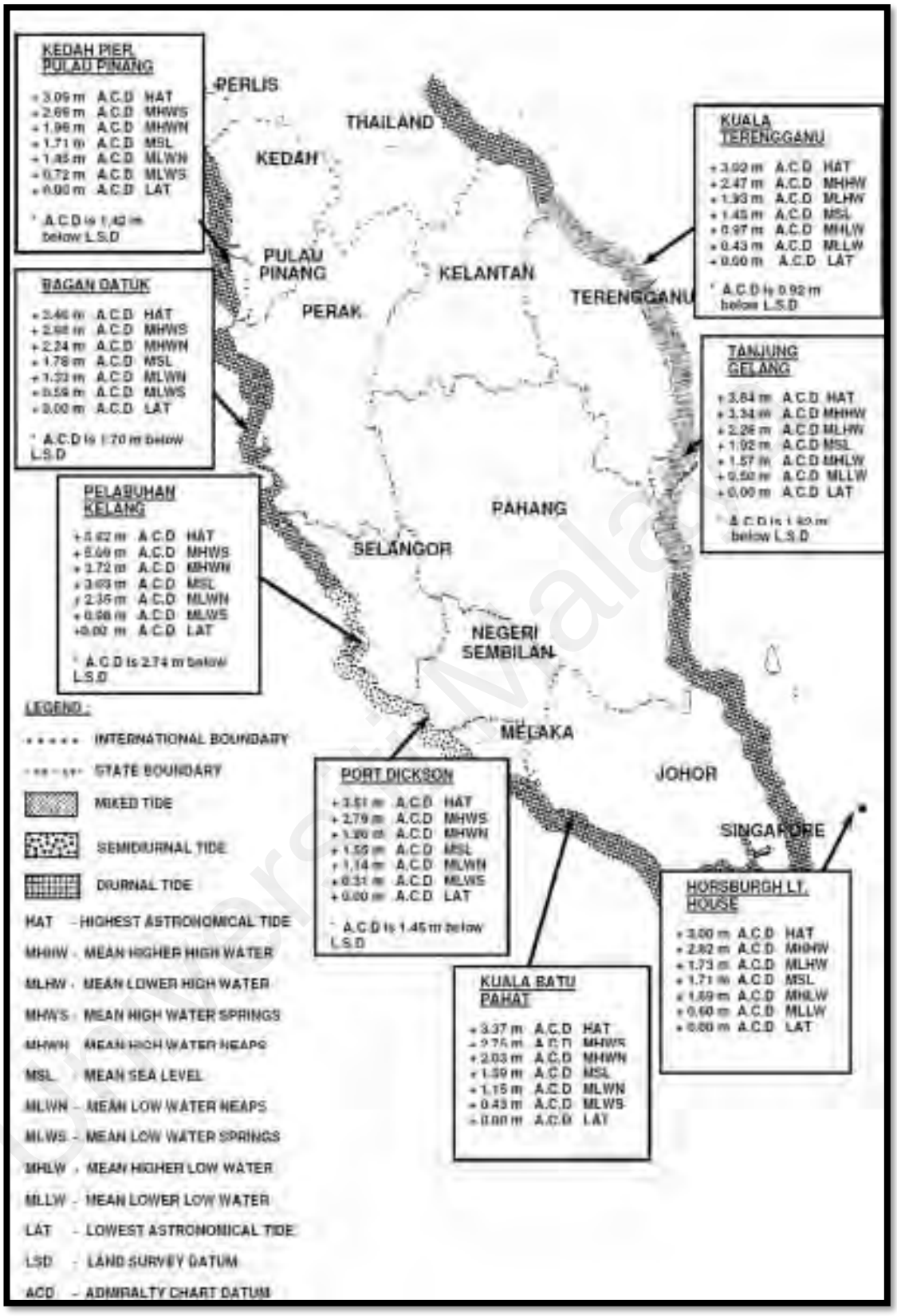

Figure 2.15: Tidal levels at the standard ports in Peninsular of Malaysia (ref: Tide Tables of Malaysia published by Royal Malaysian Navy (2015))

2.6.3 Current Flow

The understanding of the circulation of the current flow is very important to assess the impact of the large-scale deployment of tidal extraction energy to the coastal area. In most area in Malaysia the current flow is low, especially at Malacca Strait (**Figure 2.11**), which is sheltered by Peninsular and Sumatera, the current magnitude is generally less than 1 m/s covering the full water column throughout the year except during the monsoon monsoons (Northeast Monsoon and Southwest Monsoon in February and August each year). The water flows in southeast direction during the flood tide and flow out on north west direction during the ebb tide (**Figure 2.16**). The overall flows in the Malacca Strait is to the North-West, but from May to September there is a tendency for South-East currents to prevail in some North and central parts but the predominance is very slight.

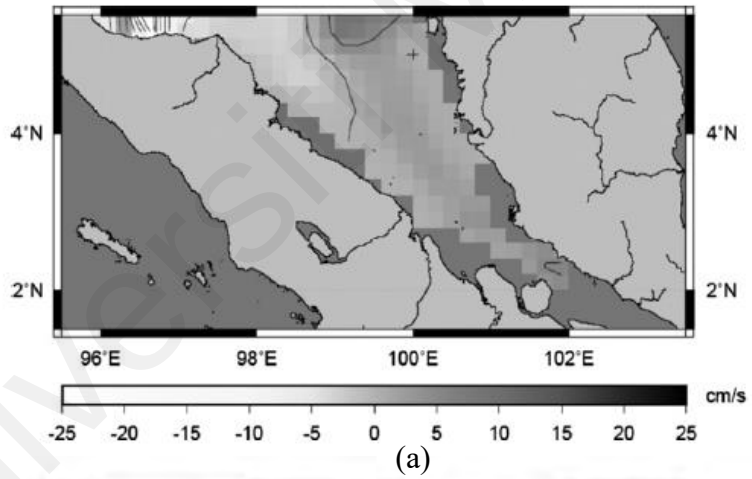

(a)

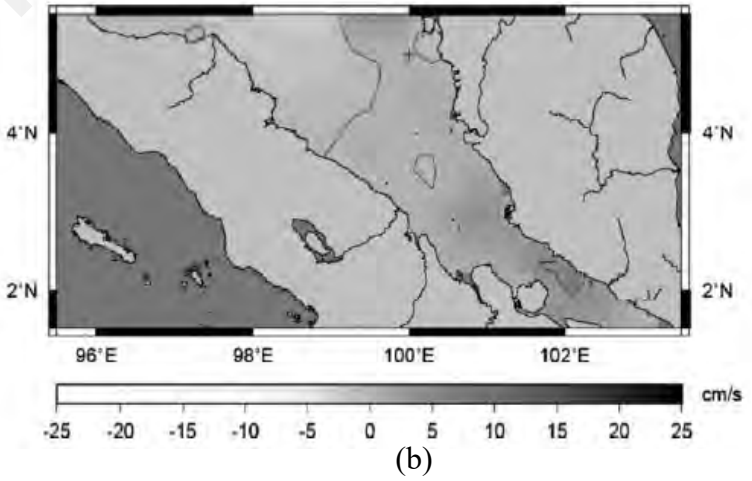

(b)

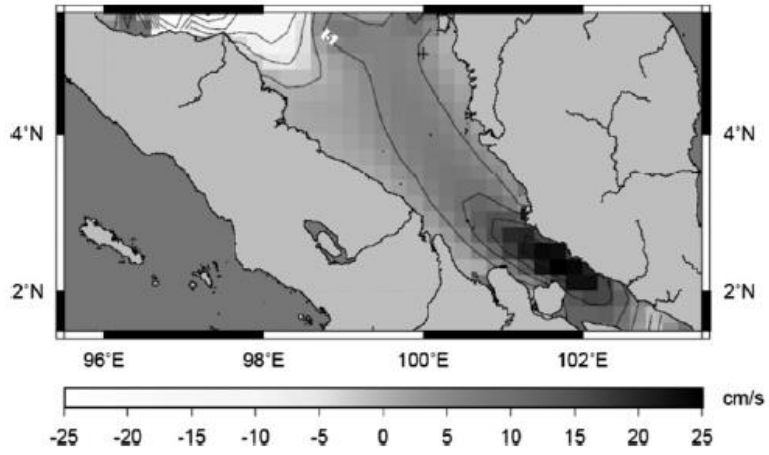

(c)

Figure 2.16: Current magnitude (a) at around 10 -70 cm/s on the surface along the Straits of Malacca, (b) in range of 10 – 30 cm/s at 30 -50 m layer from sea surface, and (c) at the bed of the strait at 10 – 20 cm/s at 30 -50 m layer from sea surface during pure tide condition

2.6.4 Wind

The Straits of Malacca lies within the equatorial region of low atmospheric pressure and has a typical tropical climate. Typhoons are not experienced and gales are infrequent. The predominant winds over the Malacca Strait are monsoon winds.

Northeast monsoon occurring form November to March has higher strength and gustiness in January. The nominal wind speed ranges from 2.5 m/s to 5 m/s, but may be as high as 10 m/s to 12.5 m/s for short periods in the northern part of the Strait (National Geospatial-Intelligence Agency, 2016).

Southwest monsoon that happens from May to September achieves its highest strength and gustiness in July and August. The nominal wind speed is about 5 m/s, reaching 7.5 m/s to 10 m/s in the Northern approaches. Squalls are common in the Malacca Strait, the most significant of which occur between April and November and are referred to as Sumatras. These squalls are usually accompanied by thunderstorms and torrential rain. (National Geospatial-Intelligence Agency, 2016).

2.6.5 Waves

The coast along the Straits of Malacca is exposed to mild wave condition. This is because the Straits of Malacca is well protected by the Sumatra Island from the Indian Ocean, by limiting the winds fetch length and wave heights to the Strait. Generally, the wave height in Straits of Malacca ranges from 0.5 to 1.0 meters, while the wave period is range from 3 to 9 seconds (Gan, 2014). The wave from the northern part of the Straits of Malacca has longer period that is travelling into the strait from the Andaman Sea. The southern part of the Straits of Malacca is dominated by South West (SW) monsoon waves. The east coast of Peninsular Malaysia is exposed to more severe wave condition as compared to the west coast, especially during the North East (NE) monsoon (Mastura, 1992).

2.6.6 Geomorphology

The hydromorphodynamic characteristic in the Straits of Malacca is complicated due to the high variation of bathymetry and a shallow sub-bottom reflector within the Strait, which is interpreted as a Pleistocene lowered sea level alluvial-delta-fan system (Emmel & Curray, 1982). Generally, the coast along the coastline of western of Peninsular Malaysia in the Straits of Malacca is sedimentary-morphodynamic type. It is formed by fine sediment that deposits within a coastal intertidal zone, normally silts and clay are found, the deposition of these materials forms a broad tidal flats (Healy et al., 2002).

2.7 Resource Assessment of Tidal Current Energy

It is crucial to conduct resource assessment on a potential site for commercialization of tidal stream energy. This assessment must be carried out to quantify the amount of available extractable energy from a potential site which also directly influence the site

selection decision. There are several other considerations in site selection decision, e.g., hydro-enviro impacts, operation and maintenance (O&M) and access of power distribution network (Blunden & Bahaj, 2006). However, the main consideration for site selection is dependent on the amount of available extractable energy from a potential site. It is worth to mention that tidal resource assessment has begun since about 50 years ago (~1970's) by several researchers such as Cave et al. (1987), Fraenkel & Musgrove (1979) and Wyman & Peachey (1979). Continual development and improvement on tidal resources assessment approaches is still on-going to date. This is to ensure that high accuracy of tidal resource assessment can be achieved so that underestimation/overestimation of resources can be avoided. Underestimation of resource may result in a project may assume not viable due to insufficiency of resources, while overestimation may result in underperformance between actual and anticipated extractable energy.

According to Blunden & Bahaj (2007), tidal current energy resource assessment is an iterative process, which contains of four main fundamental steps as follows:

a. Site selection should be done by assessing the current flow speed and the range of depths (depends upon the type of tidal energy converter device)

b. Determination of sizing and rating of the tidal energy converter maximizes the extracted energy over the converter device's lifespan. Long term variations in flow speed, deviations of flow from rectilinear movement and vertical flow must be taken into account during the site selection stage.

c. Investigation of arrangement variations to achieve maximum energy extraction.

d. Investigation of the effect of single and array tidal turbine deployment on the sea

2.7.1 Kinetic Energy Flux from Tidal Flow

The first step of tidal energy resource assessment introduced by Blunden & Bahaj (2006) is no doubt the most crucial stage to determine a suitable site for tidal energy extraction (Blunden & Bahaj, 2006). The quantification of extractable energy can be determined by the kinetic energy of the available tidal current flow, which can be expressed as:

$$E_k = \frac{1}{2}\dot{m}v^2 \quad (2.\ 1)$$

where $\dot{m}$ is the mass of the moving fluid (kg) and v is the velocity of the fluid (m/s)

The mass of the moving fluid flow can be represented as:

$$\dot{m} = \frac{m}{t} = \rho v A \quad (2.\ 2)$$

where ρ is the fluid density (kg/m^3), A is the cross-sectional area of the moving fluid flow, and t is the duration of the moving fluid flow.

Power (P) (commonly known as available extractable power resource) then can be calculated by dividing equation (2. 1) by time and substituting for $\dot{m}$ to give:

$$P = \frac{1}{2}\rho A\, u^2 \quad (2.\ 3)$$

Where u is referred to free-stream current speed of the fluid.

2.7.2 Methodologies for Tidal Stream Resource Assessment

According to Boyle et al. (2003), tidal current energy resource assessment methodologies can be estimated with the following methodologies:

a. Theoretical resources assessment

The extractable energy in a region is assessed without considering technical, environmental and economic factors, i.e., undisturbed resource assessment.

b. Technical resource assessment

Technical assessment through maximum accessible tidal energy extraction utilising the latest tidal turbine technology.

c. Practical resource assessment

The practicality resource is limited by electricity grid accessibility and transportation issue. Public opinion may limit the sea area and the implementation technology may also reduce the technical resource extractability further as this issue can only become clear when planning consent is solved and environmental submission is made.

d. Accessible resource assessment

The practicality of implementation is very likely limited by site specific constraints, e.g., energy policies, planning limitations and environmental impact.

e. Viable resource assessment

The viability of implementation can be constrained by commercial limitation, e.g., market rewards, timing, development costs and timing.

The most commonly applied assessments are the theoretical and technical resource assessments. Preliminary stage in tidal current energy resource assessment had been conducted by B&V (2004) and Blunden & Bahaj (2006) using tidal farm method. This method determines the extractable tidal current energy by assuming that each tidal turbine device extracts certain percentage of the theoretical resource based on the efficiency of the selected tidal turbine device. Therefore, it can be said that the extractable energy is dependent on the type of tidal turbines for the efficiency of extraction, size of the farm

and numbers of tidal turbines to be deployed. This method is straight forward. However, this approach does not consider the changes of the available resources due to tidal current energy extraction of each device/farm in vicinity. More recent research has indicated the importance to consider the effect of tidal current energy extraction from surrounding. Tidal current energy extraction at one region will be altering the tidal current flow condition at another region, and subsequently alter the extractable tidal current energy resources (Bahaj et al., 2007; Draper et al., 2010; Myers & Bahaj, 2010; Plew & Stevens, 2013; Stallard et al., 2013; Sun et al., 2008).

Robert Gordon University (RGU) and Black & Veatch (B&V) have modified the tidal farm method for UK tidal energy extraction resource assessment (B&V, 2004; RGU, 2002). Their studies have incorporated a 'significant impact factor' (SIF) for the tidal current energy extraction impact assessment to limit the theoretical resource assessment and re-defining the technical resources as the maximum power that can be extracted without significant environmental impacts (RGU, 2002) (B&V, 2004). Therefore, the technical resource is predicted as the theoretical resource by multiplying with SIF, which an ideal site shall be determined for sites individually (B&V, 2004). A representative SIF is determined by modelling a number of case study sites. Based on previous modelling results and existing knowledge of every single site environmental sensitivity test, mid-range velocity changes and acceptable SIFs were determined for ten selected important sites. The acceptable velocity changes are within 10 – 15 % while the associated SIF values shall range from 8 – 20%. A further refinement had been conducted by Black and Veatch Consulting Ltd (2011) where sites were studied on site-by site basis. From that, various 'significant change' limits had been determined (0.2 m difference in tidal range or a 10% difference in mid-range current velocity) and the related SIFs were identified.

2.7.3 Tidal Current Energy Resource Assessment Accuracy

There are several aspects affecting the accuracy of resource assessment. Two important types of published resource assessment methodologies are: (1) the theoretical formulation of extractable power equation (2. 3), and (2) type of current velocity to be adopted.

Theoretical formulation of extractable power equation

A formula taking the effect of temporal variation in current speed into consideration was established (Fraenkel, 2002) for estimating the extractable tidal current power. For a tidal condition covering spring and neap cycle sinusoidal in nature, the mean available power can be defined as:

$$P_{mean} = \frac{1}{2}\rho A K_s K_n u_{peak}^3 \quad (2.\ 4)$$

where u_{peak} is the maximum spring velocity, K_s is the velocity shape factor (by considering the variation in velocities over a spring neap tidal cycle) and K_n is the neap/spring factor (by considering variation in spring and neap peak velocities).

For a normal sinusoidal tidal flow, K_n and K_s are normally assumed as 0.424 and 0.57, respectively by considering a 60% decrease in peak tidal current between neap and spring tides (Fraenkel, 2002). Previous studies, which used this equation include Fraenkel and Musgrove (1979); Fraenkel (2002) and Rourke et al. (2010). The assumption of 60% spring-neap for a sinusoidal tidal cycle by Fraenkel (2002) may not be applicable to all cases, in which it may be causing inaccurate estimation of mean available power (P_{mean}) using equation (2. 4). Therefore, if time-varying current velocity data are made available, a higher accuracy quantification of the mean available power for tidal current energy can be estimated using equation (2. 4) as:

$$P_{mean} = \sum_{N1}^{N_{max}} \frac{1}{2} \rho A u_N^3 \quad (2.5)$$

where N_{max} is the sum of time steps and U_N is the magnitude of the tidal current velocity at a particular number of time-step.

In practice, theoretical resource for tidal current energy turbine are restricted by physical limit and energy losses. The proportional theoretical resource for a tidal turbines' current energy extraction is identified as power coefficient, C_p, which is very much dependent on the physical limit and the design of the tidal current energy turbine. According to Rourke & Reynolds (2010), C_p for a single horizontal tidal current energy turbine is typically assumed to be equal to 0.59, which is equivalent to the Betz limit (Rourke et al., 2010). Nonetheless, in actual condition, energy losses due to turbulence and structural drag may reduce the actual power coefficient during the tidal current energy extraction process. The extractable power by an array of n numbers of tidal current energy turbines with mean available power of P_{mean}, turbine's swept area of A_T and power coefficient of C_p can be defined as:

$$P_{ext} = \sum_{1}^{n} P_{mean} A_T C_p \quad (2.6)$$

A. Type of Current Velocity Data

For applying the theoretical formulation of extractable power using equation (2. 6), it is important to highlight that current velocity has significant effect on the power calculations, for instance a 15% underestimation of velocity would be causing underestimation by 45% of power estimation. Hence the accuracy of tidal current energy resource assessment is highly sensitive by current velocity input to be adopted for estimation.

In earlier stage of tidal current energy resource assessment by B&V (2004), Fraenkel & Musgrove (1979) and Grabbe et al. (2009), tidal current velocity data from navigational charts was adopted. However, the means of measurements are generally unknown, whether it is collected from offshore rig or guesstimate from visual observation. Consequently the accuracy of the data is unknown as well. Measured current velocity data is able to ensure better accuracy (Blunden & Bahaj, 2007; Cartwright et al., 1988). Measured data could be used as rough estimate for resource assessment. However, the duration of measurement (different monsoon and tide condition may show very different current velocities) of data collection may significantly influence the accuracy of available power estimation. The duration problem may be addressed by collecting long term measurement current velocity data at a specific site in order to provide a better accuracy assessment but this still has the drawback where spatial variation may provide different current velocity; the measured current velocity data may show very different current velocity value even at nearby location. Followed by that, the spatial variation can be tackled by using high frequency radar that can measure current velocity data temporally and spatially (Lewis et al., 2019; Liu et al., 2007; Paduan & Shulman, 2004).

Henceforth, a more comprehensive method for resource assessment was engaged by using numerical model for simulating tidal current velocity flow covering the entire extent of the interest site. This method therefore can capture both spatial and temporal velocities condition, and subsequently the available power. The accuracy of the numerical results is very much relying on the accuracy of the numerical model being set-up, which is very sensitive to the computational grid's spatial resolution. Numerical model calibration and validation are also crucial in ensuring the accuracy of the simulated tidal current velocity flow. Numerical model calibration and validation can be conducted by comparing simulated tidal level and current velocity with field measured data. Higher accuracy numerical model should be able to simulate the tidal level and current velocity data as

near as possible with the measured data. To date, here are several published studies, such as Adcock (2014), Bryden et al. (2007), Carballo et al. (2009), Lewis et al. (2015) and Rourke et al. (2010) that assessed the tidal current energy resource using numerical models.

B. Tidal Current Energy Turbine Influence

The conventional method of tidal array resource assessment, P_{mean} is an undisturbed theoretical extraction resource where the influence of tidal turbines in vicinity is not taken into account during the assessment. In reality, the effect of deployment of tidal turbine can be significant to tidal turbine in vicinity (Defne et al., 2011; Neill et al., 2012; Pacheco & Ferreira, 2016). The hydrodynamic impact of any tidal current turbine may possibly affect the available power to other tidal current turbine in vicinity, and subsequently the overall power output from the array may be affected. The configuration placement optimisation of tidal current turbine array is considerably important in order to produce maximum power output with minimal environment impact. Sustainable environment should be one of the prioritized elements to be taken into account during the planning stage. Tidal turbine wake and blockage effects will reduce the potential capture of the downstream turbine (Martin-Short et al., 2015).

2.8 Numerical Modelling Approaches for Tidal Turbines Effects

Tidal Energy Extraction technology is still evolving (Neill et al., 2012). Recent researches have shown that the operation of a tidal farm may alter both the transient and residual circulations (Abanades et al., 2014; Kenyon & Cooper, 2005). For estimation of potential power output from tidal energy converter using numerical hydrodynamic modelling, it is crucial to consider the effect of tidal turbine energy extraction to the available resources (Ramos et al., 2014).

Various approaches for numerical modelling of tidal turbine are as follows:

a. Actuator disc model, which represents the tidal turbine rotor acting as an infinite porous disc. The area of porous disc is assumed to be equivalent to rotor's swept area. The extraction is included into momentum sink in the momentum equation (Batten et al., 2008; Batten et al., 2013; Churchfield et al., 2013; Sun et al., 2008)

b. Rotating reference frame, which can be applied in CFD model allows the simulation of flow rotation and adopts the blade geometry for hydrodynamic model simulation. The Coriolis and centripetal force terms are included in the momentum equation in solving the rotation of the turbine speed (Mozafari & Teymour, 2010; Mozafari et al., 2017).

c. Sliding mesh model, which can be applied in a CFD model that simulates the rotating tidal turbines in a detailed manner. It allows a portion of cells to rotate within a bigger spatial static grid. However, this model is the most expensive computational method due to the complex flow (McNaughton et al., 2015).

d. Blade element model can be applied in CFD model, which models aerodynamic condition of the rotating blade in time-averaged manner. The tidal turbine effect is simulated using momentum source term by including it into a rotor risk disc fluid region that depends on the attack angle, drag and lift coefficient and chord length (Masters et al., 2015; Mozafari & Teymour, 2010; Turnock et al., 2011).

e. Momentum sink model simulates the tidal turbine extraction by including its effect into the momentum equation to represent the axial thrust induced by the rotor and drag induced by the turbine support structure. This is the most common method for far-field modelling (Ahmadian et al., 2012; Fallon et al., 2014; Ramos, Iglesias, et al., 2013)

f. Bed roughness model simulates the wake effect of the tidal turbine by increasing the bed roughness into the model (Funke et al., 2014; Karsten et al., 2008; Sutherland, 2007). However, this approach only captures the flow current speed without considering the flow direction, which is not realistic for horizontal tidal turbine with fixed orientations.

Momentum sink model is the most common approach adopted for tidal turbine energy extraction effect assessments in far-field numerical model simulation. It is conducted by including the induced turbine thrust in the momentum equations as a momentum sink. The common equation (2.7) used for turbine thrust is linear momentum actuator disc theory (LMADT) (Houlsby et al., 2008) given by:

$$T = 0.5\rho u^2 A_T C_T \quad (2.7)$$

where, u is the upstream current velocity, A_T is the swept area of the tidal turbine and C_T is the dimensionless coefficient for the thrust and it is the function of turbine design and flow speed.

According to Houlsby et al. (2008), the theoretical maximum power coefficient (C_p) is 0.59, where it represents the extractable power for a tidal turbine. And, this happens when C_T reaches its optimum of 0.9. Another study by Blunden & Bahaj (2007) using physical modelling has discovered similar finding for different design conditions, where the discovered C_p and C_T are 0.49 and 0.8, respectively. Based on the findings by Houlsby et al. (2008) and (Bahaj et al., 2007), far-field modelling studies were conducted by assuming a thrust coefficient of 0.8-1.0 to correspond with peak turbine efficiency, typically in the range of 0.4 – 0.6 (Ahmadian et al., 2012; Ahmadian & Falconer, 2012; Fallon et al., 2014; Nash et al., 2014; Plew & Stevens, 2013; Ramos et al., 2014).

The hypothesis of C_T value near to 1 is based on the relationship of tidal turbine thrust together with undisturbed flow condition. Nevertheless, the employment of momentum sink method typically reflects that the tidal turbine thrust is calculated using the stream flow at the at the turbine itself, that varies from the undisturbed upstream current flow velocity. As the current velocity at the turbine will be lower due to the inclusion of the momentum sink, the C_T value to be assumed in the range of 0.8-1.0 may not be appropriate. Henceforth, velocity Houlsby et al. (2008) has recommended a higher value of thrust coefficient, which is 2.0 based on localised current velocity. Selection of suitable values of u and C_T in equation (2. 7**)** is crucial in ensuring the accuracy of the numerical model. This problem becomes more prominent at lower spatial grid model due to the gap in tidal flow and tidal turbine velocity becomes larger.

Enhancement of numerical model had been carried out by Gillibrand et al. (2016) and Funke et al. (2016) to tackle the problem of selecting suitable values for u and C_T. Gillibrand et al. (2016) constructed 3D model by including large average volume at the turbine location for modelling a close condition of an undisturbed upstream velocity. While Funke et al. (2016) have established a relationship between undisturbed upstream and local current velocity at the tidal turbine, where a factor of correction is formulated to be applied on the tidal turbine thrust estimation. With that, a force close to the theoretical thrust can be implemented.

Tidal turbine array configuration optimization had been studied by Funke et al. (2014) and Divett et al. (2013). Both studies modelled the hydrodynamic impacts of tidal turbines in different configurations to come out with effective and high efficiency power output with minimal environmental impact design. High resolution 2D model was previously used by both studies mentioned. The model by Divett et al. (2013) was developed to study the energy that can be extracted in different array configurations. The latter study by

Funke et al. (2014) integrated a gradient based optimization with shallow water flow model to conduct optimization in a single simulation. The simulation was conducted by repositioning the tidal turbine and flow were recalculated in iterative steps until an optimized array is achieved. For this study, one of the main objectives is the establishment of an optimization algorithm to produce optimum tidal turbine array by determining both energy extraction and hydrodynamic impact. This discussion will be elaborated further in Chapter 6.

2.9 Tidal Energy Extraction Effects to the Coastal Environment

A scientific workshop held in Seattle, Washington entitled "Environmental Effects of Tidal Energy Development" on March 22-25, 2010 has gathered both commercial professionals and academic researchers from the tidal energy sector (Polagye et al., 2011). Several environmental threats due to the development of tidal current turbines industry have been determined:

a. Static effects: causing near-field variation on water level, tidal current velocity, waves, sediment transport, benthic habitat and ecosystem interruption due to the presence of physical structure (turbines, support body structure, cables, moorings, etc.)

b. Dynamic effects: giving threats to marine aquatic life due to the rotating tidal turbine blades, pressure and velocity gradients surrounding the device.

c. Tidal current energy removal effects: causing far-field effects on water level, current velocities, sediment transport and water quality.

d. Chemical effects: causing water quality deterioration and marine aquatic life threats due to spill/leakage of lubricants, hydraulic fluids, toxic chemical from anti-fouling coatings and, etc.

e. Electromagnet effects: giving threat to marine life due to the electromagnetic fields resulting from the generation and transmission of electricity.

f. Acoustic/noise effects: giving threats to marine aquatic life due to the underwater sound/noise generation during the device installation and operation stage.

Although the marine tidal current turbine technology is technically prepared for commercialization, the impact to the marine environment still has a lot of uncertainties to date. This is due to limited number of actual site deployments and limited measured data on actual environmental effect of tidal turbines operation. Moreover, the pilot nature of deployment that coupled with the cost of data collection, and choice of data collection is bias towards collecting device performance data over environmental impact assessment (EIA) data. Due to limited field data available and cost consideration, the researchers have opted for a more convenient and economical way by studying the potential environmental impacts using numerical and laboratory/physical modelling approaches.

The approaches used in physical and numerical modelling can be different in many ways: method of tidal turbine representation, numbers and arrangement of turbines, types of impact studied, and the quantification of the mentioned impacts. Numerical model studies will be discussed in detail in the subsequent sections.

2.9.1 Pilot Studies

Literature review on pilot study is focused on placement of horizontal axis tidal turbines at shallow (< 30 m) marine area. The pilot studies for which environmental impact data are available discovered from literature review include the following:

a. Two (2) Marine Current Tidal (MCT) 1.2 MW SeaGen consisting of 16 m diameter with double bladed rotors attach to a 3m diameter monopile was deployed in Strangford Lough, Northern Ireland (Keenan et al., 2011). The maximum power for the SeaGen turbine was designed at current flow speeds of 2.4 m/s.

b. A 35kW Verdant Power's Dyno turbine consisting of 5 m diameter with 3 bladed rotor was installed in New York, USA. The maximum power for the Dyno turbine was designed at current flow speeds of 2.1 m/s (Schmitt et al., 2015).

c. A 50 kW SCHOTTEL Tidal Generator (STG) consisting of 4 m diameter 3-bladed tidal current turbine was installed at the Queen's University tidal test centre in Strangford Lough, Northern Ireland (Jeffcoate et al., 2015).

2.9.2 Laboratory Studies

Impact assessment studies for tidal turbine have been conducted by several previous researchers, e.g., Bahaj et al. (2007), Chamorro et al. (2013), Myers & Bahaj (2012), and Stallard et al. (2013) using laboratory method. These studies focused on hydrodynamic impact due to energy removal from static effect. The laboratory studies are limited to single turbine due to the dimensional limitation of test tanks or flume.

Two main types of model implemented for laboratory studies: (1) porous mesh discs as pseudo turbines and (2) scaled model rotors. The thrust exerted by the fluid on the tidal turbine causes turbine wake, a reduction in current speed downstream of a tidal turbine.

Porous disc method can be used to study the wake properties by changing the porosity of the mesh discs in accordance to desired thrust of scaled rotors. By using this method, the challenges of small scales turbine modelling can be minimised. An accurate scaled rotor testing can be problematic and cause excessive changes in the flow downstream of the tidal turbine (Bahaj et al., 2007). Therefore, porous disc approach is relatively more cost-effective. However, porous disc method has some restrictions. The static discs do not extract energy from the flow, instead they convert it to small-scale downstream turbulence and could not create downstream swirl of rotating turbine. The thrust and flow properties that accurately scaled, the far wake characteristics link well with those of full-scale model rotor (Bahaj et al., 2007). Most of the studies assessed through single disc/turbine. There are few studies that assessed through array of turbines: Myers & Bahaj (2012) studied array of 3 turbines in two-row arrangement, and Stallard et al. (2013) assessed a range of different array with different numbers, arrangement and spacings of turbines. The laboratory studies were conducted under turbulent flow regime (> 2x 10^3) with the Reynolds depth ranging from 7.5 x 10^4 to 3.0 x 10^6 by considering that the Reynolds number in actual site is usually in the order of 10^7 (Bahaj et al., 2007).

Most of the hydrodynamic impact of tidal stream technology focused on wake characteristic changes and was conducted by measuring the current velocity and turbulence at several points downstream of the tidal turbine. The measurement was conducted by measuring the near-field wake region (0 - 5/6 rotor diameter downstream) and far-field region (> 5/6 rotor diameter downstream).

2.9.3 Numerical Model Studies

Previous studies conducted using numerical model normally adopted near- or far-field modelling approaches, and almost all focused on the modelling of horizontal axis turbines.

Near-field modelling by previous researchers e.g. Mozafari et al. (2017) and Sun et al. (2008) was conducted in three dimensions (3D) with mesh sizes smaller than the turbine rotors diameters. This model is able to simulate the near field condition; however, this type of model is expensive and hence it is only limited to single turbine modelling in an idealised channel under steady flow condition. On the other hand, far-field modelling conducted by other researchers (Ahmadian et al., 2012) used much coarser mesh, where the size of the mesh is bigger than the diameter of the tidal turbine rotor. Therefore, the far-field model is not able to precisely capture flow around, and through each individual turbine. Far field model is more suitable to be used for modelling large array of turbines. The improvement of the numerical modelling allows development of multi-scale models by several studies (Ahmadian et al., 2012; Divett et al., 2013; Ramos et al., 2019). Ramos et al. (2019) which using low spatial resolution outside the tidal turbine array and high spatial resolution within the tidal turbine array to simulate the condition of the flow around individual turbines as near as possible. Both nested and unstructured methods can be applied for achieving the objective of this study.

2.10 Numerical Modelling of Tidal Current Extraction Effect

Although tidal extraction energy brings a lot of advantages as a renewable energy resource, the understanding of the potential impacts on the marine environment of the extraction of energy from the tidal flow is far from complete. Water levels, tidal currents and sediment transport could be potentially change due to the large-scale deployment of tidal extraction energy devices, which possibly could lead to the loss of major habitat and a change in the tidal zone. This can be a major concern to us as the majority habitat at the intertidal zone in Malaysia is mainly dominated by mangrove forest, which also serves as main source of food for marine life. This section discusses on the studies that were carried

out for environmental impact assessment on two important aspects. The hydrodynamic impact assessment that includes water level and current changes is discussed in Section 2.10.1, while Section 2.10.2 discusses on the sediment transport assessment due to the array of tidal extraction.

2.10.1 Impact of Tidal Turbine Deployment to Hydrodynamic

It is important to be noted here that based on the previous studies carried out, although tidal energy extraction may changes on the velocity structure, which includes of an overall reduction in flow velocity (Ahmadian & Falconer, 2012). The reduction is generally quite small even for in large scale deployment. The impact of energy extraction on current speed is only significant when the extracted energy reaches approximately 10 percent of the available kinetic energy flux (Bryden & Couch, 2006). A 2D hydrodynamic (HD) model was used by Nash et al. (2014) to study far field coastal hydraulic impacts of the effects of tidal turbine fields on tidal extraction energy. Hydrodynamic characteristic is found to have changes in areas upstream of the farm of tidal extraction energy where inter-tidal zones could be flooded and resulting the loss of habitat at the estuary. Hydrodynamic impact of tidal turbine deployment was studied in single and array tidal turbine and discussed in the following subsections.

2.10.1.1 Effect of Single Turbine

The hydrodynamic effect of single turbine deployment includes of reduced wake velocities, accelerated bypass velocities, increase of turbulence magnitude and mixing of the wake of bypass current flow, and a reduction in water level across the tidal turbine.

a. Wake Velocities

Deployment of single turbine causes significant reduction of wake velocities at the downstream of the tidal turbine due to energy removal. Wake's characteristics are complicated. Nonetheless, it can be typically characterized by wake width, wake length and depth profile. Wake length is controlled by the wake recovery rate. It can be determined by measuring and plotting velocity deficit (U_d) at the centreline of turbine downstream in longitudinal direction. This is the most commonly studied hydrodynamic impact to date. Velocity deficits (U_d) is defined as:

$$U_d = 1 - \frac{U_w}{U_o} \tag{2. 8}$$

Where U_o is the average free stream current velocity and U_w is the wake velocity after flow pass through the single turbine structure. Previous studies conducted using laboratory approach by Bahaj et al. (2007), Myers & Bahaj (2009), Myers & Bahaj (2010) and Stallard et al. (2013) indicated that the deficit of velocity is the highest nearest to the device and reduces according to distance downstream. The current velocity recovered to free-stream magnitude after some distance. In the near-wake area downstream (immediate downstream of a tidal turbine), the wake velocities showed reduction of approximately 60- 90%, while in the far-wake area (~10x rotor diameter), the current velocities recover to 10 – 20%. The current velocities recover to 5 – 10% when reaching 20x rotor diameter further downstream. The wake width at immediate downstream of a tidal turbine reman similar width as the tidal turbine. However, the mixing of the turbulence with larger current velocity at the outer boundary of the tidal turbine width and lower current velocity flow within the width of the tidal turbine causes lateral and vertical expansion distance downstream. The scaled model studies of Stallard et al. (2013) showed wake width of 1.5x rotor diameter at 1.5x rotor diameter downstream, 2.0x rotor diameter at 4x rotor diameter downstream and 3 x rotor diameter at 8x rotor diameter

downstream. Followed by that, Nash et al. (2014) conducting a single turbine effect on wake profile showed similar finding of Stallard et al. (2013). Previous studies also observed that no further expansion on wake width beyond 5x rotor diameter in distance. The tidal energy is fully dissipated at distance of 40x rotor diameter.

b. Bypass Current Velocities

The current flow is diverted near to the device, whether at both sides or in vertical manner (below and above) due to slowing flow of water passing through the device. Acceleration in current flow velocity below and above a scaled rotor is recorded in a range of 6 – 8% (Stallard et al., 2013).

c. Turbulence

The wake of tidal turbine normally refers to the turbulence intensity, an increase in turbulence level. It can be expressed as:

$$TI = \frac{\sigma}{U_o} \tag{2. 9}$$

Where U_o is the average free stream current velocity and σ is the root mean square of the turbulent current velocity fluctuation. Previous studies conducted using experimental approach showed that turbulence intensity for near and far-wake are significantly different. According to Stallard et al. (2013), the TI remains similar throughout the wake (10-12x rotor diameter downstream) and back to free-stream levels by 12x rotor diameter in the near-wake of 22 – 33%.

d. Water Levels

Based on single tidal turbine studies by Bahaj et al. (2007) and Divett et al. (2013), slight increase of water level is observed upstream and slight decrease of water level is observed downstream of the tidal turbine. However, the changes are relatively small in comparison to the total water depth, hence the water level changes can be deemed negligible. Similar

to El-Shahat et al. (2021), negligible change was observed for the water level but significant change in wave height and wave length was found. For considering a long-term sustainable design, Jiang et al. (2021) has included Sea Level Rise (SLR) on tidal level into the study showed that the sum of mean tidal current energy has increased by 6.5% for 100-year modelling scenario.

2.10.1.2 Array

The pilot studies, physical modelling and numerical modelling elaborated above found that the hydrodynamic effect of single tidal turbine is localised and insignificant to environmental effects in far-field region. Nevertheless, the cumulative effects due to large numbers of tidal turbine placed relatively close may potentially cause larger hydrodynamic effects than single tidal turbine device and subsequently may cause greater environmental responses. This is due to larger level of tidal current energy extraction and wakes from combined effects of merging of individual tidal turbines. In this section, the findings from laboratory studies and numerical modelling are discussed.

a. Merging Wake

An interaction study between wakes of a row of tidal turbine with an isolated tidal turbine discovered that spacing sufficiently large between each rotor will result in similar wake of an isolated rotor of single tidal current turbine. Reduction of tidal current turbine lifetime are found due to the wake's turbulence (Tao et al., 2021). The isolated wake at the immediate downstream of a row of tidal turbine in closer spacing will form as single expanded wake eventually further downstream. Stallard et al. (2013) discovered that wake merging occurs for tidal current turbine space at 2x Rotor Diameter or less at approximately 2 rotor diameter downstream (Stallard et al., 2013). According to Myers & Bahaj (2012), inclusion of third disc for two-row array is causing merging of three (3)

wakes and subsequently created much larger far-field wake than single tidal current turbine case. Longer wake recovery is required due to the increased merged wake width. The spacing in lateral direction can be optimised to attain acceleration tidal current bypass flow, e.g., lateral spacing of 2.5x rotor diameter achieved a 22% increment in existing kinetic energy. Three dimensional model by Sanchez et al. (2014) shows insignificant difference on the general circulation and far-field impact between the floating and bottom-fixed turbine.

b. Velocities

Previous studies on tidal current turbine array generally found substantial reduction of current velocities within the array and wakes is formed at the downstream and upstream of the array. A numerical modelling conducted by Ahmadian et al. (2012) found that 2000 units of 10m rotor diameter tidal current turbine array reduced the peak spring flood velocities from 2 m/s to 1.5 m/s. The resulting far-field wakes are observed several kilometres away from the extraction point. Higher velocity reduction is observed for lined arrangement compared to staggered arrangement (Nash et al., 2014). Higher density and capacity of array are found to have higher impact on current velocities (Fallon et al., 2014; Plew & Stevens, 2013). Suspended sediment and faecal bacteria levels are observed at the lee of the arrays from a study carried out by Ahmadian & Falconer (2012). Similar results through numerical modelling carried out through the depth integrated 2D hydro-environmental model, namely DIVAST by Ahmadian et al. (2012) for an arbitrary array of tidal extraction energy devices in the Severn Estuary and Bristol Channel. For an array of tidal current turbine placed a larger area of the channel, it was found that performance of energy generation of the tidal current turbine increases due to a reduced amount of the tidal current bypassing the system of the turbines and diverts through the opening between two turbines (Kim et al., 2012).

c. Tidal Levels

Similar to single tidal turbine deployment, array deployment may result in water level increment upstream and decrement downstream. However, the effect on water level changes is deemed negligible, unless small spacing between tidal turbine is placed. The large scale deployment of tidal extraction energy at the estuary showed negligible impact on the water level changes (Defne et al., 2011; Ramos, Iglesias, et al., 2013). A study carried out by Fallon et al. (2014) using turbine spacing of 0.5, 2 and 5 rotor diameters show that the observed impact of tidal level changes decreases as the density and capacity increased and hence the impacts of large-scale deployment is viable in the condition of applying a low density spacing of 5 rotor diameters.

2.10.2 Impact of Tidal Current Turbine on Sediment Transport

Relatively little academic interest has focused on the impacts to sediment transport (ST) compared to other areas such as hydrodynamics or biological receptors (Ahmadian et al., 2012; Ramos, Iglesias, et al., 2013; Schlezinger et al., 2013; Waggitt & Scott, 2014). It is believed that this is due to the relative scarcity of sediment in many first-generation deployment sites.

Previously Neill et al. (2009) used a 1D model to demonstrate that, for a relatively long channel with variations in tidal asymmetry, morphological impacts increase if energy extraction occurs in regions of asymmetry. Neill et al. (2012) investigated the impact of large (300MW) arrays on headland sandbanks for both idealised and realistic scenarios. They found that energy extraction of this magnitude could have significant impacts on the morphology of local sandbanks. (Robins et al., 2014) found that for smaller array deployments of 10-50MW the impact of energy extraction was less than the natural variability, but that as array sizes increased over 50MW significant impacts on sediment

transport were observable. They highlight the fact that results for the impact of tidal current energy on sediment transport are case specific. This is due to the range of hydrodynamic, bathymetric and sedimentary properties of sites where energy extraction is being planned. In high energy environments suitable for tidal current sites sediment is often spatially varying with regions of swept rock, sand and gravel (MeyGen, 2012). (Robins et al., 2014) also note that use of 3D modelling would give more accurate results. Use of a 3D model allows for energy to be extracted at a specific level in the water column, which allows for more realistic representation of the hydrodynamic impacts, which will force changes to sediment transport. (Robins et al., 2014) highlighted the option for focusing on the changes to bed shear stress rather than actual sediment transport, which could be appropriate for regions where detailed description of sediment is unavailable.

The numbers of turbine for tidal extraction energy gives different sediment transport impacts in the shallow channel. The effects due to the tidal extraction array may be up to few kilometres away from the site, which may also implicate the benthic fauna (Martin-Short et al., 2015). Studies carried out by Nash et al. (2014) and Yang et al. (2013) demonstrated that tidal energy extraction has some effects on the flushing time. The study results of Logan et al. (2016) showed that the large scale tidal extraction energy could reduce the suspended sediment concentration and thus it may affect the physical and biological processes at the intertidal areas in the region of the macrotidal basin.

2.10.3 Other Potential Impacts of Tidal Energy Extraction

The previous sections described the potential energy extraction effects due to the tidal current turbine deployment in altering water level, current velocities and sediment transport. The changes of the described parameters may in turn cause changes on water flow mixing and bed disturbance, which subsequently causing significant environmental

impacts on the water quality, benthic, flora and fauna. Water quality impact assessment studies were conducted by Ahmadian & Falconer (2012) on the bacteria level changes, Sheng, Thompson, Greenberg, & Hill (2012) on salinity and temperature level changes, and Nash et al. (2014) and Yang et al. (2013) on flushing time changes.

Tidal flushing study is an analysis to assess the capability of water exchange within a specific water body. A study by Yang et al. (2013) showed increase of flushing time of water immediate to the array, and it increases as the numbers of tidal turbines increases. However, another study by Nash et al. (2014) showed different finding where array with much larger spacing between tidal turbine, i.e., 5x rotor diameter has significantly reduced the increment on flushing time, even for fairly large numbers of tidal turbines tested (1000 units).

The benthic living in tidal environment is normally attached to the sediments on the seabed and therefore a direct interaction between the benthic and sediment transport can be expected. However, water quality parameters (e.g., salinity, bacterial and nutrient concentrations) are inter-related, changes to one might subsequently affecting another. Hence, most of the water quality modelling conducted to date by using single parameter is not sufficient to provide a comprehensive picture. It is recommended that a complete hydro-biogeochemical modelling to be conducted.

2.10.4 Potential impact to Straits of Malacca

The mangrove forests in Malaysia occurring mainly along the west coast of Peninsular Malaysia, at the estuaries of Sarawak (1st Division), Rejang (6th Division) and Trusan-Lawas (5th Division) rivers of Sarawak and along the east coast of Sabah (Abd. Shukor, 2004) are susceptible to erosion due to the hydrodynamic changes in the sea. Deployment of turbine arrays is likely to cause areas of tidal current reduction due to energy extraction; while at the same time may accelerate the tidal flows in other areas due to the obstruction

effects. For deploying the tidal stream at west coast of Malaysia where mangrove forest occurs commonly along the coast, particular concerns are the extent to which the altered tidal environment as a result of energy extraction will change the natural combined mud sandy bay area, which consists of non-cohesive and cohesive sediment transport regime and consequently the sea bottom morpho dynamics, which may have some implications on mangrove forest, beach stability and coastal ecology.

2.11 Summary

The literature review of published studies has determined the conventional methodologies to tidal energy resource assessment and highlighted the importance to include the tidal energy extraction effects on the tidal regime, and therefore the power availability of extraction.

Reviewing the previous approaches of potential site selection and quantification showed that precision of estimation relies on the current velocity data and calculation of power availability. One of the most common methods adopted is numerical modelling for tidal energy resource assessment; nevertheless, the accuracy of the prediction depends on the accuracy of the numerical model. Considering this, field measurements capturing the bathymetry, water level, current velocity, Total Suspended Solid (TSS) and bed grab sampling at the actual site were conducted at the study site. The numerical model should be accurately modelled to assess a feasible extractable energy at a potential site. A high definition well calibrated and validated numerical model is set up for energy extraction potential and environmental impact assessment. The developed approach is calibrated and validated using the two sets of Acoustic Doppler Current Profiler (ADCP) measurement data. Tidal current energy resource assessment was conducted from larger scale that covering the whole Negeri Sembilan Coastline. The selected headland was further studied

in detail on the suitable zone for energy exploitation. Based on the modelling results, a suitable tidal current turbine deployment sites are determined and assessed in detailed. This research is deliberated in detail in Chapter 4. Momentum sink is the most commonly applied method for tidal turbine inclusion in far-field modelling. It is included as additional force into the momentum equation. For this study, the tidal energy extraction model is developed using the momentum sink approach, the development details of the model are elaborated in Chapter 3.

The energy removal effects due to tidal current turbines deployments may possibly be causing environmental effects and the impacts increase with increase size of energy removal. It is important to account for the impacts of tidal energy extraction in optimizing the array deployment layout. The magnitude of environmental impact is highly depended on the quantity of energy seized by the tidal turbine array. Based on literature made, it is suggested that effect of energy removal by single tidal current turbine is localised and is deemed negligible to the environment, and in terms of sediment transport, it showed fairly small far-field effects. Whilst, tidal energy removal in array deployment may be causing significant changes in tidal level, current velocity, sediment transport, flushing, water quality and it may affect areas in several kilometers away from the deployment area. This study is looking into current velocity for energy dissipation and electrical power generation assessment. It is noticed that most of the changes shown in the literature are focused on current velocity changes. This is the commonly studied parameter as the determination of velocity changes is quick and rather simple. Determination of water quality changes is more complicated and requires a substantial number of parameters to be included in the analysis and therefore longer simulation is required. The benthic zone at the nearshore and estuary of Straits of Malacca is an important habitat for the marine benthos life that live on or in the sea bottom. Hence, use of bed shear stress and sediment transport changes as an impact factor was also explored based on availability of the data.

3 METHODOLOGY

3.1 Introduction

Numerical modelling shall be the main approach for this study. As such, field measurement works are required to assist in the development of the coastal model. This chapter is divided into two main sections. The first section very briefly discusses the methodology for the field measurements, which described very briefly as most of the works were done by the Third Party (Surveyor). While, the second section discusses in detailed the methodology of numerical modelling carried out this study. The overall workflow process to achieve objectives of the study is as illustrated in **Figure 3.1**.

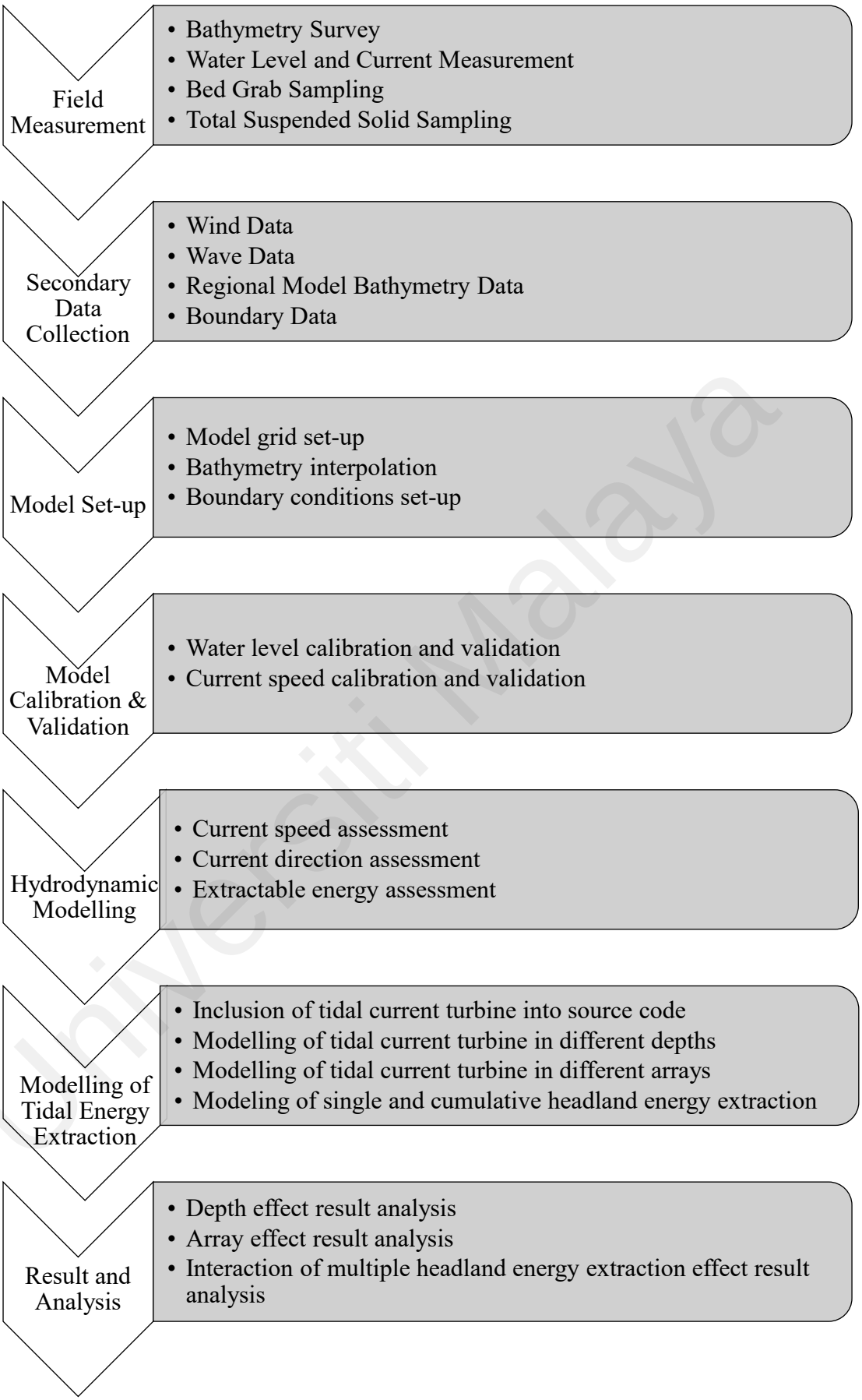

Figure 3.1: Work flow diagram of overall workflow process

3.2 Field Data Measurement

3.2.1 Data Requirement

Data requirement varies with the type of modelling to be carried out. Hence it is necessary to initially determine the simulation that will be conducted and with that, subsequently all the data required during the modelling are determined.

3.2.1.1 Data for Hydrodynamic Modelling

The basic data required for the hydrodynamic, HD, module are tides, wind, wave and bathymetry. For current work, the wave effect was not considered as the focus of the study is mainly to assess the tidal energy extraction resource and effect from tidal current flow.

a) Tidal Data

The tidal data to be used as input to the model maybe in the form of tidal constituents. These data are obtained either from the tables published by the Royal Malaysian Navy or any reliable source (e.g., IHO, TOPEX/Poseidon global inverse solution) or through actual measurement at predetermined locations and analysed to identify the tidal constituents. For this study, the tidal data for boundary condition was obtained from TOPEX/Poseidon global inverse solution TPXO 7.2 developed by Oregon State University. The detail on the tidal data input at the boundary is as described in Section 3.3.13.

b) Wind data

Wind data normally can be obtained from Malaysia Meteorological Department ((MMD) or from other reliable source such as BMT, GROW that was derived from global data. For this study, the wind and wave data are obtained from BMT Eastern Australia Pty Ltd (BMT). The details of wind and wave data are described in Section 4.2.2.6.

c) Bathymetry Data

The bathymetry data for the hydrodynamic modelling work is normally obtained from the Admiralty Chart of Sea Map for the deep-sea areas. In order to model the actual hydrodynamic condition at the study area, bathymetry survey is highly required to be carried out at the nearshore area (fine grid model area). It is important to ensure that the interval of the bathymetry survey for the fine grid area must not be more than twice the fine grid size in order to achieve a well-defined modelled seabed domain at the study area. The survey data must be processed into Geographical Lat/Long coordinates and reduced to Admiralty Chart Datum (CD) to the modeller to proceed with modelling. For this study, the bathymetry at the nearshore seabed condition of the study area was measured by the Third Party (Surveyor). The seabed condition that covering the regional model was obtained from Admiralty Chart published by Royal Malaysian Navy. The details of the seabed data is further elaborated in Section 4.2.2.3.

3.2.1.2 Data for Model Calibration and Validation

Tidal level and current velocity need to be measured for calibration and validation of the hydrodynamic module. Measurement must be carried out for at least two separate locations, which consists of one calibration and one validation stations.

a) Tidal level measurements

The water level measurement for at least two weeks (fourteen days) is required to include the spring and neap tides. For this study, the water level measurement was made by Third Party (Surveyor). The detail of tidal level data is elaborated in Section 4.2.2.1.

b) Current Velocity Measurements

The current velocity needs to be measured for at least three days neap and three days spring tides. As for two-dimensional model calibration, it is important to make sure that

the measurement to be made at appropriate depth of the water column to obtain the representative depth-averaged current velocity data. However, a constant tide may not be suitable for tide conditions whereas the setting for high tide may not be suitable for low tide, and vice versa. Therefore, necessary correction must be made to these values when processing the data to obtain a representative depth-averaged current velocity for calibration and validation. For this study, the current velocity measurement was made by Third Party (Surveyor). The detail of current velocity data is elaborated in Section 4.2.2.2.

3.2.1.3 Data for Sediment Transport Modelling

The key input to sediment transport will be the bathymetry, tidal current flow pattern from the validated hydrodynamic model, wind and seabed sediment characteristics. The locations of measurements for the sampling need to be selected with care so that the data can be applied for the desired task. During the actual site measurements, it is quite normal that the sampling location maybe shifted due to various reasons, like site problem, misinterpretation of the instruction, human error, etc. The results and descriptions of marine data collected for this study are given in Section 4.2.2.

3.2.2 Field campaign procedures

3.2.2.1 Establishment of Survey Control Station

Site reconnaissance is a main component to establish the survey control station at the survey area. The boundary stones found at the study area, i.e., Lot 263 (PA 11020) was established at the survey area (**Figure 3.2)**. Traversing method is a normal approach used for site reconnaissance that ties with the existing boundary stones nearest to the survey area. However, these boundary stones must be verified to ensure its accuracy to be adopted as a datum for the horizontal control survey. The datum for planimetric control

survey can be tied with the old boundary stones of Lot 263 (PA 11020) in Horizontal Coordinate System. For the coordinate system, it was fixed with a boundary stone published by the Government Survey Department (JUPEM), i.e., PA 11020. The established boundary mark (**Figure 3.3**) was then adopted to establish the control station in this survey work.

The vertical control datum was established based on JUPEM's Benchmark and Royal Malaysian Navy, which was verified to BM N027 and BM N0154 within the survey area. Close loop levelling and GPS static observation were used to transfer the reduced level to all control stations. National Geodetic Vertical Datum (NGVD), which was established by JUPEM for Peninsular Malaysia was adopted for this survey (**Table 3.1**).

Figure 3.2: Location of Lot 263 (PA 11020)

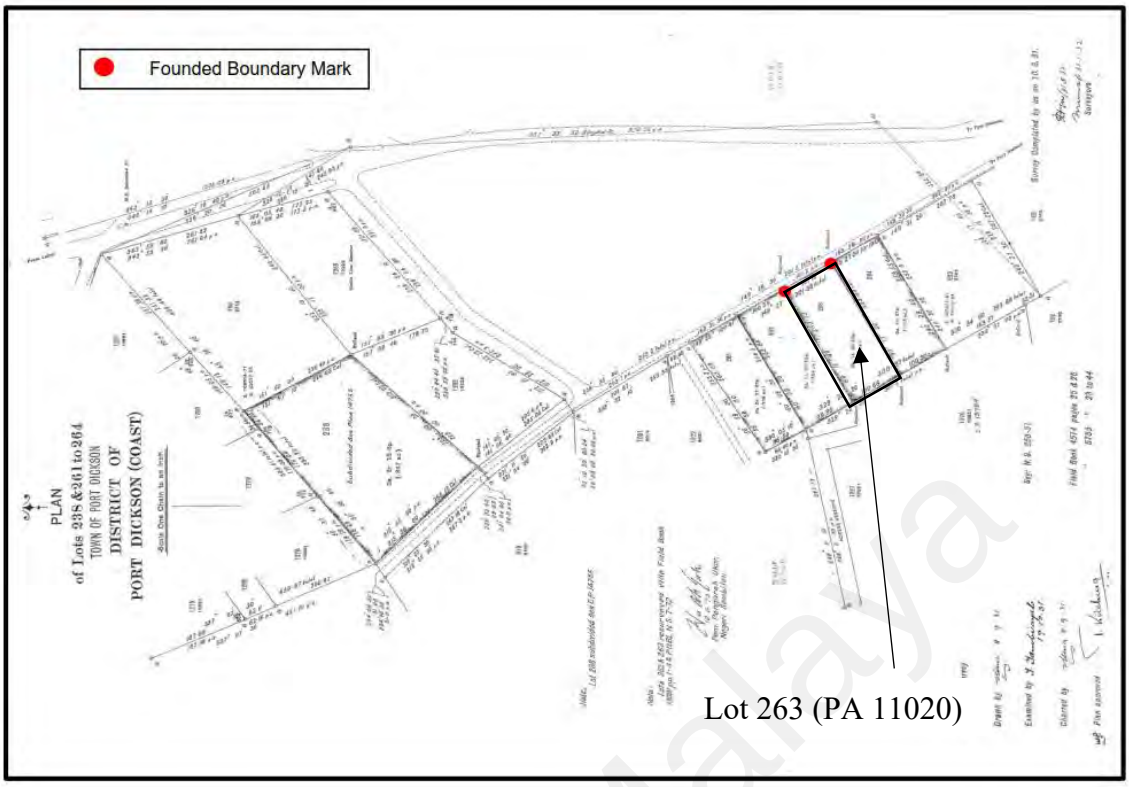

Figure 3.3: Founded Boundary Mark at Lot 263 (PA 11020)

Table 3.1: Description of datum for vertical control

BM no.	Reduced Level in NGVD (m)	Reduced Level in Chart Datum (m)	Location description
BM N0038	3.363	-	In front of Port Dickson Town roundabout.
BM N1547	2.045	-	Located at Linggi-Port Dickson Road, in front of a business premise, 30 meters before Carltex Petrol Station
BM N0237	5.928	-	Jetty KTM, Port Dickson
TLDM 1000N	-	5.36	Jetty KTM, Port Dickson

3.2.2.2 Tidal Observation

Automatic water level recorder (RBR Virtuoso & Aanderaa) tide gauges were deployed in the study area to record the tidal level. The tidal observation data was captured between 1st July 2015 to 4th August 2015 at Jetty KTM, Port Dickson. TP1 (RL= 3.844m in NGVD) was used as a reference station and levelled from the BM N0237 (**Table 3.2**). **Figure 3.4** shows the location of the tide gauge (RBR Virtuoso and Aandera)

and manual tide reading. The manual tide reading, TP1A (RL = 3.836m in NGVD) was placed at the corner of Jetty KTM, Port Dickson. Manual tidal observation was recorded using a measuring tape for every 10-minute interval.

Table 3.2: Coordinate of the tide gauge (RBR Virtuoso and Aanderaa) and Manual Tide Reading

Tide Gauge/Tide Reading	WGS 84 Coordinate System		Reduced Level in NGVD (m)	Date of Deployment		Remarks
	Latitude (N)	Longitude (E)		Start	End	
Tide Gauge (RBR Virtuoso)	2°31'12.18"N	101°47'46.77"E	3.844	1 July 2015	4 August 2015	At Jetty KTM, nearby with BM N0237 at the corner of Jetty KTM
Tide Gauge (Aanderaa)						
Manual Tide Reading	2°31'12.04"N	101°47'45.98"E	3.836	1 July 2015 22 July 2015	15 July 2015 27 July 2015	At the corner of Jetty KTM, beside of BM N0237

Figure 3.4: Locations of Tidal Gauge and Tide Reading

3.2.2.3 Positioning and Navigation

StarFire Real-Time Differential Global Positioning System (D-GPS) was adopted as the navigation system for positioning the survey boat during the bathymetry survey. The mobile systems consisting of 66 channels, and dual frequency Navcom SF3050 GPS receiver was used to track the satellite vehicles. **Figure 3.5** illustrates the working system of Star Fire Real-Time Differential Global Positioning System.

StarFire D-GPS was integrated into a laptop computer, which operates a HYPACK ® 2009a Hydrographic Survey Software for the navigation and acquisition of positioning data. The Hypack General Navigation, Positioning and Processing Package read the the D-GPS position in WGS-8 and transformed it into local position, i.e., Negeri Sembilan State Cassini Coordinate System. The data captured from the survey can be displayed in real time through the antenna or offset position of the survey vessel. The survey information, e.g., coordinates (Easting & Northing), distance offline, distance travelled and distance to end of line, survey speed, and real time digital depths are displayed in the HYPACK ® 2009a Hydrographic Survey Software. The survey data were stored in the computer disk drive for data logging. The data logger, a built-in device of the computer, was used to record and store the survey data over time or in relation to location travelled.

The D-GPS Star Fire navigation system (bathymetric survey) were verified at some known points: STN A3, STN A8A, which are the survey stations for positioning system integrity check **(Figure 3.6)**. The positioning system integrity check needs to be carried out to identify if there is any gross error within the system or blunder during the system set-up. **Table 3.3** gives the survey stations coordinate used in the integrity check. Integrity checks for the bathymetric survey were carried out on 1st July 2015, 2nd July 2015 and 27th July 2015 and 31st January 2019.

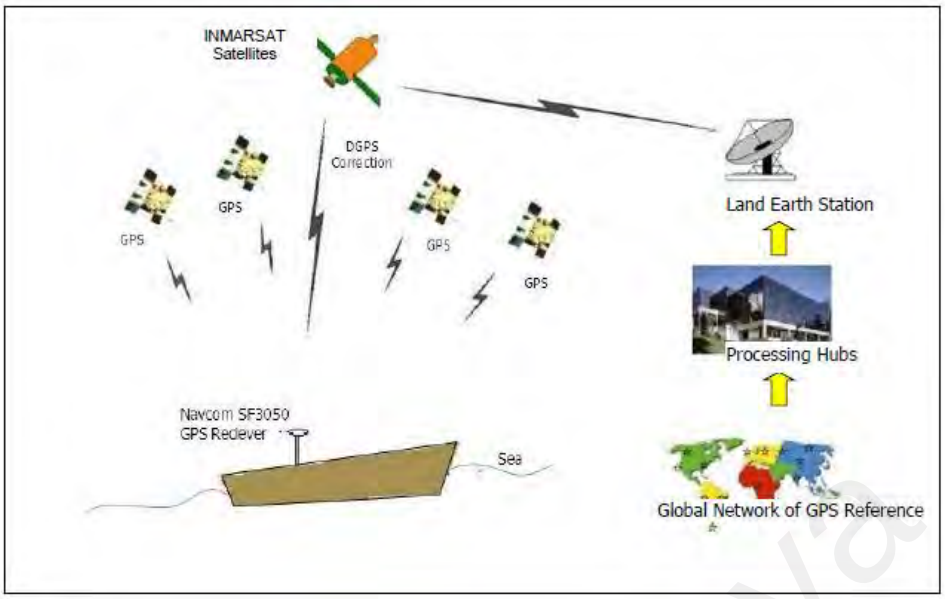

Figure 3.5: Star Fire Real-Time Differential Global Positioning System (D-GPS) Concept

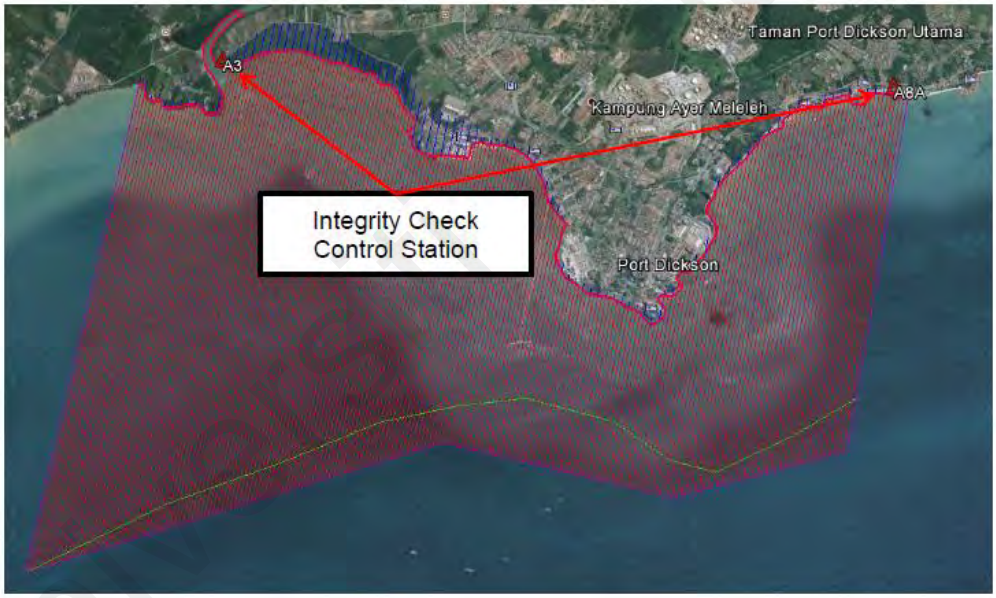

Figure 3.6: Locations of the Control Station for integrity check

Table 3.3: Coordinate of the control stations used in the integrity check

Control Stations	Negeri Sembilan State Cassini Coordinate System		Remarks
	Easting (m)	Northing (m)	
A3	-16920.670	-15509.984	Nail on Tarred Road
A8A	- 12711.695	- 23204.696	Pipe in Concrete

3.2.2.4 Bathymetric Survey

Continuous echo soundings with a single high frequency echo sounder (210 kHz) precision echo sounder were used as the measurement tool to capture the bathymetry along the designated profiles. The measured depths were logged into the online navigation system at intervals of not more than 10 metres interval along the surveyed lines profiles. The bathymetry surveys must be extended as far inshore as possible to ensure capturing maximum bathymetry data, the coverage of the survey is shown in **Figure 3.7**. The echo sounders were calibrated with sounding, known as "Bar Check" method. Soundings were reduced to the adopted Chart Datum (CD) and also to National Geodetic Vertical Datum (NGVD) from observed water level.

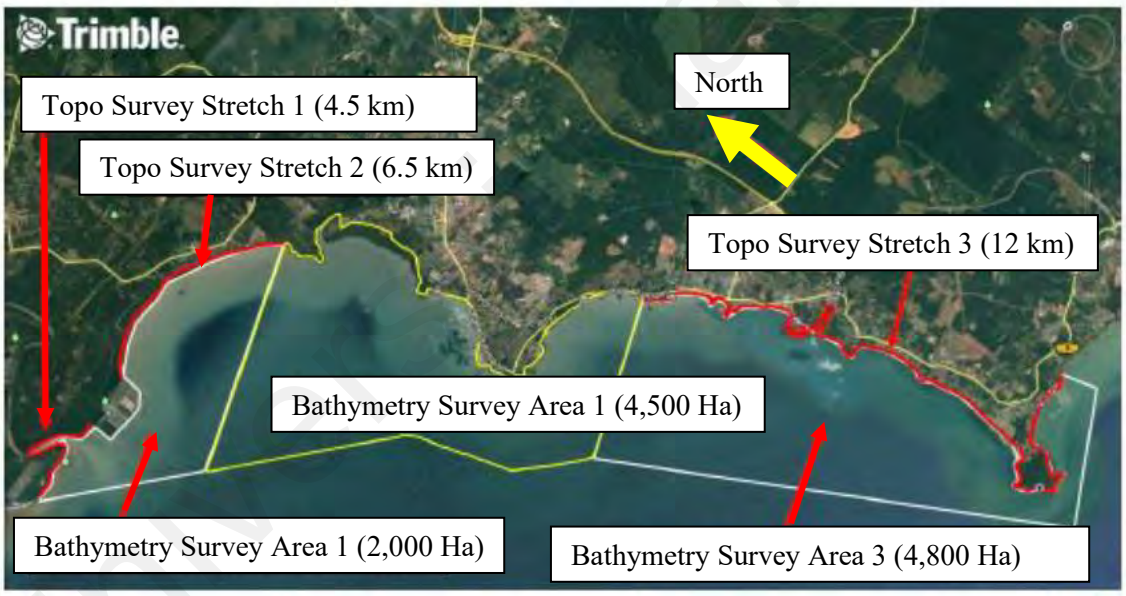

Figure 3.7: Bathymetric survey coverage

The bathymetric survey was carried out using several equipment listed as below:

no	Equipment	Description
1	Echo Sounder	ODOM ECHOTRAC MK III version 3.28 Dual Frequency echo sounder (operated on dual high frequency mode (~30kHz &210 kHz) c/w dual frequency transducer

2	Navigation and Positioning	• Real Time StarFire D-GPS System • World Wide-Differential GPS • Mobile Station (Survey Boat) Navcom Star Fire SF3050 GPS Receiver. • Hypack Navigation and Positioning with Processing Package. • Notebook/Laptop Computer.
3	Data Processing	• DELL i3 PC System • HYPACK Processing Survey Package. • Terramodel Release 10.43 Post Processing Package • utodesk's AutoCad 2000 Package • Canon iPF 700 Plotter
4	Water Level Measurement - Tidal Observation	• RBR Virtuoso • Aanderaa • Measurement tape

The geodetic information of the bathymetric survey is as listed as below:

a. Geodetic Data

- Spheroid: Malayan Revised Everest
- Semi-major axis (a): 6 377 304.063 m
- Semi-minor axis (b): 6 356 103.039
- Eccentricity Squared (e2): 0.006 637 846 6302
- Reciprocal of flattening (1/f): 300.8017

b. Origin of Meridian reference

- Projection: N. Sembilan / Melaka
- Origin of Meridian of Reference: Gun Hill
- Longitude of Origin (CM): E 101° 56’ 28.”22
- Latitude of Origin: N 02° 42’ 44.”27
- False Easting: - 242.005 m
- False Northing: - 948.547 m

c. Satellite Datum

- Spheroid: WGS-84
- Semi-major axis (a): 6 378 137.000 m
- Semi-minor axis (b): 6 356 752.314 m

- Eccentricity Squared (e2): 0.006 694 380 023
- Reciprocal of flattening (1/f): 298.257 223 563
- Datum transformation parameters from WGS-84 to Malaysia Revised Everest, Kertau Datum are as follows:
    - dx = + 11.0m
    - dy = - 851.0m
    - dz = - 5.0m

3.2.2.5 Acoustic Doppler Current Profiler (ADCP)

The Nortek 600 kHz Acoustic Doppler Current Profiler (ADCP), a hydroacoustic current meter comparable to a sonar was used to measure tidal level, current velocities over a depth range using the Doppler effect of sound waves scattered back from particles within the water column.

Piezoelectric transducers, component of ADCP is able to receive and transmit the sound signals. The distance is estimated using the traveling time of the sound waves and the water velocity along the acoustic path in accordance to the frequency shift of the echo. Other components of an ADCP are: receiver, electronic amplifier, a clock for travelling time measurement, temperature sensor, a pitch/roll sensor for orientation determination and a compass for heading/direction determination. The doppler shift is determined through the use of analog-to-digital converter and a digital signal processor. Water velocities are determined using a temperature sensor by estimating the sound velocity at the device position to estimate the frequency shift. The equation of seawater state was used for the calculation by assuming that the salinity has a preconfigured constant value.

The ADCP was deployed on the seabed with its beam looking upwards. It was mounted within 'Barnacle' fiber glass trawl-resist bottom-mounted frame as a platform with its sensor head protruding slightly out from the frame. Accessories, such as tracking

underwater beacon, satellite alerting and tracking beacon, and lead ballast weights compliment the seabed platform. The ADCP was powered by a single 50 Wh alkaline battery pack. Configuration summary of the ADCP is given in **Table 3.4.**

Table 3.4 : Summary of ADCP configuration

Parameter	Station ADCP1
Location	Lukut, Port Dickson
Coordinates	Lat 2.545622º Long 101.769789º
Depth During Deployment	13.1 m
Seabed Terrain	Flat
Mounting	Sand Dollar
Accessories	Transponder ID: 14
Instrumentation (ADCP)	AquaDopp Profiler 600KHz
ADCP Mounting Height	70 cm
ADCP settings: **Current profile interval** **Number of cells & Size** **Cell size** **Averaging** **Blanking distance**	10 minutes 30 x 1 m 1 meter 60 seconds 0.5 meter
Tide gauge settings: **Sampling interval Averaging**	10 minutes 60 seconds
Platform deployment	01 February 2019 @ 15:00 PM
Platform recovery	06-February 2019 @ 10:00 AM

The platform was deployed at its respective station with the assistance of SCUBA divers once the suitable depth and substrate were determined. The platform was lowered to seabed with plaited rigging rope and the deployment station's coordinates were fixed using handheld GPS. The DGPS coordinates were also fixed at the same time via HYPACK navigational software package. It is important to make sure that the platform's orientation is sitting horizontally flat on the seabed during deployment. Diver handheld homing device was deployed from the boat in order to confirm each respective platform ID. The environmental conditions observed during both field trips (seabed platform deployment and recovery) were recorded, as given in **Table 3.5** below.

Table 3.5: Environment conditions during field campaign

Platform ID (Station)	Station 1 Lukut (ADCP1)
Weather	Windy
Sea State	Choppy
Observed Surface Current	Slight
Seabed Type	Hard Mud
Bottom Terrain	Flat Hard Mud

For this study purposes, two units of Nortek 600 kHz Aquadopp Profiler (ADCP) with internal logging unit complete with moorings were deployed from the survey vessel to collect the current profiling data and the survey was carried out for a 15-day period with the data sampled at 10-minute interval. The field team recovered both platforms after 15 days of data recording period. During the recovering, a diver down-line (weighted anchor ~ 10kg) was anchored as close as possible to the deployment target guided by D-GPS and Navigation software package. The surface marker was also used as diver's down line (DDL) during the recovery. The divers have descended through DDL and performed underwater search guided by transponder. They were rigged up with airlift bag (ALB) and partially inflating it during the recovery. The ALB was fully inflated once the divers are cleared from hazard zone (directly under platform) to enable the platform to surface.

With that, divers then ascended through DDL and signaled to inform the boat to approach. The platform was hauled on board manually after divers detach the ballast weights and adding auxiliary rigging lines to the platform. The platform was brought back to the shore to disassemble and clean for data retrieval. The current speed and direction data were logged at 10 minutes interval. The procedure of installation and retrieval is as shown in **Figure 3.8** to **Figure 3.11**.

Figure 3.8: The installation and setting up of ADCP at site

Figure 3.9: Scuba diving check on the device position and marking of buoy

Figure 3.10: Retrieval of ADCP with the aid of Airlift Bag (ALB)

Figure 3.11: Recovered platform and ADCP device

3.2.2.6 Soil Sampling

Soil samples were collected using a Van der Veen type grab sampler at nine (9) soil samples designated locations. Nine (9) samples were sent to laboratory for test and analysis of particle size distribution, D50, bulk density and dry density. Proper soil test at the predetermined locations needs to be carried out to derive the seabed sediment characteristics. Each sample collected shall be of a minimum mass of one kilogram, stored in a clear plastic bag and placed in another bag before being tied and labelled. All samples collected were sent to an accredited laboratory for particle size distribution (wet sieving method including hydrometer test where required) in accordance with BS1377: Part 2:1990 or ASTM 0422-63(2007) Standard Test method for Particle Size Analysis of Soils. The grab sampling locations are shown in **Figure 3.12** and **Table 3.6**. For the bed grab sediment sampling, the test included:

- Particle Size Distribution
- Specific Density
- Bulk Density
- Dry Density
- Percentage of Material
- Sediment D_{50}

3.2.2.7 Water Sampling

Water samples were collected using Jabsco Water Pump came with water hose and 500 ml HDPE bottles at 0.2D, 0.5D and 0.8D at nine (9) sampling locations (same locations as soil sampling) with the total of 27 water samples. Each bottle was capped and labelled accordingly based on the occasion. Water samples were sent to the laboratory for total suspended solid (TSS) analysis. **Table 3.6** and **Figure 3.12** show the coordinates and locations of all samples.

Table 3.6: Coordinates locations of soil and water sampling

Points	Latitude	Longitude	Seabed RL in CD
P1	2.591642°	101.712328°	0.66 m
P2	2.593489°	101.758469°	1.35 m
P3	2.549208°	101.790811°	2.17 m
P4	2.529161°	101.780744°	18.51 m
P5	2.517111°	101.819317°	1.46 m
P6	2.504381°	101.829439°	0.93 m
P7	2.489189°	101.838906°	2.51 m
P8	2.481000°	101.843439°	3.27 m
P9	2.450592°	101.849667°	9.53 m

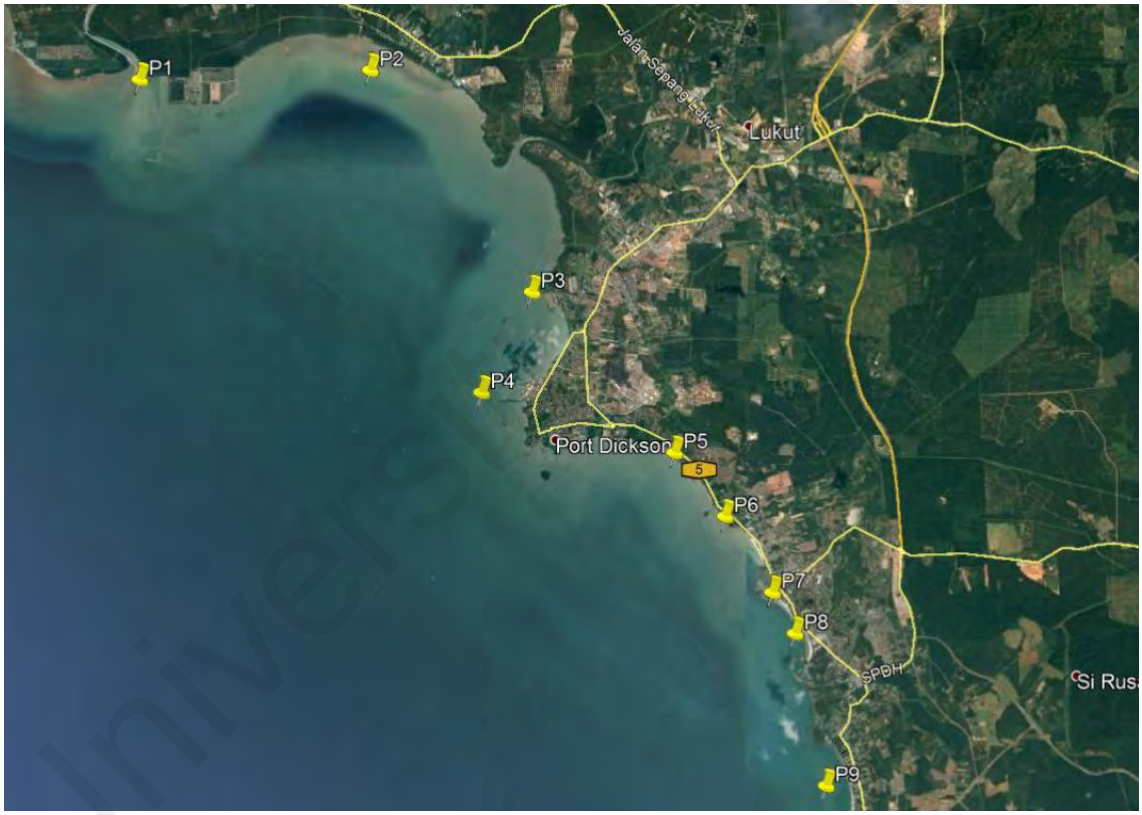

Figure 3.12: Location of soil and water sampling

3.2.3 Field Data Check Analysis

Quality input data is pertinent to ensure that the numerical model properly simulates the modelling scenarios for the research work. Hence, critical analysis of the data needs to be made before they are applied into the numerical model. Some of the crucial components that need to be checked are as follows:

a. Measurement Location

The locations of measurement for tidal level, current velocity, and TSS need to be checked with care to ensure that the obtained data can be adopted for the modelling. Therefore, the record of the surveyor needs to be checked and verified to identify the exact locations of the data collected. The measurement location check for tidal level, current velocity, TSS are elaborated in 4.2.2.1, 4.2.2.2, 4.2.2.3, and 4.2.2.5.

b. Bathymetry Data

It is necessary to measure the bathymetry of the tidal level, current velocity and sampling location as to check the consistency of the bathymetric data from other available reliable source, such as Royal Malaysian Navy Bathymetric Chart. If there are significant difference, it is essential to analyse the data to identify the cause of faults, if any, and make reasonable decisions on the most proper values to be adopted. Seabed data check is elaborated in Section 4.2.2.3.

c. Tidal Level Data

As two locations of tidal level measurement were made for this work. The results from these two stations were compared with one another to verify if there were large difference between levels as well as their phase. If significant difference is observed and not tally with their relative location, it is necessary to analyse the tidal data to examine if there are any fault or errors, e.g., equipment setting errors, local interference (near to jetty or navigation channel) to make sure necessary corrections can be made if possible. Otherwise, the unreliable datasets or noise can be removed. Tidal level data check is elaborated in Section 4.2.2.1.

d. Current Velocity Data

Similar to tidal level data, the current velocity data was measured at two stations within the model domain. It is advisable to conduct the current velocity measurement using fixed-position recording instrument in order to reduce interference caused by boat

movement, handling, etc. The measured current data shall be checked with the phase of current and tidal levels (at adjacent location). It is expected to have slack condition (low current velocity) to occur during the high and low tides, while high current velocity during mid-flood and mid-ebb tide. If there is no distinct pattern for the correlation of the phase, the data needs to be checked for its validity before it can be adopted for modelling. Tidal level data check is elaborated in Section 4.2.2.2.

3.3 Numerical Modelling

Negeri Sembilan and Tg Tuan Headland model was developed using Deflt3D software in this study. Delft3D model suite was developed by Deltares, a research institute working in the field of estuarine, river and coastal areas. It is a multi-dimensional (two dimensional or three dimensional) model that can be used to simulate tidal flow, sediment transport, morphological changes, waves, water quality and ecology. This model suite consists of several modules, which are capable to interact with each other. Two main modules used for this research are Delft3D-FLOW (Hydrodynamic Module) and Delft3D-SED (Sediment Transport Module).

The FLOW module is developed based on the depth integrated solution of the Navier-Stokes equation. It calculates non-steady flow and transport condition arising from meteorological and tidal forcing on a boundary fitted grid (rectilinear/curvilinear). This module integrates the properties of tidal forcing, earth's rotation (Coriolis force), density driven flows, advection-diffusion solver, space and time varying wind and atmospheric pressure, advanced turbulence models, time varying sources and sinks, and drying and flooding of inter-tidal flats. The applied model is similar to the established numerical models, such as MIKE 21, POM and TELEMAC.

Sediment transport was modelled with Delft3D-SED module, which simulates the process of sediment transport changes due to the tidal turbine deployment. The basis of the model is the advection-dispersion transport. All sediment particles are transported by the flow (advection) and turbulent mixing (diffusion). The sediment transport module is a sub-module of the DELFT3D-FLOW. This module is used to model the transport of cohesive and non-cohesive sediments. For cohesive sediment fractions, the fluxes between the water phases and the bed are calculated with the well-known Partheniades-Krone formulations (Partheniades, 1965).

3.3.1 Model Description

Numerically assessing the tidal turbine installation site and the energy extraction impact around the headland requires a dedicated modelling approach that accounts for large-scale oceanic flows over the Malacca Strait and sufficient model resolution in time and space (x, y, t) at the Tg Tuan Headland area. In order to achieve this, Delft3D, which is an integrated flow and transport modelling system software was adopted as modelling tool for this research.

Delft3D is a multi-dimensional numerical model adopted to simulate the water level and current velocity variations induced by forcing function such as tides and/or meteorological forcing. The numerical model solves the unsteady shallow water equation in two-dimensional (depth-averaged) manner. It also includes the effect of density gradient difference due to non-uniform salinity and temperature distribution. The flow model can be used to predict the flow in shallow seas, coastal areas, lagoons, rivers, estuaries and lakes. This module solves the Navier-Stokes equations for an incompressible fluid, under shallow waters and the Boussinesq assumptions. In the vertical momentum equation, the vertical accelerations are neglected in which it leads to

the hydrostatic pressure equation. The equations include of the continuity equations, transport equations and motion horizontal equations for conservative constituents. It is formulated in spherical and orthogonal curvilinear co-ordinates, where spherical co-ordinates follow the curvature of earth while curvilinear co-ordinates follow the flat horizontal plane of reference for water level and sea bed level.

The tidal flow of the model is forced by tidal constituents at the open boundaries, pressure gradients, density gradient and the free surface's wind stress. Source and sink terms are also included into the equations for simulating the discharge and withdraw of water in the numerical model.

Delft3D comprises several modules that provide the facility to undertake this study. The study generally begins with the Delft3D-FLOW module. From Delft3D-FLOW, details such as velocities, water levels, density, salinity, eddy viscosity and eddy diffusivity can be provided as inputs to the other modules. For this study, Delft3D-FLOW module was used to set up Negeri Sembilan and Tg Tuan Headland model for tidal current energy resource and impact assessment. It is also adopted as hydrodynamic basis to be used for Delft3D-SED module for sediment transport impact assessment. In the vertical direction, σ co-ordinate system (σ-model) introduced by Phillips (1957) (Phillips, 1985) was used for setting up the model**. Table 3.7** summarizes the modules used in this study.

Table 3.7: Delft3D modules used in this study

MODULE	GENERAL DESCRIPTION	FUNCTION
Delft3D- RGFGRID	• For generating orthogonal curvilinear grids, in Cartesian or spherical coordinates	• To construct boundary fitted grid generation
QUICKIN	• For preparing and manipulating grid-oriented data, such as bathymetry, initial conditions for water levels, salinity, constituents and other parameters.	• Data interpolation to computational grid
Delft3D- FLOW	• A multi-dimensional hydrodynamic simulation program that calculates non-steady flow and transport phenomena resulting from tidal and meteorological forcing on a curvilinear and boundary-fitted grid. • The hydrodynamic module is based on the full Navier-Stokes equations with the shallow water approximation applied. The equations are solved with a highly accurate unconditionally stable solution procedure.	• To conduct hydrodynamic modelling (i.e. water level and current). • The results of hydrodynamic modelling will serve as the inputs to the other modules.
Delft3D- SED	• The sediment transport module can be applied to model the transport of cohesive and non-cohesive sediments. • It is a sub-module of the water quality module that all processes contained in the sediment transport module are also present in the water quality module. • For cohesive sediment fractions, the fluxes between the water phase and the bed are calculated with the well-known Partheniades-Krone formulations (Partheniades, 1965).	• To study the sediment transport and dispersion of the plume.

MODULE	GENERAL DESCRIPTION	FUNCTION
	• For the transport of non-cohesive sediment, Van Rijn et al. (2000) approach is followed. The settling velocity of non-cohesive sediment fraction is computed following the method of Van Rijn (1993).	
QUICKPLOT	• Post-processing tool for Delft3D. • Standalone program based on technology of The MathWorks Inc. It can be seamlessly integrated with the MATLAB environment.	• Post-processing

3.3.2 Justification of Model Choice

The Delft3D numerical model, developed by Deltares, a well validated multi-dimensional model and hence suitable to be adopted for development of Negeri Sembilan and Tg Tuan high-resolution model in tidal current energy resource and impact assessment. In addition, Delft3D has been applied in major coastal and ocean investigations and engineering studies worldwide. Carballo et al. (2009), Chatzirodou and Karunarathna (2014) and Ramos, Iglesias, et al. (2013) adopted Delft3D to perform energy extraction assessment using 2DH momentum equations.

Three-dimensional numerical modelling is able to simulate and reproduce the hydrodynamic condition over the whole water column depth as well as able to reproduce the hydrodynamic condition of the turbine rotor depth. However, practical application of this model is limited due to high computational time and costs required. While the two-dimensional numerical modelling, which using depth-averaged approach, requires much lower computational time and costs and shows better advantage for practical application

as the study area for this study is a well-mixed water bodies, which do not have significant vertical variation over the water column depth. However, as the tidal current turbine is given in depth-averaged form in the model, the hydrodynamic changes outcome at the certain depth of the two-dimensional model will be much lesser than those measured at the centreline of the tidal current turbine. These changes are important for near-field impact assessment, nevertheless, current study is focused on far-field impact assessment and, based on the savings of computational consideration, a two-dimensional model is deemed adequate.

3.3.3 Governing Equations of Tg Tuan Hydrodynamic Model

Delft3D-FLOW solves the Navier Stokes equations for an incompressible fluid under shallow waters and the Boussinesq assumptions. Considering that Tg Tuan within the Straits of Malacca is a vertically well mixed flow strait, the use of depth-averaged model of Delft3D-FLOW is sufficient in the numerical simulations.

The shallow-water equations are obtained by reducing the vertical momentum equation to the hydrostatic pressure assumption. Also, the fluid is assumed to be incompressible in the process of simulation. The mass and momentum equations are given by equation (3.1) and equation (3.2), respectively and equation (3.3) is the transport equation used to solve problems related to temperature and salinity:

$$\frac{\partial \zeta}{\partial t} + \frac{\partial[(d+\zeta)U}{\partial \xi} + \frac{\partial[(d+\zeta)V}{\partial \eta} = Q \qquad (3.1)$$

$$\frac{\partial U}{\partial t} + U\frac{\partial U}{\partial \xi} + V\frac{\partial U}{\partial \eta} - f.V = -g\frac{\partial \zeta}{\partial x} - \frac{g}{\rho_o}\int_{-d}^{\zeta}\frac{\partial \rho'}{\partial \xi}\,dz + \frac{\tau_{s\xi} - \tau_{b\xi}}{\rho_o \cdot (d+\zeta)} + \upsilon_h \nabla^2 U \quad (3.2)$$

$$\frac{\partial V}{\partial t} + U\frac{\partial V}{\partial \xi} + V\frac{\partial V}{\partial \eta} - f.U = -g\frac{\partial \zeta}{\partial \xi} - \frac{g}{\rho_o}\int_{-d}^{\zeta}\frac{\partial \rho'}{\partial \eta}\,dz + \frac{\tau_{s\eta} - \tau_{b\eta}}{\rho_o \cdot (d+\zeta)} + \upsilon_h \nabla^2 V$$

$$\frac{\partial\,(\zeta + d)c}{\partial t} + \frac{\partial\,[\,(d+\zeta)Uc\,]}{\partial \xi} + \frac{\partial\,[\,(d+\zeta)Vc\,]}{\partial \eta} = D_h \nabla^2 c - \lambda_d\,(d+\zeta)c + R \quad (3.3)$$

where d= local water depth relative to a reference plane; U= vertically integrated eastward components of the velocity; V = vertically integrated northward components of the velocity; Q = intensity of mass sources per unit area; f= Coriolis parameter; υ_h = kinematic horizontal eddy viscosity; ρ_o= reference density; ρ' = is the anomaly density; $\tau_{s\xi}$ = ξ-components of the wind stress acting on the sea surface; $\tau_{s\eta}$ = η-components of the wind stress acting on the sea surface; $\tau_{b\xi}$ = shear stress in ξ-components at the bottom; $\tau_{b\eta}$ = shear stress in η-components at the bottom; c = temperature or salinity; D_h = horizontal eddy diffusivity; λ_d = first order decay process; and R = the source term per unit area.

3.3.4 Governing Equations of Sediment Transport Modelling

Sediment transport was modelled with Delft3D-SED module, which supports both transport of bed material and suspended sediment material of cohesive and non-cohesive suspended sediments. The basis of the model is the advection-dispersion transport. All sediment particles are transported by the flow (advection) and turbulent mixing (diffusion).

There are two processes governing sediment transport: settling of sediment particles and sediment exchange between the water column and the seabed. Settling of sediment particles is dependent on settling velocity. For the sediment exchange between the water column and the seabed, deposition and erosion are involved. Deposition only occurs when the bed shear stress is below a critical value of $\tau_{cr,d}^{(\ell)}$ whereas erosion only occurs when the bed shear stress is above a critical value of $\tau_{cr,e}^{(\ell)}$.

For cohesive sediment fractions the fluxes between the water phase and the bed are calculated with the well-known Partheniades-Krone formulations (Partheniades, 1965):

$$E^{(\ell)} = M^{(\ell)} S\left(\tau_{c\omega}, \tau_{cr,e}^{(\ell)}\right), \tag{3. 4}$$

$$D^{(\ell)} = \omega_s^{(\ell)} c_b^{(\ell)} S\left(\tau_{c\omega}, \tau_{cr,d}^{(\ell)}\right), \tag{3. 5}$$

$$c_b^{(\ell)} = c^{(\ell)}\left(z = \frac{\Delta z_b}{2}, t\right) \tag{3. 6}$$

where:

$E^{(\ell)}$: erosion flux [kg m^{-2} s^{-1}]

$M^{(\ell)}$: user-defined erosion parameter [kg m^{-2} s^{-1}]

$S\left(\tau_{c\omega}, \tau_{cr,e}^{(\ell)}\right)$: erosion step function:

$$S\left(\tau_{c\omega}, \tau_{cr,e}^{(\ell)}\right) = \begin{cases} \left(\frac{\tau_{c\omega}}{\tau_{cr,e}^{(\ell)}} - 1\right), & \text{when } \tau_{c\omega} > \tau_{cr,e}^{(\ell)} \\ 0, & \text{when } \tau_{c\omega} \leq \tau_{cr,e}^{(\ell)} \end{cases} \tag{3. 7}$$

$D^{(\ell)}$: deposition flux [kg m^{-2} s^{-1}]

$\omega_s^{(\ell)}$: fall velocity (hindered) [ms^{-1}]

$c_b^{(\ell)}$: average sediment concentration in the near bottom computational layer

$S\left(\tau_{c\omega}, \tau_{cr,d}^{(\ell)}\right)$ deposition step function:

$$S\left(\tau_{c\omega}, \tau_{cr,d}^{(\ell)}\right) = \begin{cases} \left(1 - \frac{\tau_{c\omega}}{\tau_{cr,d}^{(\ell)}}\right), when\ \tau_{c\omega} < \tau_{cr,d}^{(\ell)} \\ 0, \qquad when\ \tau_{c\omega} \geq \tau_{cr,d}^{(\ell)} \end{cases} \tag{3. 8}$$

$\tau_{c\omega}$: selected maximum bed shear stress due to current and waves as calculated by the wave-current interaction model

$\tau_{cr,e}^{(\ell)}$: user-defined critical erosion shear stress [N/m^2]

$\tau_{cr,d}^{(\ell)}$: user-defined critical deposition shear stress [N/m^2]

Due to limitation of sediment distribution data for Straits of Malacca hydrodynamic model, the regional model was initialized with assumed constant sediment distribution map to define the mixture of cohesive and non-cohesive sediment bed thickness based on TSS and bed grab sampling data collected at the study area. The sediment source and properties of the TSS and bed grab sampling are given in Section 4.2.2.4 and Section 4.2.2.5. The initial result in sediment suspension is sourced from the silty sand which comprises 5m depth of non-cohesive sediment and thin layer of 0.05 m cohesive sediment, where depths modelled are relative to the Mean Sea Level (MSL). The initial condition for sediment concentration was initialized at 41 mg/l for cohesive sediment and zero concentration for non-cohesive sediment. The cohesive sediment concentration is adopted based on average TSS value obtained from field measurement data. The non-cohesive sediment within the numerical model is defined as consisting of 0.2 mm diameter of d_{50} grain size based on the average composition of the bed grab sampling. Based on an sediment transport assessment in the locality of a detached low-crested breakwater on

Pulau Carey, which is about 80 km from northward of Tg Tuan, the monsoons (Northeast and Southwest) play an important role in affecting the sea-bed elevation at the intertidal zone (Fitri et al., 2019). Hence, monsoon effect was included as part of the assessment in this research work. The details of the wind and wave data adopted in the numerical modelling are given in Section 4.2.2.6.

3.3.5 Tidal Current Energy Resource Evaluation

The site selection assessment along Negeri Sembilan Coastline was first performed by evaluating the tidal current resource potential at multiple headlands at this coastline. The evaluation was carried out by means of power density assessment using the validated two-dimensional Delft3D-FLOW numerical model to solve equation (3. 1) to equation (3. 3). The equation of power density (per m^2) is expressed as

$$P_{ex} = \frac{1}{2}\rho U^3 \tag{3. 9}$$

where ρ = fluid density and U = the depth-averaged velocity of the stream. The energy density for tidal current extraction was calculated using the following equation:

$$P_{ex} = \sum_{h=1}^{8760} [\frac{1}{2}\rho U^3]_T \tag{3. 10}$$

3.3.6 Governing Equation for Tidal Energy Extraction Modelling

The near-field and possibly the far-field flow patterns may be affected by deploying a turbine array in a free-stream flow (Martin-Short et al., 2015). It is expected that the current speed will slow down when water flows through the turbine blades by adding drag

in the horizontal momentum equations (Lesser et al., 2004). The momentum equations for flow in the in ξ- and η- directions are given by:

$$\frac{\partial u}{\partial t}+\frac{u}{\sqrt{G_{\xi\xi}}}\frac{\partial u}{\partial \xi}+\frac{v}{\sqrt{G_{\eta\eta}}}\frac{\partial u}{\partial \eta}+\frac{\omega}{d+\zeta}\frac{\partial u}{\partial \sigma}-\frac{v^2}{\sqrt{G_{\xi\xi}}\sqrt{G_{\eta\eta}}}\frac{\partial \sqrt{G_{\eta\eta}}}{\partial \xi}$$
$$+\frac{uv}{\sqrt{G_{\xi\xi}}\sqrt{G_{\eta\eta}}}\frac{\partial \sqrt{G_{\xi\xi}}}{\partial \eta}-fv \qquad (3.\ 11)$$
$$=-\frac{1}{\rho_0\sqrt{G_{\xi\xi}}}P_\xi+F_\xi+\frac{1}{(d+\zeta)^2}\frac{\partial}{\partial \sigma}\left(\nu_V\frac{\partial u}{\partial \sigma}\right)+M_\xi$$

and

$$\frac{\partial v}{\partial t}+\frac{u}{\sqrt{G_{\xi\xi}}}\frac{\partial v}{\partial \xi}+\frac{v}{\sqrt{G_{\eta\eta}}}\frac{\partial v}{\partial \eta}+\frac{\omega}{d+\zeta}\frac{\partial v}{\partial \sigma}-\frac{uv}{\sqrt{G_{\xi\xi}}\sqrt{G_{\eta\eta}}}\frac{\partial \sqrt{G_{\eta\eta}}}{\partial \xi}$$
$$+-\frac{u^2}{\sqrt{G_{\xi\xi}}\sqrt{G_{\eta\eta}}}\frac{\partial \sqrt{G_{\xi\xi}}}{\partial \eta}-fu \qquad (3.\ 12)$$
$$=-\frac{1}{\rho_0\sqrt{G_{\eta\eta}}}P_\eta+F_\eta+\frac{1}{(d+\zeta)^2}\frac{\partial}{\partial \sigma}\left(\nu_V\frac{\partial v}{\partial \sigma}\right)+M_\eta$$

The v_V represents the vertical eddy viscosity coefficient. P_ξ and P_η represent the pressure gradients. Density variations was neglected in the existing model, except in the baroclinic pressure terms.

In this numerical model, “Porous disc” was assumed as a thin hydraulic structure relative to the model grid size. It acted as a semi-permeable barrier to add friction to the flow and covered only part of the water column (Deltares, 2021). The porosity was controlled by an energy loss coefficient that was prescribed across the height of the structure. Flow discontinuity in static pressure passing through the rotor-center line may

occur due to deployment of the device (Roc et al., 2013). The general energy extraction due to flow thrust force inserted on the turbine rotor, where the effective swept area of a device is perpendicular to the undisturbed fluid flow, can be expressed as follows:

$$F_\xi = -\frac{P_{ex}}{U_\xi} \tag{3. 13}$$

where F_ξ is the retarding force on the fluid as it passes through the rotor, P_{ex} is the energy extraction; and U_ξ is the incoming tidal current velocity perpendicular to the cross section of the tidal turbine (**Figure 3.13**).

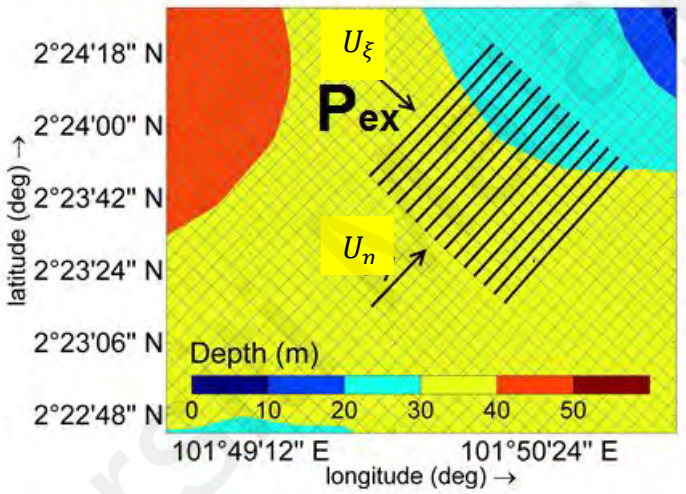

Figure 3.13: The arrangement of the tidal farm at cell in the η-direction perpendicular to flow

Momentum sink approach (momentum loss added in the Navier-Stokes equations) was adopted for estimating the speed reduction due to tidal energy extraction by the tidal turbine farm (Chen et al., 2013; Defne et al., 2011; Hasegawa et al., 2011; Ramos, Iglesias, et al., 2013; Shapiro, 2011; Yang et al., 2013). M_ξ and M_η respectively represent the contributions due to external sources or sinks of momentum (external forces by hydraulic structures, discharge or withdrawal of water, wave stresses, etc.). An array of tidal turbine works as an additional quadratic friction term (momentum loss). The momentum equation in the ξ-direction can be expressed as:

$$\frac{\partial U}{\partial t} + U\frac{\partial U}{\partial \xi} + V\frac{\partial U}{\partial \eta} - fV = \frac{\partial}{\partial x}\left(\mu\frac{\partial U}{\partial x}\right) + \frac{\partial}{\partial y}\left(\mu\frac{\partial U}{\partial y}\right) - \frac{1}{\rho}\left(\frac{\partial p}{\partial x}\right) + f_{\xi} - M_{\xi} \quad (3.14)$$

where μ is the kinematic water viscosity and f_{ξ} is the horizontal Reynolds stresses. The momentum sinks of turbines perpendicular to the flow is given by:

$$M_{\xi} = -\frac{c_{loss-u}}{\Delta\eta} u\sqrt{u^2 + v^2} \quad (3.15)$$

$$M_{\eta} = -\frac{c_{loss-v}}{\Delta\xi} v\sqrt{u^2 + v^2} \quad (3.16)$$

where M_{ξ} or M_{η} has the form of an acceleration term, where c_{loss-u} or c_{loss-v} is the quadratic friction coefficient, the input term in the model, u or v is the incoming flow velocity, and $\Delta\xi$ or $\Delta\eta$ is the grid resolution in the ξ- and η -direction. A porous disc was used to represent a turbine to the flow along the ξ- or η-direction of the grid (**Figure 3.13**). During the simulation, the porous disc was assumed as a thin hydraulic structure relative to the model grid size. It acts as a semi-permeable barrier that posed friction to the flow. The total drag force of N number of turbines, C_D can be expressed as (Vennell et al., 2015):

$$C_{D,total} = \frac{A_T}{2A_c} N\,(C_s + C_T) \quad (3.17)$$

where C_T is a single turbine's thrust coefficient based on the area swept by the blades A_T, C_s is the gross drag coefficient of one turbine, and A_c is the cross-sectional area of a channel. Hence, the total drag force on the fluid $F_{D,total}$ due to power extraction by an array of tidal turbine arranged in η -direction is expressed as:

$$F_{D,total} = C_{D,total}\rho A_c {U_\xi}^2 = \frac{A_T}{2A_c}\rho N(C_s + C_T){U_\xi}^2 \quad (3.\ 18)$$

The momentum loss term (M_ξ) in equation (3. 14) can be written as a relationship between the total drag force and the mass of one grid cell in Delft3D:

$$-\frac{\frac{N}{2}\rho A_T(C_s + C_T){U_\xi}^2}{\rho\Delta\eta\Delta\xi\Delta h} = -\frac{c_{loss-u}}{\Delta\eta}U_\xi^2 \quad (3.\ 19)$$

where h is the cell depth and $\Delta\eta$ is the cell size in the η -direction (parallel to the flow). Hence, c_{loss-u} is defined as:

$$c_{loss-u} = \frac{N\ A_T(C_s + C_{T1})}{2\Delta\eta h} \quad (3.\ 20)$$

The water flow through each tidal turbine is unique due to the change of bathymetry. The loss coefficient, c_{loss-u} should be adjusted by considering the incoming velocity of the turbine rotor as the operational conditions affect the $C_{D,total}$. However, Delft3D is unable to address the variation of c_{loss-u} required for this study. To simplify the problem, this research assumed all the turbines are subjected to constant flow magnitude and drag coefficient. Thus, the force and power produced by respective turbines in an array can be expressed as:

$$F_\xi = \frac{\rho}{2}A_T(C_s + C_T)\left|U_\xi\right|U_\xi \quad (3.\ 21)$$

$$P_\xi = \frac{\rho}{2}A_T(C_s + C_T)\left|U_\xi\right|^3 \quad (3.\ 22)$$

where C_T is the turbine's thrust coefficient based on the area swept by the blades A_T, and C_s is the gross drag coefficient of the turbine. Derivation of loss coefficient from previous studies (Ainsworth & Thake, 2006; Chen et al., 2013; Gorban et al., 2001; Yang et al.,

2013) are referred. C_{T1} and C_s are respectively set at 0.5 and 0.33 (Ainsworth & Thake, 2006; Gorban et al., 2001; Yang et al., 2013).

The turbine array is oriented in the η-direction so as to impede flow in the ξ-direction with the diameter of turbine blade is 10 m. The amount of energy supplied by the turbine is influenced by three factors, namely the incoming flow velocity of turbines U_ξ, the swept area A_T of tidal turbines, and the turbine efficiency C_T. Each marine energy current converter unit requires a rated output, which defines the maximum amount of power that can be produced by each turbine (Fraenkel, 2002). No additional energy would be converted for flow velocities higher than these values. The peak flow velocity at Tg Tuan Headland is 2.5 m/s. The optimal design of rated power level depends on the costs related with capturing energy from peak velocity at the Tg Tuan Headland site that may only occur for short period of time. In this study, it is assumed that horizontal axis turbines are used where the deployment site for typical horizontal axis turbines should have a water depth ranging from 20 to 50 m, and the flow should be uniform preferably with a peak spring flood velocity of 2.0 – 2.5 m/s and median velocity exceeding 1.0 m/s (Fraenkel, 2007; Fraenkel, 2002; González-Gorbeña et al., 2015; Lewis et al., 2015; Myers & Bahaj, 2005). Note that the minimum tidal flow speed to enable the horizontal axis turbines to generate power (cut-in speed) is 1.0 m/s (Lewis et al., 2015). The yearly average energy is given by:

$$P_{ex\_yearly} = \sum_{h=1}^{8760} [\frac{1}{2} \rho C_T A_T {U_\xi}^3]_h \qquad (3.23)$$

3.3.7 Model Accuracy, Stability and Resolution

The model accuracy depends on the ability of the Finite Difference Scheme in solving the governing equations correctly during simulation. A successful hydrodynamic model can be justified by the convergency, consistency, accuracy and stability of the model.

The finite difference equations adopted is used to resolve the governing differential equations. As the finite difference equation is an approximation of actual solution of the governing differential equation and therefore some truncation errors should be expected. For the finite difference scheme, it is highly preferable for the spatial distance step ($\Delta\xi$ and $\Delta\eta$), and time step (Δt) to have convergence to zero, where the finite difference equation is converged to the original differential equation and negligible truncation error. If this is fulfilled, the finite difference scheme is considered consistent with the differential equation.

The stability of numerical model is mainly dependent on the round off errors produced during the calculation of the finite difference equations. The limitation of a numerical model is due to its incapability in generating solution of a finite difference equation to an infinite number. While solutions are solved to a finite number and round off error is produced for every individual calculation. A finite difference scheme shall only consider stable if the overall effect of the round off error is negligible. Therefore, a solution that vary very slightly from the actual solution of the finite difference equation can be achieved.

The stability of finite difference equation is governed by the Courant condition (Nash et al., 2014). For implicit models, the dependent parameters are affected by the coupling sets of governing equations containing of unknown parameters of the next time-step. Delft3D-FLOW, which is an implicit numerical model, is stable regardless of the time

step. Therefore, the selection of model resolution is not limited by the Courant stability criteria.

Even though a finite difference scheme has achieved its convergence and stability, truncation error that may occur during the computational process may result in inaccurate model result. In order to make sure that the model is sufficiently accurate, an appropriate constraint should be decided for a finite difference scheme based on the degree of acceptance on truncated error. This constraint is employed into the model by limiting the time-step using Courant-Friedrichs-Lewy number (CFL) to achieve a model with good stability. The Courant-Friedrichs-Lewy number (CFL) can be expressed as:

$$CFL = \frac{\Delta t\sqrt{gh}}{\Delta\eta, \Delta\xi} \tag{3. 24}$$

For Delft3D-FLOW model, the accuracy of the model declines when CFL exceeds a value of ten (CFL<10). The restriction is more limited depending on the type of application, scale of velocity, scale of length, with or without density coupling, etc. With that, the model time-step is restricted by applying the CFL equation in the form of:

$$\Delta t = \frac{min(\Delta\eta, \Delta\xi)}{\sqrt{\frac{\Delta\rho}{\rho} gh}} \tag{3. 25}$$

and

$$\Delta t = \frac{min(\Delta\eta, \Delta\xi)}{max(|u|, |v|)} \tag{3. 26}$$

The equation above can later be adopted to identify the maximum time-step (Δt_{max}) allowed for a selected grid spatial resolution, $\Delta\eta, \Delta\xi$.

3.3.8 Model Architecture

Delft3D-FLOW model comprises of a key program together with a number of subprograms of different functions. The key program demands the subprograms to execute commands required. **Figure 3.14** showed a flowchart of the architecture of Deflt3D-FLOW numerical model and explains the function of every sub-program involved. The input and output data are opened in subprograms 1 and 2. The model input data includes of domain (grid parameters, bathymetry, dry points and thin dams), time frame, initial condition, boundary conditions, physical parameters, and numerical parameters; monitoring and additional parameters are read in and stored in subprograms 3, 4, 5, 6, 7, 8, 9 and 10.

All variables are initialised in sub-program 5. The hydrodynamic in the η and ξ direction are computed during the first time-step in sub-programs 5 - 7 (initial condition, boundaries and physical parameters). The flooding and drying are checked in subprogram 8 (Numerical parameters). Sub-programs 3-10 are executed every time-step for the entire simulation of the numerical modelling process. The bed roughnesses (Manning/chezy and eddy viscosities) are calculated in subprogram 7, where they are called for recalculation of time-step specified in the input data file. Any output data specified are written to output files in subprogram 11 (in 2D through map file or extraction point through history file).

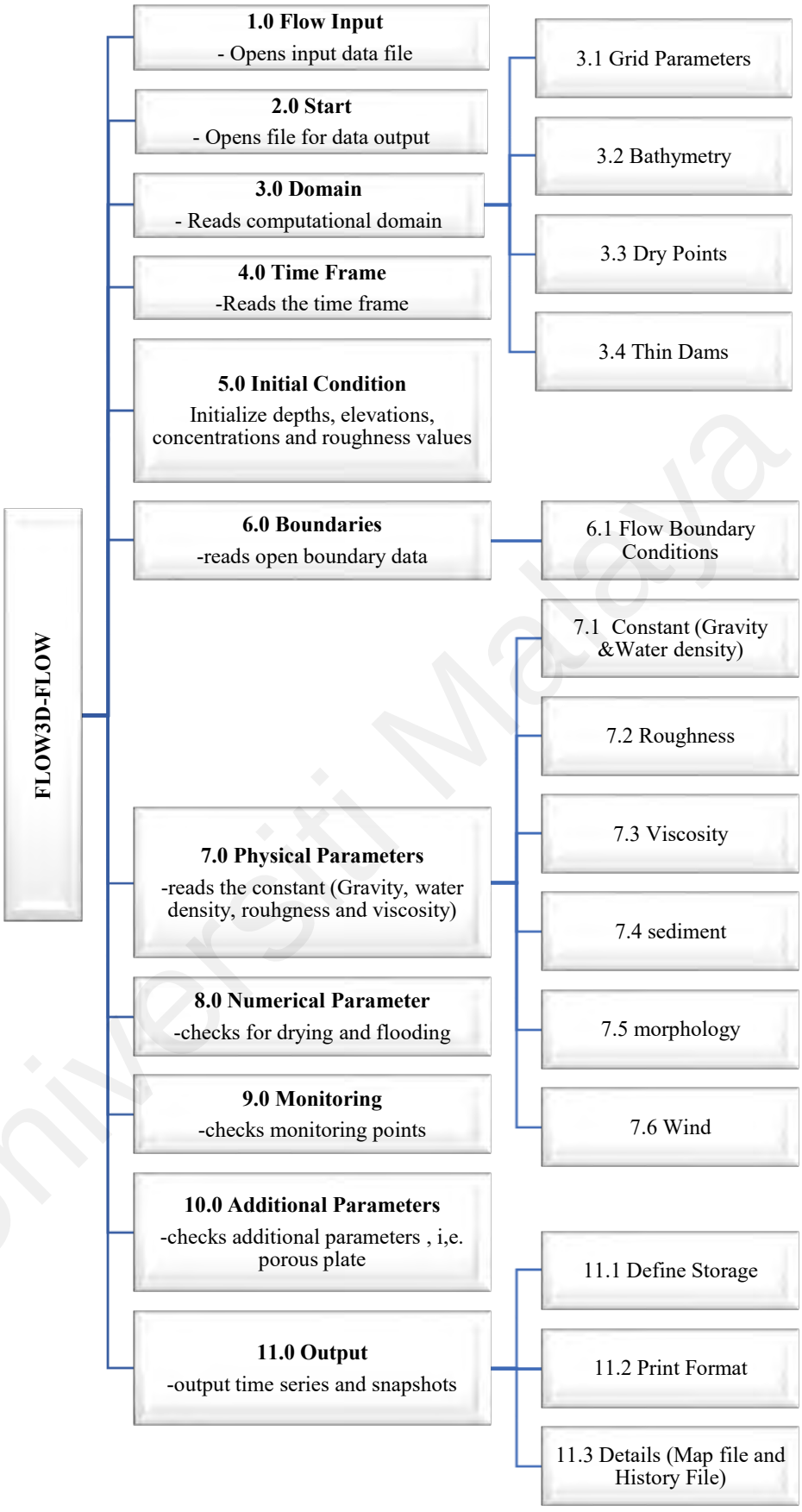

Figure 3.14: Flowchart of model sub-programs

3.3.9 Model Grid Resolution

The model area is covered by curvilinear grid, where the grid is assumed as orthogonal and well-structured. An example of well-structured constructed grid is as shown in **Figure 3.15**. The numerical grid can be defined either in spherical or Cartesian co-ordinate system. The numerical grid was generated using RFFGRID module in this study.

The numerical grid of the computational space is transformed from physical grid vertices space. The quantities of the geometrical $\sqrt{G_{\xi\xi}}$ and $\sqrt{G_{\eta\eta}}$ are introduced in the transformation equations. The transformation from physical space to computational space is as shown in **Figure 3.16**.

The developed variables: tidal level and current velocity (u, v and w) describe the condition of the flow. **Figure 3.17** clearly indicates the water level, density and velocity points (u, v and w) through top and three-dimensional view. The tidal water level (pressure) points are defined in the centre of a cell in continuity. The current velocity components are perpendicular to the grid cell surface.

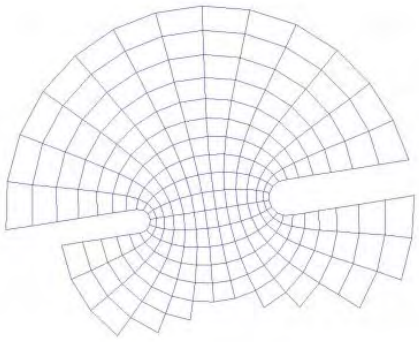

Figure 3.15: An example of Delft3D-FLOW structured grid (Deltares, 2021)

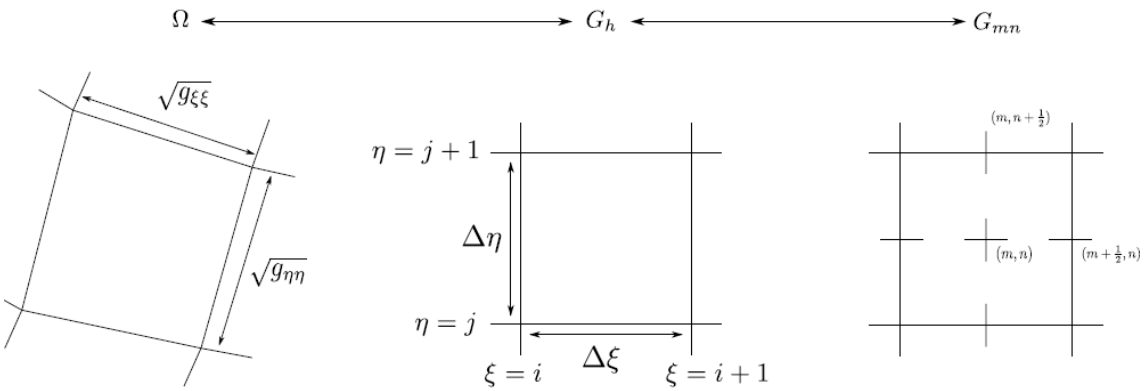

Figure 3.16: Transformation from physical space to computational space (Deltares, 2021)

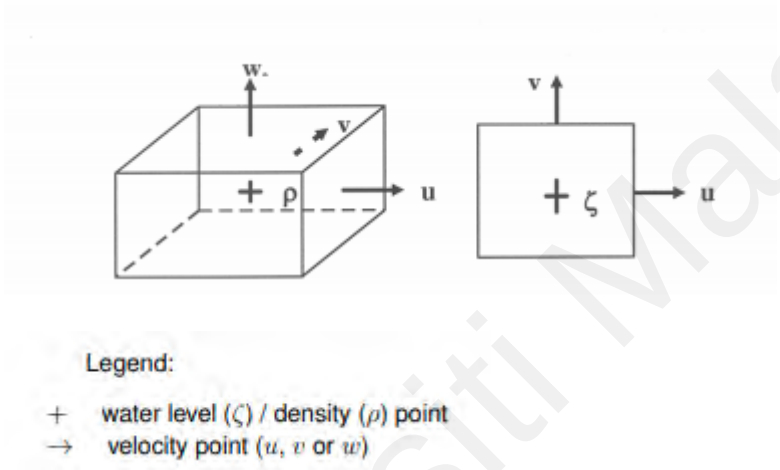

Figure 3.17: Three-Dimensional (left) and top view from top (left) of water level, density and velocity points (Deltares, 2021)

The continuity equation is derived for incompressible fluids ($\nabla \bullet \vec{u} = 0$). The continuity equation in depth-averaged manner is given by:

$$\frac{\partial \zeta}{\partial t} + \frac{1}{\sqrt{G_{\xi\xi}}\sqrt{G_{\eta\eta}}} \frac{\partial((d+\zeta)U\sqrt{G_{\eta\eta}})}{\partial \xi} + \frac{1}{\sqrt{G_{\xi\xi}}\sqrt{G_{\eta\eta}}} \frac{\partial((d+\zeta)U\sqrt{G_{\xi\xi}})}{\partial \eta} = Q(d+\zeta) \tag{3.27}$$

with U and V, are the depth-averaged velocities in ξ– and η-direction, respectively and Q represents the contribution of water due to discharge/withdraw of water, precipitation and evaporation.

Staggered grid is advantageous to be applied in this study as the boundary condition can be applied in considerably simple and straight-forward method. It is also possible to apply a lesser number of discrete variables. Other than that, staggered grid application also prevents oscillations in the tidal water levels for shallow water solvers.

In vertical direction, the Delft3D numerical model offers two types of vertical grid system, which are a boundary-fitted σ co-ordinate system (σ-model) and the Cartesian Z co-ordinate system (Z-model) that the grid is strictly horizontal. The σ co-ordinate system is defined as:

$$\sigma = \frac{z - \zeta}{d + \zeta} = \frac{z - \zeta}{H} \tag{3. 28}$$

For σ co-ordinate grid, it is assumed that the number of layers over the whole horizontal computational area is consistent, regardless of the local water depth. Where z represents the vertical co-ordinate in physical space, ζ is the free-surface elevation above reference plane (z = 0), d is the depth below reference plane (z = 0) and H is the total water depth ($d + \zeta$), refer to **Figure 3.18**.

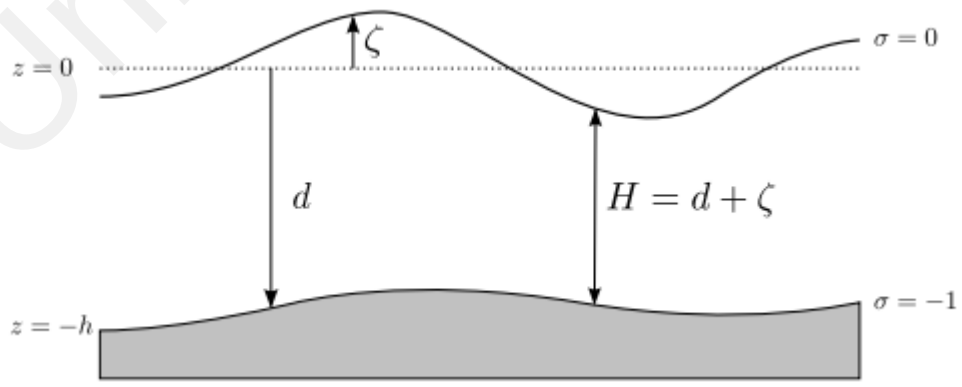

Figure 3.18: Free surface elevation (ζ); reference plane (z = 0); water depth (d) and the total water depth (H) (Deltares, 2021)

For cartesian grid in Z co-ordinate, it is suitable to be applied in coastal areas, lakes and estuaries where stratified flow and steep topography that may occur concurrently. The Z-grid model has nearly parallel lines with density interface with steep bottom slopes, which can reduce artificial mixing of scalar properties in the model, i.e., salinity and temperature. This study adopted σ co-ordinate as the flow at the study area was not stratified and the measurement data indicated that bathymetry of the seabed at the study area is gentle.

In Delft3D-FLOW numerical model, the vertical velocities are solved using continuity equation. The partial differential equations set combining the initial and boundary conditions set are solved on a finite difference grid. The model domain is covered in curvilinear grid to discretise the 3D (Three-Dimensional) shallow water equations in space, where the numerical grid is assumed to be well structured and orthogonal.

3.3.10 Quality of the Grid

A good quality numerical model grid was constructed by fulfilling the following criteria:

- Land-water boundaries: The land-water boundaries must be closely and properly fitted.
- Orthogonality: It is measured by the cosine value of the cell centre. The orthogonal value should be less than 0.04 for inner model area and 0.05 – 0.10 for outside of interest area. The grid deviated from the cosine zero will result proportionally in errors in the direction of the pressure gradient in FLOW3D.
- Smoothness: It is determined by the ratio of changes in neighbouring grid cell. The rule of thumb allows it to be less than 1.1 at study area and allow an increment up 1.4 further away. Smooth changes on the grid spacing throughout the computational area

is necessary for a stable simulation. A good quality grid is supposed to have orthogonal and smooth changes over the model domain.

- Aspect ratio: It is measured by the ratio of grid cell dimensions in M and N directions. A range of 0.5 -2 is required. If the numerical model is set-up for one-dimensional flow condition (cross-shore or longshore processes), a larger value up to 5 can be accepted.

With the criteria above mentioned, it can be said that construction of high-quality numerical model grid is an iterative process and therefore serious time and effort are required.

3.3.11 Negeri Sembilan Model

In this study, a high-resolution depth-averaged model depicting the Straits of Malacca as shown in **Figure 3.19** was constructed using Delft3D-RGFGRID to generate a curvilinear and boundary-fitted spherical co-ordinate.

The length of the model domain was 247 km from the northern boundary to the southern boundary. The regional model was modelled sufficiently far from the study area so that any numerical disturbance at the boundary would not disturb the model results in the area of interest. The regional model grid size was set at 1200 m x 1200 m at the outer (ocean) boundary for deeper sea depth; whereas, the grid size of the local model was gradually reduced to 100 m x 100 m to sufficiently model the headlands hydrodynamic conditions. In addition, 100 m x 100 m grid is designed for modelling the 10 m diameter tidal turbine with 9D spacing in ξ - and η -direction.

A single curvilinear model was developed (as illustrated in **Figure 3.19**) covering about 120 km x 90 km from the center of the Project Area. Notable areas within the model

domain from Kuala Selangor (north) to Parit Jawa (south) include Pulau Rupat, Tg Sepat, Port Dickson, Pasir Panjang and Pelabuhan Klang. The high-resolution computation domain consisted of a grid spacing ranging from 300 m to 100 m in which finer grids has been applied at the Project Area and its surrounding. Eventually, this grid setting allowed for higher computational efficiency while maintaining the model stability and accuracy. The bathymetry within the computation domain combines the following sources:

- Bathymetric survey data (described in Section 3.2)
- Digitized Admiralty Charts

The bathymetric survey is used to refine the water depths surrounding Project Area while for the Admiralty Charts are used to supply the bed profiles beyond the extent of the survey data. The depths of grid vertices are interpolated from these sources and adjusted to MSL vertical datum (approximately +1.55 mCD). **Figure 3.20** shows the bathymetry within the computational domain. The details description of the bathymetry data adopted for the modeling are provided in Section 4.2.2.3.

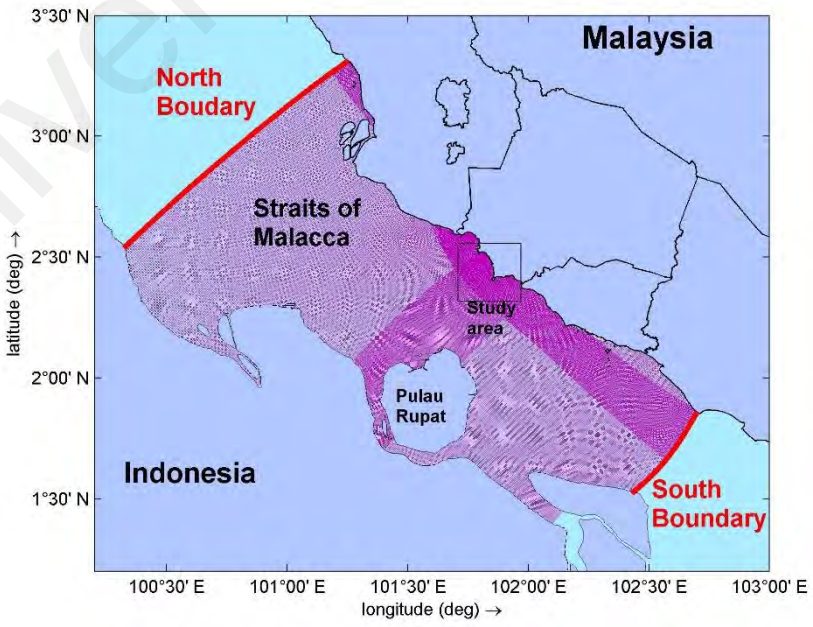

Figure 3.19: Boundary and model domain grid

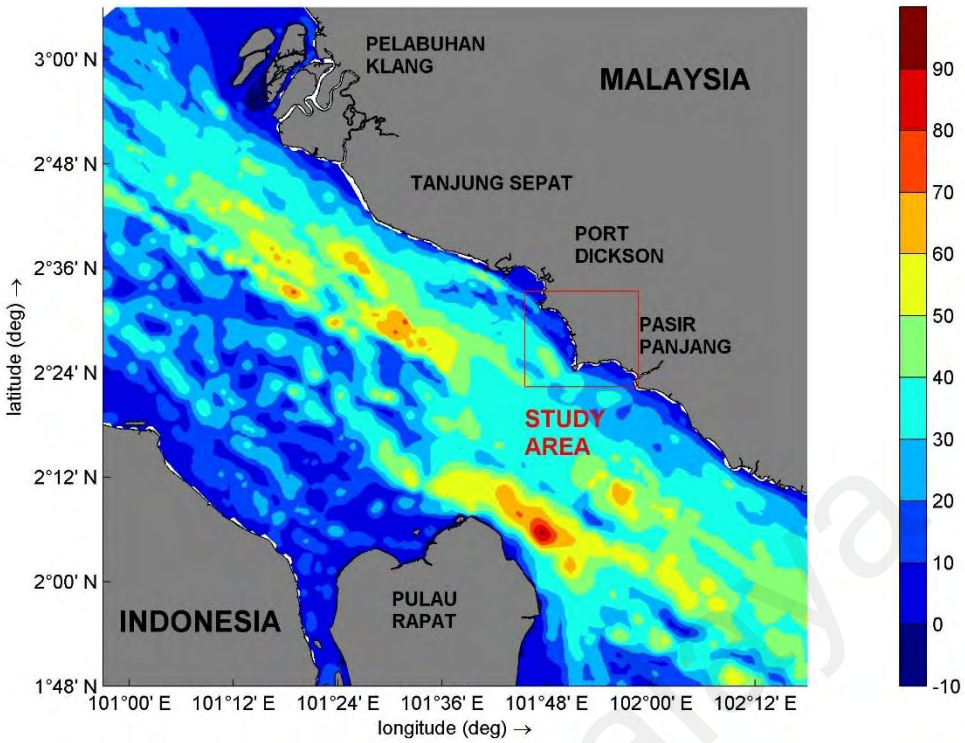

Figure 3.20: Interpolated Bathymetry within the model (in m MSL)

3.3.12 Boundary Conditions

The domain of the model comprises of division along 'land-water' lines (coast line or river bank), which are called as closed boundary and division across the flow field that is called as open boundary. Closed boundary is natural boundary while open boundary is artificial 'water-water' boundary. Open boundaries are used to limit the computational area as well as to reduce the computational effort for the numerical model. The open boundary of the numerical model should be set up as far as possible from the study area. For the Negeri Sembilan Model, the north and south boundary are open boundaries to allow the tidal flow into the model while the Peninsular and Sumatera land are set as closed-boundary. Hence, the long wave propagating out of the study area will not be affected by the open boundaries where the reflection should be negligible.

For Delft3D-FLOW, the flow at the open boundary is assumed to be sub-critical. This means that Froude Number is smaller than one, where the flow magnitude is smaller than the wave propagation velocity. Froude number is defined as:

$$r = \frac{U}{\sqrt{gH}} \tag{3. 29}$$

Where U is the incoming current velocity, g is the gravitational force, and H is the depth of flow. Two boundary conditions are specified at the inflow and one boundary condition is specified at the outflow. Ebb and flood tides require different numbers of boundary condition. The first boundary condition is defined when setting up the model, while the second boundary condition is given by the built-in function of the Flow3D-FLOW numerical model. The velocity component at the inflow of the open boundary is given as zero. The open boundary of the numerical model is set at location where the grid lines of the boundary is normal to the flow in order to get a realistic flow pattern near to the open boundary.

The momentum equation of vertical velocity direction is parabolic. It is governed by vertical eddy viscosity as well as seabed (bed stress) and free surface (wind stress) at the boundary. The kinematic conditions (ω) for σ -grid has considered the impermeability of the surface and bottom. It can be defined as:

$$\omega|_{\sigma-1} = 0 \quad \text{and} \quad \omega|_{\sigma+1} = 0 \tag{3. 30}$$

a. Bed boundary conditions

The momentum equation of the boundary conditions at the seabed is:

$$\frac{vV}{H}\frac{\partial U}{\partial \sigma} = \frac{1}{\rho_o}\tau b\eta \tag{3. 31}$$

Where $\tau_{b\eta}$ is the bed shear stress component in η direction. It may be the combined influence of wave and flow. However, for this study, the bed shear stress is only restricted to flow.

b. Depth-averaged flow

The shear stress at the bed by turbulent flow for two-dimensional depth-averaged flow modelled in this study us given by quadratic friction law as:

$$\overrightarrow{\tau b} = \rho_o g \vec{U}\left|\vec{U}\right| \quad \frac{\rho_o g \overrightarrow{U\left|\vec{U}\right|}}{C_{2D}^2} \tag{3. 32}$$

Where $\left|\vec{U}\right|$ is the depth-averaged horizontal current velocity magnitude.

The 2D-Chezy coefficient (C_{2D}^2) is calculated using Manning formulation:

$$C_{2D}^2 = \frac{\sqrt[6]{H}}{n} \tag{3. 33}$$

Where H is the total water depth (m) while n is the Manning coefficient ($m^{-1/3}s$).
Bed grab sampling data and land-use data were used to determine the bed roughness and flow resistance.

c. Surface boundary condition

The momentum equation of free surface boundary condition is defined as:

$$\frac{vV}{H}\frac{\partial U}{\partial \sigma}\Big|_{\sigma=0} = \frac{1}{\rho_o}|\overrightarrow{\tau_s}|cos\theta \tag{3. 34}$$

$$\frac{vV}{H}\frac{\partial v}{\partial \sigma}\Big|_{\sigma=0} = \frac{1}{\rho_o}|\overrightarrow{\tau_s}|sin\theta \quad (3.35)$$

Where θ is the angle between wind stress vector and local grid direction is constant. The model setup in this study has excluded the wind effect, the stress at the free surface is therefore zero.

d. Open Boundary Conditions

Open boundary is artificial 'water-water' boundaries in order to achieve an effective computational domain area as well as to reduce the computational effort. In actual condition, waves can travel across the open boundaries without reflections and unhampered. The water level and current flow velocity should be set to have a stable mathematical initial boundary condition.

For current work implementation, the tangential velocity is prescribed as zero. The flow is assumed to flow in perpendicular direction to the open boundary. The boundary condition in this study is obtained from IHO tide station database. The water level is given as (only U-direction flow is given here for the sake of simplicity in description):

Water level: $$\zeta = F_\zeta(\mathrm{t}) + \partial_{atm} \quad (3.36)$$

Where, F_ζ is the boundary forcing of incoming flow from $\zeta - direction,$ and ∂_{atm} differential of atmospheric pressure (N/m^2). Linear interpolation is adopted to create the boundary condition at the intermediate grid points throughout the boundary. The water level boundaries are consistent with average pressure where the input signal is corresponding to Mean Sea Level.

e. Closed Boundary Conditions

Closed boundary is transition between land and water. Two types of boundary conditions are set, i.e., one side of the boundary is with water flow normal to the boundary and the other side of the boundary is with the shear stress along the boundary. No flow is penetrating through the boundary with flow normal to the boundary. Free slip is applied to the closed boundary as the numerical model domain for this study is set considerably large where the influence of side wall can be neglected.

3.3.13 Tidal Harmonics

A tidal resource investigation was conducted to quantify the available tidal power and to determine the potential tidal energy berths along the multiple headlands of Negeri Sembilan coastline. Followed by that, tidal resource zone assessment focused at the potential headland was further conducted in this study. This study has considered both current flow velocity magnitude and direction for the tidal resource assessment.

The Delft3D-Flow model was developed to include the water level in time series at the open boundaries, described in Section 3.3.5. The flow was driven by a number of environmental forces, i.e., tides at the open boundaries, wind stresses at the free surface and pressure gradients. Conventional tidal harmonical analysis used least squares fit method to discrete the tidal level and current into tidal harmonic constituents. Modification was made on nodal correction and interference to improve the accuracy of the conventional method. There are several numbers of available tools that can be used to perform tidal harmonic analysis, e.g., T_T tide (can be implemented into MATLAB), TASK (tidal analysis software kit) designed by National Oceanography Centre and written in Microsoft windows), TAPPY (tidal analysis program in python), MIKE 21 tidal analysis and prediction module.

TOPEX/Poseidon global inverse solution TPXO 7.2 developed by Oregon State University from the DDB tide database tool was chosen to perform the tidal analysis (Egbert & Erofeeva, 2002). TOPEX/Poseidon global inverse solution TPXO 7.2 is part of the 'tide database' toolbox from Delft Dashboard (DDB), an open source standalone Matlab-based graphical user interface (i.e., GUI) and OpenEarth suite (Van Koningsveld et al., 2010). DDB was developed by Deltares as a rapid tool for setting up coastal and estuarine models. This tool has been developed in Matlab version 2013B and tested up to Matlab version R2016a. It can be opened from the command line through Matlab or execute as a standalone tool. The DDB software is free and the extracted data could be easily implemented into Delft3D-FLOW model. There is no license required and the software can be easily downloaded from the Deltares Wiki (https://publicwiki.deltares.nl/display/DDB). TPXO adopted in this study is a series of global ocean tide model, which best-fits, in a least-squares sense of the Laplace Tidal Equations and altimetry data (Egbert et al., 1994; Egbert & Erofeeva, 2002). The model considered tides as complex amplitudes of earth-relative sea-surface elevation for eight harmonic primaries (i.e. M2, S2, N2, K2, K1, O1, P1 and Q1), two long periods (i.e. Mf, Mm) and three non-linear harmonic constituents (i.e. M4, MS4, MN4), on a 1440 x 721, ¼ degree resolution full global grid. The files are saved as NetCDF on the Deltares OpeNDAP server as phases and amplitude. The information produced from DDB can be viewed within DDB on a map or exported as*.mat or *.tek file.

The tide is derived from long term analysis of observed data at the selected tidal stations. The basis of tidal prediction is developed by Doodson's tidal potential model (Doodson & Warburg, 1941). It was developed by considering the position of the sun and moon and governs the tide generating forces. It could be determined using the astronomical variables, which are:

S(t) = Moon's mean longitude

H(t) = Sun's mean longitude

L = Mean lunar time

P'(t) = Mean longitude of the solar perigee

P(t) = Lunar perigee's mean longitude

N'(t) = Mean ascending's node longitude in negative direction

The analysis of tidal harmonic is derived depending on the generating force of each tide represented by the harmonic cosine curve, at the same time of oscillation by astronomic force production, which is known as tidal constituents or harmonic. Every tidal constituent is relying on a different astronomical phenomenon. Principal solar S_2 and lunar M_2 are constituents due to the earth rotation relative to the sun and moon while the constituents for lunar elliptic, L_2 and N_2 are consequences of the furthest and nearest, respectively between the moon and earth. For the study area at Negeri Sembilan coastline, M_2 and S_2 are dominant constituents relative to the major diurnal constituents K_1 and O_1, and hence the resulting tide is semi-diurnal.

The frequency of each tidal constituent can be defined by 'Doodson Number', which is used to identify both phase and speed of a tidal constituent. The frequency of every tidal constituent is known, and with that, if tide level measurement is conducted for a considerably long time-series, it can be divided into its representative constituents. Every tidal constituent is given with an alphabet to represent the astronomical force and a symbol, which representing the number of tidal cycles per astronomical cycle. For example, M_2 (principal lunar semidiurnal constituent), M refers to the moon while subscript 2 refers to two complete tidal cycles for every astronomical cycle. The tidal constituent can be classified into three main groups (Mann & Lazier, 2013) as:

a. Semidiurnal: ~12-hour of tidal period, consists of two full tidal cycles per day. The symbol is given with subscript 2.

b. Diurnal: ~ 24 hours of tidal period, which is one tidal cycle per day. The symbol is given with subscript 1.
c. Long period: the tidal period ranges from days to years, the symbol has no common pattern.

Further grouping on tidal constituents is given as 'over-tide', that is influenced by the non-linear of other bathymetry and tidal constituents and more commonly applicable to shallow water and estuaries. The tidal period for these constituents is less than 9 hours. The subscript for these tidal constituents is 4 or 6, which is approximately 4 or 6 numbers of tidal cycles per day. Tidal harmonic analysis is used to calculate the constant of tide at a certain location to enable the forecasting of astronomical tide. The height of a tide can be represented by:

$$h(t) = \sum_{j=1}^{M} A_j \, cos \, [2\pi(\delta_j t - \theta_j)] \tag{3. 37}$$

where $h(t)$ is the height of the tide at time t, M is the chosen harmonic constituent number, j is the individual constituent, A_j is the amplitude of the constituent, δ_j is the frequency of the constituent, θ_j is the constituent phase, measured in radians. Typical example of tidal curve resulting from combination of tidal constituent is as shown in **Figure 3.21** below.

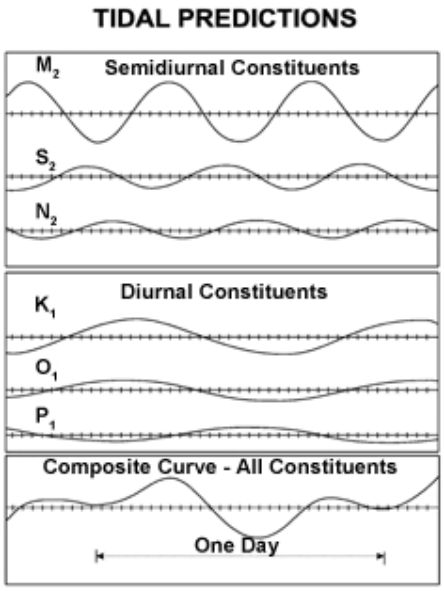

Figure 3.21: A tidal curve resulting from combination of tidal constituents (adopted from Naval Postgraduate School of Department of Oceanography (2015)

The nearest available tidal station to the project site is the Port Dickson, Negeri Sembilan. The tidal pattern at the project site is described as mixed type with predominantly semi-diurnal as shown in **Figure 3.22**. **Table 3.8** shows the predicted tidal elevations at Port Dickson.

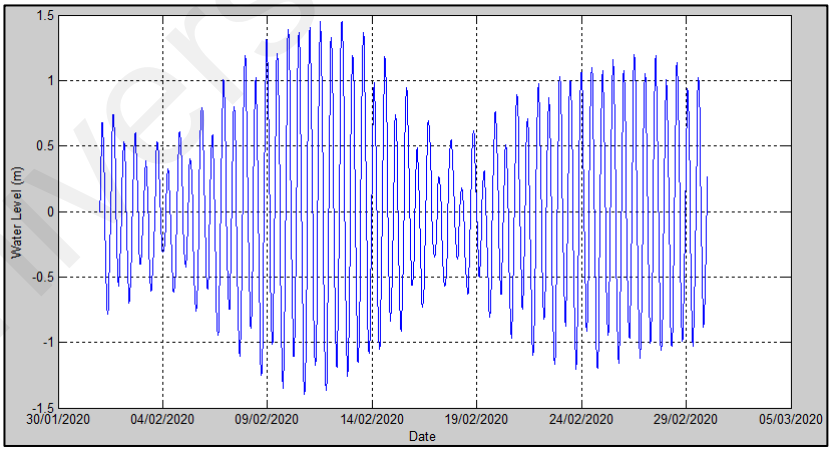

Figure 3.22: Predicted tidal elevation at Port Dickson (February 2020)

Table 3.8: Tidal Elevation at Port Dickson

Event	Tidal Height (m, ACD)
Highest Astronomical Tide (HAT)	3.51 m ACD
Mean High Water Spring (MHWS)	2.79 m ACD
Mean High Water Neap (MHWN)	1.96 m ACD
Mean Sea Level (MSL)	1.55 m ACD
Mean Low Water Neap (MLWN)	1.14 m ACD
Mean Low Water Spring (MLWS)	0.31 m ACD
Lowest Astronomical Tide (LAT)	0.00 m ACD

3.3.14 Calibration and Verification

The calibration and verification process of the numerical model were carried out by comparing the simulated result (i.e., water level, current speed and current direction) against the measured data at both ADCP 1 and ADCP 2. Root Mean Square Error (RMSE) statistical approach was used in order to define a good calibration.

$$RMSE = \sqrt{\frac{\sum_{i=1}^{N}(P_i - O_i)^2}{N}} \quad (4.1)$$

where;

P_i = Simulated parameter

Oi = Measured parameter

N = Number of observation data

The output from the simulated model must be able to reproduce the flow condition and tidal elevation of the study area based on the measured tidal level and current speed.

3.4 Summary

The field campaign includes data collection for bathymetric, water level, current, bed grab sampling and TSS sampling as discussed in Section 3.2. The field measurement and secondary data collected for the research were served as input for the numerical modelling. Followed by that, the requirement and work methodology for numerical modelling with Delft3D-FLOW model is given in Section 3.3. The numerical model calibrated using the ADCP data was used for tidal energy resource assessment, performance and impact assessment as discussed in the subsequent chapters.

4 RESOURCE ASSESSMENT

4.1 Introduction

Identification of suitable tidal current energy extraction site is basically relying on the available tidal current resource. Strong tidal currents can normally be observed in estuaries, narrow straits, islands, and around headlands (Draper et al., 2013; Finkl & Charlier, 2009). The South China Sea and Straits of Malacca, which surround the Malaysian shoreline offers abundance of tidal stream energy for exploration and exploitation (Lim & Koh, 2010; Rourke et al., 2010). Lim & Koh (2010) used Princeton Ocean Model (POM) to identify the locations for great potential for harvesting of tidal energy extraction in Malaysia. In South China Sea region, Pulau Jambongan, Kota Belud and Sibu were identified to be the most viable spots for harnessing of tidal energy (Lim & Koh, 2010). Whereas, for Straits of Malacca, which has separated Peninsular of Malaysia and Sumatera, several viable sites with high tidal current flow were identified within Straits of Malacca that include Kapar, Pontian, Alor Setar and Tanjung Karang (Lim & Koh, 2010; Sakmani et al., 2013). However, these sites found within Straits of Malacca are not suitable for tidal current energy extraction due to their limited depths, i.e., the water depth is mostly less than 20 m. Further of that, Bonar et al. (2018) has conducted a tidal stream resource assessment study within Straits of Malacca. This study found that Port Dickson is the most promising site as it has the highest extractable energy in comparison to other sites assessed, i.e., Pulau Pinang, Klang, Pulau Langkawi and Pulau Pangkor.

Past studies on marine energy in the Straits of Malacca were mainly undertaken using low spatial and temporal resolution flow data. Such models might not be able to provide the detailed hydrodynamic characteristic for a local tidal stream site (Lim & Koh, 2010;

Sakmani et al., 2013). Sakmani et al. (2013) assessed the suitability of the sites for tidal turbine installation in the Strait of Malacca. One of the site assessments was held in Pangkor Island, Perak in which the site suitability for tidal energy extraction was concluded merely based on a single set of site data measured using an Acoustic Doppler Current Profiler (ADCP) deployed at a sheltered area and through responses given by local fishermen and divers through interview. Thiébaut et al. (2019) found significant change in spatial pattern of velocity (power density) distribution throughout the Alderney Race by merging high resolution velocity measurements with the tidal stream potential modelling estimation. Similar to Alderney Race, the flow velocity condition in this Strait varies throughout the strait. To provide sound judgements on such a feasibility study, a validated high resolution 2D hydrodynamic model is deemed to be crucial.

This study assessed the site suitability based on three main characteristics as listed in **Table 4.1** (Fraenkel, 2007; Fraenkel, 2002; González-Gorbeña et al., 2015; Myers & Bahaj, 2005) to determine a suitable site for Tidal Energy Converter (TEC) efficient power extraction. This chapter discusses the development for a multiple-headland coastline site selection assessment based on three main characteristics of typical tidal stream energy site justified by Lewis et al. (2015), i.e., to determine a suitable site for Tidal Energy Converter (TEC) efficient power extraction. The deployment site for typical tidal stream energy should have a water depth ranging from 20 to 50 m, and the flow should be uniform preferably with a peak spring flood velocity of 2.0 – 2.5 m/s and median velocity exceeding 1.0 m/s (Fraenkel, 2007; Fraenkel, 2002; González-Gorbeña et al., 2015; Lewis et al., 2015; Myers & Bahaj, 2005). Note that the minimum tidal flow speed to enable the horizontal axis turbines to generate power (cut-in speed) is 1.0 m/s (Lewis et al., 2015).

Table 4.1: Site requirements for Tidal Energy Converter (TEC) (Fraenkel, 2007; Fraenkel, 2002; González-Gorbeña et al., 2015; Lewis et al., 2015; Myers & Bahaj, 2005)

Variable	Site Requirements
Depth	20 - 50 m
Average Current Velocity	> 1.0 m/s (Ideal 2 – 2.5 m/s)
Tidal Current Field	Defined axial direction

4.2 Negeri Sembilan Hydrodynamic Model

Flow determination at the study site is the prerequisite for investigation of the tidal energy potential near headlands. In this study, Delft3D numerical model was used to build a 2D Negeri Sembilan hydrodynamic model for investigation of the local hydrodynamic conditions near headlands H1, H2, H3 and H4 in Negeri Sembilan. Similar to the established numerical models, such as POM, TELEMAC and MIKE 21, Delft3D has the capability of generating a high-resolution simulation of a hydraulic problem, and has been adopted by a number of researchers in conducting tidal current energy viability and energy extraction study by using 2DH momentum equations (Carballo et al., 2009; Chatzirodou & Karunarathna, 2014; Chatzirodou et al., 2015; Ramos & Iglesias, 2013). Instead of idealised headland modelling study or case study at an actual study site adopting secondary source of modelled coarse-resolution bathymetry data, the tidal array site selection assessment is more representative through real-field data measurement for model set-up, calibration and validation. Hence, the numerical model of this study is set-up using the measured bathymetry to be calibrated and validated with measured water level and current velocity data. The details including the source and coverage of the measured bathymetry are elaborated in Section 4.2.2.3. Moreover, complicated geomorphological condition for different-sized headlands can be accurately captured in this research.

4.2.1 General Description of Study Area

The Peninsular Malaysia and Sumatra are separated by the Straits of Malacca. The west coast of Peninsular Malaysia has a long stretch of shoreline of approximately 800 km, extending from Perlis (the north-most) to Johor (the south-most). Straits of Malacca is an essential shipping waterway due to its strategic location for ships to sail between East Asia and Europe and an important habitat for livings of high ecological values, such as fisheries, mangroves forest and coral reefs.

The tidal current in Straits of Malacca is generally low (<1 m/s) due to the geographical condition of this strait being sheltered by Sumatera Island (Koh & Lim, 2008; Lim & Koh, 2010; Sakmani et al., 2013; Shukri et al., 2013). Yet, the tidal current flows passing through the restricted channel of Straits of Malacca might be enhanced. Negeri Sembilan, which is a constricted channel located at the central west coast of Malaysia, was selected as the study area of this case study. Previous study showed that current velocity in the middle of the strait which is constricted due to the protruded shoreline and the islands shows higher current velocity at this region (Sakmani et al., 2013).

Semi-diurnal tides are dominant where occurrence of two high waters and two low waters of similar heights are observed within a tidal day. Annually predicted tidal observations obtained from the 2019 Tide Tables of Malaysia published by Royal Malaysian Navy illustrates that Port Dickson standard port is the nearest port to the Project Site. Tidal levels at Port Dickson are listed in **Table 4.2**. The tidal range for spring and neap tide at this area are 2.48 m and 0.82 m, respectively.

Table 4.2: Tidal Levels at Port Dickson (Royal Malaysian Navy, 2019)

Tide	Elevation in Chart Datum (m)
Highest Astronomical Tide (HAT)	3.51
Mean High Water Spring (MHWS)	2.79
Mean High Water Neap (MHWN)	1.96
Mean Sea Level (MSL)	1.55
Mean Low Water Neap (MLWN)	1.14
Mean Low Water Spring (MLWS)	0.31
Lowest Astronomical Tide (LAT)	0.00

Negeri Sembilan has approximately 55 km of shoreline length. The land area of Negeri Sembilan state is approximately 6686 km² and is located on the western coast of Peninsular Malaysia, bordered by Selangor and Kuala Lumpur in the north, Melaka to the south and Pahang to the east. It comprises seven administrative districts, which are Seremban, Jelebu, Tampin, Rembau, Port Dickson, Kuala Pilah and Jempol. The State is generally hilly and mountainous with low hills interspersing in the river valleys. The three main river systems are Sg Linggi flowing south and discharges directly into the Straits of Melaka; while Sg Triang, which is tributary of Sg Pahang and Sg Muar, flow eastwards towards Johor before discharging into the Straits of Melaka.

The cultural history of Negeri Sembilan has enabled the inland valleys of the upper basins to be well settled and cultivated. The lateritic soil makes it suitable for the cultivation of rubber and oil palm. The State is mainly covered with agricultural landuses, such as oil palm and rubber plantations, vegetable and livestock farms and fruit orchards. Seremban is the main agricultural distribution centre and the administrative capital of the State. The manufacturing sector is a major contributor to the State's economy. Tourism industry is also expected to grow and will continue to become an important contributor to the state economic growth. The coastal region of Negeri Sembilan especially Port Dickson will remain as the key tourism district. Moreover, coastal zone in Negeri Sembilan also has been used for mining and trading.

Negeri Sembilan coast can be broadly divided into three bays (**Figure 4.1**), which coincide with the demarcation of the three main sediment cells, namely Lukut Cell C1 (Sg. Sepang - Port Dickson Headland), Port Dickson Cell C2 (Port Dickson Headland - Tanjung Tuan) and Pasir Panjang Cell C3 (Tanjung Tuan -Sungai Linggi) (JPS, 2008).

Figure 4.1: Negeri Sembilan Cell Division based on ISMP Negeri Sembilan (JPS, 2008)

Lukut Cell C1 is an indented bay extending from Sg Sepang to Port Dickson headland stretching about 21 km (**Figure 4.2**). Jimah Power Station is constructed on reclaimed land east of Sg Sepang. In front of the mangrove is an intertidal sand flat, which widens eastwards and beaches are formed when the fringing mangroves have been removed. Towards the minor headland, a large area has been cultivated with oil palm and a stretch of coast has been protected with laterite stone revetment. At the southern area, two small

pocket lateritic beaches bounded by ironstone headlands are found. The mudflat is rich in bivalves and cockles. Bukit Keramat located west of Sg Lukut river mouth is a sedimentary outcrop in front of which is a lateritic shore platform. Mangroves occupy most the Sg Lukut Besar estuary. On the east bank of Sg Lukut Besar river mouth, mangrove on the narrow neck have been cleared for pond aquaculture project. Towards the south is Tg Gemuk headland with low cliffs and rocky platform in front. The pocket beaches here are dark brown in colour. Towards south, reclamation has been undertaken for the construction of Shell jetty and the Tuanku Jaffar Power Station (TJPS). Seawalls lined most of this stretch of Port Dickson town. At the south of TJPS is a small sand-mud beach bounded by the Kapor headland (ISMP Negeri Sembilan, 2008).

Port Dickson Cell C2 extends from Port Dickson headland to Cape Rachado/Tanjung Tuan for about 21 km along the coastline (refer to **Figure 4.3**). The cell is characterised by submerged laterite shore platforms extending from headlands and rocky shore. Based on ISMP Negeri Sembilan, the stretch of Cell C2 is complex due to the number of natural features, such as natural rocky headlands and protrusions and man-made structures (marinas, reclamation, coastal protection structures, etc). Based on ISMP Negeri Sembilan (2008), the beach profiles near the shoreline tends to be flat and wide in the northern areas, whereas the beaches become narrower and steeper in the southern stretches. The beach is generally sandy with little fine sediments. The suspended sediments in Cell C2 is considered as the lowest level along the Negeri Sembilan coastline as there are no major river discharges along the cell. The suspended sediments may however increase during monsoon seasons.

Referring to **Figure 4.4**, Pasir Panjang Cell C3 is within the shallow bay between Tg Tuan to Tg Serai in Melaka. This stretch comprises of Negeri Sembilan portion of the bay with a length of 19 km, terminating at Sg Linggi. Thin belts of mangroves are found

scattered along the rocky coast. Smaller headland within the bay includes Tg Menyala, Tg Terus, Tg Mengkudu, Tg Minyak and Tg Pasir Panjang and Tg Selamat. These smaller headlands are just minor protrusions with rocky platforms at the shorefront. Several rocky islands surrounded by laterite shore platforms are Pulau Babi, Pulau Perjudi, Pulau Mengkudu and Pulau Tikus. Cell C3 has several beaches but these beaches are small and their quality inferior to those in Port Dickson Cell C2. The southern area of Cell C3 is less developed.

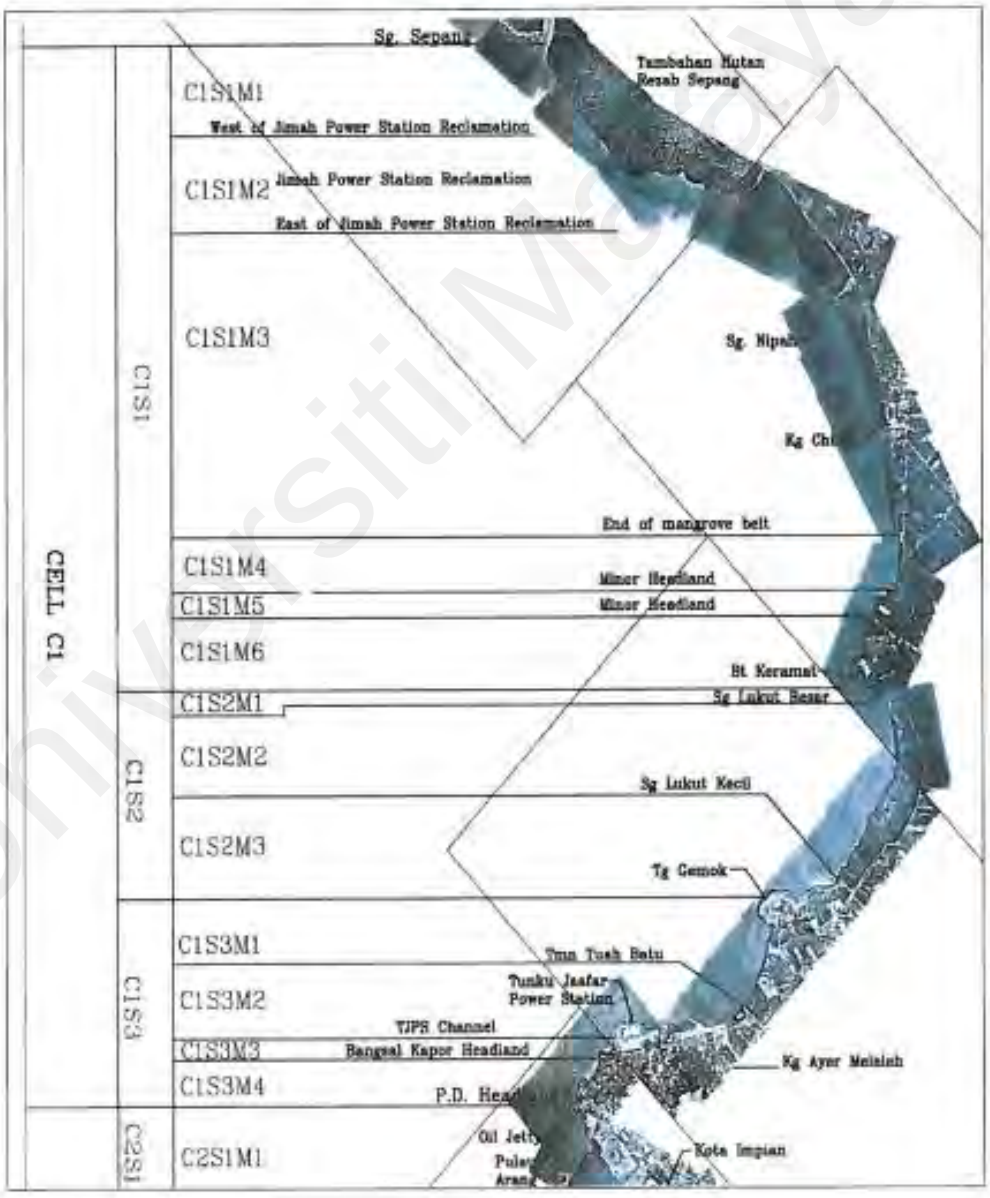

Figure 4.2: Shoreline of Cell C1 (JPS, 2008)

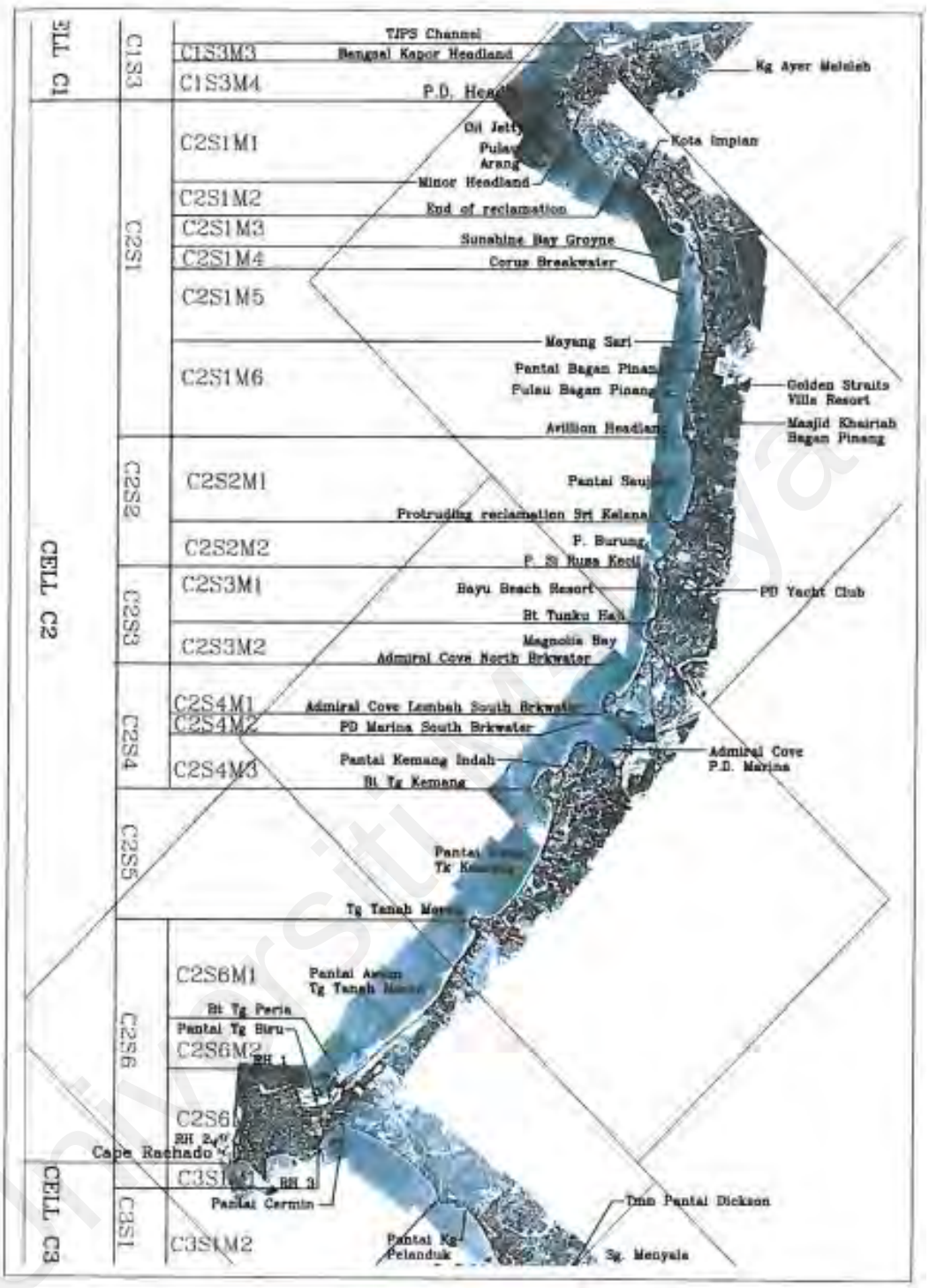

Figure 4.3: Shoreline of Cell C2 (JPS, 2008)

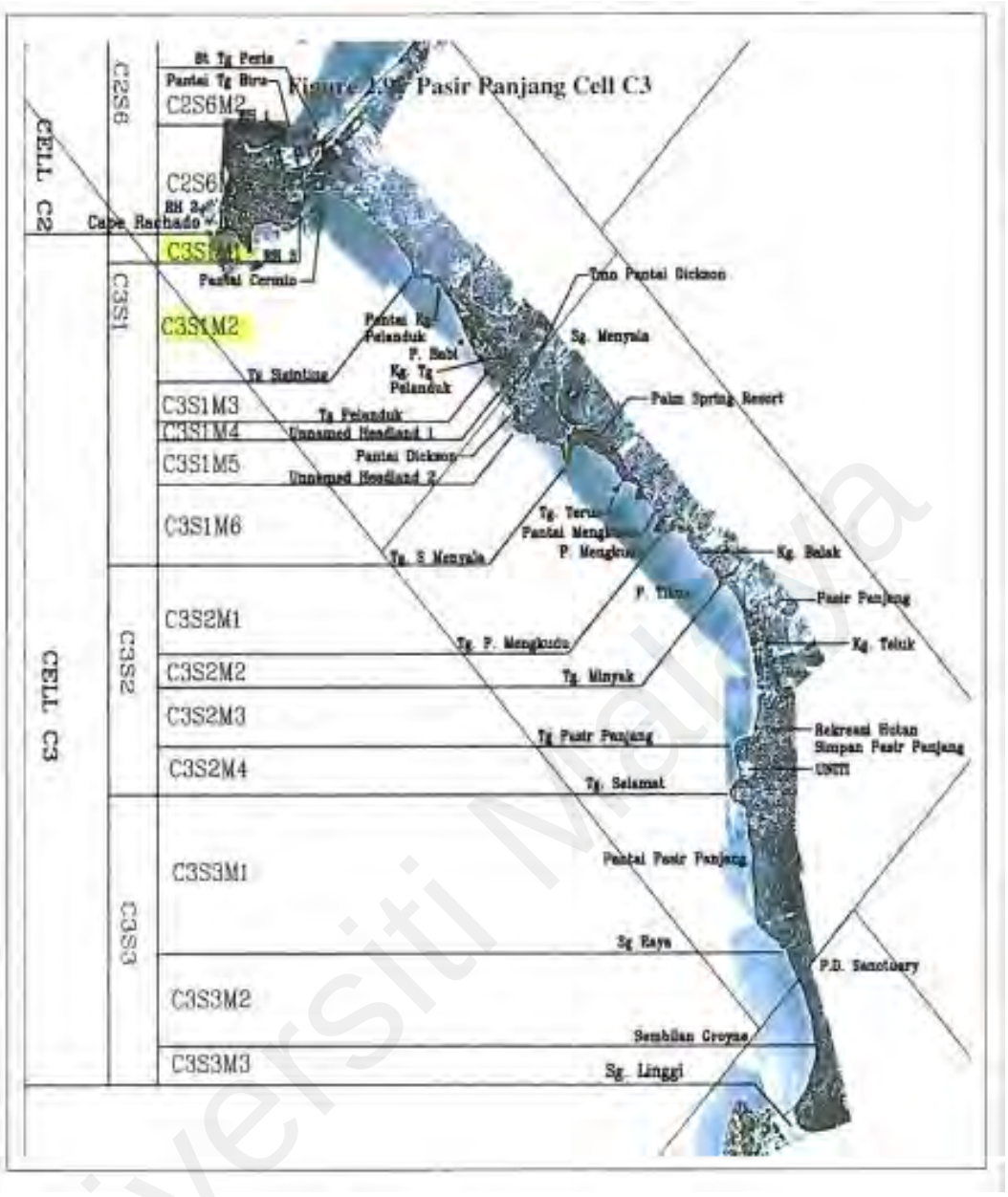

Figure 4.4: Shoreline of Cell C3 (JPS, 2008)

4.2.2 Marine Condition of the Study Area

4.2.2.1 Tidal Condition

Two Acoustic Doppler Current Profilers (ADCPs), ADCP1 and ADCP2 were deployed to measure the water level at the study area (**Figure 4.5**). The water level measurement is deemed sufficiently covering the whole study area of approximately 55 km length at each bay of the study area (**Figure 4.6**). Every location of water level

measurement had been carried out for at least 16 days to cover both neap and spring tide events.

Water level measurement for ADCP 1 was carried out from 15 July 2015 to 06 August 2015. ADCP 1 was deployed within Lukut Cell C1, which is an indented bay extending from Sg Sepang to Port Dickson headland stretching about 21 km. High Water Spring and Low Water Spring observed within this bay during the measurement period are 1.70 m and -1.24 m, respectively. The tidal range within this bay is 2.94 m during spring tide and 1.71 m during neap tide. The tidal level in time series over the 22 days plotted for the ADCP 1 is as shown in **Figure 4.5a**.

ADCP2 was measured water level and current velocity at the most southern bay of Negeri Sembilan. It is deployed within the Pasir Panjang Cell 3, a shallow bay between Tg Tuan to Tg Serai in Melaka with a length of 19 km. The tidal measurement was carried out from 5 January 2016 to 19 January 2016. The High-Water Spring and Low Water Spring for ADCP2 are 1.15 m and -1.18 m, respectively. The tidal range observed during the measurement period within this bay is lower than ADCP1 during spring and neap tide. The tidal range observed during spring and neap tide are 2.33 m and 1.26 m, respectively.

The tidal level is checked against tidal elevation at Port Dickson tide station (**Table 4.3**). It was found that the measured tidal level of ADCP1, located nearer to Port Dickson, is similar with the standard port value. Spring tide occurs during new and full moon as the gravitational pull of the moon and sun are aligned (in the same direction), and therefore generating tidal ranges greater than average monthly range (Hicks, 2006). The high and low water of ADCP 1 during spring tide is slightly higher than Standard Port Dickson tide station due to larger depth (~ 10m CD) and slightly more offshore measurement location was selected, where higher tidal level is expected. When went further southward at ADCP2 (**Figure 4.5b**), located near to Linggi, the spring tide at this

location was slightly lower than Port Dickson tide station due to the lower deployment depth (~ 5m CD) at this station. The lunar and solar force are misaligned during the first and last quarter throughout the lunar phase and thus smaller tidal range during neap tide in comparison to average tidal range. The tide is uniformly distributed throughout the three bays during neap tide. The tidal level variation for ADCP1 and ADCP2 are similar with Port Dickson tide station, generally < 0.2m difference.

The tidal range for ADCP1 is very similar with Port Dickson Tide Station due to the vicinity of the deployment location, about 3 km offshore from the Port Dickson Tide Station. While the tidal range for ADCP2 is observed to be smaller as the depth of the deployment location was much shallower (~ 5m) in comparison to Standard Port and ADCP 1. As neap tide is mainly govern by the gravitational pull of solar force, the tidal range during neap tide is not causing large variation in a localized area (10 km radius), and therefore similar tidal range was observed for ADCP1, ADCP2 and Port Dickson tide station. In overall, the measured tidal data capture was found to be acceptable based on the data comparison and analysis discussed. The data is deemed suitable to be used for the subsequent numerical modelling.

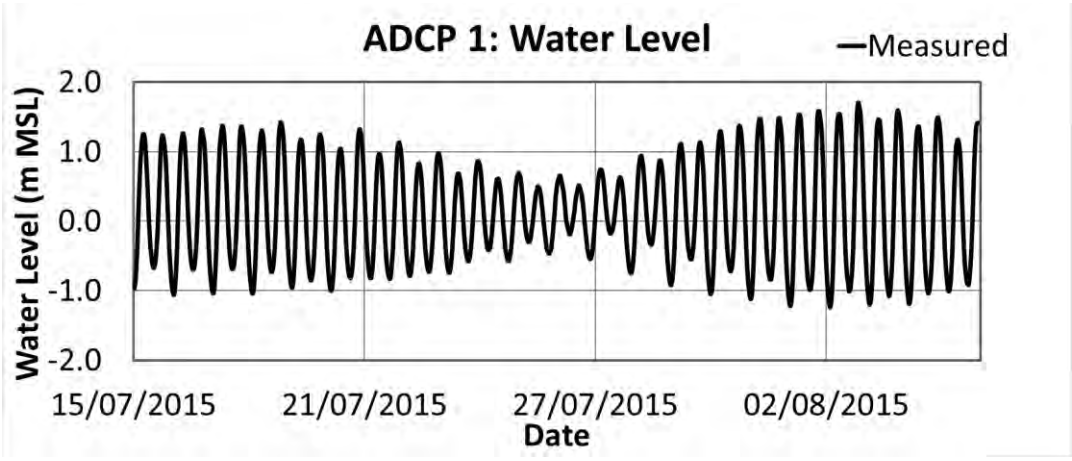

(a)

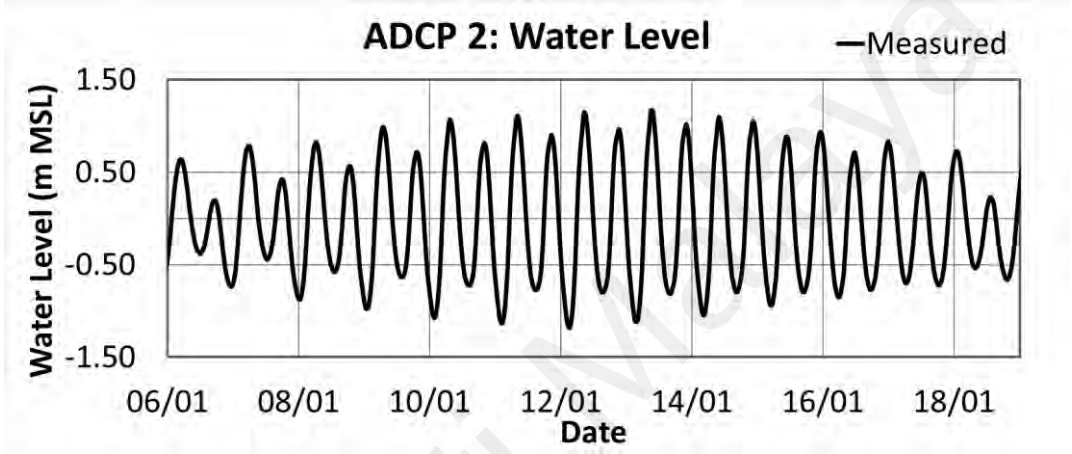

(b)

Figure 4.5: Tidal level measurement for (a) ADCP1, (b) ADCP2.

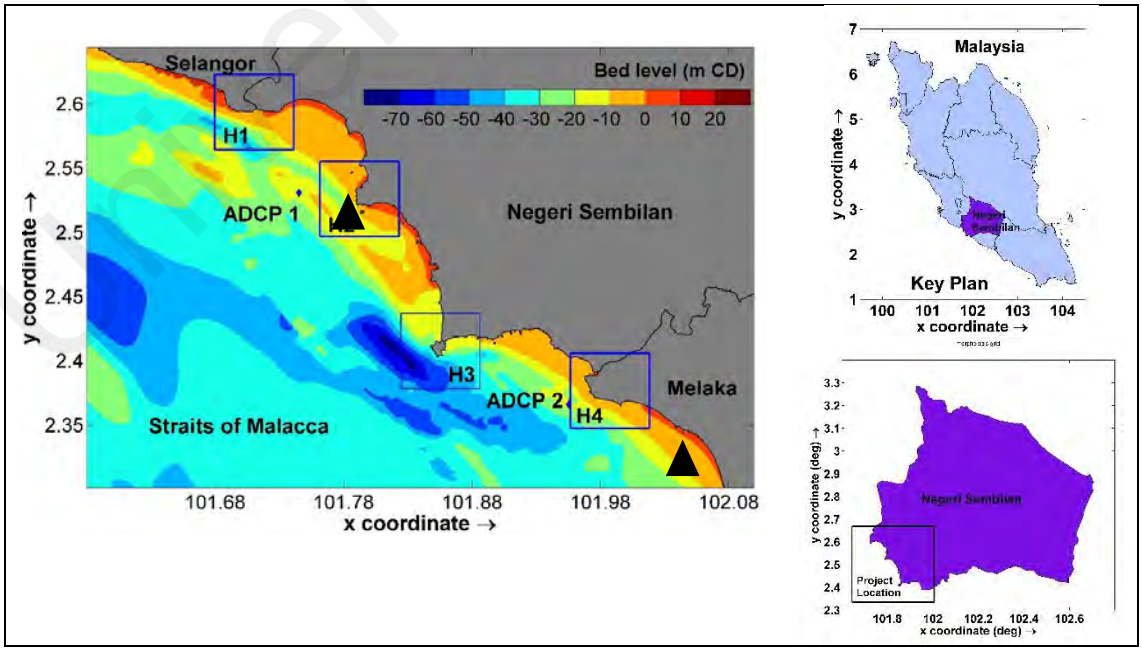

Figure 4.6: Interpolated local bathymetry and Location of ADCP1 and ADCP2

Table 4.3: Observed tidal data at ADCP1 and ADCP2

Description	Measured data		Standard Port
	ADCP1 (m MSL)	ADCP2 (m MSL)	Port Dickson
Mean Tidal level			
Mean High-Water Spring (MHWS)	1.33	0.96	1.24
Mean High-Water Neap (MHWN)	0.55	0.52	0.41
Mean Low Water Neap (MLWN)	-0.38	-0.52	-0.41
Mean Low Water Spring (MLWS)	-0.99	-0.96	-1.24
Lowest Astronomical Tide (LAT)	-1.23	-1.17	-1.55
Neap Tidal Difference	0.93	1.04	0.82
Spring Tidal Difference	2.32	1.92	2.48
Maximum Tidal Level			
Higher High Water Spring (MHWS)	1.70	1.15	
Higher High Water Neap (MHWN)	0.97	0.72	
Lower Low Water Neap (MLWN)	-0.74	-0.54	
Lower Water Spring (MLWS)	-1.24	-1.18	
Maximum Spring Tidal Difference	2.94	2.33	
Maximum Neap Tidal Difference	1.71	1.26	

4.2.2.2 Current Velocity

Two numbers of Acoustic Doppler Current Profilers, ADCP1 and ADCP2, were deployed at the same locations as described and illustrated in **Figure 4.6** to measure the current velocity at the study area. The time series of the current velocity data is as shown in **Figure 4.7**.The current velocity measurement was done in the same duration concurrently with water level measurement to cover both neap and spring tide events.

A summary of the measured mean and maximum currents at ADCP1 and ADCP2 are tabulated in **Table 4.4**. The data showed that three bays of Negeri Sembilan shoreline had similar mean current speed, approximately 0.5 m/s during spring tide. The most northern bay and middle bay also had similar maximum current speed, ~ 0.9 m/s during tide. While the maximum current speed captured during neap tide varied, 0.76 m/s, 0.58 m/s and 0.64 m/s.

The measured current data for ADCP 1 and ADCP 2 are checked with the phase of tidal levels as illustrated in **Figure 4.7**. It can be observed that low current velocity during slack is observed to coincide with the high and low tides. Besides that, high current velocity is observed during mid-flood and mid-ebb tide. A distinct pattern for the correlation of the phase verified the validity of the measured current velocity to be adopted for numerical modelling.

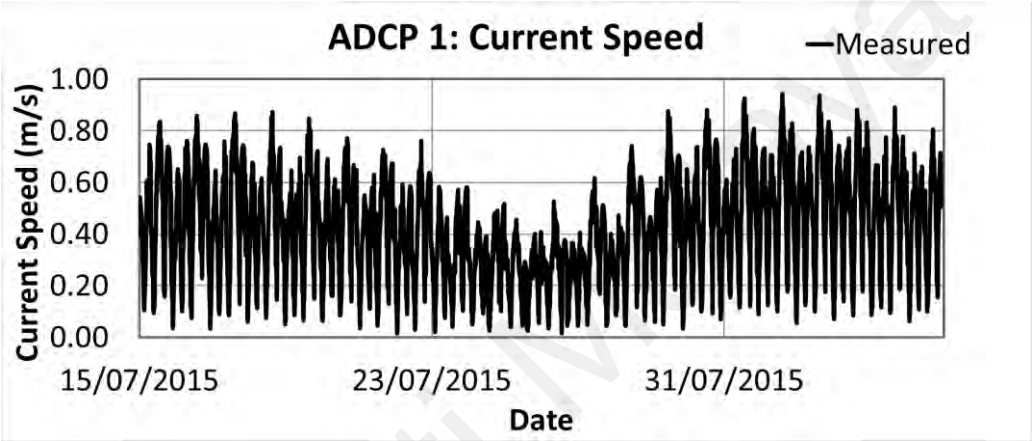

(a)

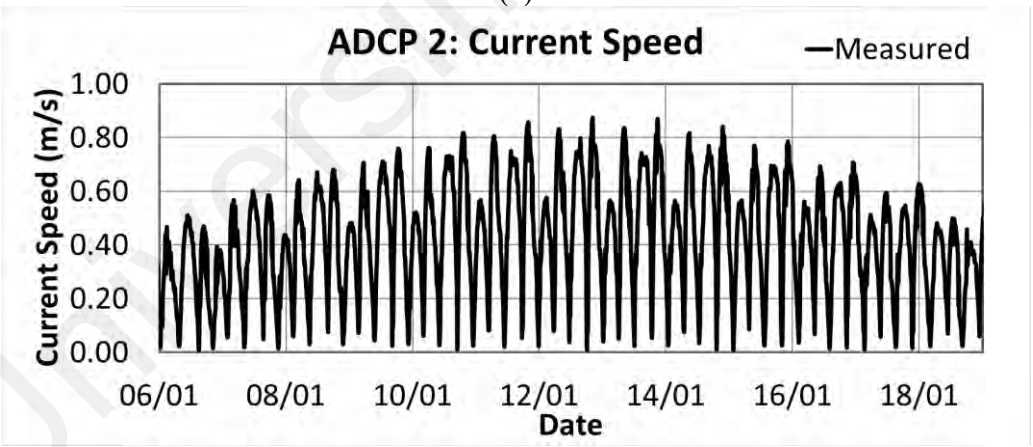

(b)

Figure 4.7: Current velocity measurement for (a) ADCP1 and (b) ADCP2

Table 4.4: Recorded mean and maximum current at ADCP1 and ADCP2

Station	Tidal Condition	Mean Current Speed (m/s)	Maximum Current Speed (m/s)
ADCP1	Spring	0.49	0.94
	Neap	0.30	0.76
ADCP2	Spring	0.50	0.87
	Neap	0.35	0.64

4.2.2.3 Seabed Condition

The bathymetric survey was carried out in 2018 and 2019 within the study area. The survey area covers approximately 37 km along the coastal zone from Kuala Sg Sepang to Tg Tuan Headland as shown in **Figure 4.8**. The sounding intervals for sea bathymetric survey are 50m and 100m. The bathymetric survey also covered drainages and rivers.

The bathymetry of the study area ranged from about -65m to 65 m MSL. The tip of Port Dickson and Tg Tuan Headland have considerably deep seabed, ranging from 25 to 65 m MSL at the offshore area of the headland. The tip of Tg Tuan Headland is observed to have deepest seabed, up to 65m MSL. An elongated of tidal ridges of 20 km length is observed within Cell 1 and Cell 2 bay. The depth of the tidal ridge is range from 0 to 10 m MSL. A deeper area which parallel with the shoreline is observed along the Port Dickson and Tg Tuan Headland. Despite that, Kuala Sg Sepang Headland is observed to have shallow seabed, generally less than 25 m MSL. The measured bathymetry was checked against with the Admiralty Chart from Royal Malaysian Navy. In overall, the pattern of seabed changes is similar with the Admiralty Chart data No 3546 (Pelabuhan Klang to Melaka) (**Figure 4.8**) obtained from Royal Malaysian Navy published on 30th June year 1989. However, the magnitude is slightly different due to the changes of seabed condition over the years. A more detailed bathymetry data at the nearshore area can be adopted for numerical modelling.

It is to be highlighted that the most southern bay (Tg Tuan to Kuala Sungai Linggi Headland) of Negeri Sembilan shoreline was not able to be captured during the course of study due to funding issue. However, bathymetric measurement at this bay should be carried out once sufficient fund is made available.

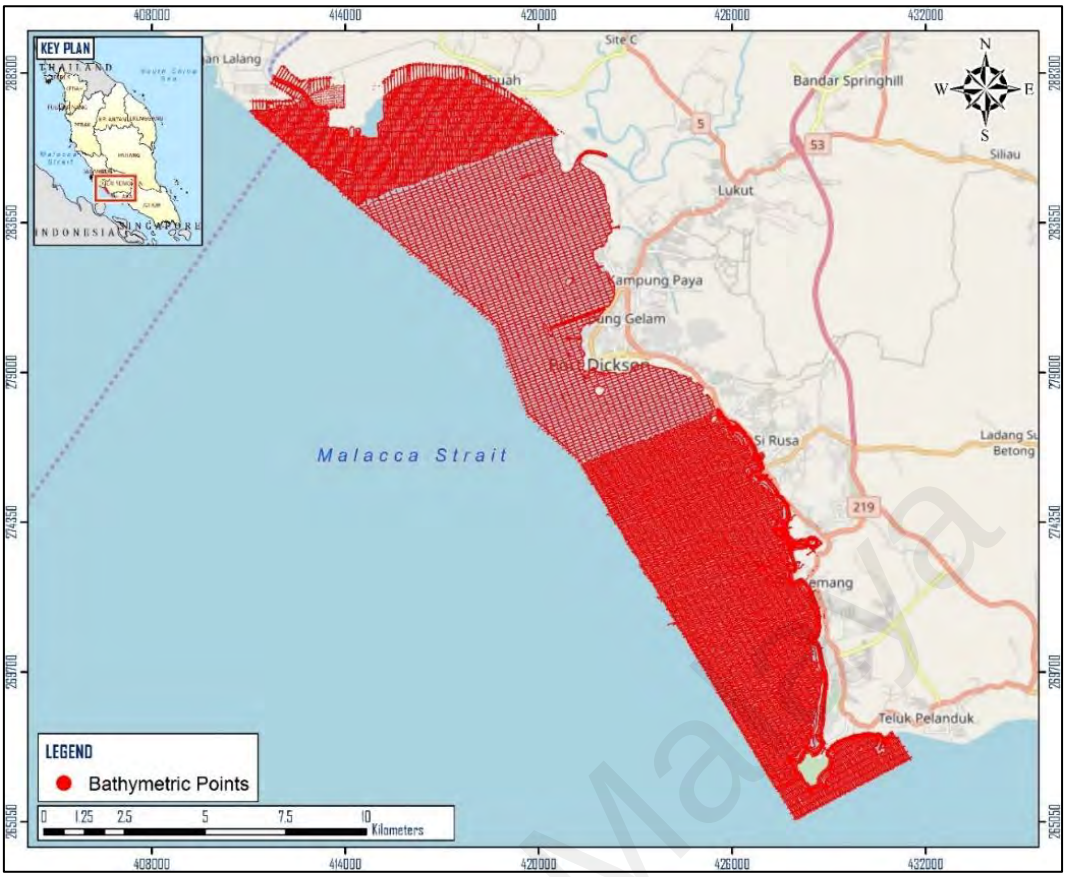

(a)

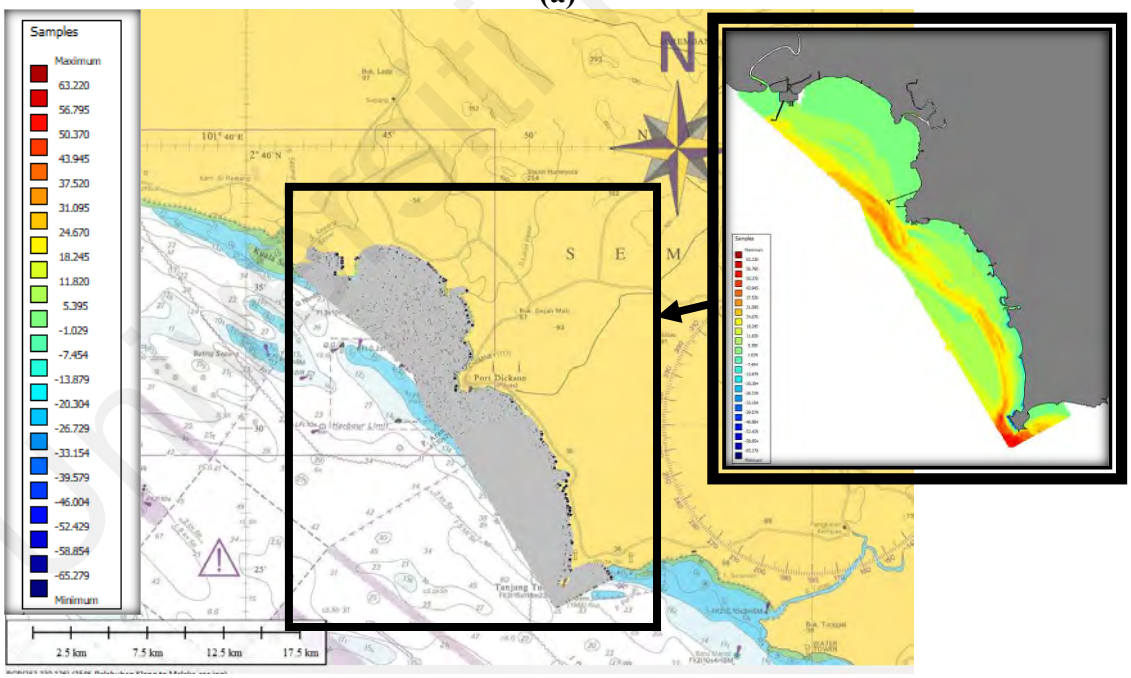

(b)

Figure 4.8: The bathymetry data validation with (a) coverage location (b) Admiralty Chart No 3546 (Pelabuhan Klang to Melaka)

4.2.2.4 Marine Water Quality - Total Suspended Solid (TSS)

Water sampling for Total Suspended Solid (TSS) had been carried out for this study. First water sampling survey which capturing 12 sampling points was carried out in March 2018 and second water sampling survey was carried out in February 2019 by collecting samples at nine water sampling points along the Negeri Sembilan shoreline. The locations of water sampling are as shown in **Figure 4.9**.

TSS is the total suspended solids in the water column sampled, which included a complex mixture of solid organic and mineral substances. TSS results are tabulated in **Table 4.5**. The results of the TSS recorded ranged from 30 mg/L to 64mg/L. The highest average TSS value of 82 mg/L was located near Tanjung Tuan Beach and the lowest of 15mg/L at near Kampung Paya.

Table 4.5: TSS obtained from Water Sampling (February 2019)

Stations	Total Suspended Solids (TSS) (mg/L)			
	Top	Middle	Bottom	Average
P1	17	53	20	30
P2	37	30	33	33
P3	7	7	30	15
P4	47	73	73	64
P5	43	7	57	36
P6	43	7	20	23
P7	137	57	53	82
P8	57	57	77	64
P9	27	47	7	27

Table 4.6 shows the TSS data captured in year 2018. The TSS recorded are ranged from 4mg/L to 6mg/L. The highest average TSS value of 9mg/L was at Sungai Linggi River mouth. The TSS levels at all sampling stations are considered less than 10mg/L.

Table 4.6: TSS obtained from Water Sampling (March 2018)

Stations	Total Suspended Solids (TSS) (mg/L)			
	Top	Middle	Bottom	Average
WS1	6	4	5	5
WS2	4	3	6	4
WS3	5	4	4	4
WS4	6	6	5	6
WS5	6	4	4	5
WS6	5	4	4	4
WS7	8	10	9	9
WS8	6	6	5	6
WS9	5	4	5	5
WS10	6	6	3	5
WS11	4	6	4	5
WS12	4	5	4	4

4.2.2.5 Seabed Soil

Grab sampling was taken at the same locations concurrently with TSS water samplings. The Particle Size Distribution (PSD) graphs obtained from grab sampling is used to determine the mean grain size (D_{50}) and the settling velocity of sediment within the Project site.

Grab sampling results from grab sampling March 2019 are tabulated in **Table 4.7**. Based on the tabulated results, P9 which located near Teluk Kemang has the highest clay and silt content with 24% and 48%, respectively. Point P1 at Sungai Sepang rivermouth as shown in **Figure 4.9** contains the highest percentage of sand with 89% and 10% of clay and silt sediments. The study area site comprises of high percentage of sand sediment above 70%, with low content of clay sediments less than 20%.

The sampling data taken in March 2018 is tabulated in **Table 4.8**. The grab sampling results showed that the samples near the coastline especially at the river mouth have higher clay and silt content, particularly point WS7 near Sungai Linggi river mouth with 96%, point WS3 at Sungai Sepang Besar river mouth with 61%, and point WS10 at Sungai Lukut river mouth with 56%. Point WS5 at the Avillion Admiral Cove has 29%

of fine sediments. The proposed Project site comprises of high percentage of sand sediment above 90%, with low content of clay and silt sediments less than 10%. Data of 2019 was checked with 2018, it was found that the seabed material of the study are mostly remain similar. Hence latest data captured in year 2019 will be used for modelling purpose

Table 4.7: Results from Grab Sampling (February 2019)

Sampling No.	Bulk Density (Mg/m3)	Dry Density (Mg/m3)	D_{50} (mm)	Grain Size Analysis (%)			
				Clay	Silt	Sand	Gravel
P1	1.61	1.26	0.1529	10		89	1
P2	1.87	1.41	0.1064	2	18	80	0
P3	1.74	1.19	0.0997	4	24	72	0
P4	1.57	0.91	0.0519	15	41	44	0
P5	1.77	1.19	0.5477	8		72	20
P6	1.62	0.99	0.0889	4	38	57	1
P7	1.90	1.40	0.1529	18		79	3
P8	1.55	0.85	0.0385	18	48	34	0
P9	1.54	0.77	0.0240	24	48	27	1

Figure 4.9: Grab and water sampling location points

Table 4.8: Results from Grab Sampling (March 2018)

Sampling No.	D_{50} (mm)	Grain Size Analysis (%)			
		Clay	Silt	Sand	Gravel
WS1	0.45	5		91	4
WS2	0.49	4		96	0
WS3	0.034	13	48	36	3
WS4	0.42	4		96	0
WS5	0.19	12	17	69	2
WS6	0.5	3		97	0
WS7	0.006	35	61	4	0
WS8	0.43	3		95	2
WS9	0.41	3		96	1
WS10	0.0049	22	34	41	3
WS11	0.62	1		98	1
WS12	1.2	4		69	27

4.2.2.6 Meteorological Condition

Four monsoon seasons can be distinguished based on the wind flow over west coast of Peninsular Malaysia, namely, southwest monsoon, northeast monsoon and two shorter periods of inter-monsoon seasons (**Table 4.9**).

Table 4.9: Monsoon seasons experienced in Malaysia.

Monsoon	Month(s)
Northeast (NE)	November to March
Southwest (SW)	May to September
Inter-monsoon (i)	April
Inter-monsoon (ii)	October

The Strait of Malacca lies within the equatorial region of low atmospheric pressure and has a typical tropical climate. The southern sea area of the Strait tends to be less pronounced with light and more variable winds. Typhoons does not occur, and gales are infrequent. Squalls are common in the Strait of Malacca.

The predominant winds over the Strait of Malacca are monsoon winds. The NE Monsoon blows from November to March, while the SW Monsoon blows from May to September. The months of April and October are considered as the Inter-monsoon period,

which is a period of rest between the NE and SW Monsoon seasons that allows for the monsoon winds to change directions. The most significant period when squalls tend to occur are between April and November. These squalls are usually accompanied by thunderstorms and torrential rainfall.

The presence of elevated land masses, such as hills and mountains around the meteorological station influences the wind measurement. Consequently, wind data from land base stations may not be representative for the Project Site, which is located at the coastal zone. Hindcast offshore wind and wave data were thus obtained at the middle area of the Strait from BMT Eastern Australia Pty Ltd (BMT) at location 2°30'N, 101°15'E for 3-hourly time series covering a period of 28 years and 5 months from January 1990 to May 2018.

All the wind and wave roses directions are indicated as "FROM" and in nautical degrees. The overall wind speed and direction are illustrated as wind rose diagrams. The annual offshore wind and wave rose at the BMT location is presented in **Figure 4.10** and **Figure 4.11**. The location of the Offshore Hindcast data is shown in **Figure 4.12** and **Figure 4.13**.

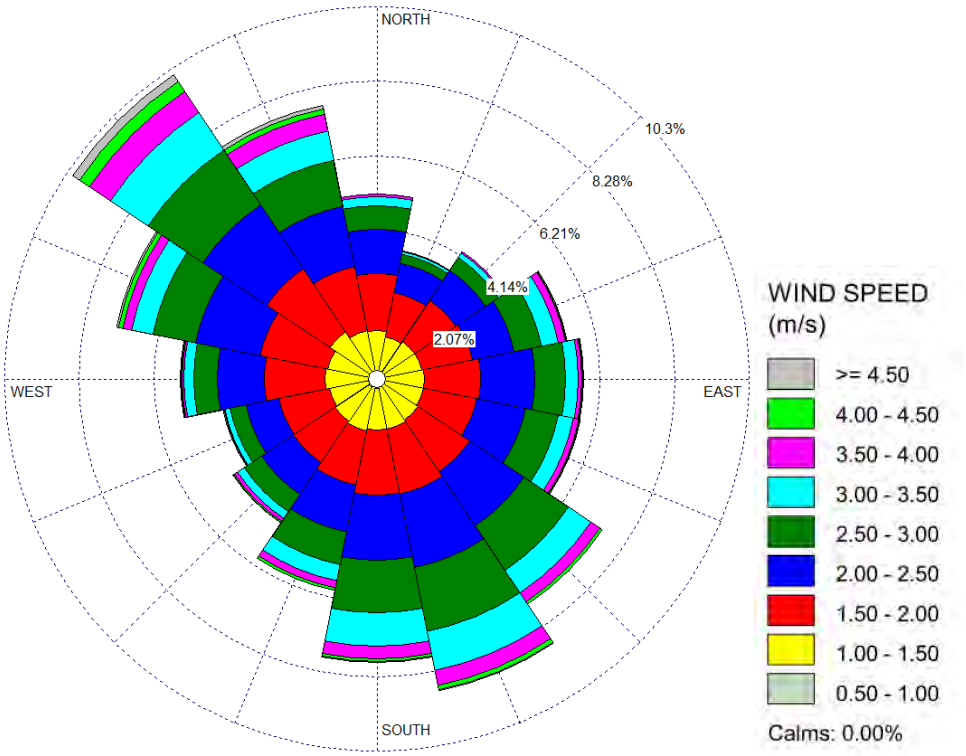

Figure 4.10: Annual Wind Rose (January 1990 to May 2018)

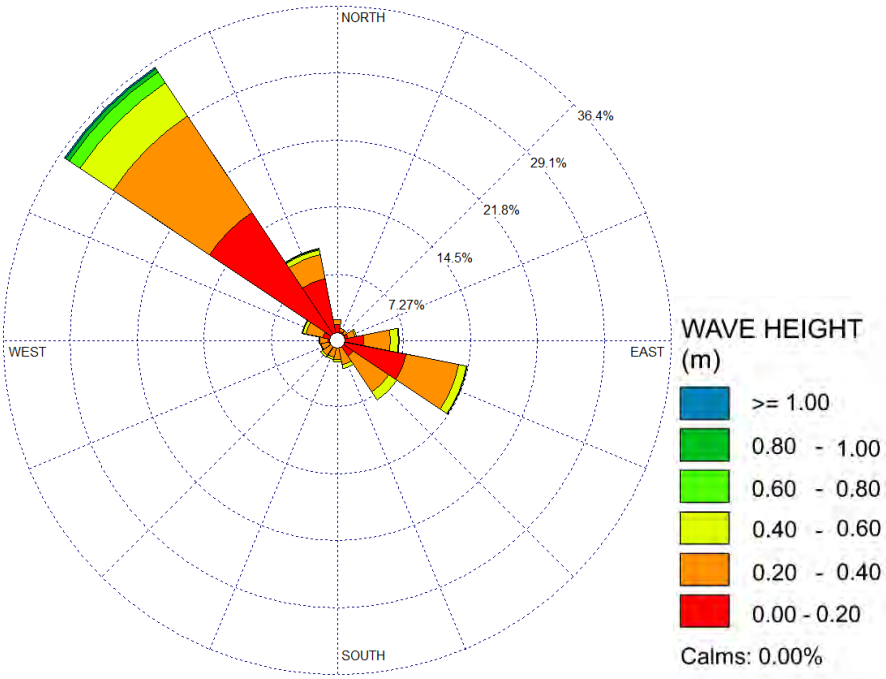

Figure 4.11: Annual Wave Rose (January 1990 to May 2018)

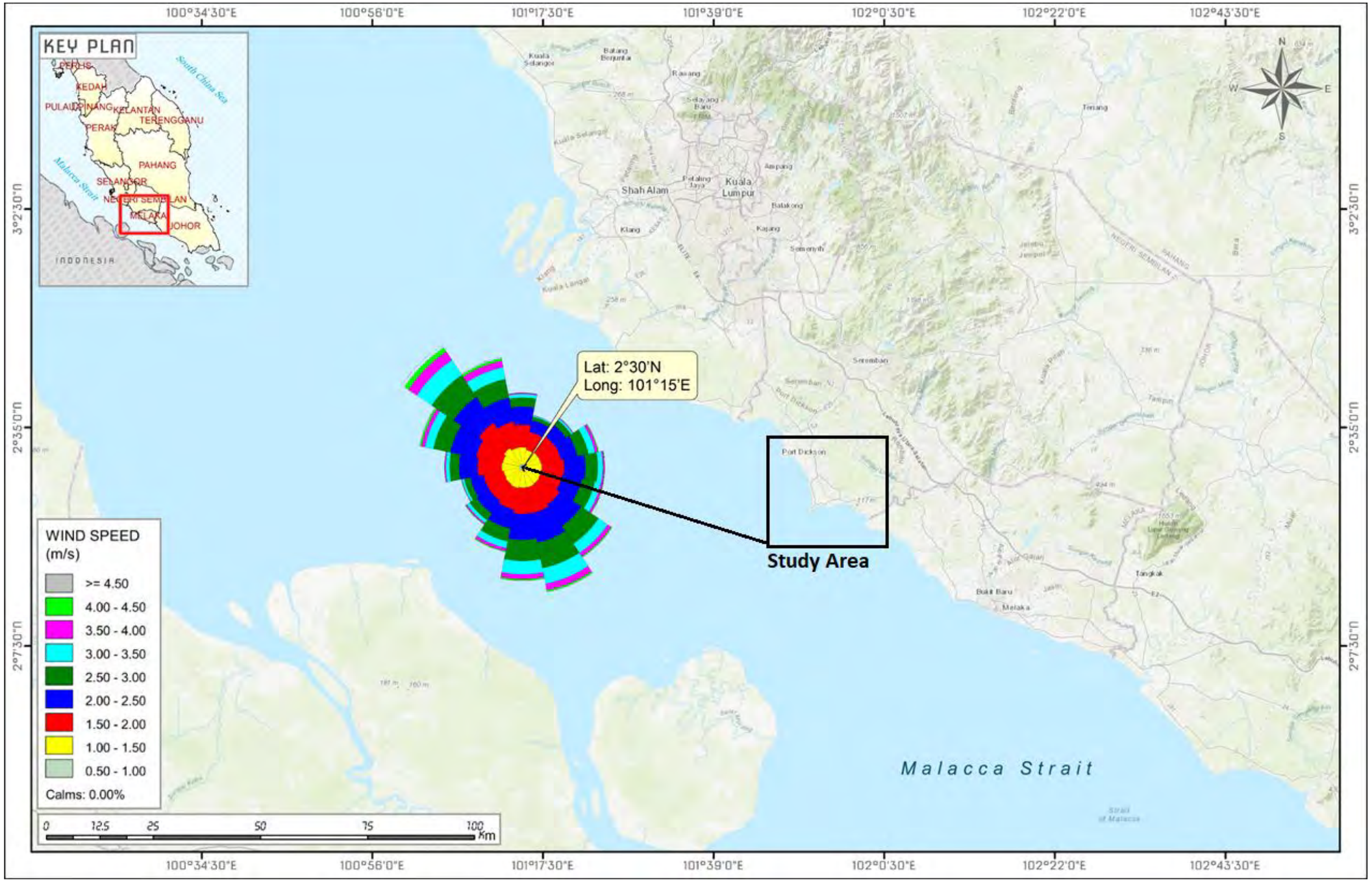

Figure 4.12: Geographical location of the offshore wind rose derived from BMT data (1990 – 2018)

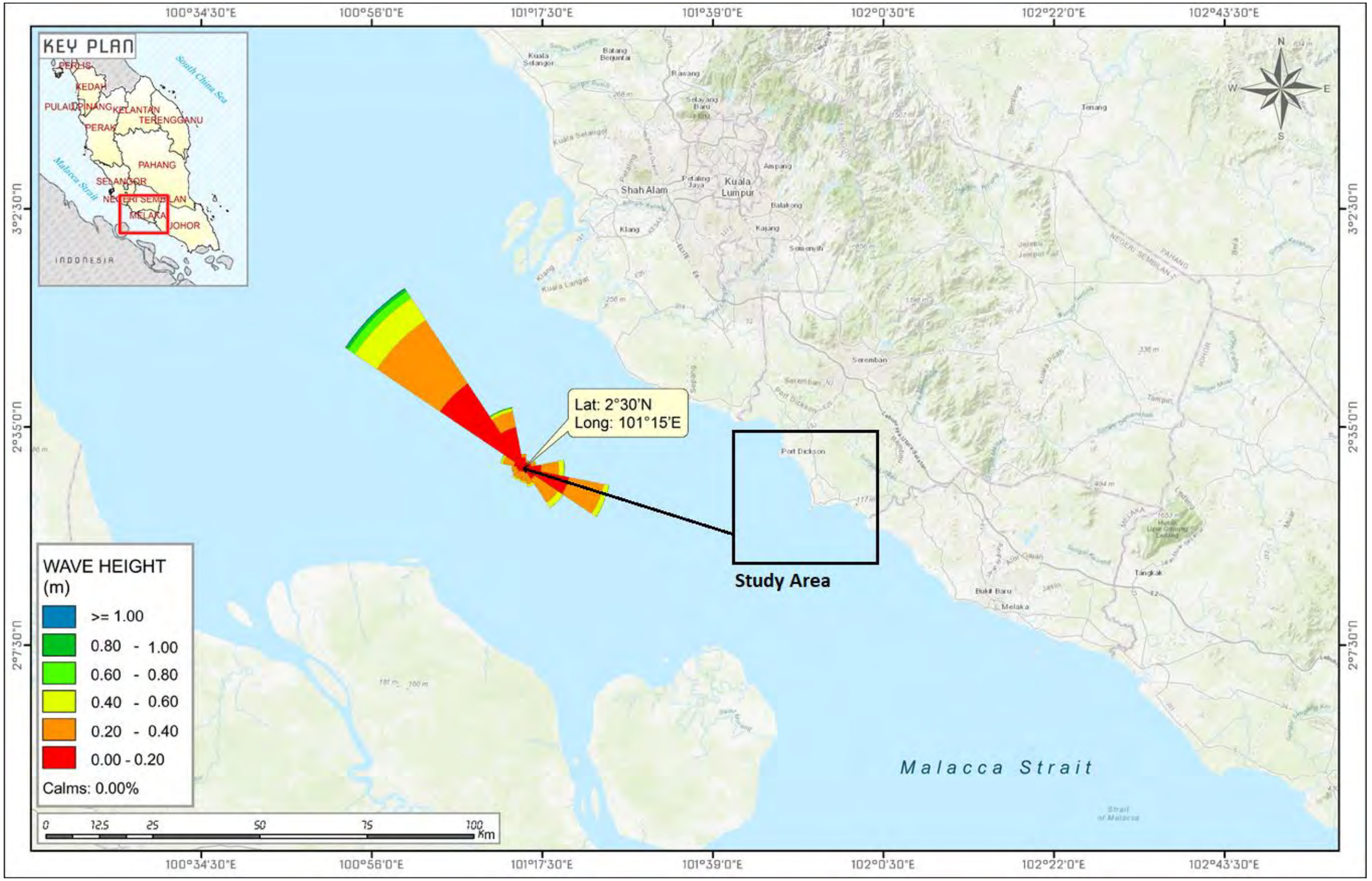

Figure 4.13: Geographical location of the offshore wave rose derived from BMT data (1990 – 2018)

The wind rose in **Figure 4.14** shows that the dominant wind directions are blowing from north west and south east direction for annual wind rose, corresponding to NE and SW monsoon seasons respectively. The typical wind speed class was between 1 m/s and 2.5 m/s coming from all directions, while the stronger winds up to 4.5 m/s blew from the dominant directions, Northwest and Southeast. Stronger winds that were beyond 4.5 m/s mainly comes from the Northwest direction. The offshore hindcast data shows that there were no calm periods (wind speed that are less than 0.5 m/s) experienced at the location throughout the whole period.

Figure 4.14 (ii) shows the wind rose during NE Monsoon, with the dominant wind blowing from Northwest and Northeast direction due to the NE monsoon. Although the monsoon winds originate from the Northeast direction, due to the presence of land masses that obstructs the wind, the dominant direction for an offshore location is influenced by the angle of the Malacca Strait, where the open water allows for the wind to blow and develop without obstruction. Consequently, the wind blows more frequently and stronger from the Northwest direction during NE monsoon.

Similarly, the same factor applies for SW monsoon as shown in **Figure 4.14(iii)**, where the dominant wind blows from the Southeast direction despite the main wind originating from the Southwest direction. The angle of the Straits of Malacca influences the dominant wind direction along the Strait. The wind roses for the inter-monsoon period in April and October are shown in **Figure 4.14(iv)** and **Figure 4.14(v)**, respectively. The general trend of the two wind roses is similar, with the wind blowing dominantly from the north west direction during the resting period. The annual wind class frequency distribution is presented in **Figure 4.15**.

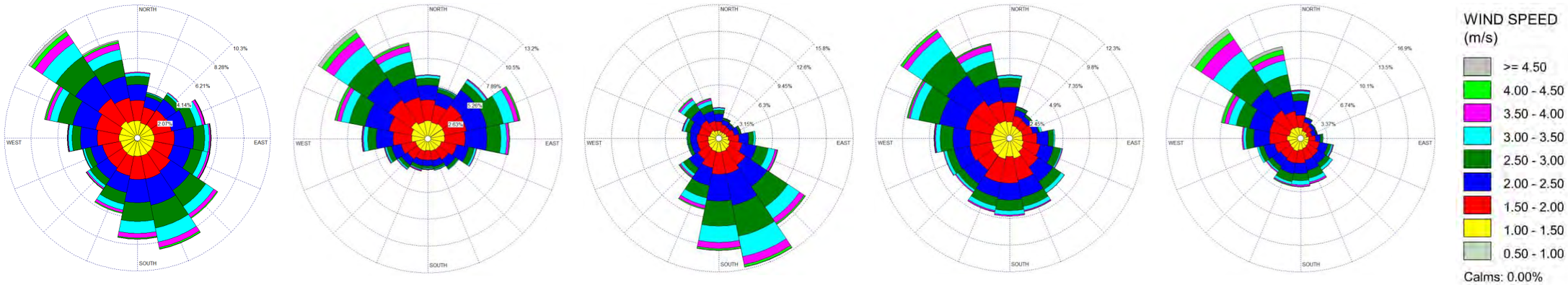

(i)
Annual Wind Rose
(January – December)

(ii)
North East Monsoon Wind Rose
(November – March)

(iii)
Southwest Monsoon Wind Rose
(May – September)

(iv)
Inter Monsoon (i) Wind Rose
(April)

(v)
Inter Monsoon (ii) Wind Rose
(October)

Figure 4.14: Annual and monsoonal offshore wind rose at Longitude 101°15'E, Latitude 2°30'N

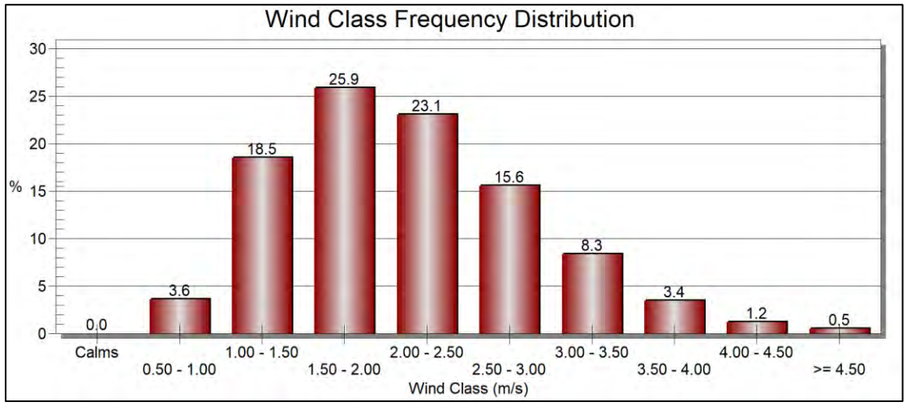

Figure 4.15: Wind class frequency distribution for 28 years of wind speed from BMT data

The overall wave height and direction are illustrated as wave rose diagrams. The monsoonal wave roses clustered by the monsoon seasons are indicated in **Figure 4.16**. The annual wave height frequency distribution is presented in **Figure 4.16**. In general, two dominant wave directions are noted coming from the northwest and southeast directions as shown in **Figure 4.16(ii)**. These dominant waves highly correlate to the direction of the prevailing winds. The overall wave heights are typically within the range of 0 m – 0.4 m. The waves coming from the north west direction is considered most dominant, with high frequency and wave heights reaching up to 1 m. The annual event frequency of the Northwest direction is around 45% of the overall records. Waves from the north west direction occurs throughout the year but shows a more pronounced and consistent development during NE monsoon and inter-monsoon seasons with event frequencies reaching up above 50%. During SW Monsoon, the dominant waves are divided into two opposing directions, north west and south east as shown in **Figure 4.16**Error! Reference source not found.**(iii)**. The waves coming from south east direction is developed by wind blowing during SW monsoon. The frequency for waves coming from north west and south directions are respectively around 32% and 36% during SW monsoon. The annual wave class frequency distribution is presented in **Figure 4.17**.

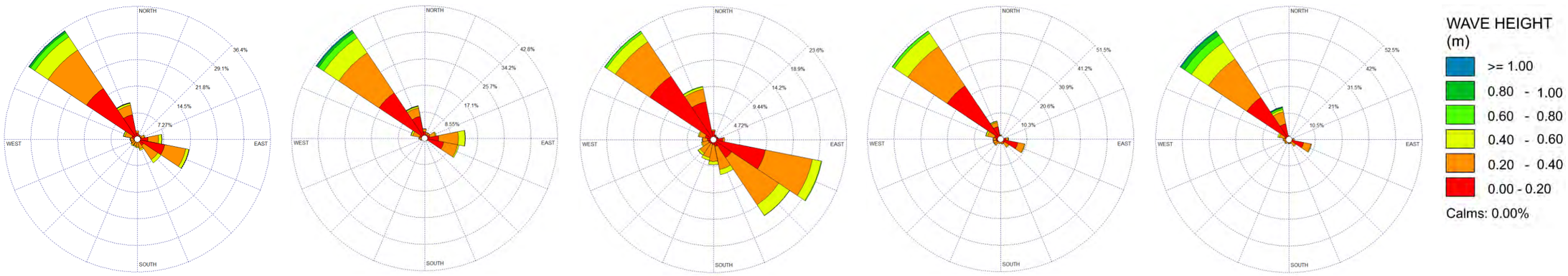

(i)
Annual Wave Rose
(January – December)

(ii)
North East Monsoon Wave Rose
(November – March)

(iii)
Southwest Monsoon Wave Rose
(May – September)

(iv)
Inter Monsoon (i) Wave Rose
(April)

(v)
Inter Monsoon (ii) Wave Rose
(October)

Figure 4.16: Annual and monsoonal offshore wave rose at Longitude 101°15'E, Latitude 2°30'N

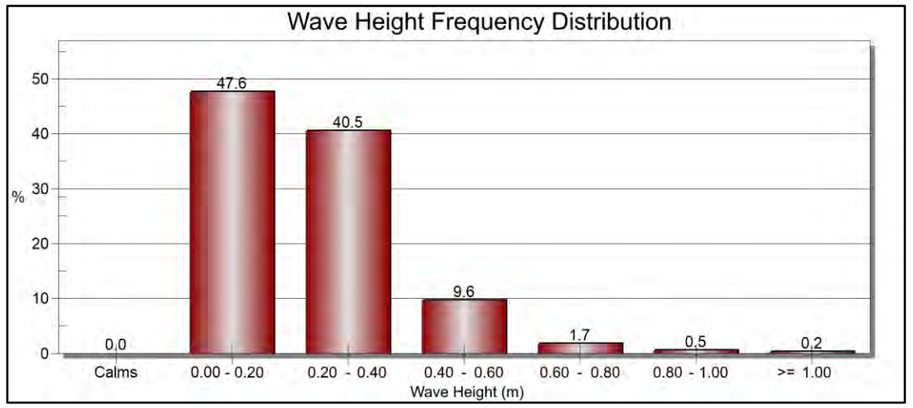

Figure 4.17: Wave class frequency distribution for 28 years of wind speed from BMT data

4.2.3 Model Domain

The workflow for numerical modelling consists of four main steps (**Figure 4.18**). As for first step, the Straits of Malacca regional model was constructed using Delft3D-RGFGRID to generate a curvilinear and boundary-fitted spherical co-ordinate. The remaining bathymetry of the model was derived from General Bathymetric Chart of the Oceans (GEBCO) data. The time series boundary conditions were generated using TOPEX/Poseidon data. Followed by that, for step two, high resolution Delft3D model was setup at the study area. The depth of the local model was interpolated using measured bathymetry data as described in Section 4.2.3.2. In the next step, the numerical model was calibrated and validated with the measured water levels and flow velocities. Result analysis based on the modelled scenarios was carried out for time and spatial velocity, extractable energy, as well as tidal energy extraction effect analysis.

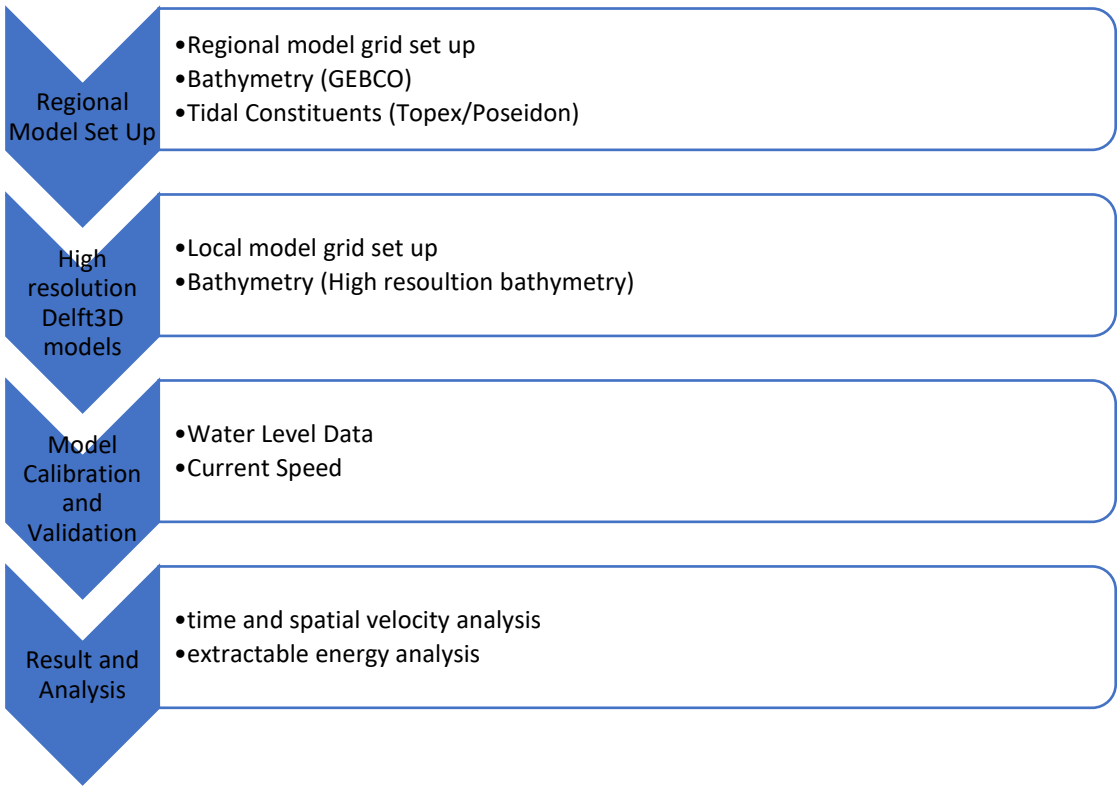

Figure 4.18: Schematic representation of the work process of Delft3D modelling for tidal current resource assessment

4.2.3.1 Model Grid Domain

Flow determination at the study site is the prerequisite for investigation of the tidal energy potential near headlands. In this study, tidal resource assessment was firstly carried out by setting up a high-resolution depth-averaged model depicting the Straits of Malacca as shown in **Figure 4.19**. The model domain grid was constructed using Delft3D-RGFGRID to generate a curvilinear and boundary-fitted spherical co-ordinate. The length of the model domain was 247 km from the northern boundary to the southern boundary. The regional model was modelled sufficiently far from the study area so that any numerical disturbance at the boundary would not disturb the model results in the area of interest. The regional model grid size was set at 1200 m x 1200 m at the outer (ocean) boundary; whereas, the grid size of the local model was gradually reduced to 100 m x 100 m to sufficiently model the four headlands hydrodynamic conditions at Negeri Sembilan Coastline.

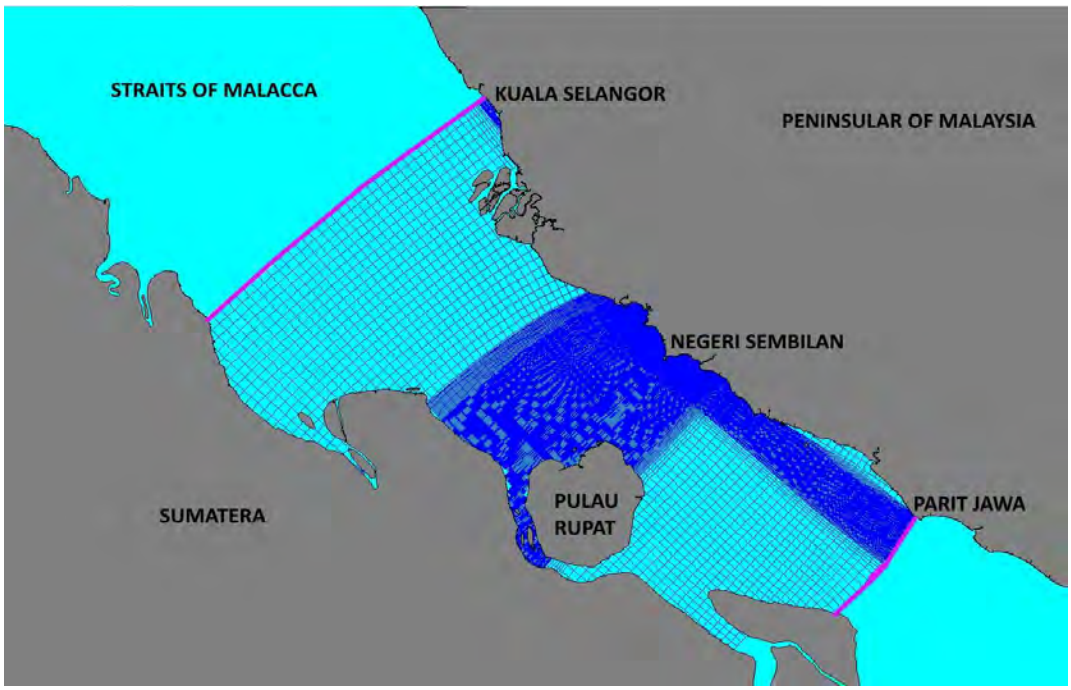

Figure 4.19: Boundary and model domain grid

4.2.3.2 Interpolated Depth

The bathymetry interpolated for the model is as shown in **Figure 4.20**. The free surface level and bathymetry were related to a horizontal plane of reference to MSL. The bathymetry of the study area was derived from General Bathymetric Chart of the Oceans (GEBCO) data (Weatherall et al., 2015) together with the survey data collected along the headlands of Negeri Sembilan as described in Chapter 3. The survey techniques, data collection, post processing, accuracy of positioning and sounding adopted in the bathymetry survey were undertaken in accordance to the International Hydrographic Organization (IHO) and Hydrographic Department of Royal Malaysian Navy (RMN) regulations as described in Chapter 3.

Figure 4.20a shows the local bathymetry of the Negeri Sembilan coast. The beach gradient of headlands H1, H2 and H4 are relatively mild compared to the headland of H3. **Figure 4.20b** shows the local bathymetry of the focused zone of Tg Tuan Headland. For three selected zones at Tg Tuan Headland, it can be seen that Zone B has deeper depth than Zone A and Zone C. When focused into the tip of Tg Tuan Headland, the depth at the tip of the headland varies from 25 – 65 m MSL.

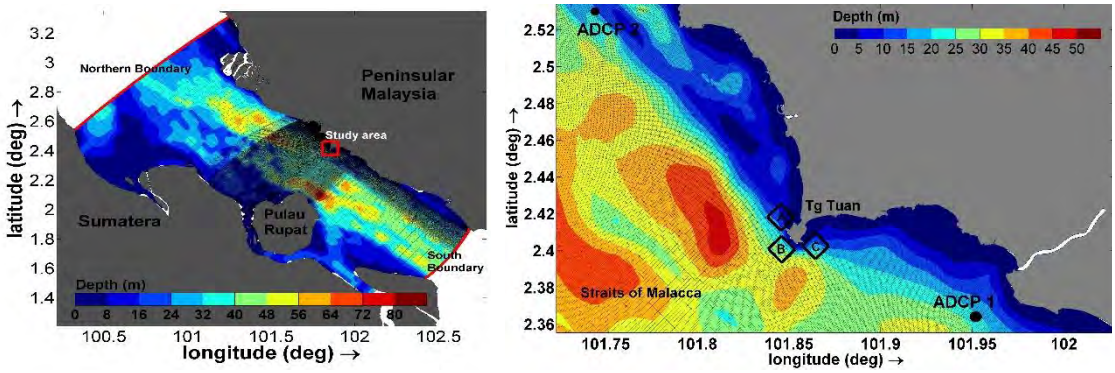

(a) (b)

Figure 4.20: Numerical model setup with interpolated bathymetry: (a) regional model grid and regional model interpolated bathymetry with northern and southern open boundaries; (b) local model grid with interpolated bathymetry-with two ADCP locations

4.2.3.3 Open Boundary

The flow was driven by a number of environmental forces, i.e., tides at the open boundaries, wind stresses at the free surface and pressure gradients. In order to include the large-scale, oceanic circulation effects in the regional model, time series boundary conditions at the northern boundary (Kuala Selangor) and southern boundary (Parit Jawa) of the developed model is as shown in **Figure 4.20a**. The boundary conditions were generated using TOPEX/Poseidon global inverse solution TPXO 7.2 developed by Oregon State University (Egbert & Erofeeva, 2002). TPXO adopted in this study is a series of global ocean tide model, which best-fits, in a least-squares sense of the Laplace Tidal Equations and altimetry data (Egbert et al., 1994; Egbert & Erofeeva, 2002). The model considered tides as complex amplitudes of earth-relative sea-surface elevation for eight primaries (i.e. M2, S2, N2, K2, K1, O1, P1 and Q1), two long periods (i.e. Mf, Mm) and three non-linear harmonic constituents (i.e. M4, MS4, MN4), on a 1440 x 721, ¼ degree resolution full global grid. Based on the Courant-Friedrichs-Lewy criterion (Courant et al., 1928), the existing model ran with a time step of 60 seconds as to ensure numerical stability.

4.3 Results

4.3.1 Varying Seabed Roughness

The seabed roughness within the model domain has a significant influence on tidal processes. The tidal current prediction to the local seabed friction was assessed. Four different Manning friction coefficients for seabed roughness were investigated. Simulations were performed over each 19 days (a total of 4 individual model runs), which covered the spring and neap tides. One location of the ADCP (ADCP 1) was used for the calibration purpose. RMSEs were calculated and weighted. For each of the bed roughness

cases considered, RMSE smaller than 10% is desired. **Table 4.10** provided the RMSEs of ADCP 1 for each simulated model, as plotted in **Figure 4.21**.

Simulation 1 with Manning value 0.020 with the least friction has over predicted current speed (**Figure 4.21**) with overly fast pace of phase change. The time series comparison of Simulation 1 with measured data shows that the current speed and water level data of Simulation 1 are much higher than measured data over the 19 days simulation. Considerably big error, with RMSE of 14.11% and 19.90% of RMSE was obtained. A larger Manning was further considered. Based on Simulation 2 with 0.025 Manning value, the magnitude of current speed for Simulation 2 is relatively more compatible with measured data; however, the phase of the current speed and water level movement are still different, slightly faster than the measured data (**Figure 4.22**). The RMSEs for simulation 2 for water level and current speed are 9.37% and 12.23%, respectively; much lower than obtained in Simulation 1. Therefore, a higher Manning value of 0.03 was further tested.

A satisfactory simulation result was obtained for Manning value 0.03, as illustrated in **Figure 4.23**. Although the current speed magnitude of simulation 3 is slightly lower than the measured data, the phase of simulated water level and current speed has matched the measured water level almost perfectly with much lower RMSE of ~ 7.01% and 9.53% , respectively were obtained. In order to test the sensitivity of the model, a higher Manning value of 0.035 was further simulated. Under-prediction of current speed and water level are observed, where the error has increased to 8.00% and 12.17%, respectively. An optimal value was achieved by adopting Manning value of 0.03. Model was further validated using ADCP 2 at the southern area of the study area. The overall performance of the model is discussed in the next section.

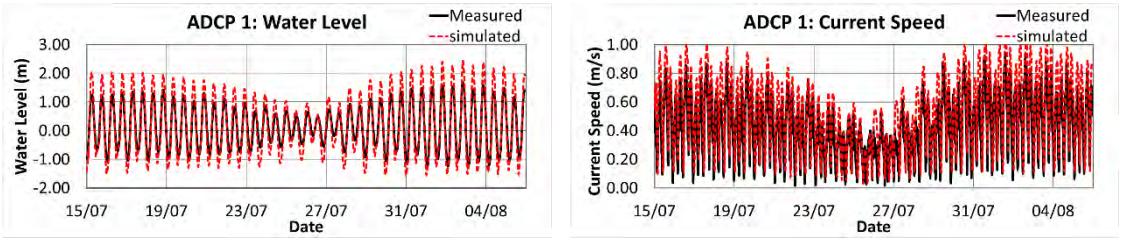

(a) (b)

Figure 4.21: Measured and predicted time series of (a) water level and (b) flow velocities for Simulation 1 (Manning = 0.020)

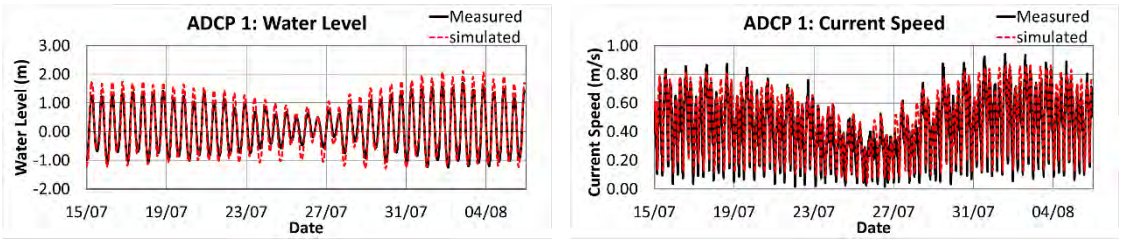

(a) (b)

Figure 4.22: Measured and predicted time series of (a) water level and (b) flow velocities for Simulation 2 (Manning = 0.025)

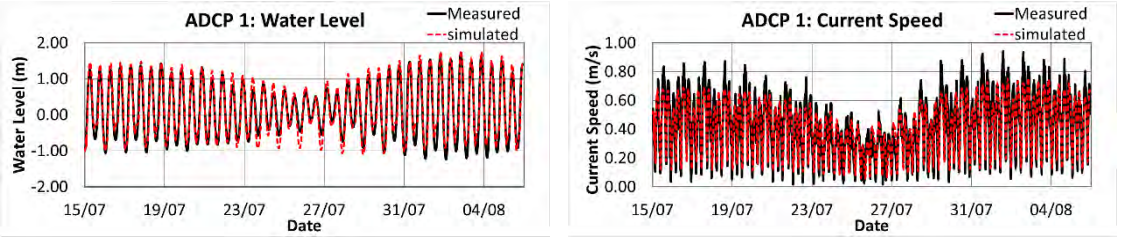

(a) (b)

Figure 4.23: Measured and predicted time series of (a) water level and (b) flow velocities for Simulation 3 (Manning 0.030)

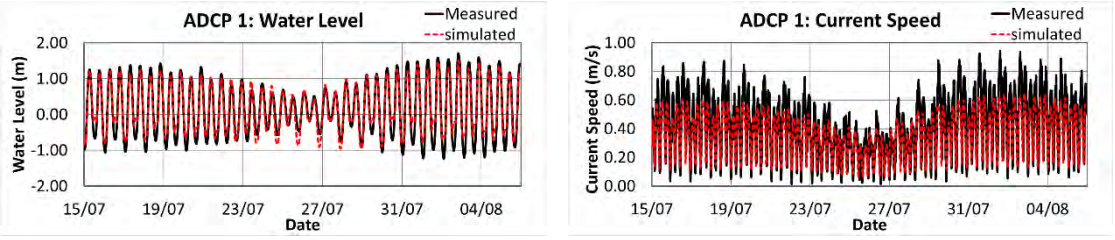

(a) (b)

Figure 4.24: Measured and predicted time series of (a) water level and (b) flow velocities for Simulation 4 (Manning = 0.035)

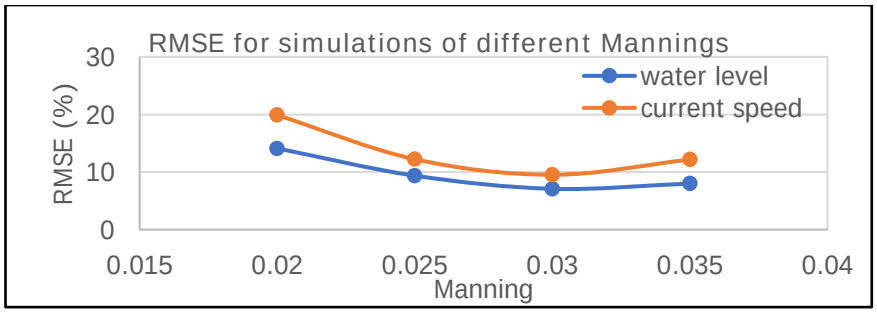

Figure 4.25: RMSE of ADCP 1 for Manning variation 0.02 – 0.035

Table 4.10: RMSEs for simulations of water level and current speed with different Manning's coefficients.

Simulation	Manning	% of RMSE	
		Water level	Current speed
1	0.020	14.11	19.90
2	0.025	9.37	12.23
3	0.030	7.09	9.53
4	0.035	8.00	12.17

4.3.1.2 Model Performance

Bathymetry is one of the main factors that governs the natural kinetic energy at the headland area. Thus, assessment of power output due to the presence of headlands using higher resolution coastal models, complemented with detailed ADCP measurements, provided a good preliminary evaluation for this study. High resolution hydrodynamic coastal models produced in this study was used for analyzing fluid flows, improving complex simulation scenarios prior to installing tidal farms, establishing maximum energy extraction area and assessing the hydrodynamic disturbance of energy extraction.

The calibrated Negeri Sembilan model using ADCP 1 (**Figure 4.23**) as discussed above has been further adopted for validation against measured water level and current velocities at ADCP2. The comparison of simulated data with measured data for ADCP 2 is graphically shown in **Figure 4.26**. A good agreement between the simulated data and the measured data for ADCP was achieved.

In assessing the overall performance of the numerical model, two Acoustic Doppler Current Profilers, ADCP1 and ADCP2 were respectively located at the northern and southern coast of Negeri Sembilan as depicted in **Figure 4.20b**. The high-resolution Delft 3D hydrodynamic model was used to reproduce water level and current speed at these locations in which the coordinates are given in **Table 4.11**. The measurement of water level and current speed covered both spring and neap tides. Due the narrowed shape of

the Negeri Sembilan within the Strait, the trough of the ebb tide travels faster than the crest of the flood tide, and therefore the ebb tide has shorter duration than flood tide (Fallon, 2012). This is because same volume of water is flowing through every stage of the tide and inducing larger ebb tide velocities than flood tide velocities. It is known as ebb-domination.

Table 4.11 summarizes the discrepancies between the measured and simulated data for ADCP1 and ADCP2. The RMSE percentage of both water level and current speed for ADCP1 and ADCP2 are less than 10%, and the coefficients of determination, r^2 are well beyond 0.9. Therefore, it is proved that the hydrodynamic model appeared to be suitable and capable of assessing the energy extraction potential at the headlands of Negeri Sembilan as well as the resulting impacts to the environment (described in the next chapter).

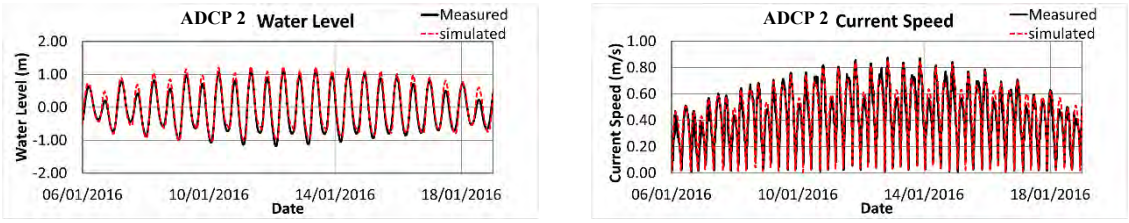

(a) **(b)**

Figure 4.26: Measured and predicted time series of (a) water level and (b) flow velocities for ADCP 2 during the validation period.

Table 4.11: Comparisons of water level and current between the measured and simulated water levels and current speeds at two stations (ADCP 1 and ADCP 2).

Station	**Longitude Coordinates (Deg)**	**Latitude Coordinate (Deg)**	**Water level**			**Current speed**		
			r^2	**RMSE**	**% of RMSE**	**r^2**	**RMSE**	**% of RMSE**
ADCP 1	101.74538 E	2.53059 N	0.95	0.043	7.1	0.96	0.008	9.1
ADCP 2	101.35083 E	2.36608 N	0.98	0.017	5.5	0.90	0.006	8.8

4.3.2 Natural Kinetic Energy Extraction

The common tidal resource estimations based on a single tidal cycle can significantly misestimate the tidal energy potential of a site. An annual resource estimate introduced differences of up to 35% depending on whether a simulation of one tidal cycle, one lunar month, or a full year (Mestres et al., 2019). The simulation considered in this study was carried out for a duration of 14 days covering both spring and neap tidal cycles.

The flow is believed to be accelerated when passing the headland. This study started with the tidal energy harnessing at the Negeri Sembilan, which consists four headlands along the coastline of about 55 km length. in. A numerical model is required to accurately simulate the problem by resolving the secondary flows (Ainsworth & Thake, 2006; Batten & Bahaj, 2006) for the assessment of depth-effect interference on tidal energy extraction. A comprehensive and detailed resource assessment by looking into headland selection specifically at the Negeri Sembilan Coastline, and subsequently a detail zone selection based on the selected headland was conducted. The findings discussed in this chapter will form a good basis for further study on the development of innovative and suitable tidal energy technologies.

4.3.2.1 Case study 1: Multiple Headlands at Negeri Sembilan

Negeri Sembilan, which is located at the central west coast of Malaysia, was selected as the study area. The state is bordered by approximately 55 km of shoreline encompasses three bays that are confined by four headlands (H1 – H4) along the coastline as demonstrated in **Figure 4.27**. The four headlands extending from Kuala Sepang Besar to Kuala Linggi are identified as the potential sites for tidal energy exploitation in Negeri Sembilan. The channel widths normal to the selected headlands are given in **Table 4.12**. The headland of Kuala Sg Sepang (H1) has the widest tidal flow passage, followed by the

headland of Port Dickson (H2), the headland of Kuala Sg Linggi (H4) and the headland of Tg Tuan (H3). The tidal current flows in the southward direction during flood tides and in the northward direction during ebb tides. During the occurrence of flood tides, H1 is the first headland to receive the incoming tidal flow, and H4 is the last headland to respond to the tides.

Table 4.12: Channel width with reference to the Negeri Sembilan headlands

Headland Location	Headland ID	Channel Width (km)
Kuala Sepang Besar	H1	75
Port Dickson	H2	63
Tg Tuan	H3	38
Kuala Linggi	H4	46

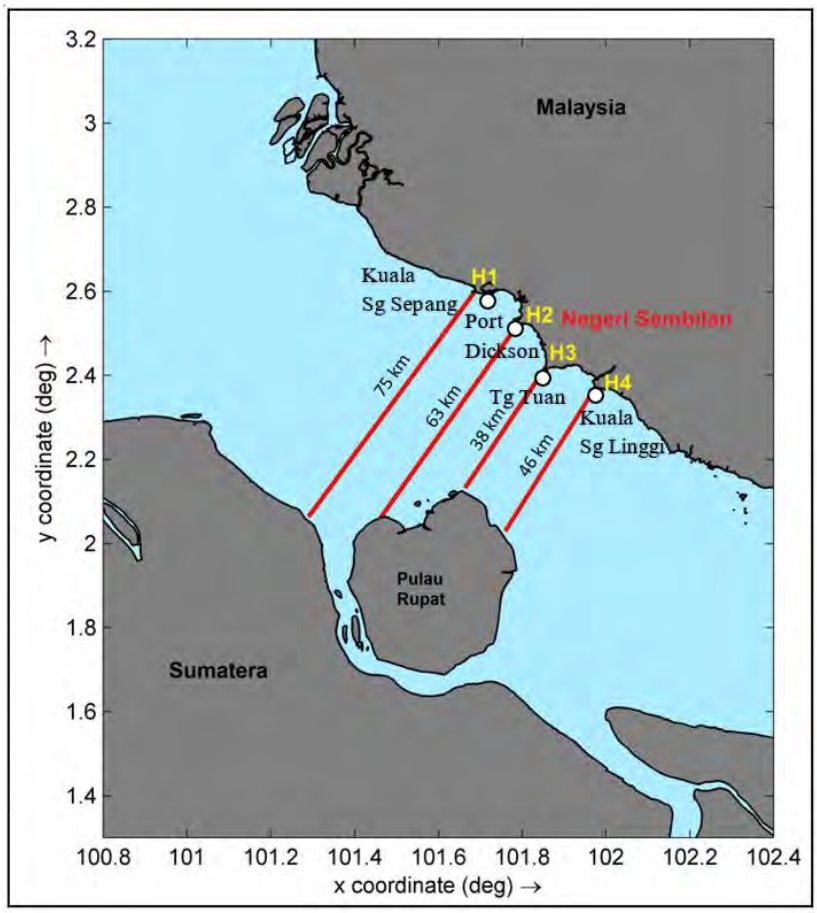

Figure 4.27: Channel flow passage along the Negeri Sembilan coastlines

The modelled flow velocity during mid flood and ebb tides are shown in **Figure 4.28**. It is seen from the figure that the tidal current propagates from southeast towards northwest during ebb tide and reverses during flood tide. The peak velocity is higher

during flood tides. The current velocity pattern at H3 is significantly different from those at H1, H2 and H4 (**Figure 4.29a** and **Figure 4.29b**). At H3, the recorded current velocity is the highest among all giving the mean and maximum velocities of 1.5 and 2.4 m/s, respectively. This is due to combined effect of the channel geometry in which the presence of Pulau Rupat close to the Indonesia coast is constricting the channel width to 38 km (**Figure 4.27**), as well as the local geographical condition at this headland. Headland H3 extends far more offshore to the deeper sea than Headland H1, H2 and H4 allowing it to receive higher current velocity during mid flood and mid ebb tides. High current velocity at H3 is also due to the presence of the submarine ridge fronting the headland. Other than that, with reference to the bathymetry map in **Figure 4.20**, the reduction of current velocity at H1, H2 and H4 is principally due to mild gradient of the beach. A sandbar is noticed in front of H1 and H2 and hence high bed shear and bottom friction are the two main factors retarding the tidal current strength.

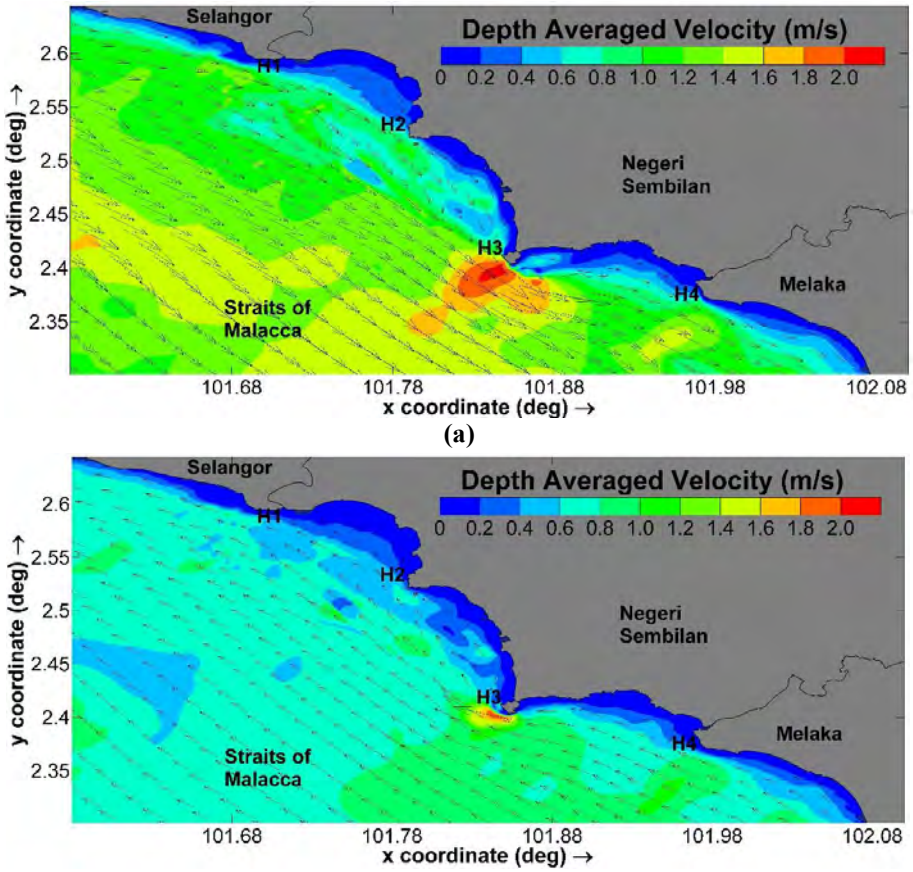

Figure 4.28: Natural distribution of flow velocity at the study area during (a): mid-flood tide and (b): mid-ebb tide

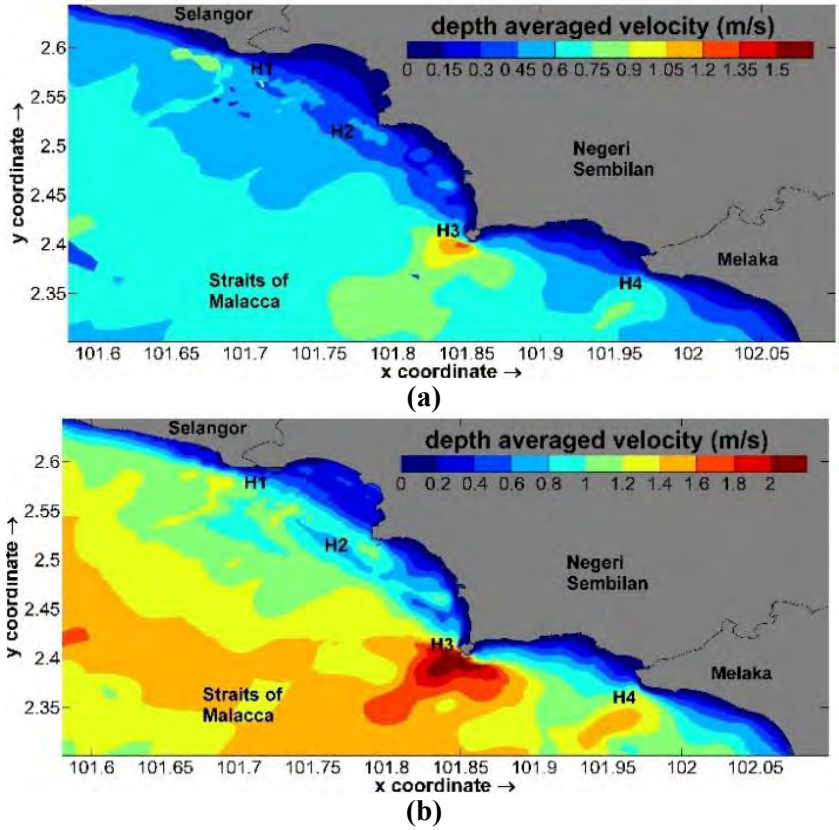

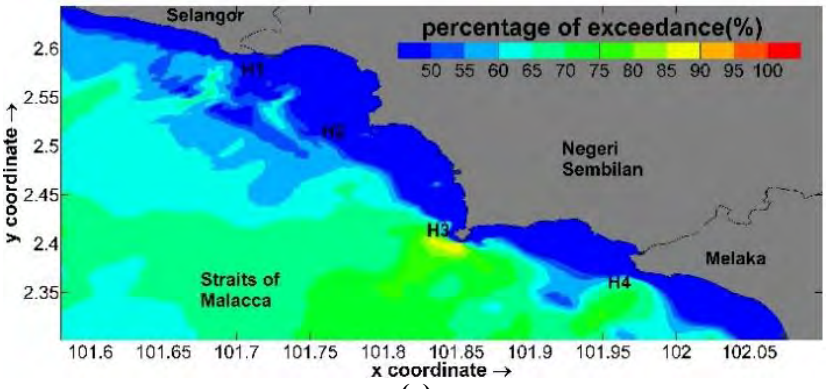

(c)

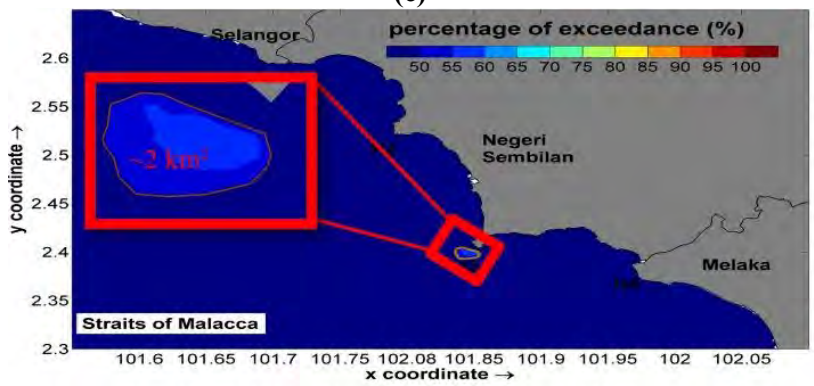

(d)

Figure 4.29: 2D map plot for assessment of the area of interest around the location of the headlands H1 – H4 for (a) mean current velocity (b) peak spring (c) percentage of exceedance for current speed > 0.5 m/s (d) percentage of exceedance for current speed > 1.0 m/s

Table 4.13 shows the summary of the mean and maximum velocities at Headlands H1, H2, H3 and H4. The variation of current velocities at Headland H1, H2 and H4 is small. The mean and maximum velocity for Headlands H1, H2 and H4 are range from 0.5 m/s to 0.8 m/s and 1.2 to 1.5 m/s, respectively. Note that the current velocity at H2 is observed to be relatively small partly due to the restriction imposed by the offshore sandbar located parallel to the headland as illustrated in **Figure 4.29.**

Table 4.13: Summary of the mean and maximum velocity at Headlands H1 to H4

Headland	H1	H2	H3	H4
Mean Velocity (m/s)	0.7	0.5	1.5	0.8
Maximum Velocity (m/s)	1.3	1.2	2.4	1.5

In terms of site suitability for installation of tidal turbines, Fraenkel (2002, 2007) and Myers & Bahaj (2005) recommended that the deployment site should have a water depth ranging from 20 to 50 m, and the flow should be uniform preferably with a peak spring flood velocity exceeding 2.0 m/s and median velocity exceeding 1.0 m/s (Fraenkel, 2007; Fraenkel, 2002; Myers & Bahaj, 2005). Note that the minimum tidal flow speed to enable the horizontal axis turbines to generate power (cut-in speed) is 1.0 m/s (Myers & Bahaj, 2005).

Figure 4.20 shows the bathymetry conditions of the Headlands H1, H2, H3 and H4, in which the water depth ranges from 15 to 50 m. The water condition at the study sites is deemed to be suitable for deployment of tidal turbines. **Figure 4.29** graphically demonstrates the 1.0 m/s exceedance probability analysis covering both neap and flood tides at the study area. It is apparent from the figure that Headland H3 has median current velocity (> 50% of probability of occurrence) of 1.0 m/s. Comparing to another potential tidal energy extraction site within Straits of Malacca studied by Sakmani et al. (2013) that the highest current speed was only up to 0.48 m/s; the current speed at Headland H3 demonstrated as a much better tidal stream energy site to be explored. The area of extractable energy at headland H3 that fulfills the median peak velocity and water depth criteria is demarcated in brown outlined area (~2 km^2) as indicated in **Figure 4.29d**. This brown outlined area can cater 233 numbers of 10 m diameter horizontal tidal turbine (Fraenkel, 2007; Fraenkel, 2002; Myers & Bahaj, 2005) where both lateral and longitudinal spacing between rows of 10 times the rotor diameter, as suggested by Chen et al. (2015) and the Legrand (2009), can produce maximum energy of 56 GWh/annum. The flow regime is converted into power output using theoretical potential in equation (3.9). According to Seng et al. (2008), 3.3 kWh of natural gas can be replaced by 1 kWh of any distributed generation electricity. Hence, with 56 GWh/annum of energy generation from tidal turbine, a total amount of 185 GWh of natural gas can be replaced

every year. Based on the outputs shown in **Figure 4.30d**, the energy extraction of tidal turbines installed at Headlands H1, H2 and H4 may not be productive due to weak current activities adjacent to the headlands. Nevertheless, with the advancement of turbine technology and the plant design enhancement, the tapping of the marine energy at these locations is still feasible (Faez Hassan et al., 2012; Hassanzadeh et al., 2017). Further assessment in considering the feasibility of deployment at lower tidal current velocity sites basing on the mean velocity of Straits of Malacca, approximately ranging 0.1 – 1.0 m/s (**Figure 4.29a**) to attain cost effective deployment, sites at headlands with median velocity higher than 0.5 m/s (**Figure 4.29c**) and peak velocity higher than 1.0 m/s (**Figure 4.29b**) with seabed ranging between 20 m to 50 m were selected as potential tidal farm.

An assessment was undertaken to compare the energy output generated at Headlands H1, H2, H3 and H4 in this study. The main device scaling parameter for horizontal axis tidal turbines is the amount of turbine thrust force applied on the fluid by the rotor. The axial induction factor with a peak value of 1/3 produces an optimum value 0.9 of tidal turbine thrust coefficient (Myers & Bahaj, 2010). However, Chen et al. (2013) assumed higher mechanical lost for the marine current energy converter thas adopted much lower thrust coefficient (0.33), which is lower than the range of 0.35–0.5 mentioned by Bahaj and Myers (2004). In this exercise, the natural kinetic energy was calculated using equation (3.22) with an assumption that the turbine thrust coefficient (C_{T1}) was 0.5 for marine current energy converter whose cut-in speed is 1.0 m/s for all tidal conditions, by adopting the validated model of Yang et al. (2013). The diameter of the turbine was set at 10 m and the flow-facing swept area (A_T) was 78.57 m^2.

The maximum extractable power is shown in the 2D map plot in **Figure 4.30a**. **Figure 4.30b - e** show the plots of kinetic power measured at Headlands H1, H2, H3 and H4. The maximum potential extractable kinetic power generated by the tidal farm at H1, H2,

H3, and H4 during peak flow are 37 kW, 7.1 kW, 98 kW, and 23 kW, respectively (**Figure 4.30b – e**). The annual power output was obtained by summing the hourly production of the extractable kinetic power throughout the simulated period and converting it to the potential energy recovered over a year using equation (3.23). As for the annual energy production, Headland H3 has the highest extractable energy (6209 kWh/m^2) while H2 has the lowest energy production (31 kWh/m^2) as displayed in **Figure 4.30b – e**. At each headland, a hypothetical tidal farm of 1.5 km x 1.5 km that met the site criteria for tidal turbine installation – 0.5 m/s median velocity and minimum water depth of 20 m, was identified (appeared as in diamond boxes in **Figure 4.30a**. In comparison to the analytical assessment using larger resolution model by (Lim & Koh, 2010) that more than 1000 kW/m^2 was estimated between the narrowest channel of Negeri Sembilan, a detailed quantitative analysis in this study which focused at the Negeri Sembilan headlands (H1 – H4) by using higher resolution model demonstrated energy potential along the same coastline with length of approximately 52 km can differ quite significantly. The hypothetical 1.5 km x 1.5 km tidal farms with enhanced energy extraction potential were calculated to have power output of approximately 5.0 GWh/year, 0.3 GWh/year, 54.9 GWh/year and 2.8 GWh/year for H1, H2, H3 and H4, respectively.

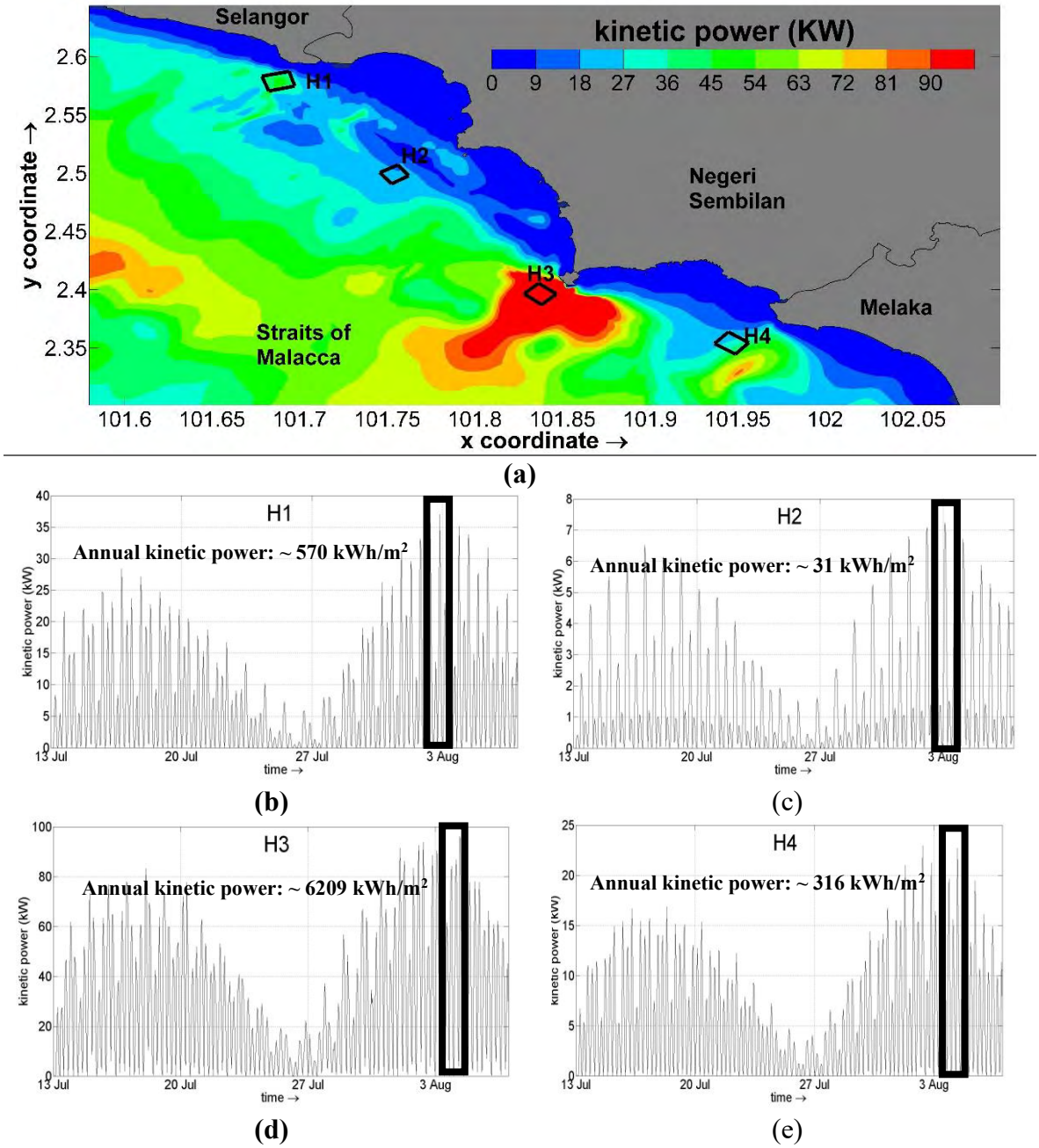

Figure 4.30: 2D map plot for (a) maximum potential extractable power; kinetic power and annual kinetic power for every single tidal turbine of (b) headland H1, (c) headland H2, (d) headland H3, and (e) headland H4 for a representative 14 days covering spring and neap tide. The black box marks the maximum potential kinetic power extractable by a single tidal turbine at peak flow.

4.3.2.2 Case study 2: Tg Tuan headland vicinity

To comprehend headland tidal resource feasibility study, a tidal resource assessment focused on a selected headland has been further studied and discussed in this chapter. Tg

Tuan Headland of Negeri Sembilan, one of the largest and most protruding headlands in Straits of Malacca is selected as case study in this research. Tg Tuan Headland is located opposite to Pulau Rapat, Indonesia as shown in **Figure 4.31a**. The headland is formed by a narrow neck of about 300 m wide. Three zones in the vicinity of Tg Tuan Headland were selected for assessment, as presented in **Figure 4.31b**. Zone A receives flooding tide flow towards the headland, Zone B is directly fronting the tip of most part of the headland, and Zone C is the sheltered area from flooding tide flow of the headland. For each zone, the available and extractable energies were determined. Note that the magnitude of the available energy was derived from the magnitude of the fluid kinetic energy in the absence of Tidal Energy Converter, TEC. The energy tapped from the headland coast is expected to power up the nearby beach resorts and hotels as listed in **Figure 4.32**.

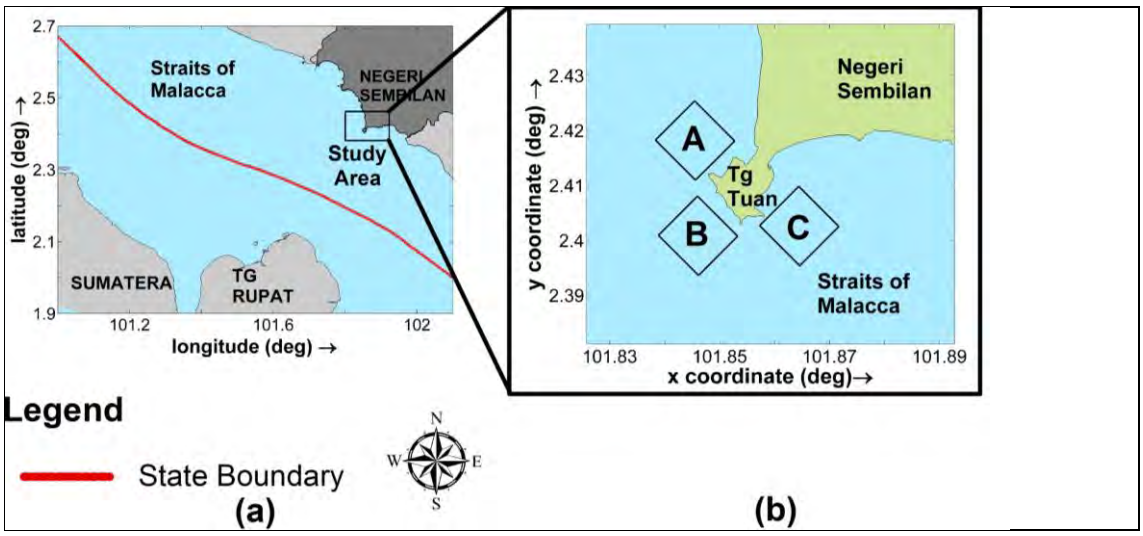

Figure 4.31: Tg Tuan Headland: (a) Geographical location and (b) the zoning for numerical modelling

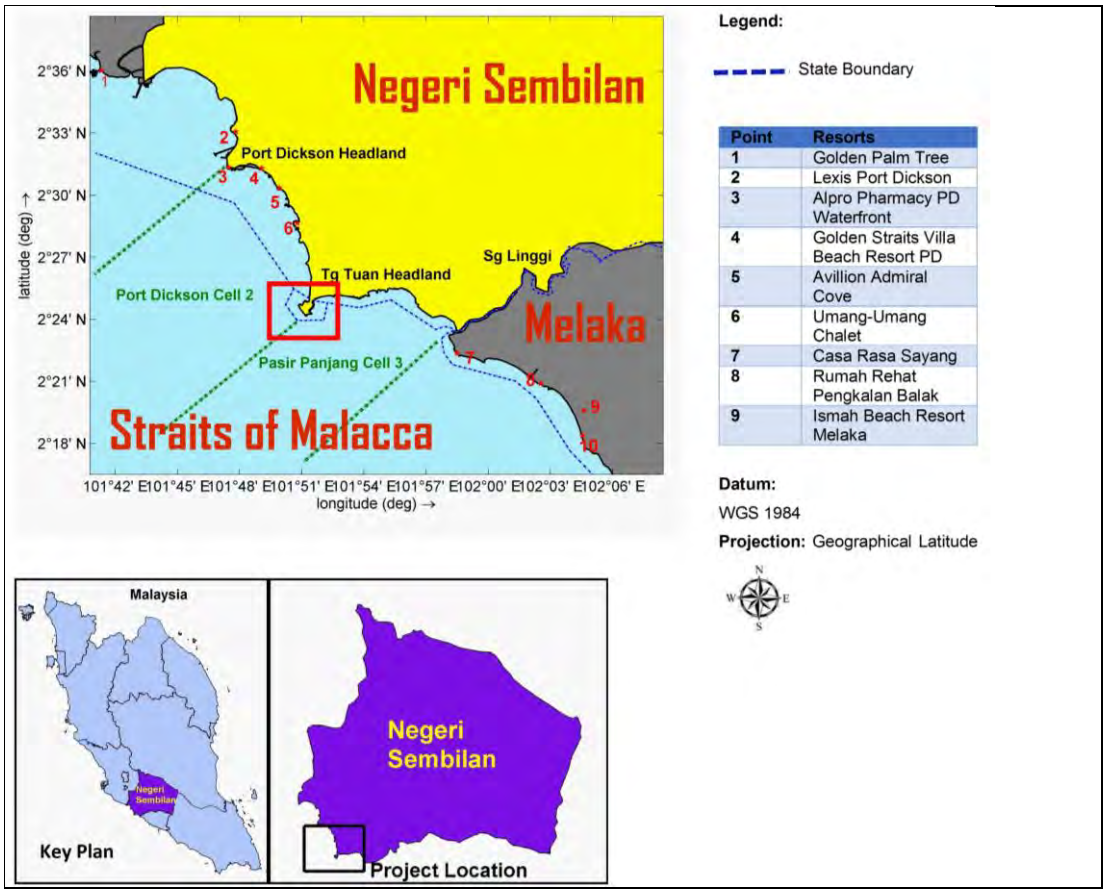

Figure 4.32: Tg Tuan Headland and its vicinity

From the analysis above, Tg Tuan Headland is identified as suitable headland for tidal energy extraction. However, complex flow circulation occurred around the headland may cause operational disturbances to the turbine rotation that limits its power take-off efficiency. It is therefore important to determine a suitable zone for TEC deployment by

applying a high resolution spatial numerical model and detail analysis at the headland area. For this numerical study, the refined model was simulated for 15 days covering spring and neap tides. The modelled flow velocity during mid flood and ebb tide are as shown in **Figure 4.33**. The tides in Zone A and Zone B propagated from southeast towards northwest during mid ebb tide and reversed during mid flood tide. A reverse of the current flow is noticeable at the downcoast (Zone C) of Tg Tuan Headland during the mid-flood tide. Similar phenomenon is also observed at Zone A during the occurrence of mid-ebb tide. A defined axial flow direction is noticeable at the tip of the headland (Zone B) during the mid-flood and mid-ebb tides.

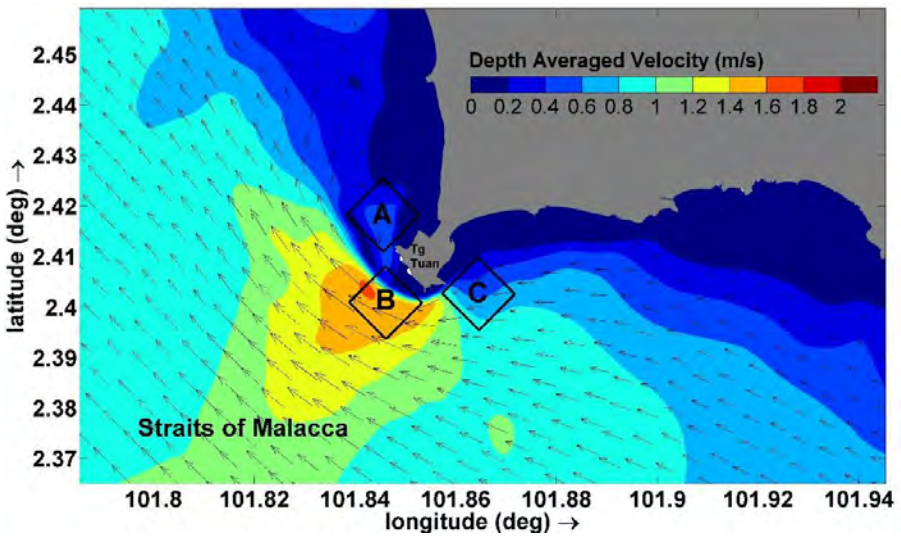

(a) Mid-flood tide

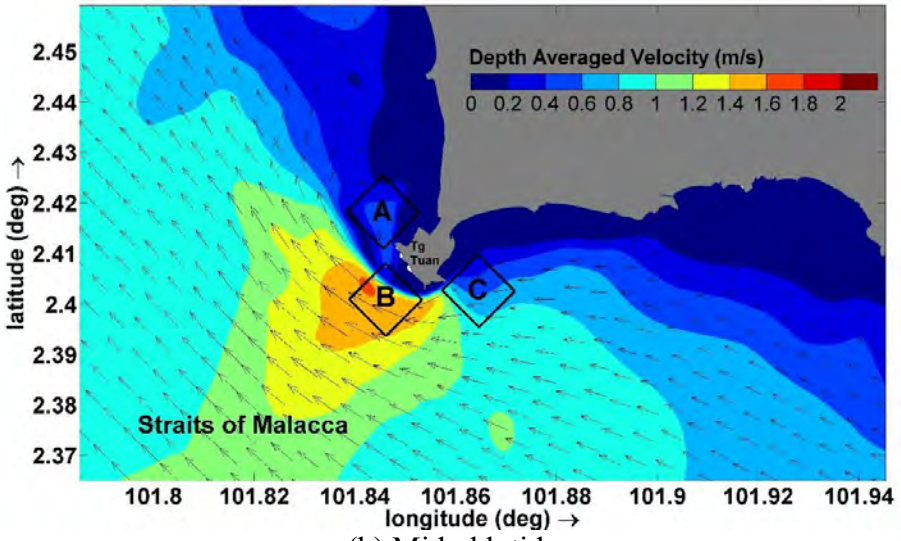

(b) Mid-ebb tide

Figure 4.33: Natural distribution of flow velocity at the study area during (a): mid-flood tide and (b): mid-ebb tide

Deviation of the tidal flow direction during flood and ebb tide is observed at the some of the headland areas due to the complicated coastline and geomorphology condition at the headland. Based on the direction vs time-series plot for Zone A, B, and C (**Figure 4.34**), Zone C is seen to have the most obvious deviation of tidal flow direction during mid-flood and mid-ebb flow; the flow direction changes swiftly during mid-ebb tide, due to the weak tidal current. Zone A has the most consistent flow direction, where the flow direction changes consistently from -20 to 160 Degrees at this zone. For Zone B, the flow direction changes from -40 to 140 Degrees. However, it was observed that Zone B has slight deviation of flow direction, up to 25 Degrees in general during ebb-tide. The anisotropic flow into the turbine rotor may significantly affect the performance of the electrical generation and induce more energy dissipation. It is therefore crucial to assess the anisotropic effect for application of the tidal stream turbine. Considering this, next chapter will be discussing the effect and performance of tidal current turbine application with anisotropic flow.

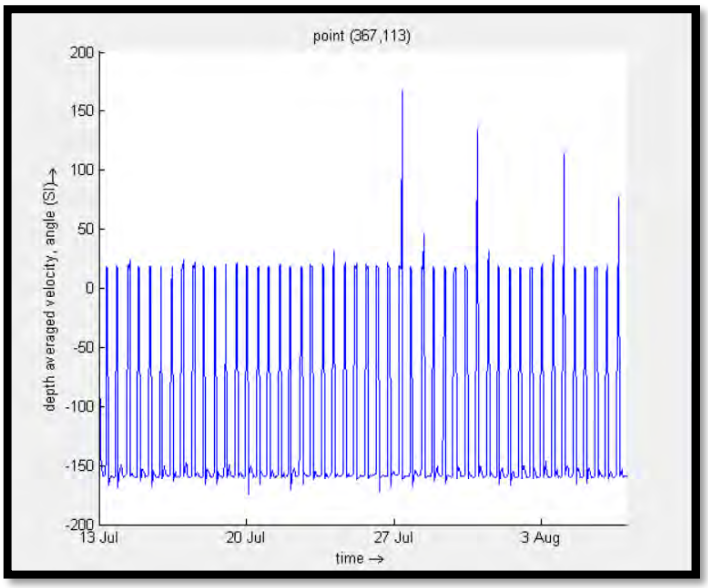

(a)

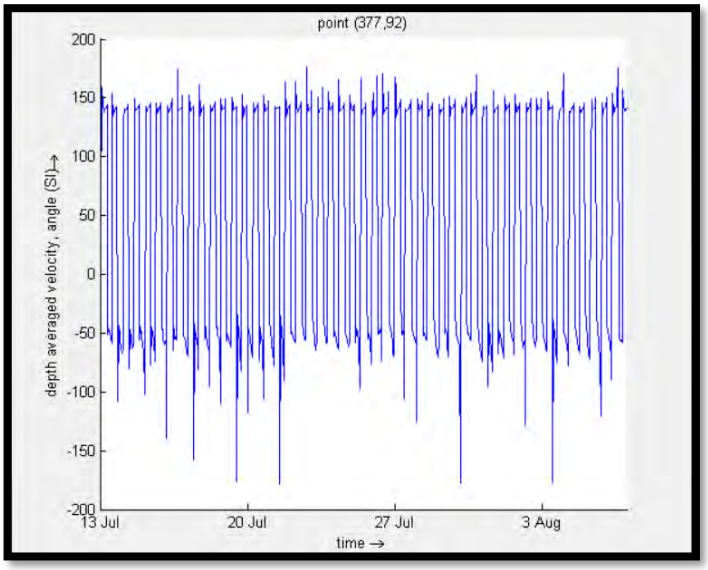

(b)

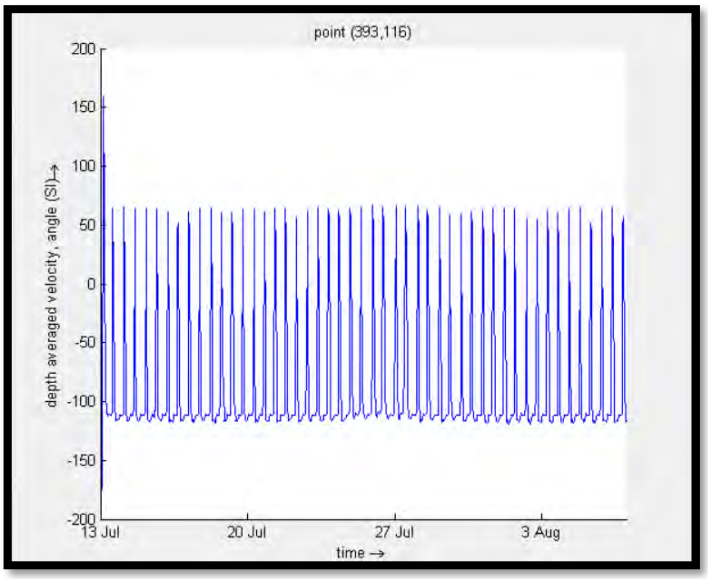

(c)

Figure 4.34: Current direction for (a) Zone A, (b) Zone B, and (c) Zone C

The velocities are not identical for both ebb and flood events, i.e., peak velocity is higher during mid-flood tide. The median velocity at the headland was determined based on the probability exceedance of 1.0 m/s at the study area. The 1.0 m/s exceedance probability analysis covering both neap and flood tides at the study area indicates that only Zone B of Tg Tuan Headland has more than 50% of probability of occurrence of alongshore currents that are higher than 1.0 m/s. This is sensible because the alongshore currents become maximal when they are less subjected to the frictional resistance from the sea bottom in greater water depths. Hence, the energy extraction of tidal turbines installed at Zone A and Zone C of Tg Tuan Headlands is less promising. Even though the depth requirement has been complied by Zone A and Zone C, the current flows remain weak due to the influence of the geographical features of the coast. In contrast, Zone B has fulfilled all the site suitability criteria prescribed by Fraenkel (2002), Fraenkel (2007), and Myers & Bahaj (2005)(see **Table 4.1**). The numerical results yielded the mean and maximum current velocities for Zones A, B and C. The mean and maximum velocity magnitudes for Zone A, Zone B and Zone C are summarized in **Table 4.14**. The recorded current velocities at Zone B have the highest mean and maximum values of 1.5 and 2.3 m/s, respectively. Among all zones, only Zone B fulfils the peak velocity requirement of 2.0 – 2.5 m/s.

Table 4.14: The average and maximum velocities at Zones A, B and C

Zone	Zone A	Zone B	Zone C
Average Velocity (m/s)	0.70	1.5	0.7
Peak Velocity (m/s)	1.2	2.3	1.2

The growth of turbine technology over the years shows possibilities for adoption at lower tidal current energy sites (Faez Hassan et al., 2012; Hassanzadeh et al., 2017). Further evaluation in allowing the TEC deployment at lower tidal current velocity sites basing on the mean velocity of 0.5 m/s, approximately ranging 0.1 – 1.0 m/s (

Figure 4.35a) is needed, to attain cost effective deployment. Zone A and Zone B are feasible sites as these two zones have median velocity higher than 0.5 m/s (Figure 4.35d) and peak velocity higher than 1.0 m/s (Figure 4.35b) with seabed ranging between 20 m and 50 m (**Figure 4.20b**).

Figure 4.36 shows the 2D map plot for potential extractable power per annum (computed using equation (3.23)) with a depth-averaged velocity greater than 1.0 m/s at Tg Tuan Headland. Computed by using equation (3.22), the maximum potential extractable kinetic power derived from Zones A, B and C for a representative 14 days covering spring and neap tides are 0.1, 2.7 and 0.1 kW, respectively (see **Figure 4.37**). The annual energy output around Tg Tuan Headland ranges from 1,500 to 11,000 kWh/m^2 (**Figure 4.36**). The tip of the headland (Zone B) has the highest extractable energy at approximately 11,000 kWh/m^2 while Zone C has the lowest extractable energy at 1,500 kWh/m^2. These results again have proved that the extractable tidal energy is largely governed by the irregularity of the shorelines and the water depths.

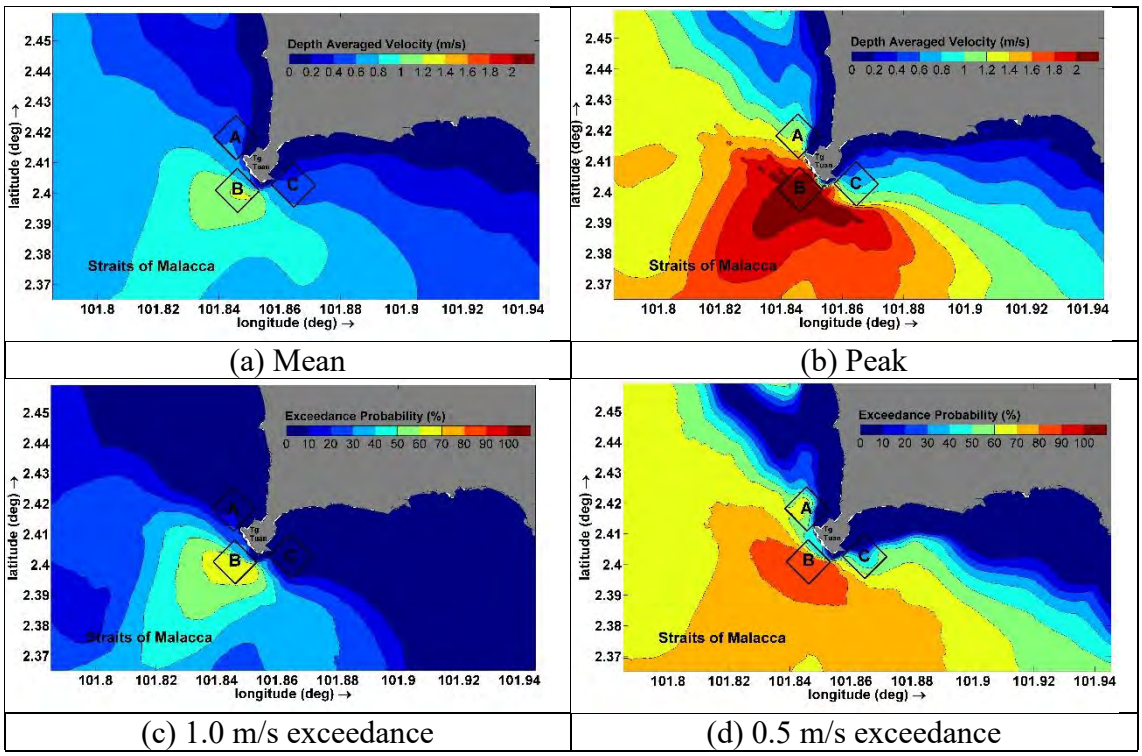

Figure 4.35: 2D map plot for assessment of the area of interest around zones 1-3 of Tg Tuan Headland for (a) mean current velocity, (b) peak spring flood velocity, (c) 1.0 m/s exceedance probability, (d) 0.5 m/s exceedance probability

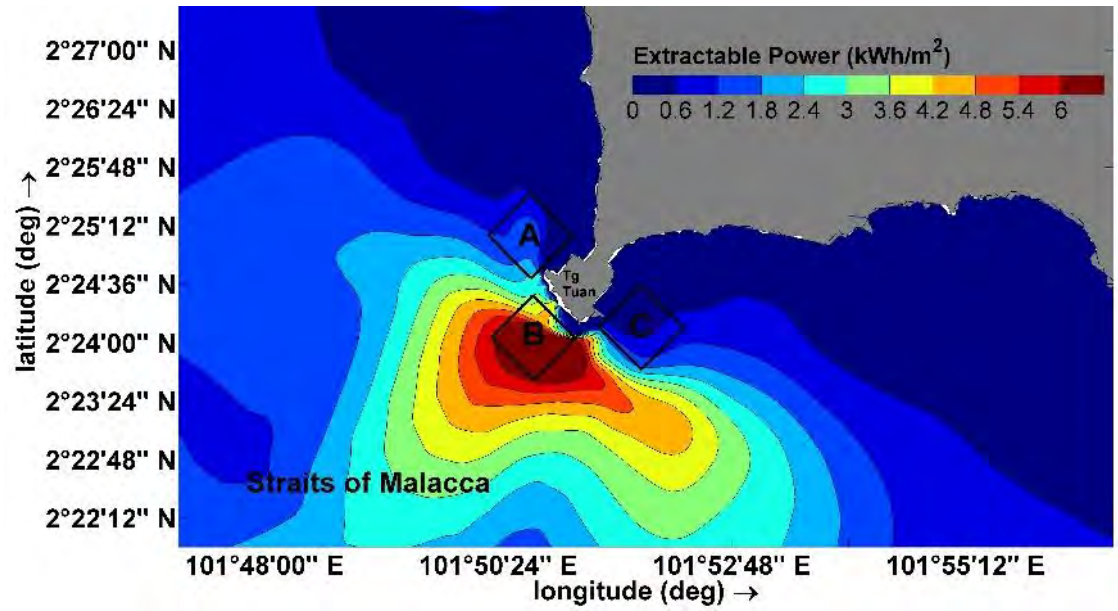

Figure 4.36: 2D map plot for potential extractable power per annum with a depth-averaged velocity greater than 1.0 m/s and potential extractable kinetic power

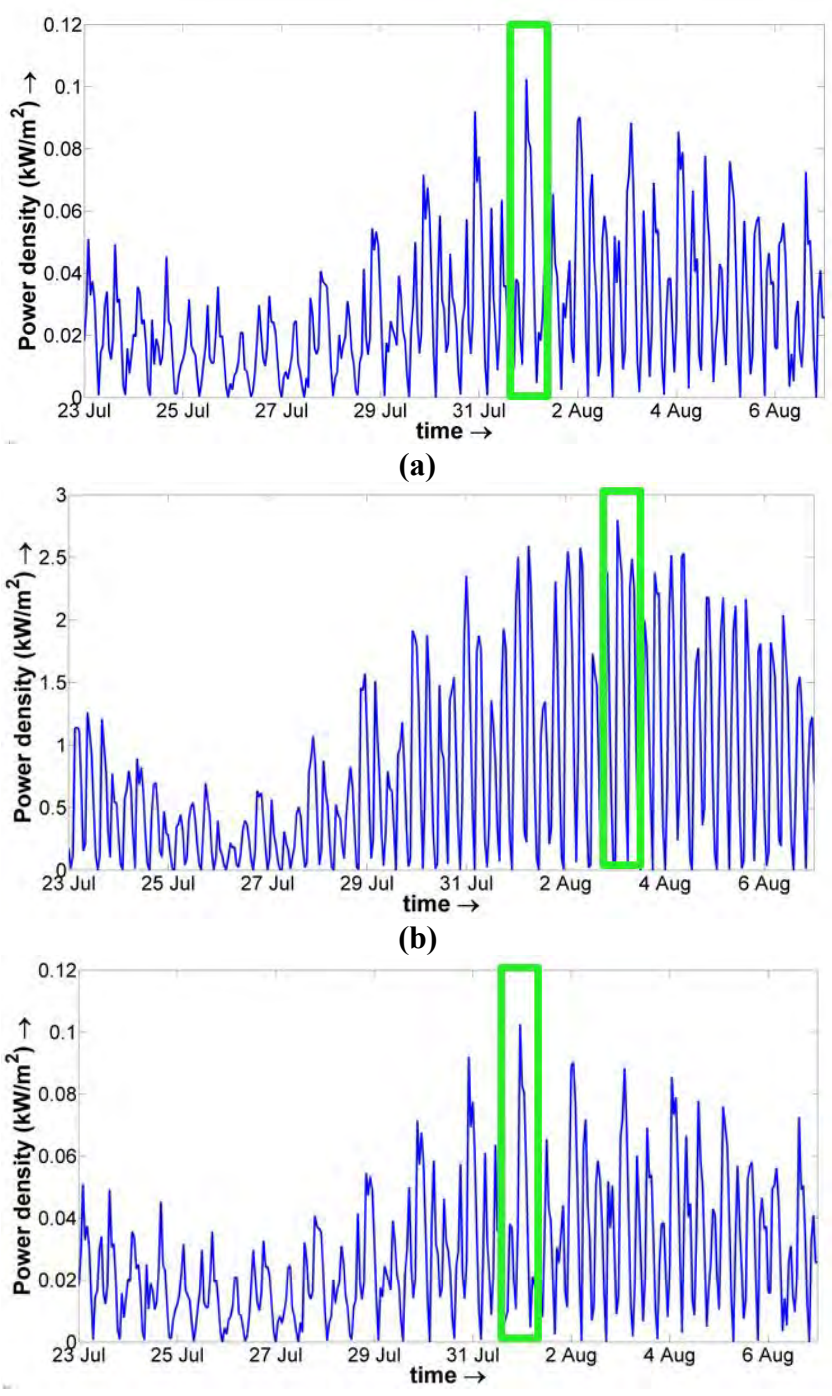

Figure 4.37: Potential extractable kinetic power with a depth-averaged velocity greater than 1.0 m/s for (a) Zone A, (b) Zone B, (c) Zone C for a representative 14 days covering spring and neap tides. The green box marks the maximum potential kinetic power extractable by a single tidal turbine at peak flow

4.4 Summary

This chapter presents the development of a tidal current resource assessment methodology which utilizes a 2D hydrodynamic model along with measured data to incorporate the actual seabed condition into the model domain. The model was validated with sufficiently long period of measured tidal and current velocity data at the case study area. The main conclusions deduced from this assessment are as follows:

- Tidal energy resource assessments require hydrodynamic models with spatial scales less than 1 km to ensure the kinetic energy resource is not overestimated. For this study, a detailed model was set-up with significantly enhanced spatial and temporal resolution than previous published studies. The numerical model was developed using measured bathymetry data extensively covering the study area to simulate the tidal flows around the headlands. Comparison of the simulated hydrodynamic model with ADCP measurement data, which were extensively deployed across the considerably long coastline (~ 40 km) of Negeri Sembilan, shows that the constructed model correctly captured the water level and current velocity throughout the model domain.

- A systematic detailed quantitative analysis conducted around the Negeri Sembilan coastline which focusing on four sites – H1, H2, H3 and H4 by using high resolution model demonstrated that energy potential along the same coastline with length of approximately 40 km can differ quite significantly. Comparison of four headlands (H1 – H4) on the estimation of the maximum power output at these four sites shows high exploitable potential for power generation at headland with narrowest channel, H3.

- Complex flow circulation occurred around the headland may cause operational disturbances to the turbine rotation that limits its power take-off efficiency. Further

analysis by assessing a suitable zone for TEC deployment was carried out by applying a high resolution spatial numerical model at the headland area. This study demonstrated that extractable tidal energy area at different zone of one headland can vary quite substantially although geographically near to each other. Hence, robust assessment using finer grid of the available power for other identified suitable tidal stream energy areas in Malaysia is crucial. The modelling results revealed that due to its high peak flow speed and suitable water depth, the water at the seaward tip of Tg Tuan Headland is anticipated to provide a power density exceeding 2.5 kW/m2, consequently making the location to be suitable for installation of a horizontal axis tidal turbine for power generation. These have further demonstrated that the tidal current energy site exploitability is greatly influenced by the irregularities of the local shorelines and the bathymetry conditions.

- The estimated natural gas substitution data (660 TJ) at H3 is a good reference for the policy maker and the utility company (Tenaga National Berhad, TNB) as they can use it to estimate the saving of natural gas. The average cost of natural gas is about RM 23.72/mmBtu or RM 1.12/kg based on the tariff rates approved by the government in accordance with section 13 of Gas Supply Act 1993 (GasMalaysia, 2019). With 56 GWh/annum of energy generation from tidal turbine, a total amount of 185 GWh or 660 TJ of natural gas can be replaced every year. With the energy content of natural gas is about 55 MJ/kg. The power output of 185 GWh/year of tidal turbines, the country or the utility company can save about RM 13.4 million (~ USD 3.2 million) of natural gas per year.

- Deviation of the tidal flow direction during flood and ebb tides at Tg Tuan Headland is observed. The anisotropic flow into the turbine rotor may significantly affect the performance of the electrical power generation and induce more energy dissipation.

The anisotropic effect to application to the tidal stream turbine will be discussed in next chapter.

Identification of feasible tidal current turbine deployment sites based on the available resource is the first stage of a tidal stream energy resource assessment. The next steps consider the tidal current energy extracted by tidal current turbine(s) and the related effects of both the sea hydrodynamic condition and on the accessible power. Accessible power is a measure of the uninterrupted current flow; yet, tidal current turbines deployment will modify the undisturbed tidal current flow, and hence affecting the available resource. This research is also keen to capture the hydrodynamic influences on available power of tidal energy extraction. This concept is established, deliberated and applied in the subsequent chapter.

5 MODELLING OF TIDAL CURRENT ENERGY EXTRACTION

5.1 Introduction

The main aim of this research was the alteration of the hydrodynamic model to include the influence of tidal current energy extraction. The model developed from this research can then be adopted to quantify the tidal current power productivity from single and array of tidal current turbines and identify optimum array configuration for achieving an optimum tidal current energy with least hydro-environmental impacts that have been in the next chapter.

5.2 Establishment of Tidal Current Energy Extraction Model

5.2.1 Turbine Representation within the Model

Tidal current energy extraction is modelled into the numerical model by applying the momentum sink method, whereby the turbine thrust is representing the retarding force was included into the model through inclusion of negative sink term into the momentum equation. This approach is commonly applied in previous far field models (Adcock, 2014; Plew & Stevens, 2013).

It is to be noted that even though tidal turbine may not be generating electrical power all the time, C_{loss} will never be zero as the drag force combination from the physical existence of the tidal turbine structure will exist in all conditions. Moreover, the limit of the electricity of the tidal turbine generator will most likely be achieved prior to tidal turbine "cut-out" at high current velocity speed. Utilizing the capabilities of Delft3D-FLOW model, it was essential to provide a time-series for C_{loss} at the beginning of every model simulation.

The tidal current turbine loss momentum will be also different with the tidal current turbine's direction. In model studies it is conventional to assume that tidal currents are rectilinear, or that the tidal current turbine is align with the current flow direction (Batten et al., 2008; Blunden & Bahaj, 2007; Neill et al., 2012). The dominant design concept of horizontal fixed-axis tidal current turbine to date has no yaw control, i.e., they could not rotate about their vertical axis. In most of the tidal current turbine designs, nevertheless, the tidal current turbine blades can pitch through 180°. Bidirectional tidal currents are thus important to maximise the tidal current energy extraction. Even though it has been recommended that energetic tidal current energy sites showed that the tendency for near bi-directional flow (Harding & Bryden, 2012), this may not true for all sites. A study at Inner Sound of the Pentland Firth, the tidal flow can be misaligned as high as 40°. The offset of the angle between the flow and the tidal turbine axis increases, resulting decrease of the tidal turbine thrust and power as a function of the angle of the cosine (Blunden & Bahaj, 2007). To achieve more realistic representation of the thrust and power, it can be represented with a cosine correction within the parameterization of the tidal turbine (Ahmadian & Falconer, 2012).

Added bed shear stress approach was applied for tidal turbine modelling by Easton, Woolf, & Bowyer (2012). The parameterization of added bed shear stress does not resolve the wake effect details behind the tidal turbines (Garrett & Cummins, 2007). A better approach, actuator disc theory is recommended. This method is much better in describing the flow field in the turbine wake regions in better detail (Harrison et al., 2010; MacLeod et al., 2002). However, higher computational cost and difficulties in implementation are required within the existing oceanographic model for actuator disc approach.

In this chapter, a physically realistic tidal current turbine related loss coefficient using actuator disc parameterization is derived. This section is based on published

characteristics of tidal current turbines available from the literature. The tidal current turbine loss coefficient accounts for the non-linear dynamics of tidal current turbine operation, the anisotropic response to the incident flow. The tidal current turbine parametrization is tested in an idealised hydrodynamic model (Section 5.3). The predicted mean and maximal tidal current turbine power, tidal current turbine force, and kinetic energy dissipation are resolved and discussed in Section 5.4. The effect of tidal current turbine direction on the power and force is also examined. The outcomes of these models are discussed (Section 5.4) and the chapter is concluded (Section 5.5).

5.2.2 Tidal Current Turbine Power

The power produced by a tidal current turbine (excluding of gearbox and generator losses) is affected by tidal current velocity and scaled by the tidal turbine power coefficient as:

$$P = \frac{1}{2}\rho C_p A_T U_{ax}^3 \tag{5. 1}$$

where C_p is the power of tidal current turbine and A_T is the swept area of the tidal current turbine blades. The deviation in current flow away from the axial direction of the tidal current turbine will affect the ability of the extraction. Hence, the tidal current speed (U_{ax}) is expressed as the component of the tidal stream velocity in the turbine axial direction as:

$$U_{ax} = U.|cos\ (\theta - \emptyset)| \tag{5. 2}$$

where θ and $\emptyset$ are the tidal current velocity direction and tidal current turbine axial directions. The C_p values were based on the published values derived from physical and numerical experiments of Batten et al. (2008) and Bahaj et al. (2007). **Figure 5.1**

illustrates the relationship between C_p and blade tip speed ratio (TSR). The TSR is a non-dimensional parameter for the tip of tidal current turbine blade, U_{tip}, and the axial tidal flow speed through the tidal current turbine and expressed as:

$$TSR = \frac{U_{tip}}{U_{ax}} = \frac{\Omega \pi D}{60 U_{ax}} \quad (5.\ 3)$$

where Ω represents the rotational speed of the tidal current turbine (revolutions per minutes) and D is the diameter of the tidal current turbine. With known tidal current turbine blade length and rotational speed, the power coefficient $C_p \ and \ C_T$ can be calculated for different tidal flow current speed based on the turbine design curves as expressed in equation (5. 1).

For current assessment, the result from published data is used for model validation. The main tidal turbine geometry and its parameters for operation are given in **Table 5.1**. This is to denote a typical first-generation tidal current turbine. For U_{ax} lower than U_{inc}, the tidal current turbine will not generate any power due to inadequate torque to surpass the loading of the generator and initializing the rotation of the tidal current blade. Whilst if U_{ax} is larger than U_{out}, the tidal current turbine will not generate any power due to the risk of damage of extra loading on the tidal current increases. For the operational range of flow speeds $U_{in} < U_{ax} < U_{out}$, the equivalent TSR was examined using equation (5. 3), where 12 RPM of rotational speed and 18 m of tidal current turbine blade diameter were assumed (Bahaj et al., 2007; Batten et al., 2008; Easton et al., 2012).

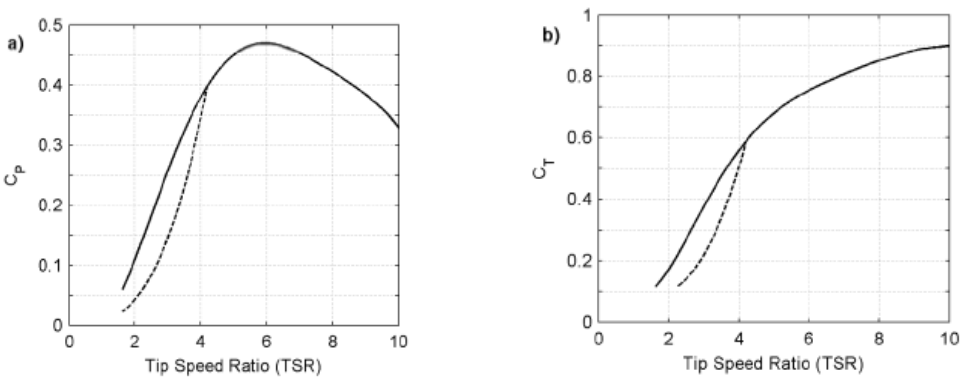

(a) **(b)**

Figure 5.1: a) Power coefficient of tidal current turbine (C_p) against Tip Speed Ratio (TSR), b) Thrust coefficient of tidal current turbine (C_T) against Tip Speed Ratio (TSR). (Solid line represents the fixed bladed pitch (interpreted from Batten et al. (2008)). Dash line represents blade pitch control above a rated current speed of the tidal current turbine) (Bahaj et al., 2007; Batten et al., 2008; Easton et al., 2012)

Table 5.1: A typical geometrical and operational parameter for a realistic tidal current turbine

Turbine Design parameters		
Turbine blade diameter	D	18 m
Swept area of turbine blades	A_T	254 m^2
Rotational speed	Ω	12 RPM
Rated speed	U_r	2.7 ms^{-1}
Cut-in speed	U_{in}	1.0 ms^{-1}
Cut-out speed	U_{out}	3.4 ms^{-1}
Support structure exposed area	As	$0.2A_T$
Support structure drag coefficient	C_S	1.0

(source: Bahaj et al. (2007); Batten et al. (2008); Easton et al. (2012))

The turbine output is maintained at rated power if the rated current speed goes above rated current speed and fall below the cut-out current speed. The design of power output will be different for different tidal current turbine designs (Bryden et al., 2007). An approach by controlling the blade pitch angle to cover the entire major axis to change the

"angle of attack" was adopted for wind turbine and found that it modified the lift force on the tidal turbine blade. This methodology enables constant rotational current speed for the operational range of tidal current speeds and was adopted for tidal current turbine in this study. However, the established C_p -TSR curve only represented a "fixed pitched" blade angle as discussed by Blunden & Bahaj (2007) and Batten & Bahaj (2006). Hence revised relationships were examined to represent tidal current turbine power control at $U_{in} < U_{ax} < U_{out}$, as described in followings:

1. The power coefficient of a fixed-pitch tidal current turbine (C_p') in operational range of TSR was calculated using the original C_p -TSR curve (solid lie in **Figure 5.1a**).

2. The power output of a fixed-pitch tidal current turbine (P') was calculated from **Figure 5.1** with the fixed-pitch power coefficient (C_p'). The power output for rated power (P_r) was calculated at rated current speed (U_{ax}=U_r).

3. A power feedback control parameter β was given for calculation of power coefficient of variable pitch tidal current turbine as:

$$Cp = \beta Cp' \quad (5.4)$$

$$\beta = 1.0 \text{ when } U_{in} < U_{ax} < U_{out} \quad (5.5)$$

$$\beta = \frac{P_r}{P'} \text{ when } U_r < U < U_{out} \quad (5.6)$$

4. The power output of variable pitch device of tidal current turbine was calculated using equation (5. 1*)* with Cp from equation (5. 4*)*.

The resulting tidal current turbine power curve for a realistic first-generation device denoted a rated power output of 1.02 MW as shown in **Figure 5.2**. For axial current speed exceeded the rated speed, the pitch control effect modified the curve of C_p vs TSR through reduction of the power coefficient (C_p) at lower TSR (dotted line in **Figure 5.1a**).

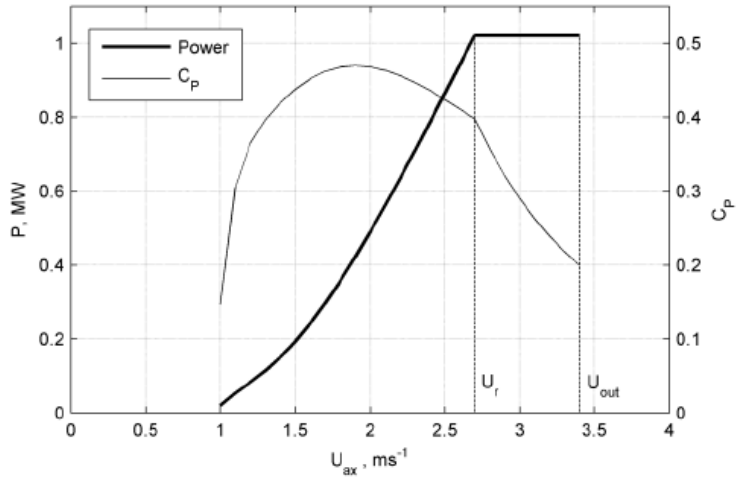

Figure 5.2: Relationship of Power Output and Power Coefficient vs turbine axial current speed. (Bahaj et al., 2007; Batten et al., 2008; Easton et al., 2012)

5.2.3 Tidal Current Turbine Forces

It is important to derive suitable values for the physical forces relating to the tidal current turbine that were consistent with the power curve described above. This is because the momentum equations relate to the physical forces which impose on the fluid element to the momentum change rate along with the continuity equation will subsequently govern the calculation in the hydrodynamic models.

The axial force refers to the force, which occurs due to variation of pressure across the tidal current turbine rotor. The axial thrust force differs quadratically with the tidal current turbine axial current speed, swept area of the device and also scaled by the axial thrust coefficient expressed as:

$$F_T = \frac{1}{2}\rho C_T A_T U_{ax}^2 \tag{5. 7}$$

where, C_T is the tidal current turbine thrust coefficient. It is to be noted that tidal current turbine power curve does not produce any power and therefore has zero thrust when it is

below cut-in speed ($U_{ax} < U_{in}$) or above the cut-out speed ($U_{ax} > U_{Out}$), as illustrated in **Figure 5.2**.

As mentioned earlier, the blade pitch angle of tidal current turbine was assumed to be different for $U_r < U_{ax} < U_{out}$ in order to ensure that the power output to stay within the limit of the tidal current turbine generator. Inevitably, the blade pitch may modify the tidal turbine rotor thrust force. The established relationship for C_T against Tip Speed Ratio is meant for fixed-pitch blade angle; hence a revision on the relationship was calculated with the assumption that the tidal turbine blade pitch control exceeded the rated current speed.

The pitch control effect was mainly to amend the curve of C_T vs TSR by lowering the thrust coefficient at lower tip speed ratio (**Figure 5.1b**). Therefore, C_T decreases as the tidal current axial current speed increases (**Figure 5.3**). When the axial speed exceeds the tidal turbine rated speed (U_r), the axial thrust coefficient (C_T) decreased very rapidly as the blades of the tidal current turbine pitched to limit the output of the power. The U_{in} of tidal turbine rotor thrust force generated 123 kN and the rated current speed produce rotor thrust force to 559 kN. The tidal current rotor thrust force decreased when it went beyond the rated current speed and the cut-out speed was 442 kN.

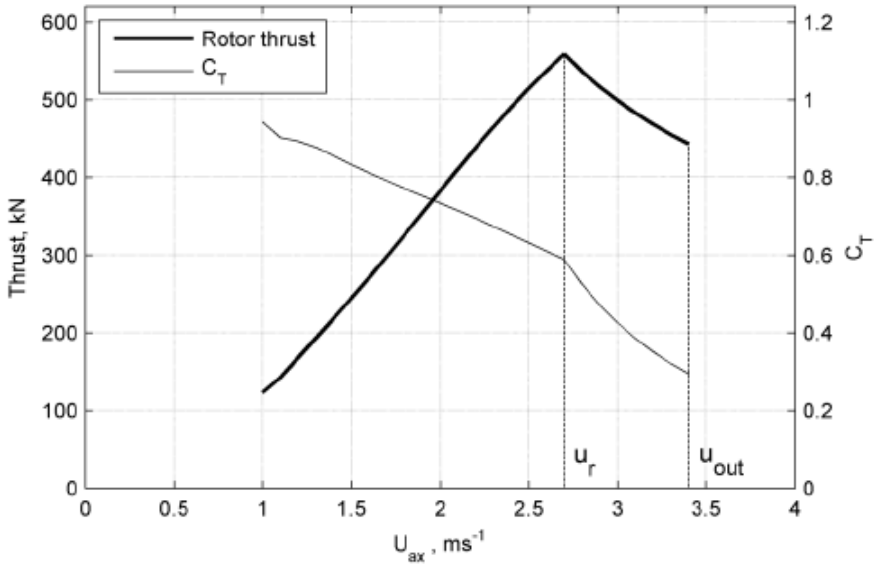

Figure 5.3: Tidal current turbine rotor thrust and coefficient vs axial current speed (Bahaj et al., 2007; Easton et al., 2012)

The turbine operation begins to commence at U_{in} of 1 m/s and was associated with an order of magnitude increase in total force F. Assuming that U = U_{ax} for $|\theta - \emptyset| = 0$, the axial tidal current turbine force was much larger than the drag force of the support structure, and hence the drag force exerted on the support structure by the moving fluid is ignored in this study. The total force due to the tidal turbine, F focused mainly on the axial thrust force, F_T. The tidal turbine rotor thrust contributed to the total tidal current turbine force to increase considerably linearly from U_{in} to U_r. The maximum tidal turbine force was achieved at 750 kN at turbine rated speed. The tidal turbine operation terminated at U_{out} and seen to have 60% reduction in the total tidal turbine force F. The drag on the support structure occurs throughout the whole operation, including $U > U_{out}$ and the current speed is quadratic in relationship (**Figure 5.4**).

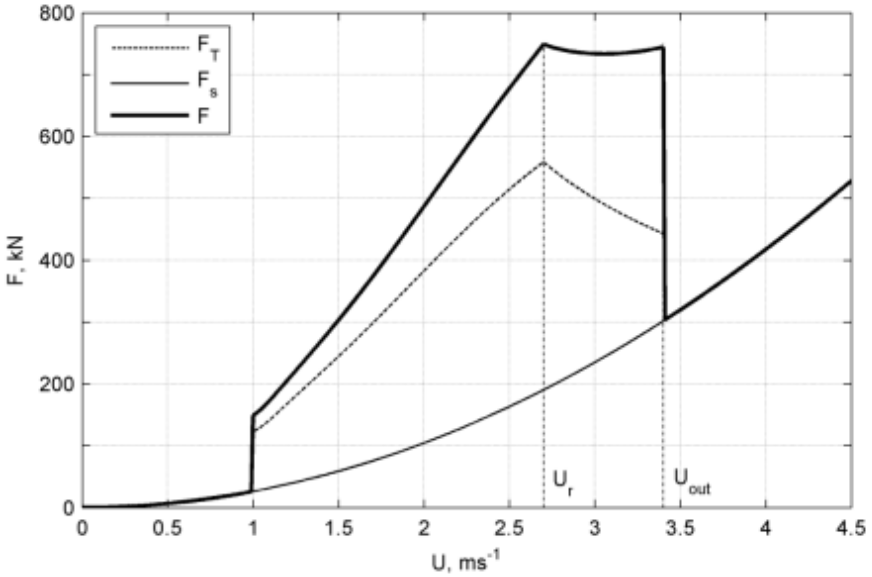

Figure 5.4: The tidal current turbine rotor thrust, turbine support structure, and total force against current speed. It is assumed that the tidal current turbine axis is parallel with the flow direction, i.e. $|\boldsymbol{\theta} - \emptyset| = 0$ (Easton et al., 2012)

5.2.4 Dissipation of Kinetic Energy

The overall kinetic energy dissipation from the flow by the tidal current turbine was calculated as:

$$\dot{E}_{turbine} = F_T U_{ax} + F_S U \tag{5. 8}$$

The $\dot{E}_{turbine}$ is differ from the extractable power P of tidal current turbine as described in equation (5. 1), as it consists of both the drag of the support structure and fluid dynamic efficiency of the tidal current turbine. It is to be noted that the overall kinetic energy dissipation is higher than the power output at all the given current speed (**Figure 5.5**). The total dissipation caused by tidal current turbine at rated current speed is two times of tidal current turbine rated power. When reaching at cut-out speed, the sum of dissipation has reached up to 2.5 times of the tidal current turbine power.

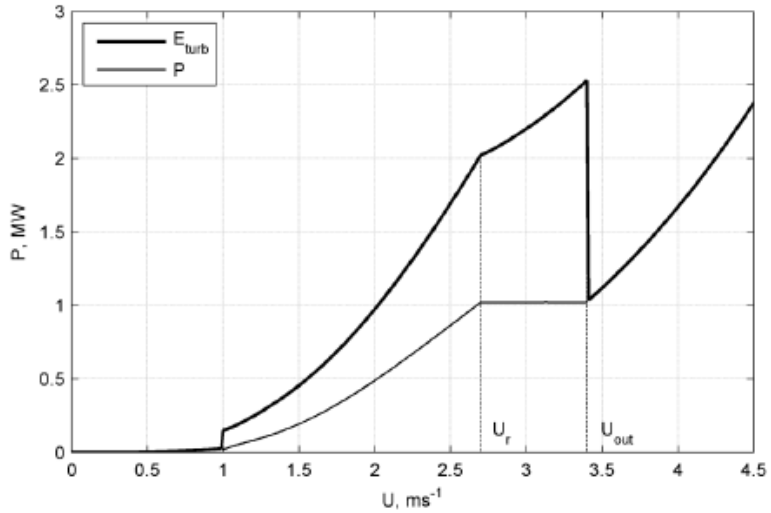

Figure 5.5: Sum of kinetic energy dissipation and tidal turbine power output vs current speed. It is to assume that the tidal current turbine axis is parallel to the flow direction, i.e. $|\boldsymbol{\theta} - \emptyset| = \mathbf{0}$ (Easton et al., 2012)

5.2.5 Tidal Current Turbine in Numerical Model Architecture

The tidal current energy extraction model is developed by extending the established hydrodynamic model of Delft3D-FLOW architecture through modification of existing subprograms and adding new subprogram to the original hydrodynamic model (Ramos et al., 2019). **Figure 5.6** illustrates a flowchart of the amended model architecture, showing all subprogram called in the model main program and highlights the additional sections established for incorporation of tidal current energy extraction.

The input and output data defined are opened in subprograms 1 and 2 for simulation. The model input data includes of domain (grid parameters, bathymetry, dry points and thin dams), time frame, initial condition, boundary conditions, physical parameters, and numerical parameters; monitoring and additional parameters are read in and stored in subprograms 3, 4, 5, 6, 7, 8, 9 and 10. The porosity of the plate is governed by a quadratic friction term where the friction term is the input parameter defined in subprogram 10 (additional parameter) as energy loss coefficient. A porous plate is a structure partially impermeable that spreads into the water column for the selected grid perpendicular to the

flow direction, which covers partial or partial or whole layers in the vertical, but the thickness of the structure is much smaller than the grid size in the grid direction perpendicular to the defined porous plate. Several previous studies conducted by Badano et al. (2018), Orhan and Mayerle (2020); Ramos et al (2013) adopted this method for studying the potential near and far-field effect of tidal current turbine energy extraction.

With the inclusion of the energy loss coefficient, subprograms 3-10 are executed every time-step for the entire simulation of the numerical modelling process. Any output data specified are written into output files in subprogram 11 (in 2D through map file or extraction point through history file).

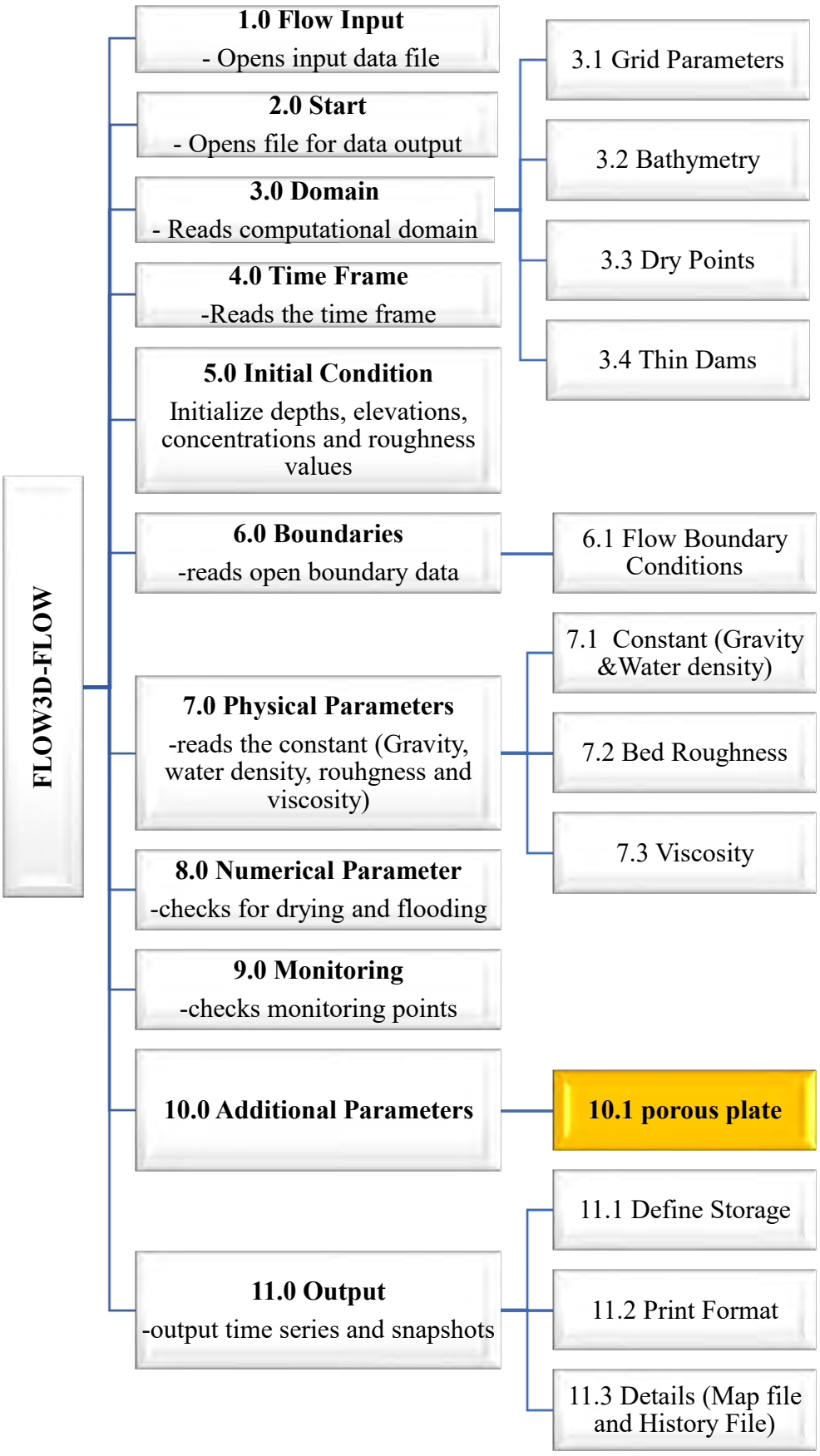

Figure 5.6: Flow3D-FLOW model subprograms with inclusion of porous plate

5.2.6 Inclusion of Energy Extraction into Source Code

In the Data Group Additional Parameters, the quadratic friction loss is specified to initiate a special feature to DELFT3D-FLOW. Keyword and value in the Data Group Additional parameters needs to be specified to initiate the calculation in the program. The keyword is used in the MDF-file to recognize the special feature. The detail of the formulation is as described in Section 3.3.6.

The porosity of the porous plate is governed by a quadratic friction term where the friction is the input parameter; the detail of friction derivation is described in Section 3.3.5. The location of the porous plate is extending over one or more layers of the water column with quadratic friction for energy losses simulation. The format of the file is free formatted and it is manually generated in offline. The values of character-type must be enclosed between two number signs (#). For the record description, it is defined as:

Record	Record description
Each record in the code	Direction of the porous plate perpendicular to the flow U: U- porous plate V: V-porous plate Begin and end indices, i.e., m1, n1, m2, n2 (4 integers) Define the layers over which the porous plate covers, i.e., k_1 and k_2 (2 integers) Friction coefficient of the quadratic friction [-] (1 real)

For the inclusion of the porous plate, it is prohibited to insert only one record per porous plate. The friction coefficient must be positive. The input items must be separated by one or more blanks. For quadratic friction, it is included into the model with following details in the numerical model.

keyword	value	description	default
Filppl	#name.ppl#	Filename for porous plate data	none
Upwppl	#Y# or #N#	Upwind advection scheme near structure	#Y#

The tidal turbine is modelled on the interface between two computational cells. As described in Section 5.2.1, large horizontal gradient may occur for water level, velocity field and in the concentration around the tidal current turbine due to the deployment of the structure. For prevention of physical oscillation in the velocities and concentrations upstream of tidal current turbine structure points, the model is switched to the discretisation of the advective terms at the designated points to an upwind approximation. Upwppl keyword is provided in the model to prevent oscillation due to large gradients. The energy preserving upwind discretization of advection is applied as below:

$$U\frac{\partial U}{\partial x}\bigg|_{m,n,k} = \frac{1}{2}\frac{\partial U^2}{\partial x}\bigg|_{m,n,k} = \begin{cases} \dfrac{U_{m,n,k}^2 - U_{m-1,n,k}^2}{2\Delta x}, U_{m,n,k} > 0 \\ \dfrac{U_{m+1,n,k}^2 - U_{m,n,k}^2}{2\Delta x}, U_{m,n,k} < 0 \end{cases} \quad (5.9)$$

It is noted that for transport equation, locally a first-order upwind scheme is used by default.

5.3 Model Experiments

The parameterization of the tidal current turbine is explored in model experiment in this section within a numerical model based on the established relationship between the tidal current flow speed and the physical force impinged by a tidal current turbine. Three main components are tested in this section: anisotropic response to the incident current flow, effect of physical structure and non-linear tidal current turbine behaviour efficacy. The Delft3D-FLOW model developed by Deltares was used. The two-dimensional hydrodynamic model is established based on Reynolds depth-averaged Navier-Stokes equations, through the application of hydrostatic and Boussinesq approximations (Deltares, 2021).

5.3.1 Hydrodynamic Model Domain and Boundaries

A rectangular channel, 14 km wide x 25 km long with 40 m depth was established in this study (**Figure 5.7**). The size of the model domain was built considerably large to ensure minimal effect of any undesirable refection at the open boundaries with the inclusion of tidal current turbine. The open boundaries are forced with a sinusoidal current flow from the west to east direction, where $U = U_0 cos\ (\Omega t)$. The amplitude U_0 is 4 m/s and frequency Ω is 0.506 radians/hour, based on a potential energy extraction site for optimum application of horizontal axis tidal current turbine (Easton et al., 2012). This setting represented a considerably strong tidal harmonic of M_2; however, it is considered representative for a spring tide at a potential tidal current energy extraction site. The grid size was 200 m and the seabed or bottom roughness coefficient was specified as 0.003, based on Negeri Sembilan calibrated and validated model domain (refer to Section 4.3.1).

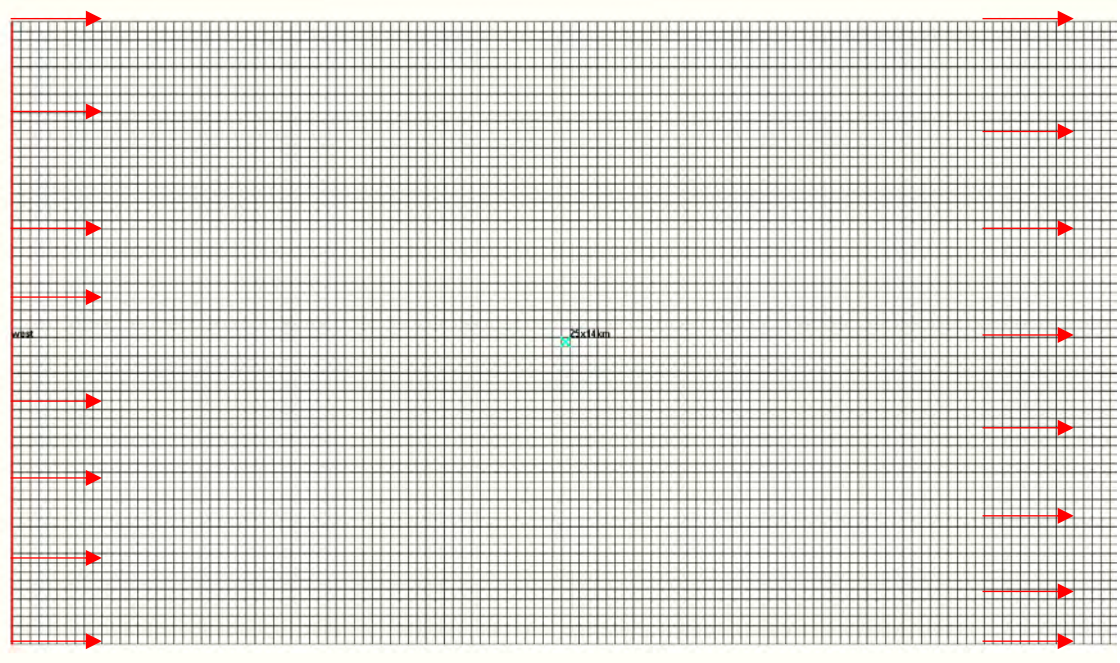

Figure 5.7: Domain of the test model showing the flow direction of tidal forcing at the open boundaries. "O" represents the location of the tidal current turbine

5.3.2 Parameterization of Tidal Current Turbine in the Model

The derivation of turbine thrust is based on Linear Momentum Actuator Disc Theory (LMADT) introduced by Betz in Year 1920's (Burton et al., 2001) that was based on wind turbine analysis application. It was further developed by Houlsby et al. (2008) for tidal current turbine using a constant flow cross section, with constant depth and parallel walls at both sides of the channel (Houlsby et al., 2008). The tidal current turbine rotor was modelled as a porous actuator disc, which removes momentum from the flow in an open channel and enables the thrust for a horizontal axis tidal current turbine to be derived. The LMADT is described graphically in **Figure 5.8**. (I) represents further upstream of the tidal current turbine, (II) represents immediate upstream of tidal current turbine, (III) represents immediate downstream of tidal current turbine, (IV) represents area where slower current flow from the tidal current turbine's wake merges with free-stream fluid from the by-pass flow and (V) represents further downstream from the turbine that water pressure backs to free-stream levels. The tidal current flow passing through the tidal current turbine is symbolized as t, whilst by-pass flow is symbolized as b.

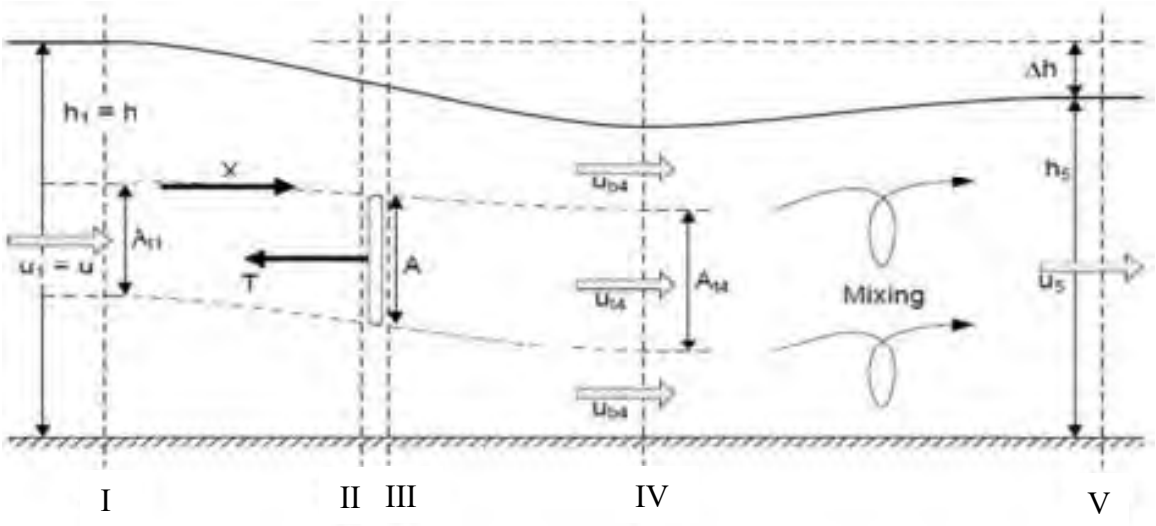

Figure 5.8: Linear momentum actuator disc theory in one dimensional channel flow (Houlsby et al., 2008)

The undisturbed flow (I) is passing through the actuator disc (from II to III) with continuous decrement in current velocity as the disc removes the momentum from the tidal current flow. Followed by that, at immediate downstream of the actuator disc (III – IV), the flow passing through the disc slows down and therefore expands to satisfy the conservation of the momentum. This has generated the turbulent mixing and wake, which reduces the velocity region further downstream of the disc. When the flow travels further downstream from the actuator disc at (V), the wake has gradually dissipated and the current flows to free-stream conditions. The tidal current energy extraction is discovered to cause a drop in depth of water, Δh, across the tidal current turbine.

The undisturbed flow at (I) travels through the channel and passess through the tidal current turbine where it exerts a forces on the rotor of tidal current turbine. Based on Newton's Third Law, the tidal current turbine imposes an equal and opposite force on the flow, which is expressed as:

$$T = \frac{1}{2}\rho U^2 A_T C_T \tag{5. 10}$$

C_T is the dimensionless thrust coefficient defined as:

$$C_T = (\beta_4^2 - \alpha_4^2) \tag{5. 11}$$

where β_4 is the bypass flow velocity coefficient and α_4 is the wake flow velocity of tidal current turbine, which represent the acceleration and decrement in the wake flows velocity and bypass, respectively.

For rated current speed, U_r, the sum of the force relating to the tidal current turbine was 749kN (**Figure 5.4**). By replacing the left side of equation (5. 10*)* to 749 kN, and substituting the values from **Table 5.1**, the value for C_{loss} was calculated as 0.79.

However, if the current flow in the axial direction is different from the rated current speed, a correction parameter, α was adopted to adjust the relationship in as:

$$F_1 = \frac{\rho}{2} A_T C_T |U_{inc}| U_{inc}\, \alpha \tag{5. 12}$$

$$\alpha = {F_1}\Big/{\frac{\rho}{2} A_T C_T |U_{inc}| U_{inc}} \tag{5. 13}$$

α is the ratio of total force from regulated force with variable pitch and the unregulated force with purely quadratic force from equation (5. 13*)*. A α parameter value was required for every time step of the model for the time-dependent quantity of the function of tidal current flow velocity.

5.3.3 Model Setup

A total of 11 models were setup for deriving an appropriate α value. Model (A) was denoted as the "uninterrupted" condition. The tidal current turbine was incorporated into model (B) – (J). For model (B), α =1.0 and the force of tidal current turbine force was quadratic in the tidal flow current speed. Next, for model (C), α was identified from equation (5. *12)* and adopted from depth-averaged current speed from model (A). Subsequent models (D) – (J) were followed by increasing the deviation of axial direction of the tidal turbine. Every test model consisted of two complete tidal flow cycles (24 hours) with 12 hours of initiation period. The parameters of tidal turbine for the validation and experiment of tidal turbine representation are given in **Table 5.2** and **Table 5.3**, respectively.

Table 5.2: Parameters of tidal turbine for the validation of tidal turbine representation

Model	$C_{turbine}$	α	α reference model	$\lvert cos\,(\theta - \emptyset)\rvert$
A	0	-	-	-
B	0.79	(5. 12)	(a)	0
C	0.79	equation (5. 12)	(a)	0
C*	0.79	(5. 12)	(c)	0

Table 5.3: Parameters of tidal turbine for the experiments of model

Model	$C_{turbine}$	α	α reference model	$\lvert cos\,(\theta - \emptyset)\rvert$
D	0.79	(5. 12)	(C*)	10
E	0.79	equation (5. 12)	(C*)	20
F	0.79	(5. 12)	(C*)	30
G	0.79	(5. 12)	(C*)	40
H	0.79	equation (5. 12)	(C*)	50
I	0.79	(5. 12)	(C*)	60
J	0.79	(5. 12)	(C*)	70

5.4 Results

Model (A) was run for scenario without momentum loss in tidal turbine. The maximum depth-averaged current velocity in the mid of the model domain was 4.0 m/s (**Figure 5.9**). As mentioned earlier, 4.0 m/s represents a considerably strong tidal harmonic of M_2 for representative spring tide at a potential tidal current energy extraction site. This is to model an optimum extraction application (Easton et al., 2012). The friction of the turbine was included in the subsequent model (B) - (J), and the simulated depth-averaged tidal current flow velocity and turbine drag force were quantified as outputs of the model. With the simulated depth-averaged tidal current flow velocity, the predicted tidal turbine force (hereafter defined as theoretical force) was identified by using the tidal turbine force curve (**Figure 5.4**). Likewise, the simulated depth-averaged tidal current flow velocity was applied to determine the tidal current turbine kinetic energy dissipation and power using the relationships detailed in Section 5.2. The average of depth-averaged current velocity, tidal turbine axial current velocity, tidal current turbine friction force, tidal current turbine kinetic energy and tidal current turbine power output from each of the simulated model are shown in **Table 5.4**.

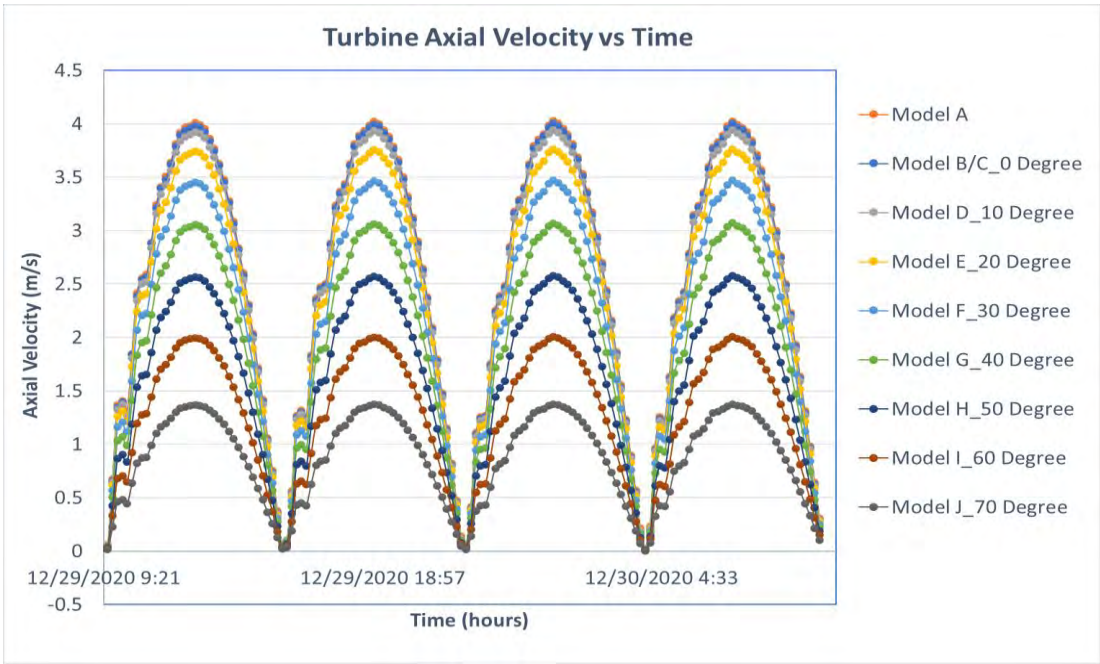

Figure 5.9: Predicted depth-averaged current velocity in various turbine axial directions

Table 5.4: Average tidal current outputs from the model tests

Model	U (m/s)	U_{ax} (m/s)	F (kN)	P (MW)	E_{turb} (MW)	$\lvert cos\,(\theta - \emptyset)\rvert$
A	2.53	-	-	-	-	
B	2.51	2.51	808.44	1.39	2.73	
C	2.51	2.51	399.99	0.65	1.19	0
D	2.51	2.47	404.56	0.65	1.21	10
E	2.51	2.36	423.81	0.65	1.29	20
F	2.52	2.18	487.91	0.68	1.56	30
G	2.52	1.93	522.98	0.68	1.75	40
H	2.52	1.62	475.94	0.52	1.62	50
I	2.52	1.26	378.84	0.28	1.3	60
J	2.52	0.86	279.45	0.1	0.97	70

5.4.1 Regulation of Tidal Current Turbine Force

The simulated tidal current turbine force for model B was quadratic in current speed as shown in **Figure 5.4**. It can be seen that the simulated tidal current turbine force for model (B) is much greater than theoretical tidal current turbine curve when the depth-averaged current velocity is less than cut-in speed ($U<U_{in}$). It is greater than theoretical force when the depth-averaged current flow velocity is between cut-in speed and rated speed ($U_{in}<U<U_r$). The simulated tidal current turbine force was equivalent to the

theoretical force when it reaches rated current speed. However, the tidal current turbine force continued to rise swiftly, deviating from the curve of theoretical tidal current turbine force.

In order to describe the tidal current turbine force more realistic to the actual device, model (C) has regulated the quadratic tidal current turbine force using the α parameter derived equation (5. 13). Although the predicted force has resembled the theoretical force more closely, some notable underestimations are discovered for depth average current velocity between rated current speed and cut-out speed ($U_r<U<U_{out}$). The inclusion of porous disc in the cell grid modified the depth-averaged current velocity of cell grid. Hence the value for α is misjudged and miscalculated. The quadratic relationship between current flow velocity and tidal current turbine force intensified although minor difference of current flow velocity occurred.

Instead of using model (A) without the structure being placed into the model, the calculation of the model is enhanced through α recalculated using the undisturbed flow (U_o) from model (C). The predicted tidal current turbine force showed excellent agreement with theoretical turbine force curve (**Figure 5.10**).

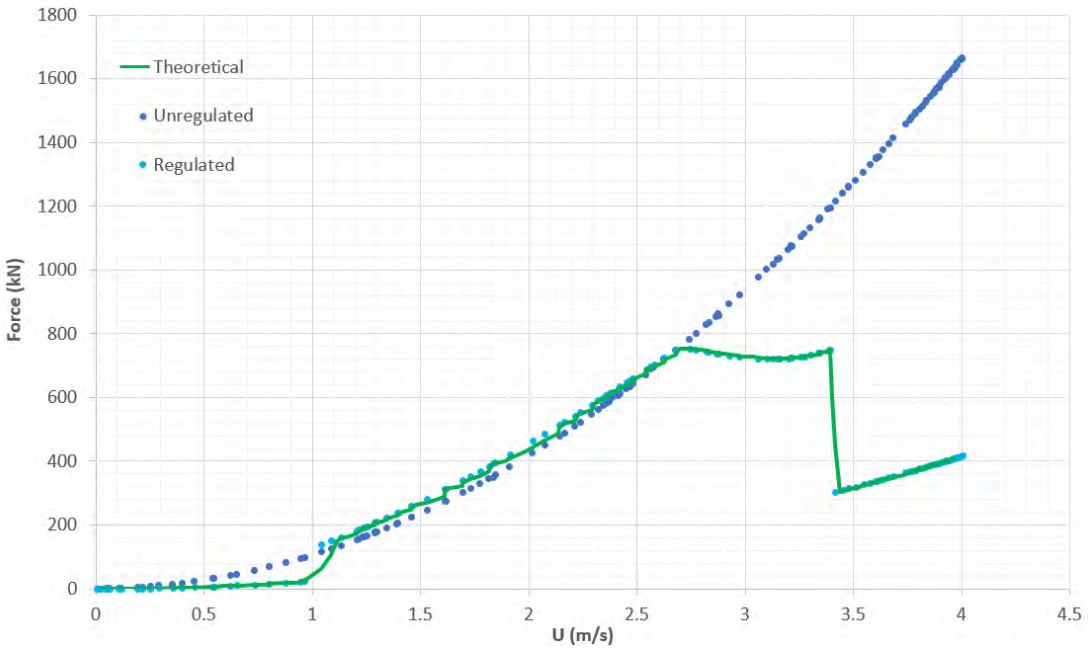

Figure 5.10: Comparison of regulated and unregulated turbine force with theoretical turbine force.

5.4.2 Power and Dissipation of Tidal Current Turbine

The tidal current turbine power coefficient, C_p, was approximately 0.40 at rated current speed (**Figure 5.2**). This constant coefficient is associated with the "unregulated" tidal turbine (model B). By substituting this constant value into equation (5. 1), the mean predicted tidal turbine power output for the model test was 1.39 MW (**Table 5.3**). It is much greater than the supposed tidal turbine rated power of 1.02 MW. By regulating the tidal current turbine for model (C) to effectively match the power coefficient C_p with the current speed (**Figure 5.2**), the mean power of tidal current turbine is reduced to a more realistic value of 0.65 MW.

The mean kinetic energy dissipation by the tidal current turbine was estimated by the product of tidal current turbine force and depth-averaged current speed equation (5. 8). The mean dissipation of kinetic energy by the regulated turbine was less than half of the unregulated tidal current turbine (**Table 5.4**). The tidal turbine regulation limits the

maximal tidal kinetic energy dissipation (**Figure 5.11**). It is observed that unregulated tidal current turbine of model (B) dissipates energy at a maximum rate of 6.59 MW, much higher rate than the unregulated tidal current turbine associated with tidal current turbine of regulated tidal current turbine (model (C)).

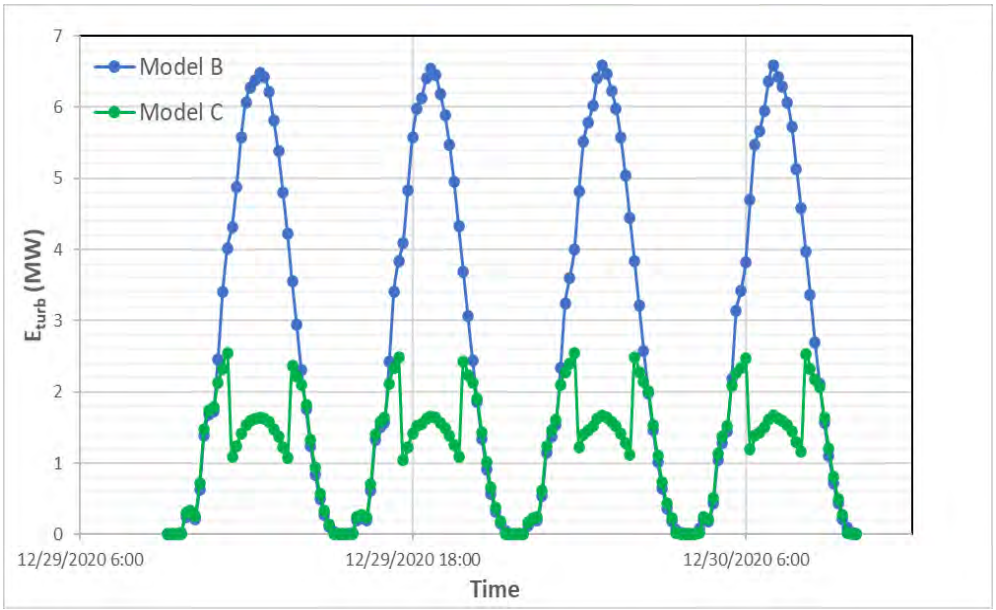

Figure 5.11: Total kinetic energy dissipated by tidal stream turbine

5.4.3 Deviation of Tidal Current Turbine Axis

The effect of deviating the relative angle between flow direction and tidal current turbine axial direction ($\theta - \emptyset$) was assessed in this chapter through model (D) – (J) (**Table 5.4**). The magnitude of tidal current turbine axial velocity decreases when the deviation of relative angle of tidal current turbine increases (**Figure 5.12**). Therefore, larger incoming current speed is required to achieve rated, cut-in and cut-out settings. This effect is similar by adjusting the tidal current turbine thrust curve rightward along the x-axis (**Figure 5.3**) and subsequent effect to the performance of the tidal current turbine.

The tidal current turbine was working within the range of operation ($U_r < U_{ax} < U_{out}$) when axial direction increased from 0˚ – 40˚ (**Figure 5.4**). Consequently, the mean

power output, tidal current turbine force and energy dissipation all increased for this interval (**Figure 5.12**; **Table 5.3**). However, when $|\theta - \emptyset|$>40˚, the turbine power, energy and force dissipation reduced rapidly as the tidal turbine axial current speed did not achieve the tidal current turbines rated speed. The energy and force dissipation reduced rapidly axial deviation more than 40 degrees is mainly because the majority of the mean and maximum axial velocity are below the rated current speed

It is to be noted that the peak tidal current turbine force (**Figure 5.12c**) and peak tidal current turbine energy dissipation (**Figure 5.12d**) were inconsistent with peak tidal current turbine power. The peak kinetic energy dissipation when turbine deviated at 40˚ was 1.2 times larger than 0˚. For the latter axial scenario, the peak tidal current turbine thrust force was attained simultaneously with peak turbine support drag force, and therefore more kinetic energy dissipation was achieved for less tidal turbine power.

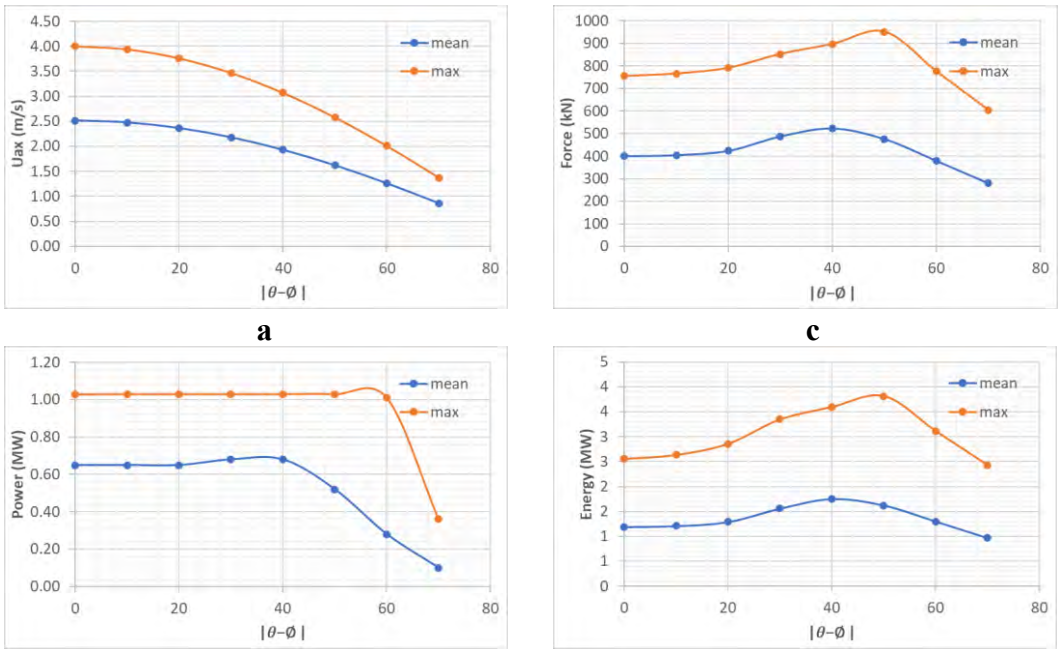

Figure 5.12: The influence of tidal current turbine on turbine performance: a) tidal current turbine axial speed, b) tidal current turbine power, c) tidal current turbine force, d) tidal turbine kinetic energy disspiation

5.5 Discussion

The fundamental principle of horizontal tidal current turbine energy extraction is straightforward where the kinetic energy of the water is transferred into the rotor of the tidal turbine. However, the explanation on the energy extraction process is more complex and thought-provoking. The extraction of the tidal current energy is non-linear and it is not isotropic to the incoming flow.

The effect of tidal stream energy extraction is normally included into a hydrodynamic model to estimate the available resource and to assess its effect to environment. The conventional method is to model the tidal current turbine by an additional constant bed friction coefficient, without differentiating in kinetic energy dissipation. This method is effective and convenient to identify the worst-case scenario for environmental impact assessment. However, real turbine does not behave linearly in current speed. It is affected by the tidal current turbine design and hydrodynamic condition. The loss coefficient of the tidal current turbine can be altered to represent the characteristic of a pitch-regulated tidal current turbine.

Only single tidal current turbine was simulated as a porous plate in the momentum equation of the 2D hydrodynamic model. The dissipation force consists of influence from the thrust of rotor and structure drag of a tidal current turbine. Realistically, the relationship between dissipation force and current speed is proved to be much more complex than quadratic force estimation (**Figure 5.4**). It is important to stress that the power production was much lesser than dissipation (**Figure 5.5**). The tidal current turbine power curve enables the interested party to determine the power output, which is important to be adopted for cost projection. In order to achieve an optimum and sustainable design, nevertheless, one should seriously take the environmental effect on

the flow into design consideration instead of only focusing on the output of electrical power.

From the analysis, on-average the unregulated tidal current turbine model (model (B)) dissipates much larger kinetic energy than regulated tidal current turbine (model (C)). For regulated tidal current turbine, greater kinetic energy is extracted when $U_{in}<U_{ax}<U_r$. While, for unregulated tidal current turbine, greater kinetic energy is extracted when U<U_r (**Figure 5.10**). Therefore, the non-linear relationship between the current speed and kinetic energy dissipation, may significantly affect the interaction between the environment and extractable energy.

The tidal turbine is included as porous plate exerted a loss on the momentum of the flow and altered the tidal current speed at the tidal current turbine location. By adjusting the tidal current turbine loss coefficient changes in the momentum loss in the local flow occured, which in turn alters the tidal current flow speed on which the tidal current turbine related loss coefficient is relied on. The porous plate inclusion method makes it easy to regulate the tidal current turbine precisely, contrast with bed friction coefficient, where model iteration with multiple repetition is required to achieve a satisfactory solution. The bed friction method may have difficulties in turbine parameterization for multidimensional array of device simulation. In comparison, the porous plate method applied in this study is simpler to be used as it can be easily adjusted via loss coefficient parameterization when modelling the multidimensional array of device.

High technology type of tidal current turbine is adopting the fixed-axis tidal current turbine and it is highly responsive to different flow direction. A fixed tidal current turbine is not isotropic to the incident flow; the force, kinetic energy dissipation and power output are heavily influenced by the flow current direction of the turbine (**Figure 5.12**).

Interestingly, the axial misalignment below 20˚ has insignificant influence on the tidal turbine behaviour, based on the environmental conditions modelled in this study.

It is important to be noted that the experiments carried out for model (C) – (J) were not meant to be used as a direct reference for tidal current turbine siting purposes. For instance, the simulation result showed that the power output could be maximised by adjusting the tidal current turbine axis to 30˚ to the incident flow direction (**Table 5.4** & **Figure 5.12**). This can be untrue if the behaviour of real site is taken into consideration. The experiment is limited to single tidal harmonic with considerably large current speed of 4 m/s and lower cut-out speed of 3.4 m/s. Realistically, variation of tidal data is expected for longer time period due to additional tidal harmony. It is highly anticipated that optimal tidal current turbine orientation would be aligned with the current flow direction when a representative spring-neap tidal cycle was simulated for an appropriate tidal turbine. However, the direction of the turbine may not be optimised for the flow in reverse direction. It was also assumed that the porous plate was not dependent on the incoming tidal current flow direction. Realistically, the tidal turbine support structure would be more streamline in the axial direction and facing a larger area of exposure to deviated incident flow.

Further from that, the values for U_{in}, U_r and U_{out} were assumed for the model tests. These values essentially control the form of tidal current turbine power curve (**Figure 5.2**) and turbine force curve (**Figure 5.3**) and therefore they are important parameters for identifying the tidal current turbine characteristics. In reality, these parameters can be adjusted to achieve maximum power output for a certain set of flow data. It is therefore assumed here (also in the next chapter) that tidal current turbine is off shelf and U_{in}, U_r and U_{out} are fixed.

Lastly, the two-dimensional hydrodynamic model is a depth-averaged model and therefore no details on the vertical flow profiles is provided. Constant value depth-averaged current speed is assumed from the top to bottom of the water acting on both turbine support structure and turbine rotor. Realistically, the current velocity acting on the turbine support structure is lower than at the turbine hub. A three-dimensional hydrodynamic model can be adopted to better model the variation between energy dissipation by the support structure and turbine rotor, but higher computationally cost could be incurred.

In order to describe the tidal current turbine force more realistic to the actual device, model (C) has regulated the quadratic tidal current turbine force using the α parameter equation (5. 12). Although the predicted force has resembled the theoretical force more closely, some notable underestimation is discovered for depth average current velocity between rated current speed and cut-out speed. (U_r<U<U_{out}). The inclusion of porous disc in the cell grid modified the depth-averaged current velocity of cell grid. Hence the value for α is misjudged and miscalculated. The quadratic relationship between current flow velocity and tidal current turbine force intensified although minor difference of current flow velocity occurs.

5.6 Summary

Chapter 4 has demonstrated that Straits of Malacca has complex flow patterns. Misalignment of flow direction during peak flood and ebb tide was observed. This chapter demonstrated the characteristics of fixed-axis horizontal tidal current turbine is very much dependent on the tidal flow nature. The quantification of kinetic energy to be extracted

by a tidal current turbine is non-linear and anisotropic to the incident current flow direction.

The uniqueness of flow at each potential headland site may be crucial for identifying the exploitable yield of energy and environmental influence of tidal current turbine energy extraction development. Considering of this uniqueness when modelling tidal current energy extraction in hydrodynamic model, it is worthy to carry out further examination. The inclusion of tidal current turbine explained in this chapter provides a useful tool for such a study. A hydrodynamic model of Negeri Sembilan Coastline with multiple headlands will be adopted to assess different scenarios involving single and arrays of tidal current turbines deployment.

6 SIMULATING REGULATED TIDAL CURRENT TURBINES DEPLOYMENT CONFIGURATIONS EFFECTS

Single and array of tidal current turbines are simulated at an energetic tidal channel with an enhanced tidal current headland. For the tidal current turbine array simulation, the turbines are 'regulated' in relation with all other turbine in the array. The dissipation of energy due to the tidal current turbine in different configurations is estimated and the generation of electrical power is quantified.

The environmental impact assessment by evaluating the bed shear stress and sediment transport parameter for the tidal channel with multiple headlands are assessed and discussed. The monsoonal effect: Northeast monsoon, Southwest monsoon and inter-monsoon (pure tide) are also evaluated for sediment transport scenario.

6.1 Introduction

6.1.1 Practical Application of Tidal Current Turbine Deployment

The practical application for tidal current energy extraction was assessed based on two main aspects: extractable energy and environmental impact. The process of tidal current turbine modification to the total flow environment is complex; it may involve near and far-field effects to the environment (Vennell, 2010). Nevertheless, owing to the complexities of actual site deployment, a number of limitations that are unlikely to be applied in real condition (Atwater & Lawrence, 2011; Polagye et al., 2011):

a. Tidal condition does not change as tidal energy is extracted.

Theoretically, it is assumed that there is no interaction of the ocean tides which the energy extraction within the channel. In reality, removing tidal energy from the sea can affect the ocean tides (Arbic & Garrett, 2010). Numerical model studies show that tidal power diverges from the analytical theories due to tidal current energy extraction (Karsten et al., 2008; Polagye et al., 2011).

b. The entire channel is occupied and allows the tidal flow to pass through the tidal turbine rotor.

In real system, it is not feasible to install the tidal current turbines in uniform line perpendicular to the flow by occupying the whole cross section of the tidal channel. Site constraints (e.g., geographical landform, water depth, marine life habitat, navigation channel, etc.) restraint the cross section of the array deployment. The gap between the tidal currant turbine for an array of deployment may dissipate the energy via turbine wake mixing. According to Garrett & Cummins (2007) and to Garrett & Cummins (2008), the unfilled occupation of a tidal channel may cause two-third reduction to the potential power generation. However, the maximum extractable energy can be achieved through rows of partial fence deployment (Vennell, 2010).

c. No flow diversion through an alternative channel

The headlands and islands may complicate the geography at the potential tidal current energy exploitation sites by creating branched and narrowed channels. It can be mitigated by deploying tidal current turbines at one branch and allow other channel to flow freely for the vessel transit and marine life preservation. However, this assumption may not be practical for the analytical expression as tidal flow will be diverted from the channel with tidal current turbines into another free channel

((Atwater & Lawrence, 2011; Bryden et al., 2007; Polagye et al., 2011; Sutherland, 2007).

Based upon the above discussion, it is difficult to achieve the maximum theoretical power of a tidal channel in practice even not accounting the engineering limitation, economic consideration and environmental regulations. Moreover, the potential tidal current energy sites in Malaysia, hardly comply to the architecture of simple tidal channel on which analytical expressions are referred to (see Chapter 4). Numerical modelling of the complex environment with accurately parameterized tidal current energy extraction allows more effective and higher quality assessment tool, aside from relatively higher computational cost requirement.

6.1.2 Tidal Current Turbine in Different Configurations

For simulating the tidal current energy exploitation in the ocean or large basin, the device has been commonly represented by an additional bed shear stress into the source terms of momentum equations. However, the parameterization of added bed shear stress does not resolve the wake effect details behind the tidal turbines (Garrett & Cummins, 2007). A better approach, actuator disc theory is adopted in this study. The tidal current energy extraction is modelled by representing the tidal current turbine thrust through inclusion of negative sink term into the momentum equation. This approach is commonly applied in previous far-field models (Adcock, 2014; Plew & Stevens, 2013).

For the quadratic friction, the tidal current turbine energy friction varies as the square of the tidal current speed is scaled by loss of the tidal current turbine coefficient. Tidal current turbine power is scaled by the cube of tidal current speed as well as the coefficient of the turbine power. Numerical modelling was set up to assess the configuration effect

of tidal current turbine based on actual site condition in quantifying the extractable power and environmental impact assessment at Tg Tuan Headland. As discussed earlier, site condition may limit the maximal extractable power at the potential site, where physically realistic values for turbine coefficient may not be applicable (Karsten et al., 2008; Sutherland, 2007; Walters et al., 2013).

Due to variation of configuration and at site condition, i.e., depth, geographical condition, arrangement of tidal current turbine array, size of tidal current turbine array, the proportion of the free-stream energy to be extracted by a turbine may vary with the flow speed through the tidal current turbine rotor. Based on the momentum loss modelling through the adjustment of the angle of the blade pitch, the power (via the tidal current turbine power coefficient) and rotor thrust (via a tidal current turbine rotor thrust coefficient) of a tidal current turbine analysis can be regulated through the procedures in Chapter 5. The regulation is crucial for ensuring a consistent output of power within the limit and minimizing the damage and failure risk of the device. Hence in 2D modelling, the parameterization of every tidal current turbine must be individually “adjusted” in relation with its arrangement of tidal current turbine at site. This increases computational expense as every model requires to specifically regulate each turbine in prediction analysis.

6.1.3 Single and Cumulative Headland Energy Extraction Effects

A vast research was undertaken to study the power take-off efficiency of an individual tidal farm in response to the operation and deployment, and the farms physical configuration, as well as the impact of the facility to the coastal water and environment. Li et al. (2019) discovered 3% reduction in wave height under the influence of a standalone turbine located 0.4 m from the free surface and 7% increment in bed stress

upstream of the turbine due to the inclusion of surface waves. Tidal turbine deployments at headlands gapped at small intervals along the coastline tend to result in flow interruption, which is likely to cause some negative impacts to the coastal livings and environment (Guillou & Chapalain, 2017; Lo Brutto et al., 2017; Wang & Yang, 2017). Drastic change of tide-induced Lagrangian circulations in the north-western coastal waters of Brittany, France as a result deployment of a series of horizontal-axis turbines was reported by Guillou and Chapalain (2017). Furthermore, tidal array may lead to localized sediment accumulation, which potentially affect the benthic ecology of the region (Haverson et al., 2018). A recent study at Ramsey Sound showed that nine tidal energy converters will cause changes to eddy propagation leading to changes in the current velocity field up to 24 km from the tidal array and subsequently will cause localized alterations to the mean and maximum bed shear stress extend to 12 km from the tidal array (Haverson et al., 2018).

The extent of the influence is largely depends upon the size, numbers, configuration and scale of the tidal turbines (Hasegawa et al., 2011). In the investigation of the far-field hydrodynamic effects of tidal energy extraction with respect to the length of the water column (i.e. the entire water column and the lower water column at 20 m above the sea bottom) in Minas Passage, Hasegawa et al. (2011) found that the tidal turbine energy extraction from the entire water column has much larger impact on the tidal elevations and circulations. Based on a 3D numerical model investigation at Pentland Firth, Inner Sound Channel, the scale of energy extraction is found to be one of the main factors that influence the changes to morphodynamics of sandbanks (Chatzirodou et al., 2019). A full scale of 300 MW Tidal energy converter, TEC, deployment study near to headland also demonstrated significant changes to the maintenance of headland sand banks over a spring-neap tide cycle, thus suggesting the importance of TEC deployment scale to be sited near to a headland (Neill et al., 2012). A similar study was carried out by Chen et

al. (2013) to assess the impact of a tidal farm consisting of 55 units of turbines within the Penghu Channel of Taiwan Strait using a numerical model. They reported that the effect of tidal turbine installation on water level and tidal current within Penghu Channel was not significant. A tidal energy extraction potential site study at Gulf of California demonstrated that regions with less energetic tidal currents but in deeper waters can be chosen due to large tidal energy resource to be explored (Mejia-Olivares et al., 2018). Hence the risk of interaction to sites geographically close to each other will grow when intermediary sites are developed (Haverson et al., 2017).

The presence of turbines near the headlands of Negeri Sembilan would modify the regional hydrodynamic regimes to a certain extent. Upon energy tapping by the upstream tidal turbine, the energy production by downstream turbines would be reduced due to reduction of hydrodynamic power (Lo Brutto et al., 2017). Furthermore, the risk of site interactions will increase in parallel with the numbers of tidal farm sites within the study area. However, the study of flow interactions and environmental impact assessment of the multiple headland tidal farms is rather limited. To further explore this problem, the effect of single and multiple hypothetical 1.5 km x 1.5 km (15 x 15 turbines) tidal farm deployment within the higher potential tidal energy extractable area in proximity of the headland within the coast of Negeri Sembilan was investigated using the momentum loss approach. A comprehensive study on the interaction risk of tidal farm along Negeri Sembilan coastline was carried in this research. The environmental impact of multiple tidal farm deployment was looked into detail with various aspects: tidal current speed, bed shear stress, sediment transport (ST) and monsoonal effect.

6.1.4 Chapter Aims and Scopes

In this chapter, tidal current turbine in different configurations is simulated at a potential tidal current energy extraction site, Tg Tuan Headland that is located within Negeri Sembilan coastline. The parameterization of horizontal fixed-axis tidal current turbines discussed in Chapter 5 is incorporated into the calibrated and validated high-resolution HD model domain developed in Chapter 4. It is foreseen that different configurations of arrangement and site condition of regulated tidal current turbine may perform differently. The assessment on hydrodynamic impact is significant for EIA purpose, as regulated tidal current turbines "dissipate" some of the kinetic energy in the tidal flow that would be extracted.

Chapter 6 is organised as follows. First section describes an overview of the modelling system (Section 6.2). Followed by that, the configuration and parameterization of tidal current turbine is described (Section 6.3). The inclusion of the tidal turbine into the model is hypothetical, but the hydrodynamics, geographical constraint, wake interactions and device spacing, were intended to be as realistic as possible. The total dissipation for each scenario, including the tidal rotor efficiency and structure drag, are quantified and the environmental stress estimation between regulated and unregulated tidal current turbine is provided in Section 6.4.

The effect of headland series on tidal energy extraction, and the resulting potential impacts to the adjacent coastline and environment by means of numerical modelling is given in Section 6.4.4. The coastline of Negeri Sembilan within Straits of Malacca, Malaysia was selected as a case study for this research project.

6.2 Model Overview

Delft3D by Deltares was applied for numerical modelling in this study. Delft3d-FLOW is a multi-dimensional hydrodynamic simulation program that calculates non-steady flow and transport phenomena resulting from tidal and meteorological forcing on a curvilinear, boundary-fitted grid. Delft3D-Flow solves the Navier-Stokes equations for an incompressible fluid, under the shallow water and the Boussinesq assumptions. In the vertical momentum equation, the vertical accelerations are neglected in which it leads to the hydrostatic pressure equation.

The applied model is similar to the established numerical models such as MIKE 21, POM and TELEMAC. Delft3D has been applied in major coastal and ocean investigations and engineering studies worldwide. Carballo et al. (2009), Chatzirodou et al. (2015), and Yang et al. (2013) have used Delft3D for energy extraction assessment by using 2DH momentum equations. It has been adopted by a number of researchers in conducting energy extraction assessment by using 2DH momentum equations (Carballo et al., 2009; Chatzirodou & Karunarathna, 2014; Chatzirodou et al., 2015; Ramos & Iglesias, 2013). The assessment in Chapter 4 demonstrated delivering reliable and useful description of the tidal flow condition at the enhanced tidal current energy extraction site, Tg Tuan Headland. The model setup and validation of the numerical model was described in Chapter 4. The model assumptions to specify the open boundaries and bed roughness coefficient are elaborated in this section.

6.2.1 Model Domain and Open Boundary

Numerically assessing the headland site selection and impact of energy extraction around the headland requires a dedicated modelling approach that accounts for large-scale oceanic flows over the Malacca Strait and sufficient model resolution in time and space

(x, y, t). In order to achieve this, Delft3D simulations were setup using a regional and higher resolution local model.

The finite difference mesh is in a spherical co-ordinate system grid that covers the whole Straits of Malacca for regional model and Tg Tuan Headland for local model. For regional model, the grid size reaching 900 m x 900 m at the outer (ocean) boundary, in water depths of roughly 200 m, sufficiently far that any numerical disturbance that might occur at the boundary may not affect the model results in the area of interest (Tg Tuan Headland). The grid size decreases to 100 m x 100 m for local model to sufficiently model the site condition at the Tg Tuan Headland.

The model was run with a time step of 60 second, which alongside the grid size ensures numerical stability according to the Courant-Friedrichs-Lewy criterion (Courant et al., 1928). The model domain was large enough to enable sufficient propagation from the open boundaries. In order to include the large-scale, oceanic circulation effects in the Regional Model, time series boundary conditions are generated at the Northern Boundary and Southern Boundary using the Oregon State University (OSU) TOPEX/Poseidon global inverse solution TPXO (Egbert & Erofeeva, 2002). TPXO was utilized to provide tidal forcing. TPXO 7.2 is a current version of a global model of ocean tides, which best fits, in a least-squares sense, the Laplace Tidal Equations and along track averaged data from TOPEX/Poseidon and Jason obtained with OSU Tidal Inversion Software (OTIS) (Egbert et al., 1994; Egbert & Erofeeva, 2002).

It is well noted that that “constant” offshore open boundaries maybe not suitable for a numerical model consisting of tidal current turbine, as the reflected tidal fluctuation is not able to travel back across the open boundaries (Garrett & Greenberg, 1977). However, this effect is more significant for considerably large-scale energy extraction model (Adcock, 2014). In this work, a relatively much insignificant quantity of energy was

extracted; only small percentage of the mean frictional dissipation of the Tg Tuan Headland. The numerical model described in Chapter 4 and **5** were then retained for the present investigation.

6.2.2 Modelling of Tidal Energy Extraction

In this study, the energy loss effects of tidal current turbines were investigated by implementing a "porous disc" fronting the headlands. "Porous disc" is assumed as a thin hydraulic structure relative to the model grid size that acts as a semi-permeable barrier to the flow, which covers only part of the water column and adds friction to the flow (Delft3D Flow Manual, 2011). The porosity is controlled by an energy loss coefficient that is prescribed across the height of the structure. Momentum sink approach (momentum loss added in the Navier-Stokes equations) is adopted for estimating the magnitudes of speed that would be reduced due to tidal energy extraction by the tidal turbine farm (Chen et al., 2013; Defne et al., 2011; Hasegawa et al., 2011; Ramos, Iglesias, et al., 2013; Shapiro, 2011; Yang et al., 2013). Detail description of energy extraction modelling are given in Section 3.3 and Chapter 5. The parameterization of tidal current turbines in different configurations is discussed in Section 6.3.2. The modelling scenarios for this study are listed in **Table 6. *1***.

Table 6. 1: Modelling scenarios for tidal turbine deployment

Assessment	Scenario no.	Modelling
Hydrodynamic	(A) Baseline (Without tidal current turbine)	
	1	existing
	(B) Depth assessment	
	2	single tidal turbine at d1
	3	single tidal turbine at d2
	4	single tidal turbine at d3
	5	single tidal turbine at d4
	6	single tidal turbine at d5
	7	single tidal turbine at d6
	8	single tidal turbine at d7
	9	single tidal turbine at d8
	(C) Headland tidal farm interaction assessment	
	10	single tidal farm at H1
	11	single tidal farm at H2
	12	single tidal farm at H3
	13	single tidal farm at H4
	14	multiple tidal farm H1, H2, H3 and H4
	(D) Tidal array in row assessment	
	15	Array in single row 1 (L1)
	16	Array in single row 2 (L2)
	17	Array in single row 3 (L3)
	18	Array in single row 4 (L4)
	19	Array in single row 5 (L5)
	20	Array in multiple rows (L1, L2, L3, L4 and L5)
Bed Shear Stress	(E) Headland tidal farm interaction assessment	
	21	single tidal farm at H1
	22	single tidal farm at H2
	23	single tidal farm at H3
	24	single tidal farm at H4
	25	Multiple tidal farm H1, H2, H3 and H4
Sediment Transport	(F) Headland tidal farm interaction assessment	
	26	without tidal farm
	27	single tidal farm at H1
	28	single tidal farm at H2
	29	single tidal farm at H3
	30	single tidal farm at H4
	31	Multiple tidal farm H1, H2, H3 and H4
	G) Monsoon effect	
	32	Without tidal farm under Pure Tide
	33	Without tidal farm under Northeast monsoon
	34	Without tidal farm under Southwest monsoon
	35	Multiple tidal farm H1, H2, H3 and H4 under Pure Tide
	36	Multiple tidal farm H1, H2, H3 and H4 under Northeast monsoon
	37	Multiple tidal farm H1, H2, H3 and H4 under Southwest monsoon

6.3 Tidal Current Turbine Modelling

6.3.1 Natural Kinetic Energy at Negeri Sembilan Coastline

As deliberated in Chapter 4, energy potential along the same coastline with length of approximately 50 km can differ quite significantly. Comparison of four headlands (H1 – H4) around the Negeri Sembilan Coastline in the estimation for the maximum power output at these four sites showed high exploitable potential for power generation at headland with narrowest channel, Tg Tuan Headland.

Subsequently, further analysis by assessing a suitable zone for TEC deployment was carried out by applying a high resolution spatial numerical model at the headland area. This study demonstrated that extractable tidal energy area at different zones of one headland can vary quite substantially although geographically they are close to each other. Hence, robust assessment using finer grid of the available power for other identified suitable tidal stream energy areas in Malaysia is crucial. The modelling results revealed that due to its high peak flow speed and suitable water depth, the seaward tip of Tg Tuan Headland is identified as a feasible tidal energy extraction site.

The identification of feasible tidal current turbine deployment sites based on the available resource will be used to assess both the sea hydrodynamic condition and on the accessible power. Accessible power is a measure of the uninterrupted current flow; yet, tidal current turbines deployment will modify the undisturbed tidal current flow, and hence will affect the available resource. This chapter aims to deliver the hydrodynamic influences on available power of tidal energy extraction.

Fraenkel (2002); Fraenkel (2007) and Myers &Bahaj ((2005) suggested that the deployment site should have a water depth ranging from 20 to 50 m, and the flow should be uniform preferably with a peak spring flood velocity exceeding 2.0 m/s and median velocity exceeding 1.0 m/s. Note that the minimum tidal flow speed to enable the

horizontal axis turbines to generate power (cut-in speed) is 1.0 m/s (Myers & Bahaj, 2005) as described in Chapter 5. Bathymetry and hydrodynamic assessment deliberated in Section 4.3.2.1 demonstrated the area of extractable energy at headland H3 that fulfilling the median peak velocity and water depth criteria is demarcated in brown outlined area (~2 km^2) as indicated in **Figure 4.30**. This brown outlined area can cater 233 numbers of 10 m diameter horizontal tidal turbine (Fraenkel, 2007; Fraenkel, 2002; Myers & Bahaj, 2005) where both lateral and longitudinal spacings between rows are of 10 times the rotor diameter.

6.3.2 Parameterization of Tidal Current Turbine Array

The water flow through each tidal turbine is unique due to the change of bathymetry. The loss coefficient, C_{loss-u} should be adjusted by considering the incoming velocity of the turbine rotor as the operational conditions affect the $C_{D,total}$. However, due to limitation of Delft3D in addressing the variation of c_{loss-u} required for this study, this research assumes all the tidal current turbines are subjected to constant flow magnitude and loss coefficient. Thus, the force and power produced by each turbine in an array can be expressed as:

$$F_\xi = \frac{\rho}{2} A_T (C_s + C_T) \left| U_\xi \right| U_\xi \tag{6. 1}$$

For a tidal current turbine array oriented in the η-direction, the impeded flow is in the ξ-direction with the diameter of turbine blade of 10 m is assumed for current assessment. The amount of energy supplied by the turbine is influenced by three factors, namely the incoming flow velocity of turbines U_ξ, the swept area A_T of tidal turbines, and the turbine efficiency C_T. Each marine energy current converter unit requires a rated output, which

defines the maximum amount of power that can be produced by each turbine (Fraenkel, 2002). The optimal design of rated power level depends on the costs related with capturing energy from peak velocity at the Tg Tuan Headland site that may only occur for short period of time. No additional energy would be converted for flow velocities higher than these values. Based on assessment made in Chapter 4, the peak flow velocity at Tg Tuan Headland is 2.2 m/s at certain spots. Although the potential site is not able to attain the cut-in speed required, for analysis purpose, an established theoretical force imposed by regulated tidal current turbines (**Figure 5.4**) is adopted for analysis hereafter.

Fixed-axis horizontal tidal current turbines is anisotropic to the incident flow. However, Chapter 5 demonstrated that the directional effect is relatively minor for critical flood-ebb misalignment (i.e., < 20°). Although there are certain areas having deviation of flow direction > 20° at some areas of Tg Tuan Headland (Zone C), these settings were deemed not favourable for tidal turbine siting. Anisotropy is therefore considered as secondary and disregarded in the configuration assessment in this chapter.

6.3.3 Modelling Tidal Current Turbine in Different Depth

The tidal flow field at the vicinity of Tg Tuan Headland is quite complex due to the protruding geographical feature. The flow field becomes even more complex in the presence of tidal turbines. Each tidal turbine absorbs the upstream energy and consequently reduces the hydrodynamic power to the turbines located downstream (Lo Brutto et al., 2017). Chen et al. (2015) found that the lateral and longitudinal spacings between turbines significantly affect the overall performance of facility.

To explore the configurational effect of tidal turbines, depth effect of tidal turbine was investigated at the selected study site (at the tip of Tg Tuan Headland). A tidal turbine

was integrated into the calibrated, high-resolution model and positioned at eight different locations with varying water depths within Zone B, i.e., 25.46 m (D1), 27.23 m (D2), 28.41 m (D3), 29.39 m (D4), 30.21 m (D5), 30.86 (D6), 31.33 m (D7) and 31.64 m (D8), as illustrated in **Figure 6.1**. An array of tidal current turbine of 10-m-diameter-blade turbines extending vertically over the entire water column oriented in the ξ-direction is presented in **Table 6.2**. The facility will impede flow in the η-direction causing a reduction of momentum at the turbine array. The influence of water depth on tidal energy extraction was assessed using eight scenarios (D1 to D8) with varying water depths (25 – 32 m). **Table 6.2** presents the specification of the depth scenarios modelled. For each scenario, the tidal turbine was distanced at an interval distance of 90 m from the turbine used in the previous scenario. The momentum loss resulted from the turbine deployment of each scenario was quantified. In these simulations, all other variables influencing the current flow, including tidal current turbine size, are held constant.

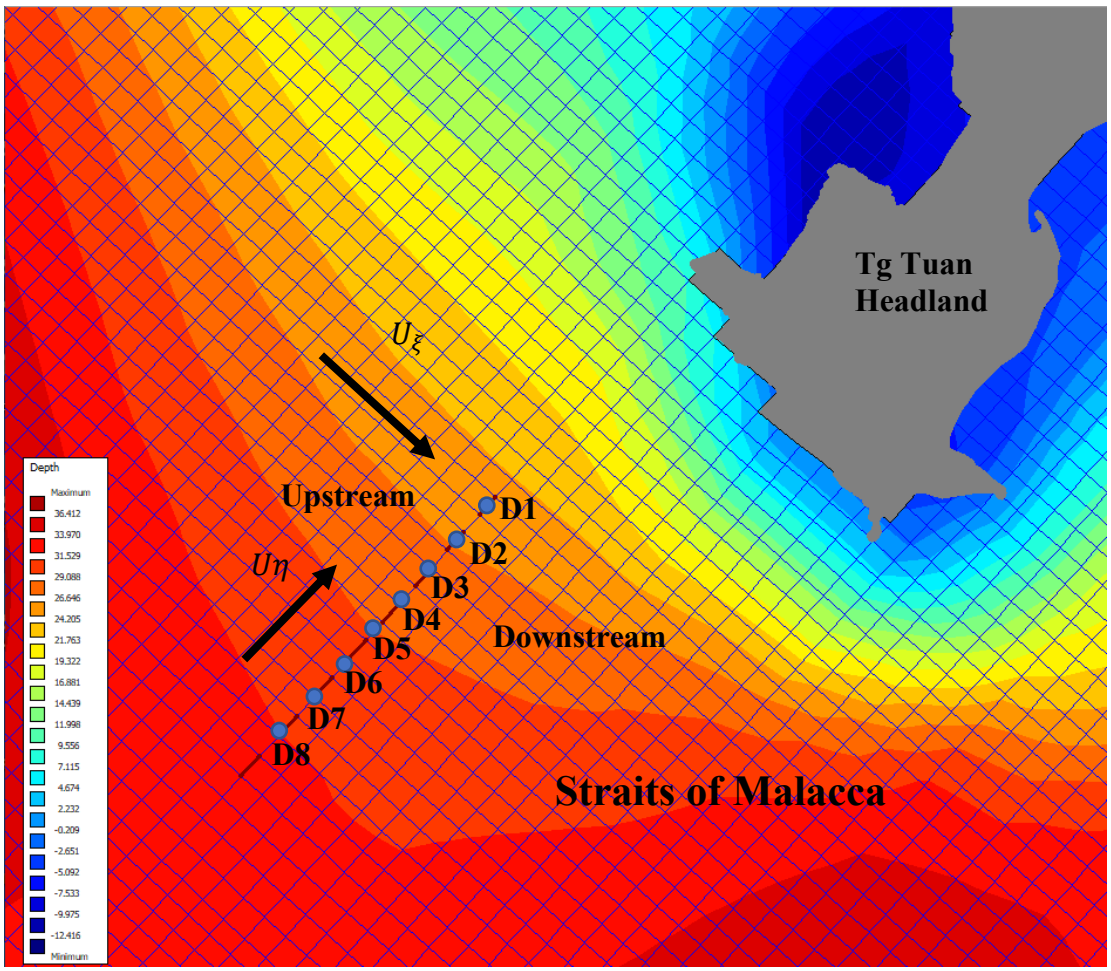

Figure 6.1: Tidal turbines aligned in the η-direction perpendicular to the current flow U

Table 6.2: Specification of tidal current turbine at Tg Tuan Headland

Turbine No.	Rated Power	Depth	Location (mid-point)	
	(MW)	**(m)**	**°E**	**°N**
D1	1.02	25.46	101.8407	2.4105
D2	1.02	27.23	101.8403	2.4031
D3	1.02	28.41	101.8392	2.4019
D4	1.02	29.39	101.8384	2.4007
D5	1.02	30.21	101.8372	2.3995
D6	1.02	30.86	101.8359	2.3985
D7	1.02	31.33	101.8351	2.3971
D8	1.02	31.64	101.8337	2.3958

6.3.4 Modelling Tidal Current Turbine Array

Guillou & Chapalain (2017) found a significant alteration of tide-induced Lagrangian circulations due to placement of a series of tidal turbines in the north-western coastal waters of Brittany, France (Guillou & Chapalain, 2017). Hasegawa et al. (2011) and Ahmadian et al. (2012) reported that the effect of tidal energy extraction may not be just limited to the vicinity of the deployment area but it could also spread to a few kilometers away from the deployment site (far-field impacts) (Ahmadian et al., 2012; Hasegawa et al., 2011). Whereas 3% decrement in wave height and 7% increment in bed stress upstream of the turbine under the effect of a standalone turbine was reported by Li et al. (2019). Similar study was also undertaken by Neil et al. (2012) and they reported that the deployment of a full scale 300 MW TEC near a headland resulted in significant deformation of the headland sand banks over a spring-neap tide cycle (Neill et al., 2012).

Furthermore, alterations in current flow and bed shear stress may also change the sediment transport patterns and the beach profiles, which are likely to cause undesirable environmental effects to the benthic and ecology in the sea (Chatzirodou et al., 2019; Haverson et al., 2018). For instance, nine tidal turbines installed at Ramsey Sound were reported to cause alterations to eddy propagation, which affect the far-field current velocity up to 24 km from the tidal farm, resulting in localized changes to the mean bed shear stress as far as 12 km from the tidal farm (Haverson et al., 2018). Nevertheless, the effect of energy extraction varies with the geographical and environmental parameters of the selected site. For example, the hydrodynamic impact assessment undertaken by Chen et al. (2015) for deployment of 55 units of turbines within the Penghu Channel of Taiwan Strait using a numerical model showed that the tidal turbine installation does not pose significant effects on water level and tidal current. Li et al. (2019) discovered that the immediate wakes resulted from tidal turbines become negligible within 9D (D is the diameter of the tidal turbine) downstream of the tidal turbine, but the far wake effect on

bed shear stress becomes apparent when go beyond this boundary by showing 2% reduction in wave height.

Other than geographical and environmental parameters, the amount of tidal energy extraction is governed by the tidal asymmetry, location, number, size, design, scale, and configuration factor of the tidal turbine deployment. Based on the study by Hasegawa et al. (2011), on the far-field hydrodynamic effect in Minas Passage, extraction of tidal turbine energy from the whole water column has greater impact on the tidal levels and flows. An assessment on large-scale tidal farm showed large-scale tidal energy current flow alterations within the strait that may possibly cause some impact to the sea conditions and subsequently to the livings in the marine environment (Guillou & Chapalain, 2017; Lo Brutto et al., 2017; Wang & Yang, 2017). In the investigation of Chatzirodou et al. (2019), they applied a range of hypothetical energy extraction scenarios was applied for different sand banks and scale at Pentland Firth, Inner Sound Channel using 3D numerical model, and the results revealed that the severity of morphological changes and the bed level alteration are subjected to the scale level of energy extraction (Chatzirodou et al., 2019). The investigation of power extraction effect on estuarine hydrodynamics based on two different schemes simulated at the Canoochee River within the coast of the state of Georgia reported that 20% kinetic power extraction was found to have substantially lesser impact on the flow than the scheme with 45% extraction (Defne et al., 2011); however the impact of both cases (20% and 45% extraction) on the currents is limited to localized area and the change in water levels was observed to be negligible. Besides that, tidal asymmetry is also one of the vital factors in affecting the effect and extent of tidal turbine deployment to the sea environment and the vicinity. Chen et al. (2015) demonstrated that the tidal turbine in a single row with higher local blockage outperformed array with lower blockage. They also found that the increment of latitudinal spacing would weaken the wake influence of the upstream turbines. Hashemi et al. (2015)

discovered that wind waves affected the performance of tidal energy resource for an array of tidal turbine off the northwest headland of Anglesey, UK (Lewis et al., 2015). In comparison with the North Sea, the wind wave effect is limited as the wind generated wave in Straits of Malacca is relatively small (less than 1 m) due to limited fetch length. Tidal turbine deployments at headlands gapped at small intervals along the coastline tend to result in flow interruption, which is likely to cause some negative impacts to the coastal livings and environment (Guillou & Chapalain, 2017; Lo Brutto et al., 2017; Wang & Yang, 2017).

As discussed, previous studies normally focused on assessment of influence for one parameter, e.g., scale, gap, wave, etc. To further explore the influence of array deployment, five different lines were considered in this test (**Figure 6.2**; **Table 6.3**). The locations of line L1, L2, L3, L4, L5 and L1-L5 were selected based on favourable sites selected in previous study for deploying tidal current turbines in Chapter 4. As shown in **Figure 6.2a**, **b** and **c**, the tidal current turbine array was placed within the potential tidal energy extraction site with median velocity (<1.0 m/s), peak velocity (>2.0 m/s) and depth range from 20 to 50 m, referring to typical horizontal tidal current turbine requirement given by Fraenkel (2002, 2007) and Myers & Bahaj (2005). However, the peak velocity found at this area is lower than rated velocity as discussed in Chapter 5. For actual deployment, customization of suitable tidal current turbine is recommended to optimize the implementation purpose.

Each line consists of 3 x 10 m diameter turbines, with 10D spacing. The tidal current turbines were aligned normal to the direction of peak tidal current velocity (**Figure 6.2c**). Staggered arrangement can be advantageous from flow acceleration between tidal current turbines and have been shown to increase energy capture (Bai et al., 2013). However, it had inadequate relevance for 2D hydrodynamic model as flow acceleration around

individual tidal current turbines were not fully resolved. Henceforth, a smaller grid size can be implemented to assess the gap and arrangement effect for individual tidal current turbine once the 2D hydrodynamic modelling issue mentioned is solved. The models that incorporated the effect of tidal turbine arrays were simulated for a total of 17 days, covering 3 days of spring tide and 3 days of neap tide, after the 2-day spin up.

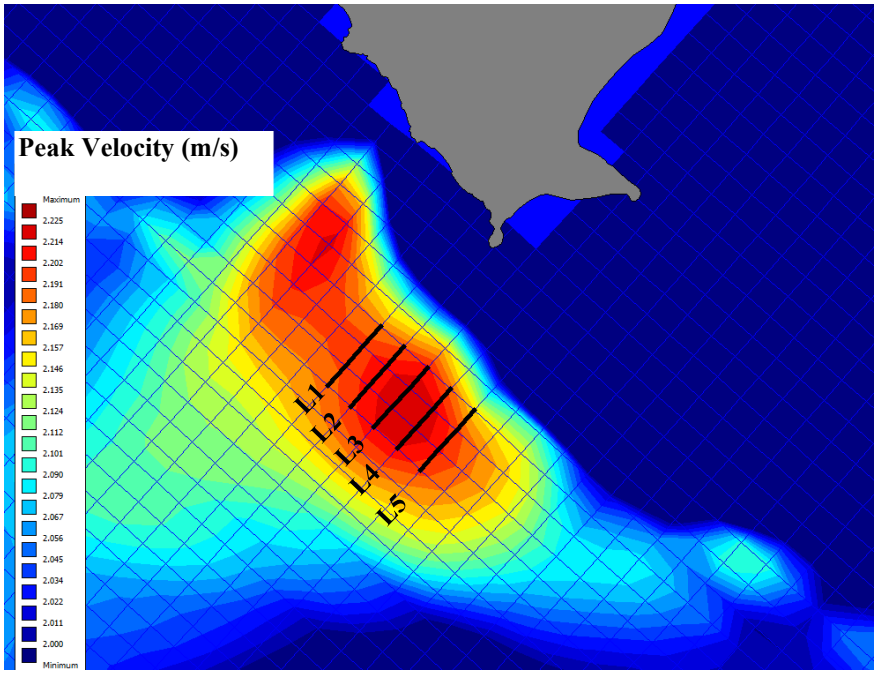

(a)

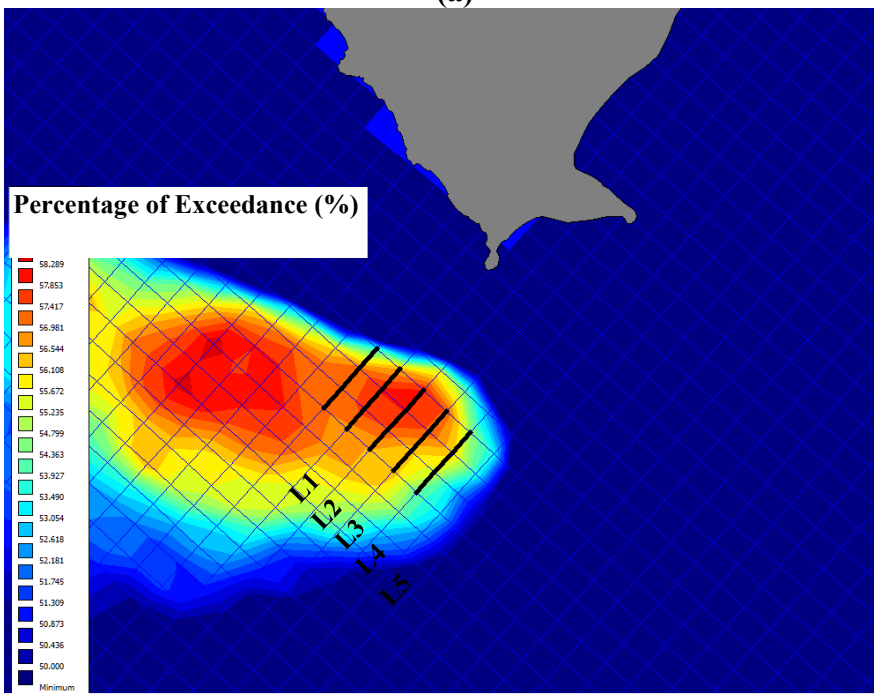

(b)

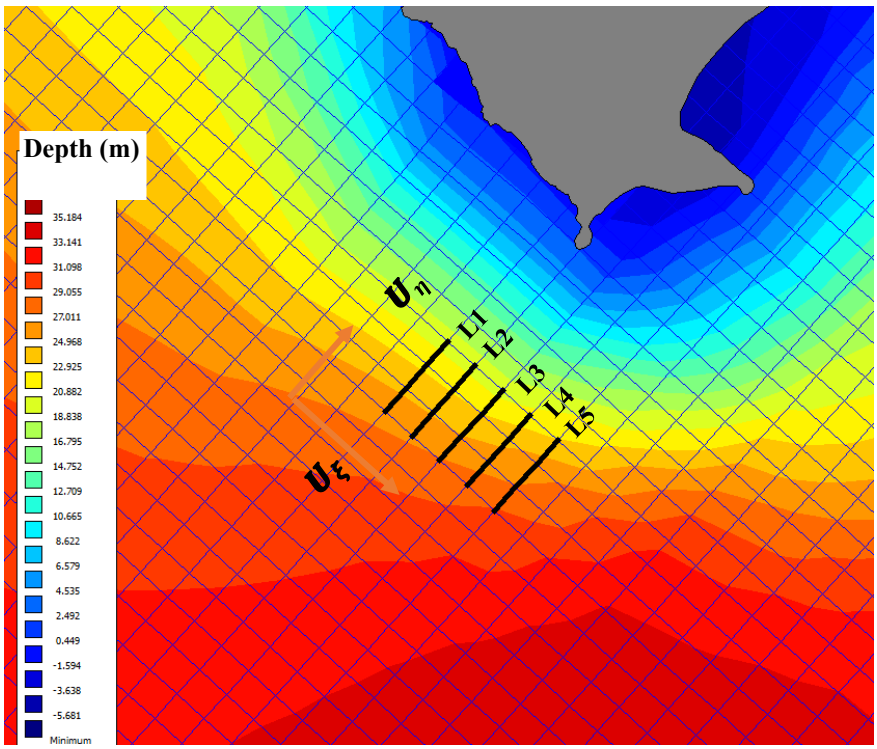

(c)

Figure 6.2: Tidal turbines (L1-L5) aligned in the η-direction perpendicular to the current flow U_ξ hypothetical deployment area within potential tidal current energy extraction site of (a) peak velocity > 2 m/s, (b) median velocity > 1.0 m/s, and (c) depth 20 – 50 m

Table 6.3: Specification of tidal current turbine testing array at the Tg Tuan Headland

Line	Turbines per row	Depth	Rated power	Centre point	
		(m)	(MW)	°E	°N
L1	3	22-27	3.24	101.8496	2.3998
L2	3	22-28	3.24	101.8503	2.3992
L3	3	22-28	3.24	101.8510	2.3986
L4	3	24-29	3.24	101.8517	2.3979
L5	3	25-30	3.24	101.8524	2.3961
L1-L5	15	22-30	16.20	101.8510	2.3986

6.3.5 Single and Cumulative Energy Extraction (H1 – H4)

The presence of turbines near the headlands would modify the regional hydrodynamic regimes to a certain extent. Negeri Sembilan, which is located at the central west coast of

Malaysia, was selected for this case study. The state is bordered by approximately 55 km of shoreline encompassing three bays that are confined by four headlands (H1 – H4) along the coastline as demonstrated in **Figure 6.3**. The four headlands extending from Kuala Sepang Besar to Kuala Linggi are identified as the potential sites for tidal energy exploitation in Negeri Sembilan. The channel widths normal to the selected headlands are given in **Table 6.4.** The headland of Kuala Sg Sepang (H1) has the widest tidal flow passage, followed by the headland of Port Dickson (H2), the headland of Kuala Sg Linggi (H4) and the headland of Tg Tuan (H3). The tidal current flows in the southward direction during flood tides and in the northward direction during ebb tides. During the occurrence of flood tides, H1 is the first headland to receive the incoming tidal flow, and H4 is the last headland to respond to the tides.

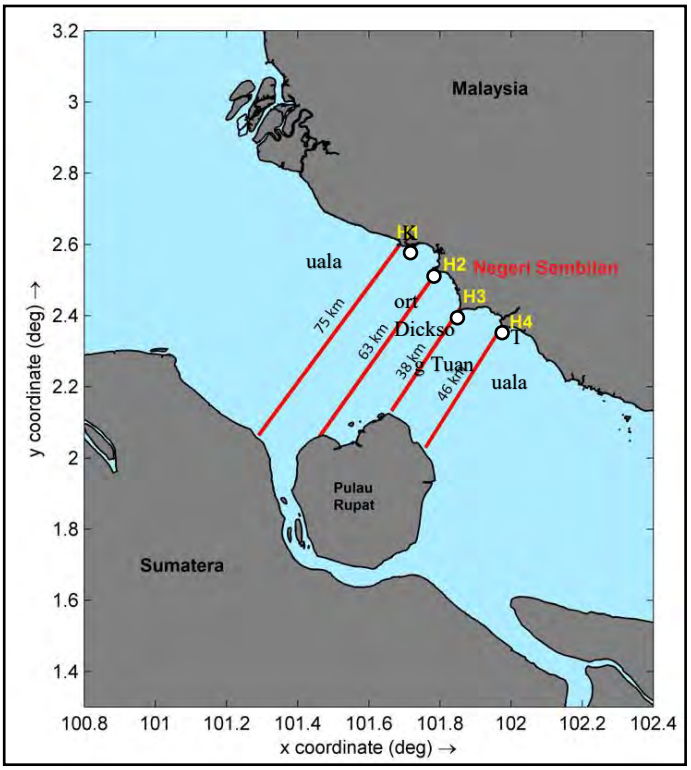

Figure 6.3: Channel flow passage along the Negeri Sembilan coastlines

Table 6.4: Channel width with reference to the Negeri Sembilan headlands

Headland Location	Headland ID	Channel Width (km)
Kuala Sepang Besar	H1	75
Port Dickson	H2	63
Tg Tuan	H3	38
Kuala Linggi	H4	46

Upon energy tapping by the upstream tidal turbine, the energy production by downstream turbines would be reduced due to reduction of hydrodynamic power (Lo Brutto et al., 2017). Furthermore, the risk of site interactions will increase in parallel with the numbers of tidal farm sites within the study area. To further explore this problem, the effect of single and multiple hypothetical 1.5 km x 1.5 km (15 x 15 turbines) tidal farm deployment within the higher potential tidal energy extractable area in proximity of the headland within the coast of Negeri Sembilan was investigated using the momentum loss approach. The specification of tidal current turbine testing array at the multiple headlands are summarized in **Table 6.5**. Higher resolution model implemented in this study provided higher accuracy of the quantification of the momentum loss by representing the turbine characteristics close to the actual scale of the turbine. Similar to tidal array effect modelling as discussed in Section 6.3.3, the effect of tidal turbine arrays was simulated for a total of 17 days (2 days warm-up) to cover both spring and neap tidal conditions.

For this analysis, the effect of the turbine was taken as the energy loss by a porous plate in the momentum equation. C_{T1} was regarded as a constant in equation (2. 7). The diameter of the turbine blades was taken as 10 m. The turbine array was oriented in the y-direction so as to impede the flow in the x-direction (**Figure 6.4**). Both the lateral spacing between turbines, Δy, and the longitudinal spacing between rows, Δx and Δy, respectively were set at 10 times the rotor diameter, as suggested by Chen et al. (2015).

Table 6.5: Specification of tidal current turbine testing array at the Multiple Headland

Line	Numbers of Turbine	Headland Location	Rated power	Centre point	
			(MW)	$°E$	$°N$
H1	225	Kuala Sepang Besar	243	101.6879	2.5808
H2	225	Port Dickson	243	101.7535	2.4997
H3	225	Tg Tuan	243	101.8400	2.3988
H4	225	Kuala Linggi	243	101.94682	2.3535
H1-H4	900	Four Headlands (H1-H4)	243	-	-

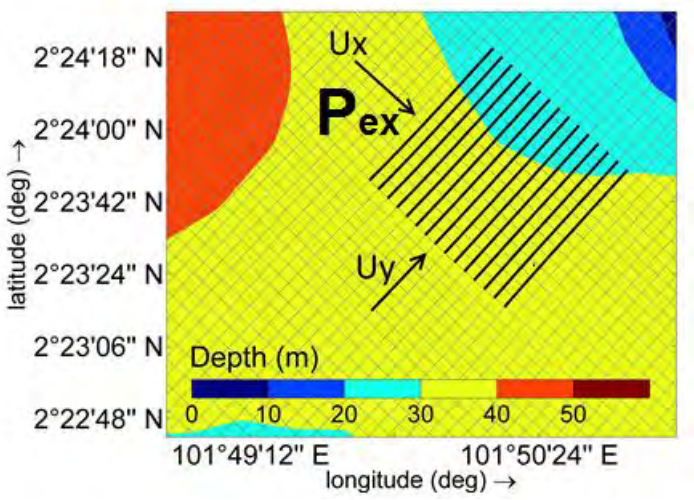

Figure 6.4: The arrangement of the tidal farm at cell in the y-direction perpendicular to flow U_{inc}

6.4 Results and Discussion

Numerical modelling was executed using the setup as elaborated in Section 6.2 and including the tidal current turbine in the model as described in Section 6.3. The numerical model was run with 30 s and simulation period of 356 hours covering full spring and neap tides plus 48 hours of warm up period. In this section, the proportion of tidal current turbine dissipation converted into electrical power was predicted using tidal current turbine power curve given in **Figure 5.5**. The results of depth effect and tidal array configuration effect are described in Section 6.4. Followed by that, environmental impact assessment of tidal current turbine deployment at Tg Tuan Headland in different headlands and cumulative effect of multiple headland deployment was provided in Section 6.4.4. The overall discussion and conclusion made based on the results of the simulation are given in Section 6.5 and Section 6.6.

6.4.1 In-concert Array Regulation

As discussed in Chapter 5, when the current speed of tidal turbine exceeds the rated current speed, the discrepancies between the regulated and unregulated tidal current

turbine force predictions were the greatest (**Figure 5.11**) and the tidal turbine became ineffective. Tidal current turbine more often operated below rated current speed. Depth-averaged current speed through the hypothetical tidal current turbine at Tg Tuan Headland did not exceed the rated current speed (**Figure 6.5**). During these conditions, regulated tidal current turbine force was higher than unregulated force. The mean and peak forces are differed by < 10% for the scenarios simulated in this test (**Table 6.6**). From the depth (25-32m) assessment, mean and peak unregulated forces ranged from 136 to 158 kN and 413 to 425 kN. On the other hand, the mean and peak regulated force is slightly higher, range from 145 – 170 kN and 461 – 477 kN. The difference of mean regulated force between the highest (D8) and the lowest (D3) magnitude was approximately 15%.

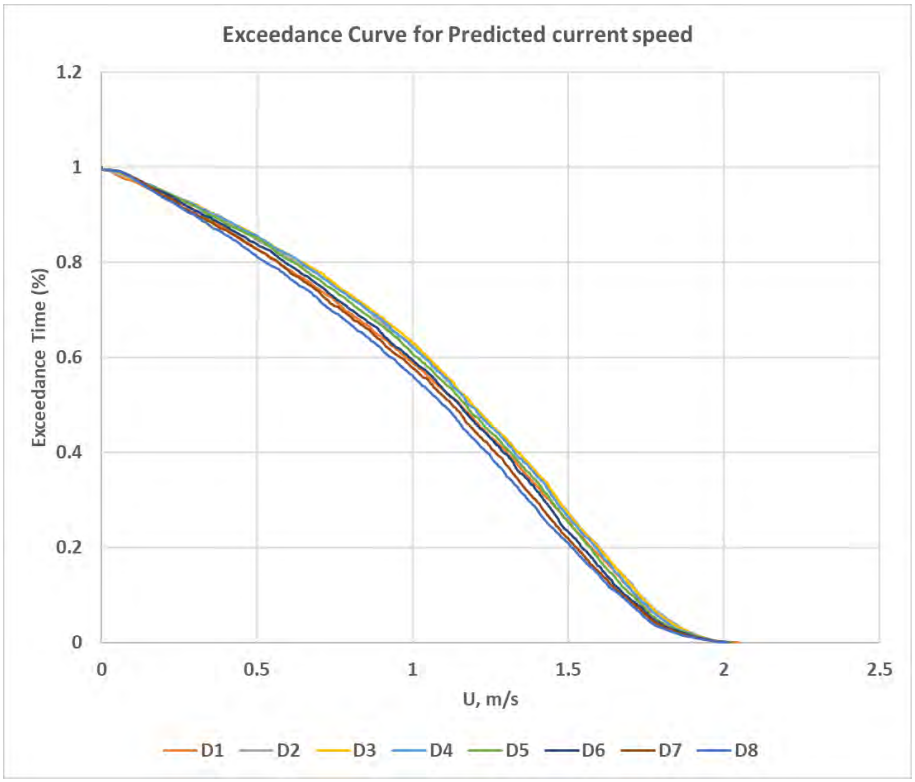

Figure 6.5: Exceedance Curve of predicted current speed for D1 – D8

Table 6.6: Mean and peak tidal current speeds and turbine's forces (regulated and unregulated)

Turbine No.	Current Speed		Unregulated Force		Regulated Force	
	Mean	**Peak**	**Mean**	**Peak**	**Mean**	**Peak**
	(m/s)	**(m/s)**	**(kN)**	**(kN)**	**(kN)**	**(kN)**
D1	1.108	2.049	150	424	159	477
D2	1.128	2.015	157	425	169	463
D3	1.133	2.009	158	411	170	461
D4	1.125	2.017	156	415	167	464
D5	1.109	2.024	151	418	162	467
D6	1.088	2.018	146	416	156	464
D7	1.065	2.017	141	415	151	464
D8	1.043	2.013	136	413	145	462

6.4.2 Depth Effects

Based on the mean kinetic energy dissipation and electrical power generation analysis, more than half of the mean dissipation was effectively extracted as electrical power (**Table 6.7**). The result from Chapter 4 can be further evidenced by this finding on selecting Tg Tuan Headland for tidal current energy extraction site; however, slight modification on the rated current speed, U_r, and size of the device maybe required, based on the site condition. D2, D3 and D4 have the highest energy dissipation (0.26 MW); however, D1 – D5 have equivalent ability in electrical power generation, 0.18 MW. D8 (~32m) has the least energy dissipation (0.214 MW) and generation of electrical power, 0.164 MW. In overall, the depth effect is not significant in changing the extractable electrical power. The difference is less than 0.02 MW compared D1 (highest) and D8 (lowest) mean electrical power extraction for about 7 m difference. In terms of energy dissipation, depth has more significant effect on the kinetic energy dissipation whereas the mean dissipation difference (0.05 MW) between D2 (highest) and D8 (lowest) is double of mean electrical power generation difference as mentioned earlier.

Table 6.7: Mean and peak kinetic energy dissipation and electrical power generation for regulated tidal turbine in different depths (D1-D8)

Turbine No.	Dissipation	Dissipation	Electrical Power	Electrical Power
	Mean	**Peak**	**Mean**	**Peak**
	(MW)	**(MW)**	**(MW)**	**(MW)**
D1	0.24	0.977	0.18	0.507
D2	0.26	0.934	0.18	0.483
D3	0.26	0.926	0.18	0.479
D4	0.26	0.937	0.18	0.485
D5	0.24	0.946	0.18	0.490
D6	0.23	0.937	0.17	0.485
D7	0.22	0.936	0.17	0.484
D8	0.21	0.931	0.16	0.482

Figure 6.6 and **Figure 6.7** relates the change of current velocity with the tidal turbine deployment depth at 500 m upstream and downstream of the turbine during ebb and flood tides, respectively. The results are presented in relative to the baseline scenario, which is pre-deployment without tidal turbine. It is noticed that the current velocity magnitude changes at 500 m upstream of the deployment locations (D1 – D8) ranging from -0.00911 m/s to 0.00098 m/s during flood tide, and 0 to 0.0098 during ebb tide. The result of this simulation agrees well with the findings of Ahmadian & Falconer (2012) and Hasegawa et al. (2011) where far-field impact to the coastal area is visible. The regional current flow is significantly controlled by the deployment depth of the tidal current turbine. D1 and D2 have current velocity magnitude changes larger than 0.001 m/s, while for deployment at further offshore at deeper depth it is insignificant, which is lesser than 0.001 m/s. The drag force acting on the tidal current turbine causes energy loss in the flow. The drag created is the results of difference between high pressure on the upstream side at stagnation zone and low pressure on the turbulent wake region in the downstream side. The rise in pressure on the upstream side is due to conversion of kinetic energy of flow to potential energy at the stagnation point. The flow depth is one of the main parameters in affecting the drag at the downstream area. Current velocity reduction is observed for

10 m tidal turbine deployment at shallower depths (<30 m) for scenario D1 – D4 as the flow is under subcritical flow condition, i.e., with Froude number smaller than 1. Slight increments in current velocity are observed for tidal turbine deployment at deeper depth (>30 m) for Scenario D5-D8 as the flow is under supercritical flow condition. The current velocity for D1 (25.46 m) and D2 (27.23 m) increased at 500 m downstream and reduced at 500 m downstream from the tidal turbine during ebb tide (**Figure 6.7**). The velocity changes further offshore at deeper area for D3 – D8 (28.41 m – 31.64 m) are also insignificant (< 0.001 m/s). The extraction at deeper depths show less impact to the surrounding coastal area. The effect of tidal deployment at downstream area is insignificant in general (< 0.002 m/s), except tidal turbine deployment at depth D1 (25.46 m) has current velocity magnitude changes of 0.0098 m/s during ebb tide. Tidal turbine deployment at deeper depth showed less impact to both upstream and downstream area. Analysis from the eight scenarios compared to baseline showed descending relationship between depth and magnitude of influence at upstream and downstream. The changes in current speed changes results showed that deployment at deeper area, which is further offshore contributed lesser magnitude of current speed changes with baseline condition compared to the shallower area.

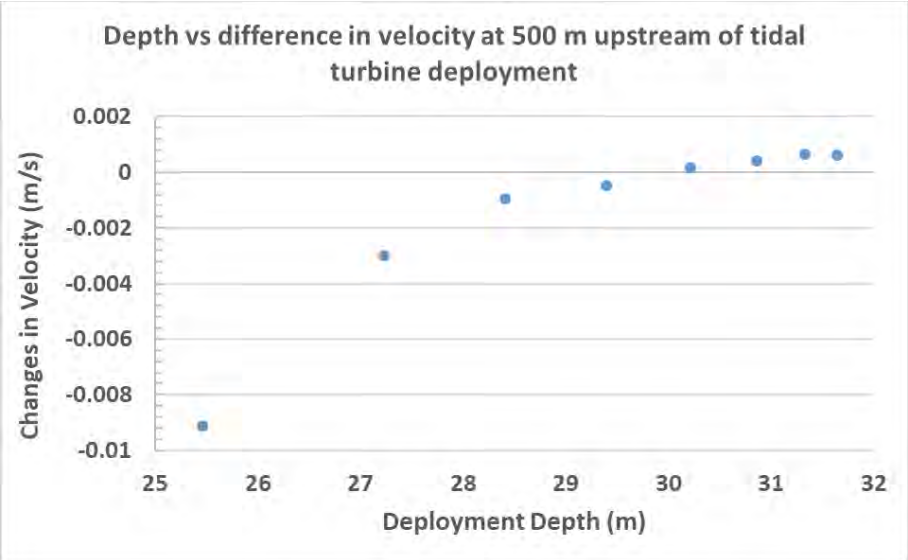

(a) Upstream

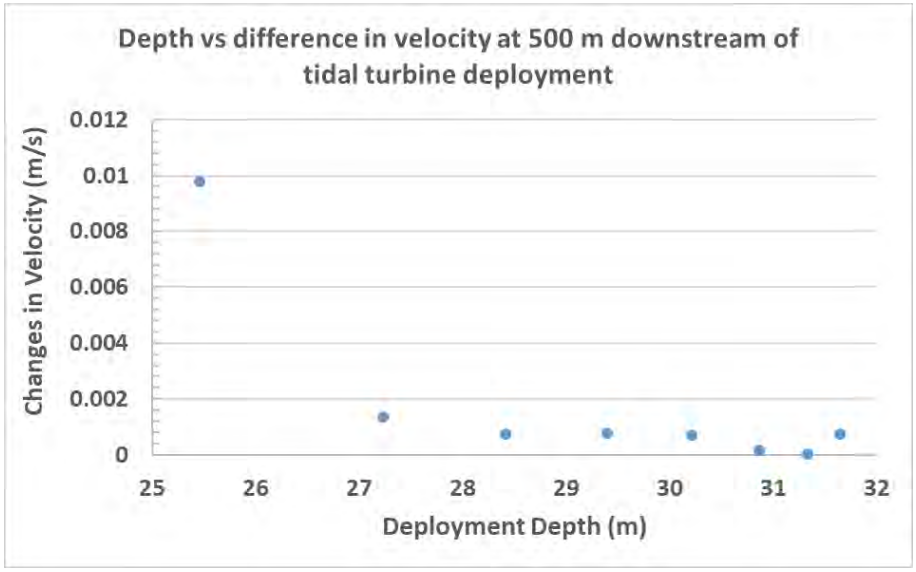

(b) Downstream

Figure 6.6: Relationship of changes in velocity at (a) upstream, and (b) downstream with tidal turbine depth deployment during flood tide condition

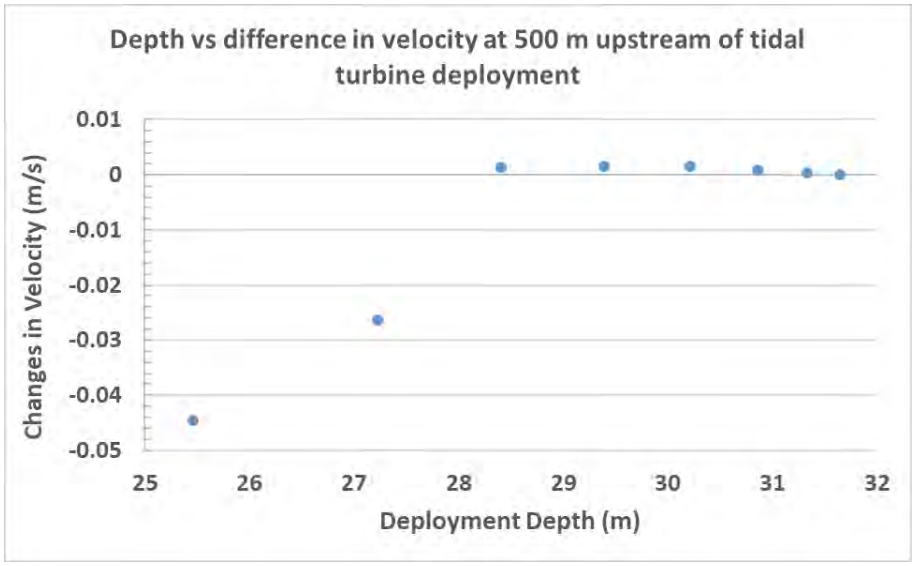

(a) Upstream

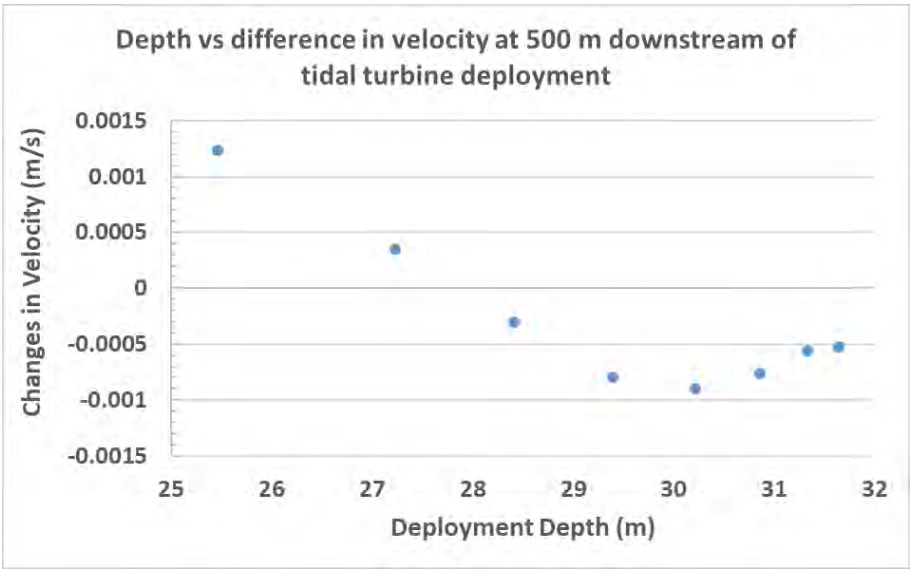

(b) Downstream

Figure 6.7: Relationship of changes in velocity at (a) upstream, and (b) downstream with tidal turbine depth deployment during ebb tide condition

However, the sea current is multidirectional. The impact of tidal turbine effect was further examined spatially in 2D map plot (**Figure 6.8**). A comparative analysis of extractable energy changes due to tidal turbine in different depths scenarios (i.e., D1, D2, D3, D4, D5, D6, D7 and D8) was done by comparing the variations of the extractable energy produced by both scenarios (pre-deployment and with-tidal-farm). **Figure 6.8** shows the mean velocity magnitude difference due to energy extraction for scenarios D1, D2, D3, D4, D5, D6, D7 and D8. Average current velocity changes are well represented over the 15 days simulated period that include of spring and neap tides. The hydrodynamic impact is varied for different TEC deployment depths which ranging from 25 m to 32 m as illustrated in **Figure 6.8(a) – (h)**. The average current velocity magnitudes yielded from the simulation scenarios of different depths (with tidal turbines) were benchmarked with the baseline or pre-deployment scenario (without tidal turbines). The changes of the average current velocity magnitudes caused by the with tidal turbine scenarios for different depths were calculated at each cell node at every time step, showing a temporarily and spatially varying difference of the scenarios simulated with

the baseline condition. It is to be noted here that the changes of average current magnitudes were calculated at each node of the cell over the simulation period.

Furthermore, the result from the mean current velocity analysis showed that 10 m diameter tidal turbine deployment at lower depth, D1 (25.46 m), compared to the baseline condition has largest visible area of influence, which extended up to about 0.9 km upstream; the maximum changes in current speed magnitude is 0.019 m/s. This is mainly because the constriction is limited and the obstruction induces a backwater effect, which extends over a longer distance upstream. On the other hand, if the Froude number of the flow is greater than one (in supercritical flow) for 10 m diameter tidal turbine in depth > 30 m, wavelike disturbances is not able to propagate upstream as the relative constriction is longer, which may cause the minimum value of specific energy to rise in the constriction section. The effect to downstream was almost invisible for the eight simulated scenarios in comparison to baseline condition as the changes in velocity is negligible (< 0.01 m/s) and the slope changes is mild and the flow near the downstream of the tidal current turbine was subcritical.

Average current velocity comparison for various scenarios (D3-D8) with baseline condition showed that the magnitude changes spread area for D3, D4 and D5 are 0.58 km, 0.5 km, and 0.49 km, respectively and the spread is not visible for further offshore deployment at D6 (30.86 m), D7 (31.33 m) and D8 (31.64 m) by having average current velocity difference of less than 2%.

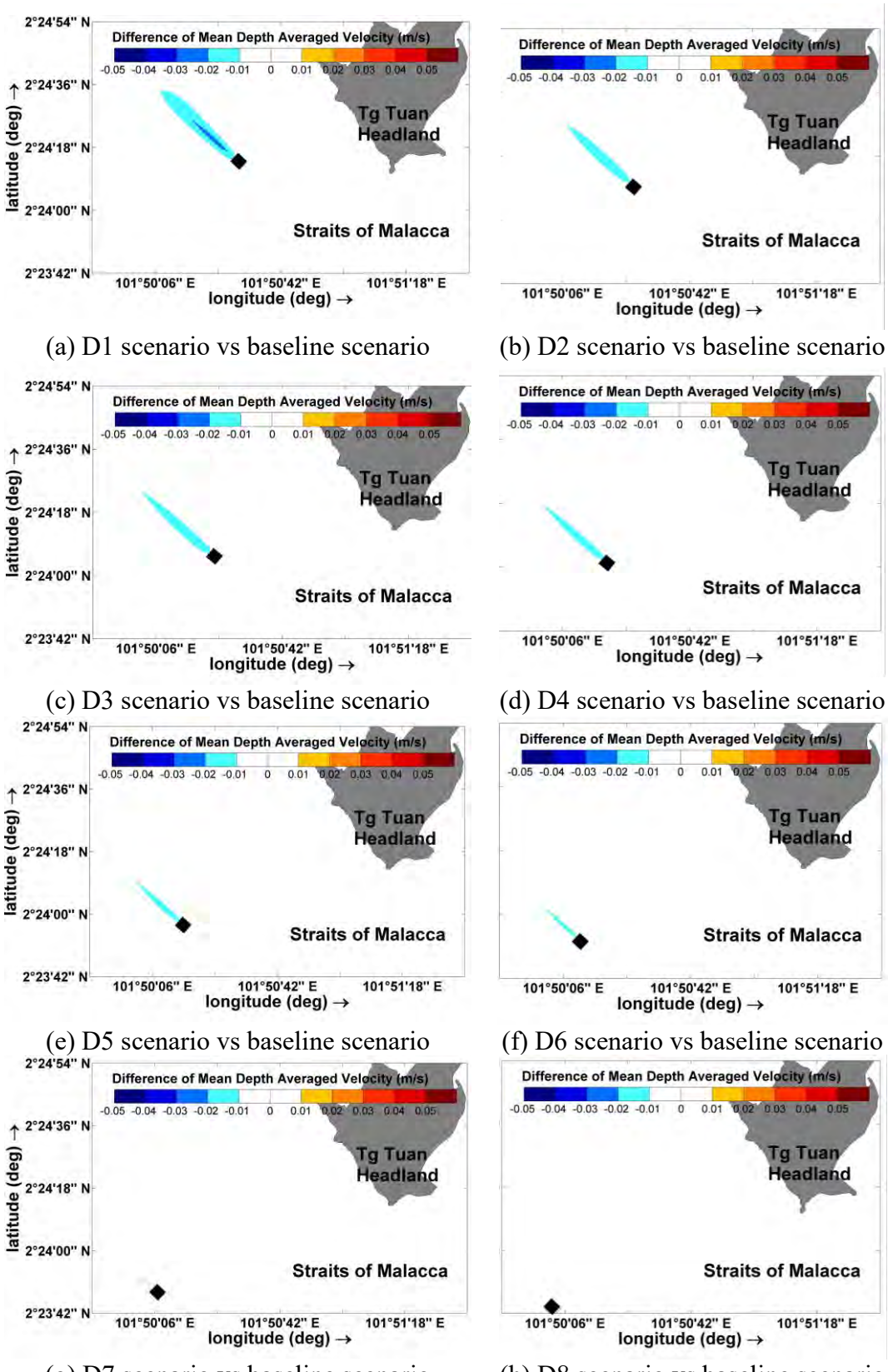

(a) D1 scenario vs baseline scenario

(b) D2 scenario vs baseline scenario

(c) D3 scenario vs baseline scenario

(d) D4 scenario vs baseline scenario

(e) D5 scenario vs baseline scenario

(f) D6 scenario vs baseline scenario

(g) D7 scenario vs baseline scenario

(h) D8 scenario vs baseline scenario

Figure 6.8: Mean velocity magnitude difference due to energy extraction for (a) D1, (b) D2, (c) D3, (d) D4, (e) D5, (f) D6, (g) D7, and (h) D8 scenarios in comparison to baseline scenario

6.4.3 Array Effects

Similar to the depth effect assessment above, more than half of the mean dissipation due to array of turbines was effectively extracted as electrical power (**Table 6 *8***). L1 and L2 have the highest mean energy dissipation (0.89 MW), with equivalent ability in electrical power generation, 0.63 MW. L2 is found to have the highest instantaneous power generation at 1.93 MW. The quantity of electrical power generation for array L1 – L5 is similar, producing about 0.61 - 0.63 MW of mean electrical power. On a per turbine basis, however, dissipation and power from L6 was lower than array L1-L5.

$$Mean\ Power\ of\ L6\ with\ constituent\ rows\ of\ power\ production$$

$$= (\frac{P_{L6}}{P_{L1} + P_{L2} + P_{L3} + P_{L4} + P_{L5}}\ x\ 100\ \%$$

$$= (\frac{2.97}{0.63 + 0.63 + 0.62 + 0.62 + 0.61})x\ 100\ \%$$

$$= 95\%$$

The mean power produced by L6 was 95% of the constituent rows of power production, which showed diminishing returns on the power generation even though this considerably low extraction was made, at considerably large gap in between each turbine (10D). Lastly, it was found that peak power production from L6 (9.2 MW) was 97% of its total electrical power capacity, less than the corresponding values for each row of the smaller array.

Table 6 8: Mean and peak kinetic energy dissipation and electrical power generation for regulated tidal turbine in different arrays (L1-L6)

Array.	Dissipation	Dissipation	Electrical Power	Electrical Power
	Mean	**Peak**	**Mean**	**Peak**
	(MW)	**(MW)**	**(MW)**	**(MW)**
L1	0.89	3.66	0.63	1.92
L2	0.89	3.68	0.63	1.93
L3	0.87	3.61	0.62	1.91
L4	0.87	3.58	0.62	1.89
L5	0.85	3.52	0.61	1.85
L6	4.19	17.42	2.97	9.2

**the onshore-offshore transmission loss is not included in the conversion of the generator*

Figure 6.9 reveals the average change of current velocity for the tidal current turbine array deployment in different configurations. The results are presented in three comparisons: single-row (SR) vs baseline, multiple-row (MR) vs baseline and multiple-row (MR) vs single-row (SR) scenarios. A total of seven simulations were modelled for the turbine configuration assessment, which consists of one number of baseline scenario, five numbers of SR scenarios, and one number of MR scenarios. A total of six scenarios were simulated in this study: (1) single row tidal array L1, (2) single row tidal array L2, (3) single row tidal array L3, (4) single row tidal array L4, (5) single row tidal array L5, (6) multiple row tidal array L6 (consists of L1, L2, L3, L4 and L5), and (7) without tidal array at the site. The configuration of SR and MR deployment were simulated for L1, L2, L3, L4, L5 and L6 and are shown in **Figure 6.2**.

It is noticed from **Table 6.9** that the mean current speed changes at each array range 0.83 – 3.20%, 1.28 - 3.48% and 0.49 – 4.53% for MR-SR, MR-Baseline and SR-Baseline comparison, respectively. The magnitude of mean current velocity changes is small, < 0.05 m/s in general. The comparison with baseline condition assessment showed that MR-Baseline scenario has larger changes in the first and second row (L1 and L2), however, due to blockage effect from the first and second row, the effect of reduction for L3-L5

was decreased and was observed to be much smaller than SR-Baseline scenario. For MR-SR comparison, the percentage of mean current velocity changes is smallest for L3, ~ 1% difference. L4 and L5 have larger changes for MR-SR scenario as L4 and L5 in MR configuration have much lower dissipation than SR configuration, due to sheltering effect from L1, L2 and L3 during flood flow condition.

Referring to **Figure 6.9**, analysis from the MR-SR based on seven simulated scenarios showed ascending relationship between row number (upstream to downstream) and percentage of current velocity changes. The drag force acting on the tidal current turbine causes momentum loss in the flow. The energy loss created is the results of difference between high pressure on the upstream side at stagnation zone and low pressure on the turbulent wake region in the downstream side. The rise in pressure on the upstream side is due to conversion of kinetic energy of flow to potential energy at the stagnation point. The blockage of structure is one of the main parameters in affecting the drag at the downstream area. By comparing MR-baseline, the reduction of peak current speed for MR has increase proportional to the numbers of array (L1 – L5) than the baseline condition. This is mainly due to increase of barrier involved causing more energy dissipation to occur. From the peak velocity comparison as shown in **Figure 6.9b**, the MR-SR current speed changes results showed that deployment of less than three rows did not reduce much the current speed, when it reached fourth row and above would reduce the current velocity and subsequently the electrical power generation significantly.

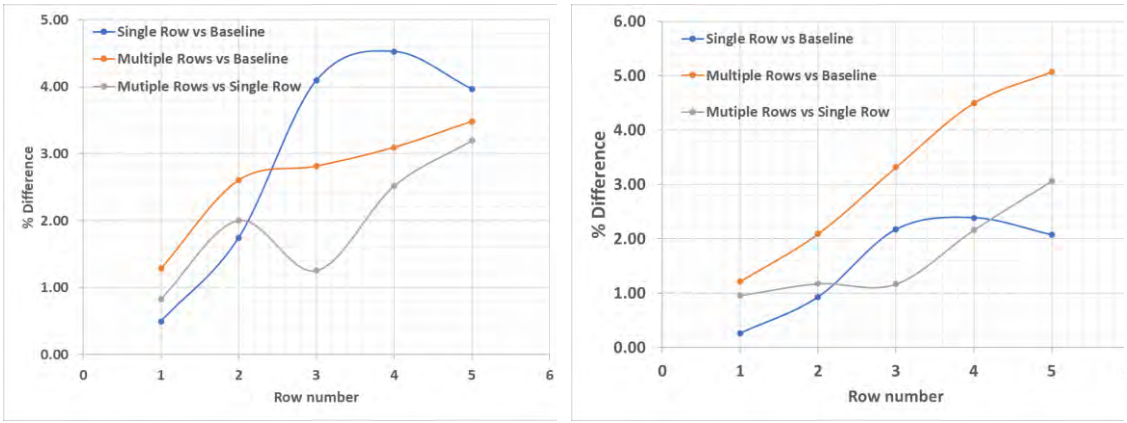

Figure 6.9: Percentage difference of current speed of (L1 – L5) for single-row and multiple-row scenarios for: a) mean current speed, and (b) peak current speed

Table 6.9: Current speed difference for L1, L2, L3, L4, L5 with baseline and L6 scenarios

Scenario	Array	L1	L2	L3	L4	L5
Baseline	mean U (m/s)	1.18	1.20	1.20	1.19	1.16
	Peak U (m/s)	2.23	2.25	2.27	2.26	2.23
Multiple-Row (MR)	mean U (m/s)	1.17	1.17	1.17	1.16	1.12
	Peak U (m/s)	2.21	2.20	2.19	2.16	2.12
Single-Row (SR)	mean U (m/s)	1.18	1.19	1.18	1.19	1.16
	Peak U (m/s)	2.23	2.23	2.22	2.21	2.18
MR - SR	% of Mean U Difference	0.83	2.00	1.25	2.52	3.20
	% of Peak U Difference	0.96	1.18	1.17	2.16	3.06
MR - Baseline	% of Mean U Difference	1.28	2.61	2.82	3.10	3.48
	% of Peak U Difference	1.22	2.09	3.31	4.49	5.07
SR - Baseline	% of Mean U Difference	0.49	1.74	4.09	4.53	3.97
	% of Peak U Difference	0.26	0.93	2.17	2.39	2.07

The hydrodynamic impact of tidal turbine effect for 3 rows and 5 rows were further examined spatially in 2D map plot. **Figure 6.10** shows the mean velocity magnitude difference due to energy extraction for 3 and 5 rows deployment scenarios. Average current velocity changes are well represented over the 15 days simulated period that include of spring and neap tides. The average current velocity magnitudes yielded from the simulation scenarios of different depths (with tidal turbines) were benchmarked with the baseline or pre-deployment scenario (without tidal turbines). The changes of the

average current velocity magnitudes caused by the with tidal turbine scenarios for different numbers of tidal current turbines were calculated at each cell node at every time step, showing a temporarily and spatially varying difference of the scenarios simulated with the baseline condition. It is to be noted here that the changes of average current magnitudes were calculated at each node of the cell over the simulation period.

The result from the mean current velocity changes analysis showed that 5 rows with 15 numbers of 10 m diameter tidal turbine deployment compared to the baseline condition has the largest visible area of influence, which extended up to about 200 m upstream; the maximum changes in mean current speed magnitude is 0.1 m/s. This is mainly because the larger area of obstruction induces a backwater effect, which extends over a longer distance upstream. The effect to downstream was almost invisible for the three rows and five rows scenarios in comparison to baseline condition as the changes in velocity is negligible (< 0.05 m/s). Average current velocity comparison for three rows turbine scenarios with baseline condition showed that the magnitude changes spread area is 100m and the spread is not visible by having average current velocity difference of less than 2%. The result of mean current speed changes showed that the three rows was an optimum array configuration in order to maximize power generation, and lesser impact to the environment for smaller array as shown in **Figure 6.10**.

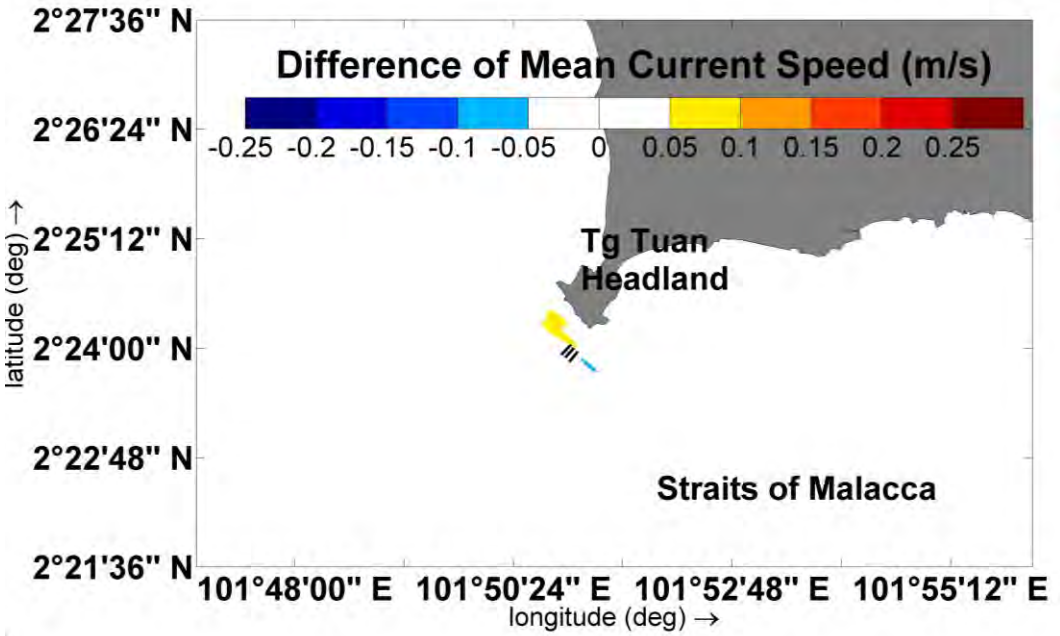

(a) Three rows

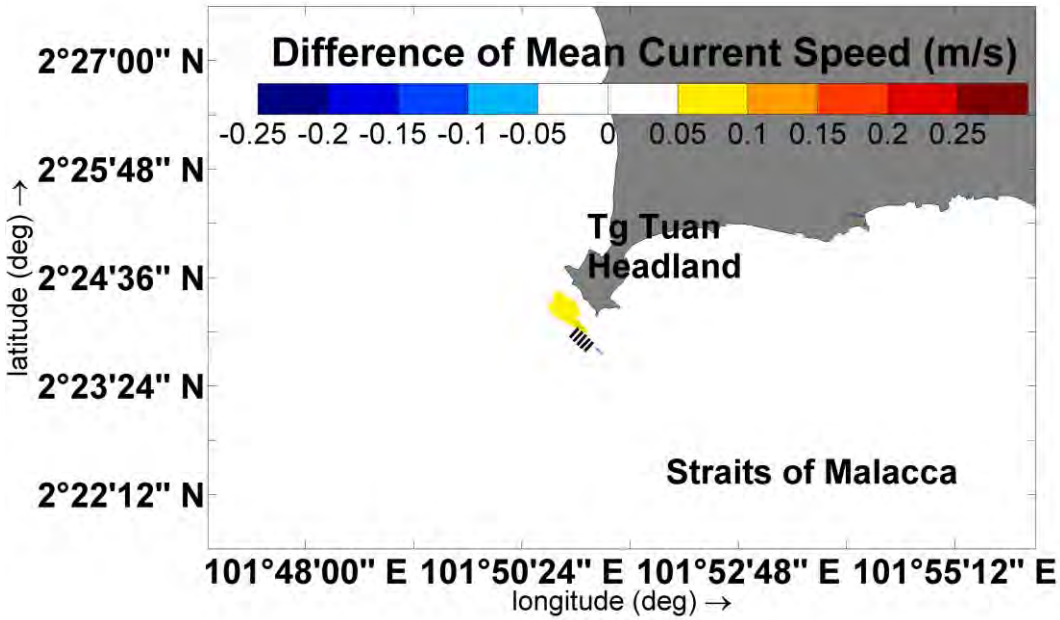

(b) Five rows

Figure 6.10: Difference in magnitudes of mean velocity magnitude difference due to energy extraction for (a) three rows and (b) five rows turbine deployment scenarios in comparison to baseline scenario

6.4.4 Interaction of Multiple Headland Energy Extraction

A total of six scenarios were simulated in this study: (1) single tidal farm – operation of tidal farm H1 only; (2) single tidal farm – operation of tidal farm H2 only; (3) single tidal farm – operation of tidal farm H3 only; (4) single tidal farm – operation of tidal farm H4 only; (5) multiple tidal farm – concurrent operation of multiple tidal farms H1, H2, H3 and H4; and (6) without tidal farm at the site. The current magnitudes yielded from the with-tidal-farm simulations were compared with the without-tidal-farm (pre-deployment) simulation.

6.4.4.1 Hydrodynamic Effect

To quantify the effect of site interactions, the zones of influence to the mean and maximum current velocities were calculated using the normalized range of difference (NRD). The variations of the current magnitudes produced by both scenarios (pre-deployment and with-tidal-farm) were determined at each cell node at every time step, giving a spatially and temporally varying difference between the two models. The range was then normalized to the maximum difference to provide a NRD 2D map plot. Note that the calculated range of difference refers to the maximum change of current magnitudes at each node of the cell over the entire simulation period. The range of difference does not represent instantaneous changes of current velocity due to the direct wake of the tidal farm at any one-time step but provides an overall indication of the total temporal and spatial extent of change.

Figure 6.11(b - d) present the NRD resulted by the tidal farms installation at H1, H2 H3, and H4. The NRD for multiple tidal farms installed at H1, H2, H3 and H4 are demonstrated in **Figure 6.1e**. For single tidal farm scenarios, it is seen from **Figure 6.11 (a - d)** that the NRD of each test scenario is considerably small and localized. In terms of spreading characteristics of the NRD, the current variation before and after installation of

the tidal farms at H1, H2, H3 and H4 for having 5.0 GWh/year, 0.3 GWh/year, 54.9 GWh/year and 2.8 GWh/year of energy extraction, is almost insignificant, similar to Chen et al. (2013b)'s study at Taiwan Strait where the influence of turbine array of 9.46 GWh/year energy extraction to the strait is small and only limited to near-field currents. Despite the variation of energy production at H2 and H4 (i.e., the tidal farms H2 and H4 produced 43 and 60 MWh/year/turbine, respectively, as given in **Figure 4.30c** and **Figure 4.30e**, the NRD spreading patterns are rather similar, having the zone of influence extended as far as 2 km southward (see **Figure 6.11b** and **Figure 6.11d**). The energy production of H1 tidal farm is 76 MWh/year/turbine (see **Figure 4.30b**), resulting in larger NRD spread at southward of the facilities. The power production recorded at the H3 tidal farm is the highest among all the single farms tested, with each turbine generating an output of 369 MWh/year (see **Figure 4.30d**). Consequently, the NRD spreading area due to the H3 tidal farm is the largest as shown in **Figure 6.11c**. It spreads up to 3.5 km southward of the tidal farm. Due to extraction of a large amount of energy at the H3 tidal farm, substantial reduction in current magnitude past the southward of H3 is observed (**Figure 6.11c**). The energy extraction effect at H3 is similar to Serhadlıoğlu et al. (2013) study at Skerries region, where the bypass flow towards the ocean side is more enhanced than the region near to the shore. The effects posed by the concurrent operation of the tidal farms at H1, H2, H3 and H4 on coastal hydrodynamics and energy concentration are depicted in **Figure 6.11e**. The NRD spreading at H1, H2 and H4 for both single and multiple tidal farm operations are almost identical. However, for H3, the spreading zone seems to elongate and overlap with that of H4. Nonetheless, the interference is marginal.

An attempt was made to conduct a comparative analysis of extractable energy changes for headlands in vicinity effect due to single tidal farm operation (i.e., H1, H2, H3 or H4 tidal farm) by comparing the variations of the extractable energy produced by both scenarios (pre-deployment and with-tidal-farm). The comparison showed that

hypothetical 1.5 km x 1.5 km single tidal farm operation at Headland H3 had the largest influence to headlands' vicinity, at headland H2 and H4, where the extractable energy reduced by approximately 4.8% and 8.7%, respectively (**Table 6.10**). Furthermore, tidal asymmetry at the site demonstrated higher reduction by 8.7% at Headland H4 (southeast) due to the influence of hypothetical 1.5 x 1.5 km single tidal farm of H3 (northwest). The flood (northwest-southeast) is stronger than the ebb. This is compatible to the previous study by Haverson et al. (2017) at Irish Sea model. Fair Head that lies to the west of Torr Head reduced energy production at Torr Head by 17%, which is much higher than 2% of energy reduction at Fair Head. The tidal asymmetry of flood (west-east) at Irish Sea is stronger than ebb. In comparison, it is also noticed that the influence of hypothetical 1.5 x 1.5 km single tidal farm of H4 was smallest compared to other headlands, < 1% of reduction.

Another attempt was also made to conduct a comparative analysis of the power production of single tidal farm operation (i.e., H1, H2, H3 or H4 tidal farm) with multiple tidal farm operation (i.e., H1, H2, H3 and H4 tidal farms). The relative efficiency of the multiple tidal farms was assessed in terms of the percentage of changes in energy production compared with the single tidal farm production. A negative percentage indicates underperformance due to concurrent multiple tidal farm operation. The energy production per annum produced by the tidal farm was derived using equation (2.2).

Table 6.11 presents energy production percentage changes of single tidal farm operation (i.e., H1, H2, H3 or H4 tidal farm) and multiple tidal farm operation (i.e., H1, H2, H3 and H4 tidal farms). It showed that tidal farm in single operation is slightly outperformed the multiple tidal farms in simultaneous operation system. The power reduction rates due to the operation of the multiple tidal farms range from 0.8 to 1.4 MWh (with performance deficiency percentages ranging from 1.3 to 6.8%), as shown in **Table**

6.11. This is due to the sheltering effect from the upstream tidal farm(s) during the occurrence of peak flood flow. In overall, the influence of the multiple tidal farms in reducing the power production is small.

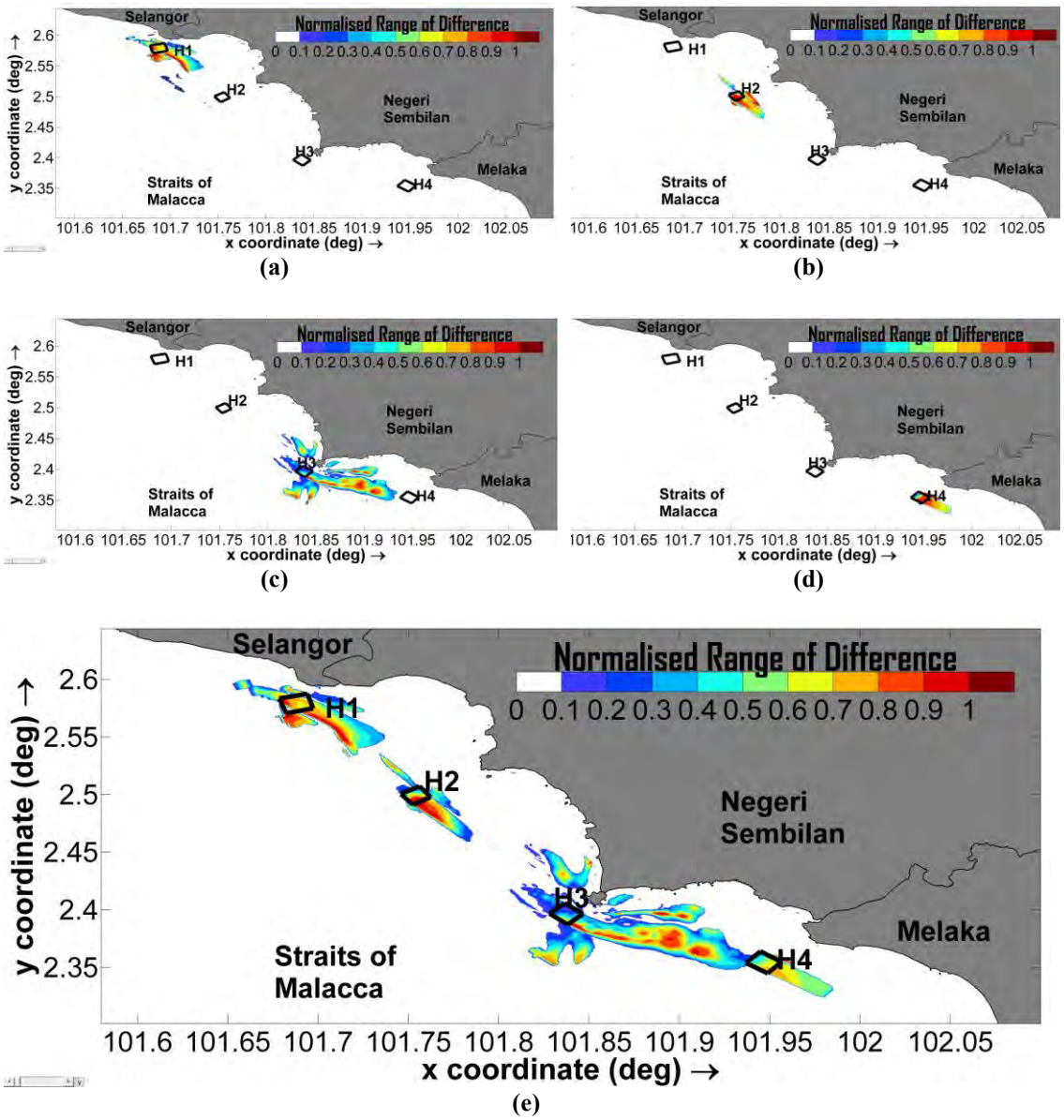

Figure 6.11: Normalized range of difference due to the tidal farm installation at (a) Headland H1, (b) Headland H2, (c) Headland H3, (d) Headland H4, (e) Headlands H1, H2, H3 and H4.

Table 6.10: Effect of single 1.5 km x 1.5 km hypothetical tidal farm to the extractable energy production at the surrounding headlands

Hypothetical tidal farm	Percentage changes in extractable energy at headland (%)			
	H1	**H2**	**H3**	**-H4**
H1		-3.6	-0.5	-0.5
H2	-2.0		-0.7	-0.5
H3	-2.0	-4.8		-8.7
H4	-0.1	-0.2	-0.9	

Table 6.11: Performance deficiency of the multiple tidal farms in concurrent operation.

Performance deficiency per annum	H1	H2	H3	H4
Magnitude (MWh)	-0.8	-1.1	-1.2	-1.4
Percentage (%)	-2.0	-5.1	-1.3	-6.8

6.4.4.2 Seabed Effect

Besides exploring the feasibility of harnessing tidal energy adjacent to headlands, this study also aimed at the potential environmental impacts caused by the tidal farm(s). For the cases of individual tidal farms, the 1.5 km x 1.5 km tidal farm at H3 causes the largest spatial and magnitude changes of tidal currents in comparison to those at H1, H2 and H4 when the tidal farms are operating individually (**Figure 6.12a**, **b**, **c**, **d**). For the case of multiple tidal farms (**Figure 6.12e**), the spatial extent of NRD spreads resembles those of the individual tidal farms. This implies that the environmental effect caused by both scenarios are nearly the same.

At increasing bed shear stress (flow velocities), surface erosion may occur. Apart from NRD spreading behaviour, the effect of bed shear stress induced by the nearshore hydrodynamic processes was also studied. The long-term impact due to the presence of the tidal farm(s) on physical littoral processes was assessed with reference to the mean and maximum bed shear stress changes. **Figure 6.12** shows the mean and maximum changes in bed shear stress as a result of installation of a single and multiple tidal farm(s) at H1, H2, H3 and H4. For single 1.5 km x 1.5 km tidal farm deployment, the mean and

maximum bed shear stress changes are relatively small in the vicinity of H1, H2 and H4 as schematically presented in **Figure 6.12 (a-d)**. Similar to the NRD finding, due to the lack of interaction with other three sites, the spatial extent of bed shear stress spreads resembles those of the individual tidal farms. The placement of tidal farm reduces the velocity and therefore the sediment would accumulate within the vicinity of the arrays with areas of erosion (increase of velocity and bed shear stress) either side.

It is observed that the peak reductions in mean bed shear stress for all the individual tidal farms simulated in this study are less than 2 Pa. These values are fairly similar to changes seen in Irish Sea (2.6 Pa) and Pentland Firth (0.8 Pa) as modelled in Haverson et al. (2017) and Martin-Short et al. (2015). It is apparent that the changes of mean bed shear stress are more prominent at H3, in which the variation of the mean bed shear stress is as high as 4 Pa. It is noticed that the bed shear stress reduction is found within the H3 tidal farm and immediately southward of the farm, and the stresses start building up beyond that as shown in **Figure 6.12c**.

Investigations at sites with high peak velocity at Fair Head, Torr Head and Mull of Kintrye was reported to have a high potential for flow interactions due to their proximity and installed capacity (Haverson et al., 2017). The energy production at Torr Head is reduced by 17%, whereas, Fair Head only reduced it by 2%. Further from the previous study, assessment for sites at 10 km distance interval with lower peak velocity (H1, H2 and H4) showed different results. The numerical outputs yielded in the present study (**Figure 6.12e**) show that the risk of interaction with the neighboring tidal farms of less than 10 km interval within the coast of Negeri Sembilan is relatively low. This subsequently poses less interference to the bottom sediment.

The coastline of Negeri Sembilan is largely bordered by a thin mangroves belt scattered along the rocky coast (Department of Irrigation and Drainage Malaysia, 2008).

It is of a great concern of the local authorities that the coastal development not to disturb the mangrove belt along the coastline. From the numerical outputs yielded in this study, the bed shear stress for H1, H2 and H4 presented a localized effect when they are operated individually (**Figure 6.12**); hence, the potential disturbances posed to the existing mangrove belt is not an issue. At H3 where the bed loading activities are more profound, the impact caused to the rocky Tg. Tuan headland is likely to be minimal. It is anticipated that the shoreline is less susceptible to erosion for minor changes on the mean and maximum bed shear stress (< 5 Pa). For the case of multiple tidal farms in concurrent operation, it is believed that the environmental effects caused by the facilities are not much different from the case of a single tidal farm.

Other than coastal mangroves, there are numerous marine life that habitats between the Kuala Sg Sepang to Kuala Sg Linggi coastal area (Department of Irrigation and Drainage Malaysia, 2008). The change to the coastal hydrodynamic regimes due to tidal energy extraction by the tidal farm(s) may cause some extent of interference to the marine life. These include coral reef, seagrass, fish, invertebrates and phytoplankton. The species to each of this marine life are listed in **Table 6.12**. It is crucial that the aquatic live remains undisturbed upon implementation of the tidal farm project along the Negeri Sembilan coastline. Some species, e.g., seagrass and seaweed, are particularly sensitive to sediment loading characteristics and may be deleteriously affected by sedimentation. It is hoped that the outcomes of this study could become a good basis for providing spatial and temporal information for environmental impact study on marine habitat due to energy extraction by tidal farms along the coast of Negeri Sembilan.

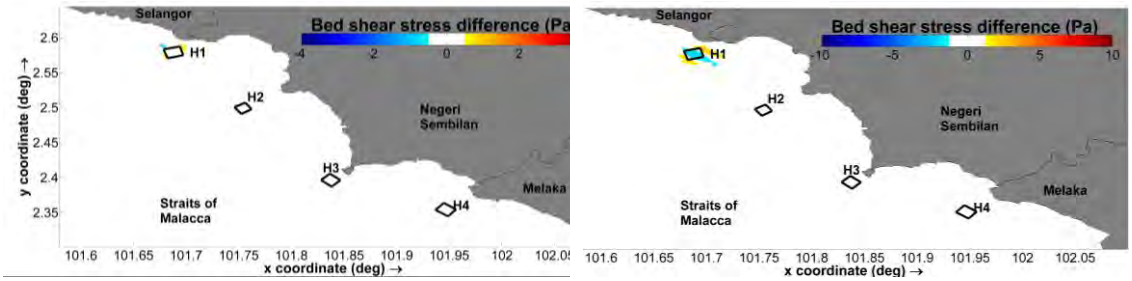

(a) (i) mean bed shear stress difference (a) (ii) max bed shear stress difference

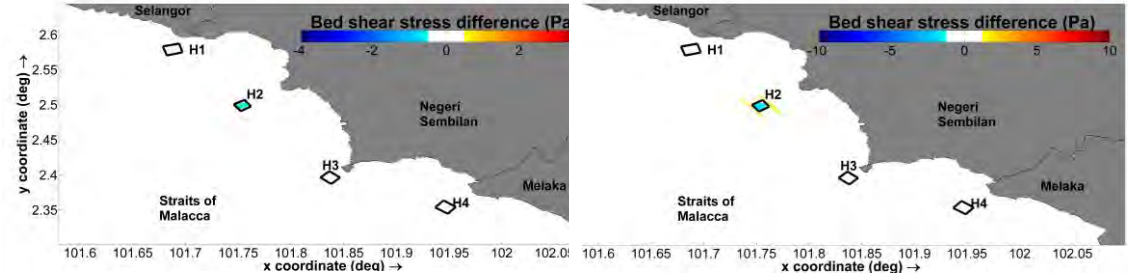

(b) (i) mean bed shear stress difference (b) (ii) max bed shear stress difference

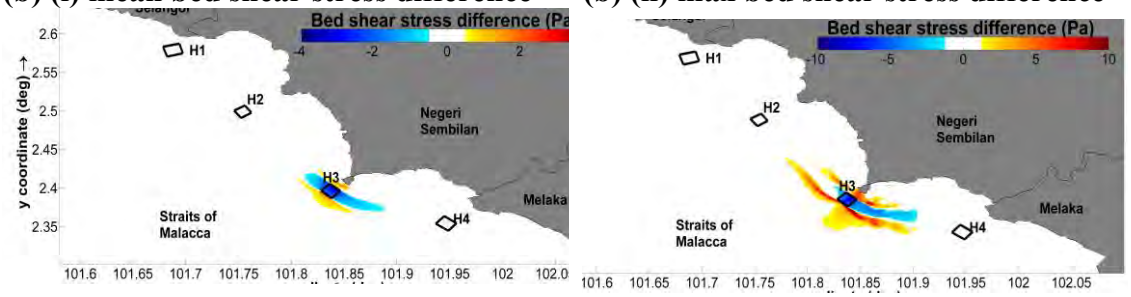

(c) (i) mean bed shear stress difference (c) (ii) max bed shear stress difference

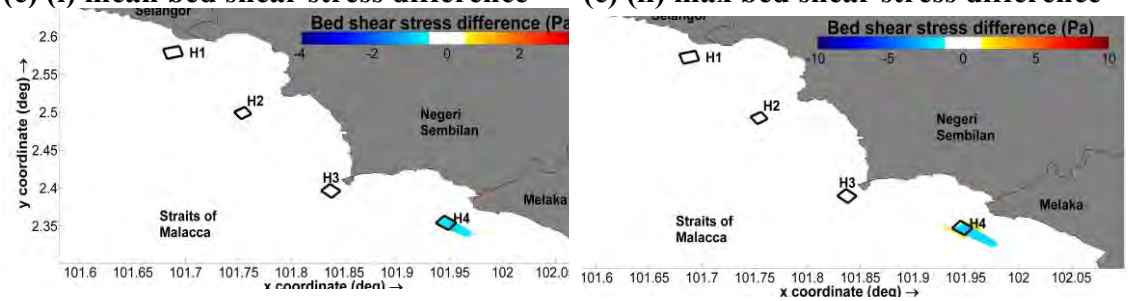

(d) (i) mean bed shear stress difference (d) (ii) max bed shear stress difference

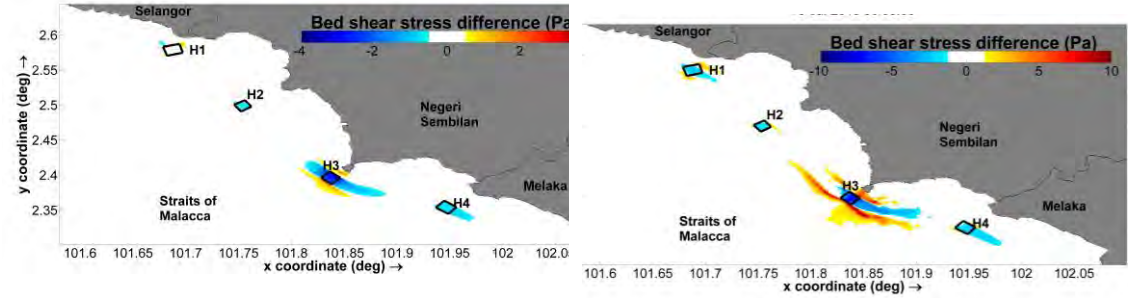

(e) (i) mean bed shear stress difference (e) (ii) max bed shear stress difference

Figure 6.12: Mean and maximum bed shear stress difference due to energy extraction of (a) H1, (b) H2, (c) H3, (d) H4, and (e) cumulative H1 – H4

Table 6.12: Species of each marine life in Negeri Sembilan coastal area

coral reef species	Seagrass	seaweed	fish inhabit seaweed meadows	invertebrate populations	Phytoplankton
Porites lutea, Porties and Goniastrea, soft coral Sarcophyton ehrenbergi. Other species found included Lobophytum pauciflorum, L. crassopiculatum and Pavona frondifera.	Echalus sp., Halodule sp. And Thalassia sp.	Glorophyta (Caulerpa spp. And Udotea spp.), Rhodophyta (Acanthophora sp., Amphiroa sp., and Gracilaria sp.) and Phaeophyta (Lobophora sp.).	rabbitfish, filefish, goatfish, boxfish, damsel fishes, sweetlips and cardinal fish	sea urchins, crabs, shrimps, scallops, mussels, snails and nudibranchs	Bacillariophyta, Cryptophyta, Dinoflagellata, and Chlorophyta

6.4.4.3 Sediment Transport variation

The inferences of deployment of large-scale tidal current turbine farm along Negeri Sembilan coastline and the impacts on suspended sediment within the coastline are investigated using the Delft3D-SED model. The tidal current turbine farm is modelled by incorporating semi-permeable structures that utilizes an energy loss term in the momentum equations of the fluid to parameterize tidal current turbine areas in the numerical model.

The results of sediment transport model results without the tidal current turbines, and for single tidal current turbine farm deployment at H1, H2, H3, H4 and multiple farm concurrent operation at H1, H2, H3 and H4 are shown in **Figure 6.13**. The sediment concentrations were simulated based on sediment concentrations in the environments with multiple grain size fractions using the actual sampling data at the site. The TSS results can be referred to **Table 4.5**. The results of the TSS recorded range from 30mg/L to 64mg/L. The highest average TSS value (82 mg/l) is found near Tanjung Tuan Beach and the lowest is 15mg/L near Kampung Paya (**Figure 4.9**). The data obtained are adequately utilised for the simulation.

Sedimentation issue within the farm area can be a concern where reduction of sediment transport can be observed within the farm (2×10^{-4} $m^3/s/m$). High sediment transport changes would affect the biological and physical order in the sea, particularly consisting of environmentally sensitive areas, i.e., seagrass, coral reef, agricultural farm, etc. The sediment transport is highly sensitive to the tidal flow changes and suggests that largest sediment transport effect occurred at the highest energy tidal farm that extracts largest power. From the sediment transport simulation, maximum tidal power extraction has the largest impact on sediment transport in the Negeri Sembilan coastline. Compared to baseline condition (pre-deployment of tidal current turbine), the sediment transport

changed significantly at the Tg Tuan Headland (H3). The effects extended as far as 10 km northward and southward, near to Port Dickson (H3) and Linggi Headland (H4). Although the effect of sediment transport seems to be obvious as indicated in spatial map shown in **Figure 6.13d**, indeed, the magnitude of change is relatively small (< 2 x 10-4 $m^3/s/m$) compared to the baseline condition. Further analysis on percentage changes on the sediment transport was made. **Figure 6.14** shows that the percentage of difference for concurrent operation of tidal farm at multiple headlands (H1, H2, H3 and H4) on sediment transport is minor (~ 10% difference) in comparison to baseline condition. Moreover, the percentage changes of sediment transport within the tidal farm are negligible (<5%) and the far-field effect is observed to be insignificant.

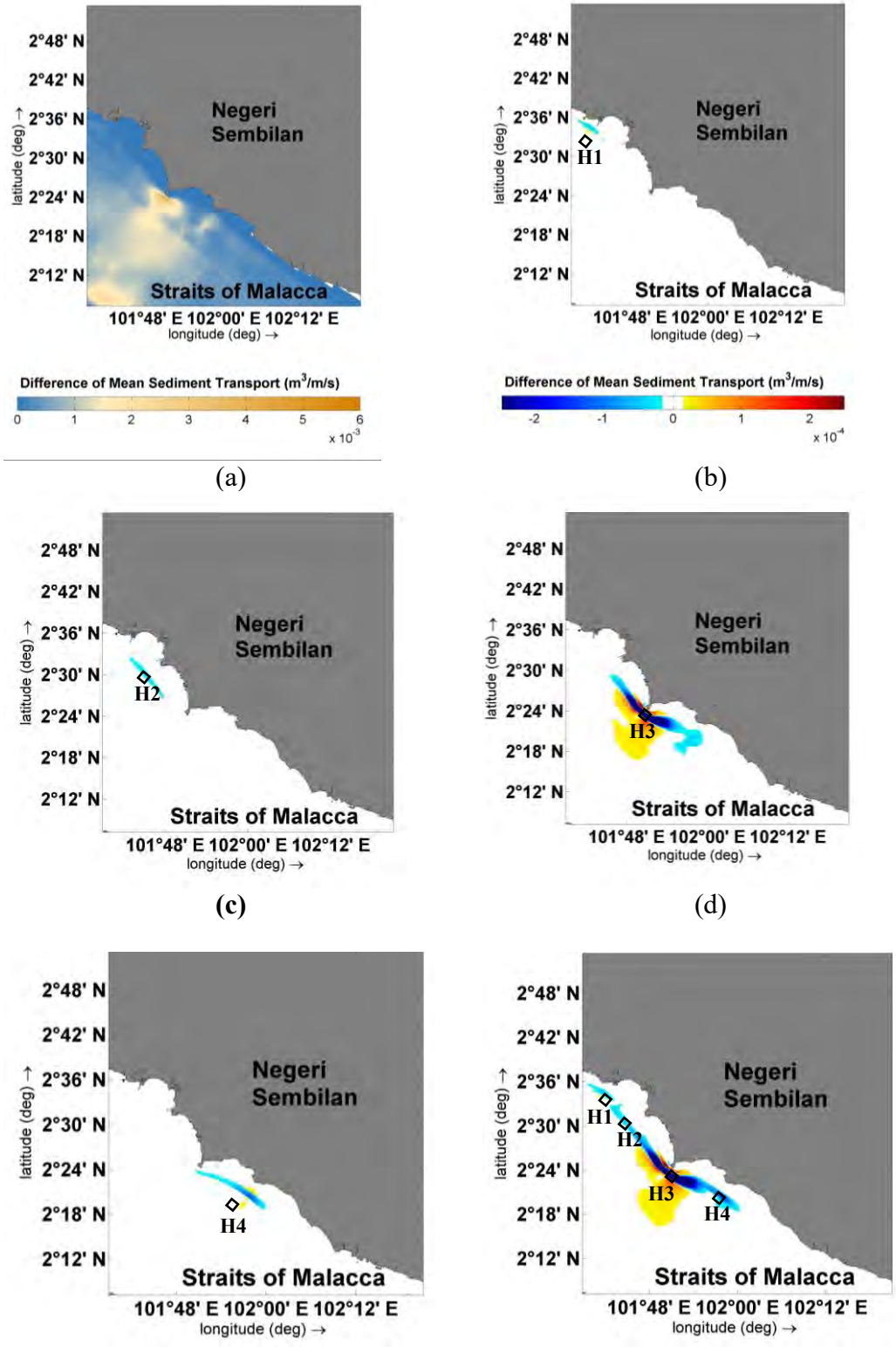

Figure 6.13: Total sediment transport for (a) baseline and difference of total sediment transport for single farm, b) H1, c) H2, d) H3, e) H4 and multiple farm f) H1-H4

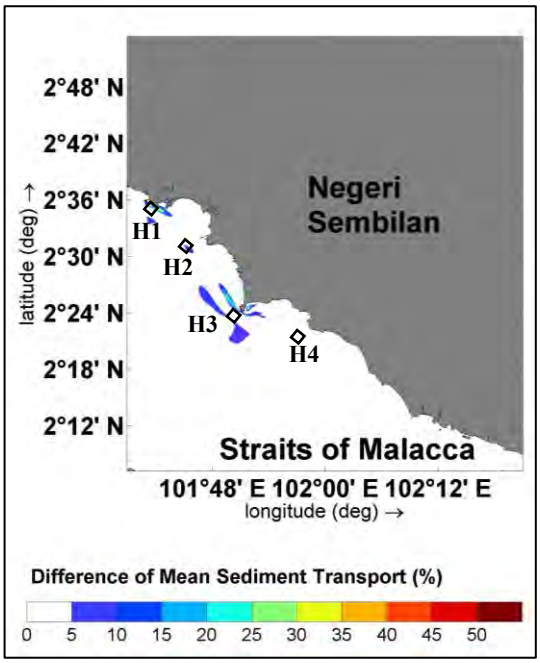

Figure 6.14: Percentage change of sediment transport for multiple farm H1-H4 along Negeri Sembilan Coastline

6.4.4.3 Monsoonal Variation

Monsoonal variation may affect the effect of tidal farm deployment. Based on the wind data obtained from BMT (1990 – 2018), the wind during NE monsoon predominantly blew from the Northwest direction at dominant speed of 2.5 - 3.5 m/s, while the wind during SW monsoon is predominantly blew from a Southeast direction at dominant wind speed similar to NE monsoon, 2.5 – 3.5 m/s. Based on the monsoonal offshore wind rose and wave rose analysis, the intensity of wind speed and significant wave height are higher during Northeast monsoon compared to Pure Tide and Southwest monsoon. For this study, a dominant wind direction of NW (300 Degrees) and SW (157.5 Degrees) with 3.5 m/s wind speed were simulated.

The simulation results shown **in Figure 6.15a(i)**, **b(i)** and **c(i)** demonstrate that the sediment transport occurs in the same manner spatially during Pure Tide, Northeast and Southwest monsoon. The monsoonal effect is not significant at the location of the study area. The sediment transport is in higher magnitude at the tip of H3 (Tg Tuan Headland)

due to higher tidal current speed at this region. The sediment transport effect within the bay is negligible, less than 1 x 10^{-3} $m^3/s/m$ is observed. Higher sediment transport is observed at the deeper area when move further offshore

Further assessment on the changes of sediment transport for Pure Tide, NE and SW monsoon showed similar result in magnitude change spatially. Contrasting with a study nearby (~ 70 km) the Tg Tuan Headland, which found that NE monsoon has significant effect on sediment transport of Pulau Carey and subsequently influences the installation of breakwater (Fitri et al., 2019). However, it is worth to mention that the data utilised in previous study has overestimated the wind speed at the study area by using the land wind speed data that captured at the nearest station, KLIA airport. The boundary condition used in the model in this study is more representative by using the offshore long-term wind data.

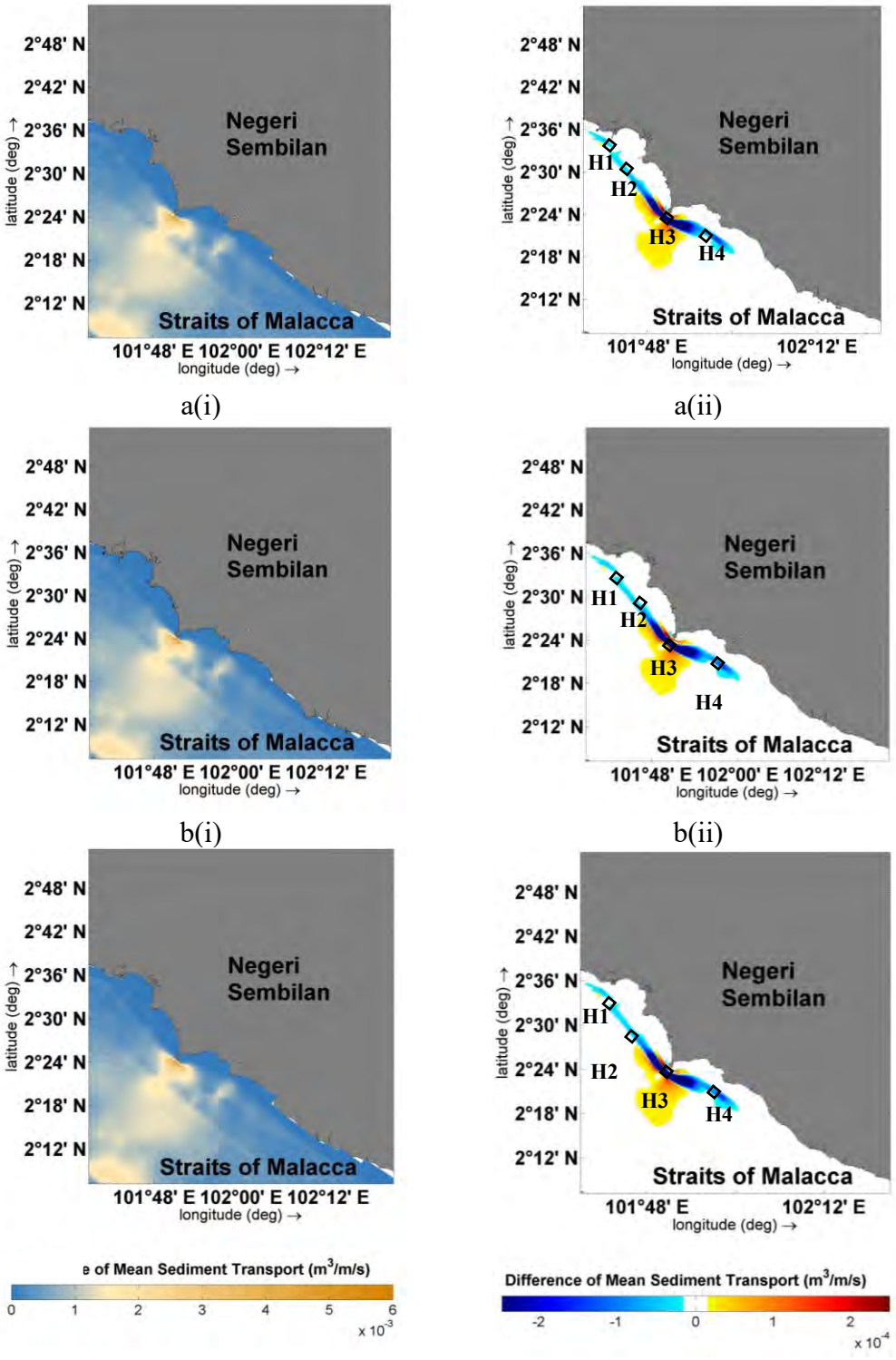

Figure 6.15: Monsoonal variation of sediment transport for: a) Pure tide, b) Southwest, and c) Northeast wind condition effect for (i) total sediment transport and (ii) change of total sediment transport for multiple farms at Headland H1, H2, H3 and H4 operation

6.5 Summary

Due to advancement of technology, further practical resource assessment is recommended to include areas with spring velocity < 2 m/s within Straits of Malacca to further explore and optimize the energy production in Malaysia. The analysis showed that the effectiveness of exploitation for a site with spring velocity < 2 m/s is encouraging as the regulated tidal current turbine force was higher than unregulated force by < 10%. Other than that, the nearest power station, Tuanku Jaafar Power Station located approximately 13 km northwest from the tip of Tg Tuan Headland, also enable the tidal resource to be tapped into the transmission line towards the national grid. In this chapter, several important aspects related to exploiting tidal current energy from a headland is demonstrated. This study provides one specific site examples (Tg Tuan Headland) that examine and quantify the effect of configuration and site condition (depth and row numbers) in affecting the performance of tidal current turbine extraction, based on kinetic energy dissipation and electrical power generation. Instead of focusing solely on the tidal turbine performance and localised dissipation, hydrodynamic far-field impact evaluation was incorporated also into the assessment as part of the assessment in energy exploitation prediction. Predicted alteration in the magnitude and distribution of the multidirectional flow was incorporated into the analyses of the changes affecting the baseline tidal hydrodynamics condition.

In overall, the depth effect is not significant in changing the extractable electrical power. The difference is less than 0.02 MW compared to D1 (highest) and D8 (lowest) mean electrical power extraction for about 7 m difference. In terms of energy dissipation, depth has more significant effect on the kinetic energy dissipation whereas the mean dissipation difference (0.05 MW) between D2 (highest) and D8 (lowest) is double of mean electrical power generation difference. Based on depth effect assessment for the deployment of a 10-m diameter tidal turbine at shallow waters (d < 30 m), the deployment

of tidal turbine results in reduction of current velocities at D1, D2, D3 and D4. From the analysis of mean current velocity relative to the baseline condition, the deployment of a 10-m diameter tidal turbine at shallow water, D1 (d = 25.46 m), has the largest upstream spatial influence, in which the affected distance is extended up to 0.9 km upstream of the facility. The maximum change in current speed magnitude is 0.019 m/s. For downstream effects, the change in flow velocity is insignificant for all the turbine locations. Further derivation on relationship for the modelled depth range from 25.4 m to 31.6 m showed descending curve of current speed changes at 500 m upstream and downstream from different depth deployment conditions during flood and ebb tides. It can be concluded that the results of current speed changes showed that deployment at deeper areas which is further offshore, contributed lesser magnitude of current speed changes with baseline condition compared to the shallower area.

For array effect assessment, diminishing returns on the power generation was showed even though considerably low extraction was made with considerably large gap (10D) was assumed in between each turbine was assumed. It was also found that peak power production from an array of 5 rows (L1-L5) of tidal array (3 turbine each row) was slightly lesser than the corresponding values for each row (single row with 3 turbines, each row of L1, L2, L3, L4 and L5) of the smaller array. The results of MR-SR current speed changes showed that deployment of less than three rows did not reduce much the current speed, when it reaches fourth row and above will reduce the current velocity and subsequently the electrical power generation significantly. Further analysis made on the mean current speed changes for MR five rows and three rows array compared to baseline condition showed that the three rows is an optimum array configuration as lesser impact to the environment for smaller array was demonstrated.

This work has conducted an interaction risk assessment using high-resolution depth-averaged hydrodynamic model, where sites with combination of higher and lower peak velocities to be exploited were assessed. Tidal energy extraction simulation results showed that the effect of single tidal farm gives minimal hydrodynamic effect to the headlands in vicinity. Slight reduction in energy production (< 7%) for headlands occurred in the vicinity due to the presence of hypothetical 1.5 km x 1.5 km tidal farm at H1, H2, H3 and H4. Results show that these four tidal farms run quite independently of each other. The results of analysis show that the interaction of intermediary sites of close proximity developed by combining higher (> 1.0 m/s) and lower peak velocities (< 1.0 m/s) is small. The environmental impact assessment using the worst-case scenario by combining four tidal farms at four headlands along the Negeri Sembilan showed that the extraction effects towards mangrove belt erosion is negligible. Using Negeri Sembilan as study site, the analysis results from this study showed positive exploitability for implementing sites with combination of higher and lower peak velocities with close proximity (~ 10 km) based on two main criteria: maximum tidal energy extraction exploitability and minimal environmental impact.

The sediment transport is highly sensitive to the tidal flow changes. Installation of tidal current turbine farm at H3 showed the largest sediment transport changes as it is the highest energy farm that extracts largest power. However, further analysis by evaluating the sediment transport changes in percentage showed that the effect of tidal farm installation is minor at the boundary of the tidal farm (~10%), and negligible within the tidal current turbine H3 farm (<5%) as the sediment transport during baseline is high (6 x 10^{-3} $m^3/s/m$). The far-field effect on sediment transport is found to be negligible for concurrent operation of tidal farm at H1, H2, H3 and H4.

The monsoonal effect to the study area is not significant. This is mainly due to low dominant wind magnitude blowing from the Northwest and Southeast direction. Other than that, the shoreline is very protected and sheltered from Sumatera Island as well as the nearest island, Pulau Rupat from developing longer fetch of wave. Hence, wave impact assessment was not carried out further for this study area. However, for other sites with high wind effect, e.g., east coast of Malaysia, Sabah and Sarawak coastline and etc, wind and wave effect assessment is crucial to be carried out to determine the monsoonal effect in tidal current turbine deployment impact assessment.

Coastal areas with lower peak velocities are rich in marine biodiversity; in order to allowing more sites with lower peak velocities to be harnessed, special care and attention must be taken. Nevertheless, there are still very few studies that focused on the tidal energy impact to marine environment/ecology even though the tidal stream industry is increasing with technological advancement. The results from this study can be used as a basis to provide spatial and temporal information for further assessment of tidal energy extraction impacts to the environment. The outcomes yielded from this study would be a good source of reference to the authorities in decision-making related to deployment of tidal turbine near Tg Tuan Headland.

7 CONCLUSION AND RECOMMENDATIONS

The findings of the research discussed in Chapter 2 to 6 are reviewed and the key conclusion discussed. Some thoughts on the use of numerical models for tidal current energy resource and environmental assessments are expressed. Recommendations are then provided for research relating to tidal current energy extraction and coastal headland.

7.1 Summary

The discussion presented in the earlier chapters of this thesis incorporates numerous resource exploitability, device engineering and environmental impact components of tidal current power generation. The development of electrical power generation from tidal current poses challenges and attractions to engineers and scientists to achieve a viable solution by attaining a harmonious agreement in both economic and environmental aspects in response to an increasing demand for energy, reducing the supplies of fossil fuels, and to combat the global climate change issue. Tidal current energy extraction is favourable due to its predictable phenomenon, characterized by earth-moon-sun gravitational force system. Other than that, to exploit kinetic energy from tidal current by applying established technologies maybe economically viable at limited number of accessible and energetic sites. In considering the complicated physical oceanography of a headland, tidal flow currents determine the patterns and stratification of sediment transport as well as the tidal fronts' position.

Tg Tuan Headland of Negeri Sembilan is the focus site of present study. This potential coastline is highly anticipated to be one of the Malaysia's first commercial-scale marine tidal current energy extraction site. However, there is none on the published information

on the flow condition at this particular tidal energy sites, or within the multiple headlands along the coast of Negeri Sembilan in general. Earlier studies for Malaysian tidal current potential sites generally focused on the economic viability in energy extraction. The scarcity of data earlier has hindered to provide accurate prediction of the potential environmental assessment in response to tidal current energy extraction. The works conducted for this thesis denotes as one of the first comprehensive efforts to address these subjects. With the strategic location, the nearest power station, Tuanku Jaafar Power Station and Jimah Power Plant, located approximately 13 km and 25km northwest from the tip of Tg Tuan Headland also enable the tidal resource to be tpped into the transmission line towards the national grid. In addition, the energy tapped from the headland coast is expected to power up the nearby beach resorts and hotels as listed and illustrated in **Figure 7.1**.

By adopting the findings from previous studies, the energy potential and effect of extraction can be further explored with a better resolution model due to the complexity of local coastline and geomorphology condition of each site. The parametrization of tidal current turbine within a precise and high reliability model also served a means of estimating the hydrodynamic response to tidal current energy extraction. A well-developed numerical model is a vital tool for advising regulators and project proponent of the doubts regarding the exploitation of tidal current energy. Various types of model are available and it is crucial that the one selected is suitable to answer the questions raised technically and practically raised. Based on the spatial scale requirement to be considered, a depth-averaged two-dimensional hydrodynamic model was applied in the present study.

The research discussed in this thesis should be of interest to engineers involved actively in the research and development of marine renewable energy and researchers in

physical oceanography. The findings should be of specifically relevance for regulators (e.g., Department of Environment, Planning Units, Drainage and Irrigation Department and etc.), private developers, and hydrodynamic model practitioners involved in tidal current exploitation research in Malaysia. Nevertheless, there are several numbers of possible opportunities to be further developed and discussed on this particular work. Some possible future researches inspired from the ideas presented in this thesis, are detailed in Section 7.4.

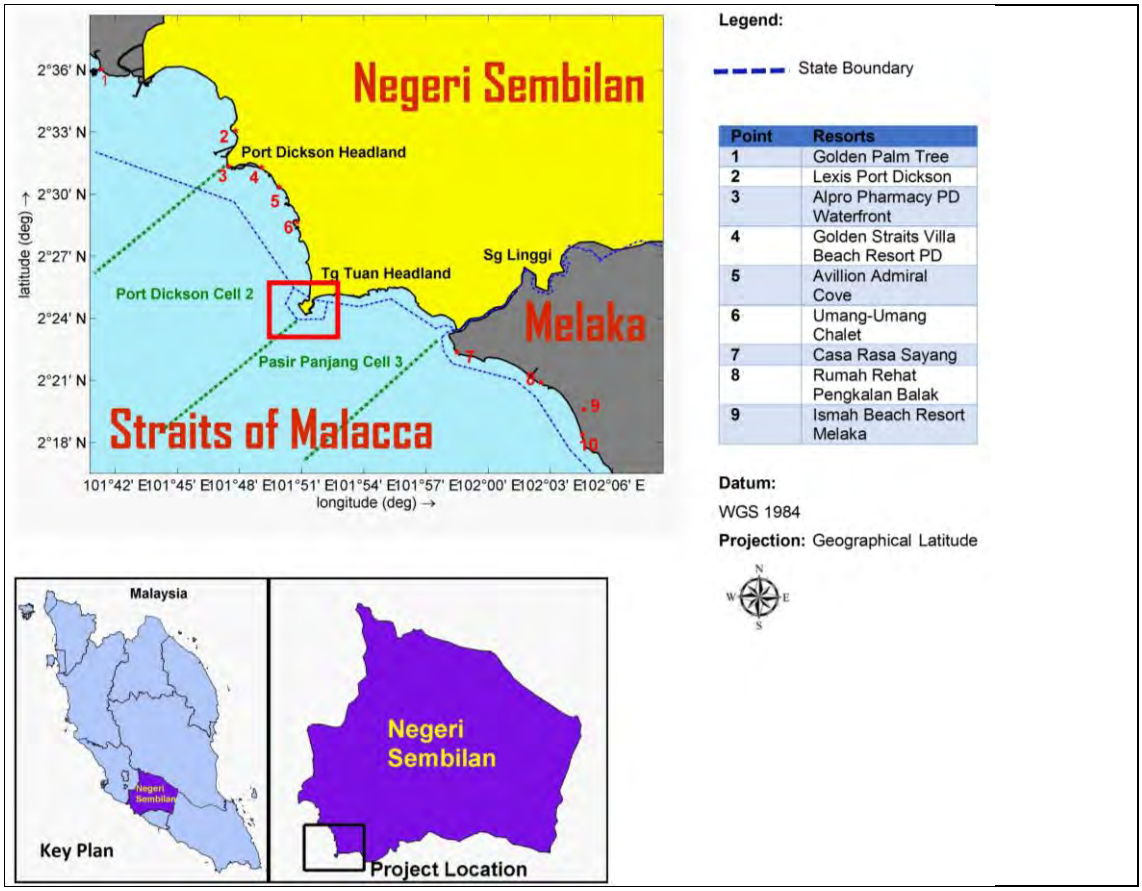

Figure 7.1: Tg Tuan Headland and its vicinity

7.2 Conclusion

By reflecting the main objectives formulated in Chapter 1, the key findings of the research discussed in Chapter 2 – 6 are summarized as below:

- Objective 1: Develop a field campaign for primary and secondary data collection requirement.

A field campaign for primary and secondary data collection requirement was successfully developed in this research based on the prerequisite for tidal current energy extraction impact assessment for this research. The primary and secondary data were checked and sufficiently applied in this study. The primary data collected in this study includes of bathymetry, tidal level, current velocity, TSS and bed grab sampling. While, wave and wind data were collected during the secondary data collection campaign. The developed field data collection campaign method and procedures as described in Chapter 3 can be used as good reference for future studies relevant to tidal current energy extraction impact assessment.

- Objective 2: Establish a hydrodynamic model capable for quantifying the electrical power resource for a tidal stream energy potential site assessment.

A two-dimensional high-resolution hydrodynamic model established in Chapter 4 was adopted to assess the tidal dynamics of Negeri Sembilan Coastline. The numerical model was found to provide a reliable and useful picture of the flow condition of Negeri Sembilan Coastline with multiple potential headlands for tidal current energy extraction. Preliminary estimation based on fully occupation of site for tidal current energy extraction under undisturbed flow condition showed that the estimated natural gas substitution data at H3 is 660 TJ. The average cost of natural gas is RM 23.72/mmBtu or RM 1.12/kg based on the tariff rates approved by the government in accordance with section 13 of Gas Supply Act 1993 (GasMalaysia, 2019). With 56 GWh/annum of energy generation from

tidal turbine, a total amount of 185 GWh or 660 TJ of natural gas can be replaced every year. The energy content of natural gas is about 55 MJ/kg. With the power output of 185 GWh/year of tidal turbines, the country or the utility company can save about RM 13.4 million (~ USD 3.2 million) of natural gas per year. This can be a good reference for the policy maker and the utility company (Tenaga National Berhad) as they can use it to estimate the saving of natural gas.

- Objective 3: Develop a methodology for parameterizing within a numerical model, the energy extraction associated with a representative array of tidal current turbine

Chapter 5 adopted the published features of horizontal axis tidal current turbine to formulate expression, which described the current speed of a tidal current turbine, power outputs and forces. The derived parameterization from this chapter can be used to simulate the tidal current turbine effect assessment in different configuration, (i.e., depth, array numbers), as further employed in Chapter 6 in this research. Another finding from regulating the tidal current turbines showed lower environmental stresses was imposed during high flow at the local grid than unregulated turbines of similar capacity. This finding enables regulators and investors to make informed decisions in response to tidal current energy extraction projects.

- Objective 4: Investigate the interactions between tidal kinetic energy dissipation and the environmental in response to power take-off of tidal stream energy for a representative configuration of tidal current turbines.

    a. Far field impact assessment showed that tidal current flow velocities would reduce within and around, and downstream with equilibrium increment of flow velocities around the turbines.

b. The result of depth effect showed that deployment at deeper area contributes lesser magnitude change of current speed with baseline condition compared to shallower area.

c. Array effect on the power generation diminishes even though low energy extraction was made. An array comprises of 5 rows (L1-L5) with 3 turbines each row was found to have lower electricity power production than each row (single row with 3 turbines each row of L1, L2, L3, L4 and L5) of the smaller array. The effect is obvious when the multiple row array reaches fourth rows and above.

d. The comparison of MR of five rows and MR of three rows with baseline condition demonstrated MR of three rows is an optimum array. MR of three rows has lesser impact to the environment, <100 m of spatial change upstream compared to MR of five rows with less diminishing on the power generation is observed.

- Objective 5: To investigate the potential risk of interaction to sites geographically close to each other when intermediary sites are developed within the coast of Negeri Sembilan

Positive exploitability was obtained for implementing sites with combination of higher and lower peak velocities with close proximity (~ 10 km). Tidal energy extraction simulation results showed that the effect of single tidal farm gives minimal hydrodynamic, bed shear stress, and sediment transport effect to the headlands in vicinity. These four tidal farms run quite independently of each other.

The outcomes yielded from this study would be a good source of reference to the authorities in decision-making related to deployment of tidal turbine near Tg Tuan Headland.

7.3 Recommendations for practitioners

At current stage, a clear set of recognized Standard of Procedures (SOP) for resource and environmental assessments is still limited. It is not possible that environmental agreement for tidal current energy extraction project will be fully secured before the responsibility held by regulators and investors are eased. Given the limited existing data and site accessibility of tidal current energy extraction project, numerical models offer as a useful tool to project developer during decision-making stage. Based on author's experience of performing this research work, necessary tasks and consideration that the modeller may take into account when conducting resource and environmental impact assessment are given below.

I. Model mesh size and bathymetry

Finer model mesh size and temporal variation in the current flow also had some effects for setting the limits of the separation of model mesh-node. The energy dissipation at the sub-grid scale of the turbulence model was mainly relies on the square of the model mesh-node separation. More numerical diffusion and uncertainties in the model prediction occur when larger mesh size model is adopted. It is recommended that model mesh size sensitivity test to be carried out in optimising the grid resolution suitable for the tidal current flow condition at the site.

An accurate and detailed bathymetry is crucial input in obtaining good quality prediction for hydrodynamic model study. This is particularly pertinent to tidal current energy extraction at headland site as it tends to have high degree of spatial variability in current flow. The model bathymetry interval adopted in this research is approximately 100 m of resolution and generally adequate to simulate position of quickest tidal current flow at the headland. Nevertheless, the numerical model is not able to capture the flow separation point and corresponding eddy in the vicinity of shallow rocky boulder that is

commonly found at headland area. The hydrodynamic at this particular area is highly complex due to its steep gradient with periodic drying and wetting model cells. It is recommended that the developers of the project consider performing a more detail geophysical site survey in order to have a more accurate bathymetry input.

II. Vessel-mounted tidal current survey for validation

In Chapters 4 and 5, the spatial variability showed the importance for characterizing the resource and environmental condition at site. A well calibrated and validated model is highly desired in order to have a high reliability baseline model, which is able to describe the hydrodynamic condition as near as possible to the actual site. Vessel-mounted tidal current survey can be used to achieve a better baseline model description by fine-tuning the seabed drag coefficient of the spatial distribution. However, this method is more complicated and will increase the difficulty during the model calibration and validation stages.

At this stage of research, the seabed-mounted instrument was used to ensure accuracy in temporal variations and the result of model calibration and validation are shown in Chapter 4. In order to improve the model description of spatial distribution characteristics at the study area, it is highly recommended to supplement model calibration and validation with observation from vessel-mounted tidal current survey data, specifically covering the tidal current energy extraction site area for model validation.

III. Detailed bed material test

For sediment transport modelling, due to limitation of sediment distribution data for regional model, the model was initialized with assumed constant sediment distribution map to define the mixture of cohesive and non-cohesive sediment bed thickness. A detail sediment distribution map shall be derived and sampled concurrently with the sonar

measurement. As the initial result in sediment suspension is sourced from the seabed sediment in the model, Soil Investigation (SI) shall be carried out to acquire the data to accurately model the thickness of the bed material. To date, there is still no data available for the sediment parameters, such as settling velocity, critical bed shear stress for sedimentation and erosion, and the erosion parameter applicable within the Straits of Malacca, an optimal sediment parameter should be derived to be applied for numerical model within the strait.

7.4 Recommendations for Future Research

The marine renewable energy sector is still in early stage into commercialization, there are more opportunities for future research. This research can be considered as a basis to cater for future studies in Malaysian sea. Some potential future researches developed from the ideas of this thesis are delineated below.

7.4.1 Coupling of 3D HD with ST model

Tg Tuan Headland is consistent with locations of localized seabed sediment deposits, as shown in Chapter 4 due to residual tidal eddies predicted behind the headland. Based on first-order-accuracy, the residual tidal eddies could maintain the seabed sediments. However, this conclusion is not confirmed as sedimentation is mainly governed by the instantaneous gradient of tidal current field. A more detailed exploration of sediment transport at the Tg Tuan Headland is necessary.

The tidal array to be deployed at the seabed adds major disturbance on the current velocity, specifically expected at the bottom layer of water column. The tidal current velocities at the seabed layer is more valuable than depth-averaged current speed for

studying sediment transport predominantly occurring at the seabed. Hence, it is recommended to conduct more detailed modelling by coupling three-dimensional hydrodynamic model with sediment transport model. This should be established in conjunction with field measurement campaign. The seabed sediment sampling and mapping (Sonar) shall be conducted concurrently to determine thickness and characteristics of each sediment fraction layer.

7.4.2 Linkage of Flow and Habitat Variables

It is crucial to understand the relationship between the tidal flow and marine habitat life at tidal current energy site to predict the ecological effect due to energy extraction. Tidal currents are the main driver for the sediment transport at the seabed and food supply to the benthic organisms. It is therefore important to determine the spatial distribution of the benthic organism in the sea. Mapping of the marine life habitat can be established to predict the benthic species distribution.

The hydrodynamic model offers a valuable tool for deriving hydrodynamic flow spatially and temporally at the potential tidal energy extraction site. By overlaying habitat mapping within a predicted hydrodynamic model is potentially more economical solution for describing the environmental constraints. Besides that, model parameterization by incorporating hypothetical energy extraction from Chapter 6 can be used to gather the statistics of tidal current flow changes. Field campaign by conducting seabed mapping can be valuable source of data to obtain the marine habitat species at the seabed of the project area. However, this might possibly only economically practical to be carried out during advanced implementation stage of the project. This study is particularly important for the fishermen who rely on fishing activity for their livings.

7.4.3 Enforcement of Environmental Impact Assessment

The tidal current energy extraction scenarios explored in this study focused on at four sites within Negeri Sembilan Coastline, Straits of Malacca. Developments are anticipated to more extensive and larger areas within the strait. Lim and Koh (2010) used Princeton Ocean Model (POM) to identify the locations for great potential for harvesting of tidal energy in Malaysia. In South China Sea region, Pulau Jambongan, Kota Belud and Sibu were identified to be the most viable spots for harnessing of tidal energy. Whereas, no suitable sites were found within Straits of Malacca due to their limited depths, i.e., the water depth is mostly less than 20 m). However, Sakmani et al. (2013) defended that Pulau Pangkor might be a suitable site for tidal turbine installation in the Straits of Malacca. Apart from that, by using a refined model resolution parallel with field measurement data at the site, this study has further proven that Tg Tuan Headland is suitable as this site fulfils the current velocity and depth requirements for established horizontal axis turbine application. Furthermore, with the advancement of turbine technology and the plant design enhancement, the tapping of the marine energy at island and headland locations along the strait is still feasible (Faez Hassan et al., 2012; Hassanzadeh et al., 2017). Therefore, it is highly anticipated to have more suitable sites that will be discovered in later stage. Although some degree of interaction between these sites may be possible as discussed in Chapter 6 based on findings from farm deployment at multiple headlands, it is not expected that these developments will significantly change the overall hydrodynamic of the sea. Further work to verify this assumption will be required. Other than that, future work will be necessary to predict the consequences of cumulative effect on the overall hydrodynamics, flow statistics as well as potential environment impact assessment. The approach established in Chapters 5 and 6 should offer a valuable framework to conduct such study.

There are twenty-one and seventeen activities stated under Schedule 1 and Schedule 2 of Environmental Quality (Prescribed Activities) (Environmental Impact Assessment) Order 2015, Department of Environment, DOE (2015). For development along shoreline and rivers, the order only requires dredging, reclamation and hotel development activities to acquire approval from DOE for development. To date, there is no specific enforcement stating that tidal farm development requires EIA submission. Hence, it is highly recommended that tidal farm should be included as one of the prescribed activities in the order, which requires Environmental Impact Assessment (EIA) to be carried out and report submission to DOE.

7.4.4 Tidal Turbine Array Modelling Verification

Incorporating tidal current turbine as actuator disc in a two-dimensional hydrodynamic model demonstrated a good prediction for energy extraction effect in the sea in comparison to conventional seabed friction approach. Although this approach was well acceptable ((Draper et al., 2014; Harrison et al., 2010) with good validation as given in Chapter 5, a few assumptions made in this work have not been verified. It has not considered the mixing increment effect in affecting the dispersion terms within the turbulence model. The turbine rotation force, which may affect the current velocity within the water column was not able to be simulated as well. With the advancement of numerical modelling technology, computational fluid dynamic (CFD) might be an alternative option to model the rotation effect of the single number of tidal current turbine to the flow. However, the cumulative effect of multiple turbine array in a regional model vary from single turbine effect. Furthermore, it will not be economically viable to conduct CFD model for tidal current turbine in large array. It is recommended that field campaign with real-time tidal current velocity measurement parallel with turbine operational data at the site can be adopted for model verification purpose. Nevertheless, it is only possible

to verify the efficacy of this methodology only when the devices are operational in the sea.

REFERENCES

Abanades, J., Greaves;, D., & Iglesias;, G. (2014). Coastal defence through wave farms. *Coastal Engineering, vol. 91*, pp. 299-307.

Abd. Shukor, A. H. (2004). The use of mangroves in Malaysia. In: Promotion of mangrove-friendly shrimp aquaculture in Southeast Asia *Tigbauan, Iloilo, Philippines: Aquaculture Department, Southeast Asian Fisheries Development Center.*, pp. 136-144

Adcock, T. A. A. (2014). *The available power obtainable from tidal stream turbines from a flow around an idealised headland, 14 - 16 April* 3rd IAHR Europe Congress, Porto, Portugal.

Ahmadian, R., Falconer, R., & Bockelmann-Evans, B. (2012). Far-field modelling of the hydro-environmental impact of tidal stream turbines. *Renewable Energy, 38*(1), 107-116. https://doi.org/10.1016/j.renene.2011.07.005

Ahmadian, R., & Falconer, R. A. (2012). Assessment of array shape of tidal stream turbines on hydro-environmental impacts and power output. *Renewable Energy, 44*, 318-327. https://doi.org/http://dx.doi.org/10.1016/j.renene.2012.01.106

Ainsworth, D., & Thake, J. (2006). *Final Report on Preliminary Works Associated with 1MW Tidal Turbine*. M. C. T. Ltd.

Araquistain, T. M. (2006). *tidal power* Tsinghua University].

Arbic, B. K., & Garrett, C. (2010). A coupled oscillator model of shelf and ocean tides. *Continental Shelf Research, 30*(6), 564-574. https://doi.org/https://doi.org/10.1016/j.csr.2009.07.008

Atwater, J. F., & Lawrence, G. A. (2011). Regulatory, design and methodological impacts in determining tidal-in-stream power resource potential. *Energy Policy, 39*(3), 1694-1698. https://doi.org/https://doi.org/10.1016/j.enpol.2010.12.048

Azman, A. Y., Rahman, A. A., Bakar, N. A., Hanaffi, F., & Khamis, A. (2011). Study of Renewable Energy Potential in Malaysia. *IEEE First Conference on Clean Energy and Technology CET*.

B&V, B. a. V. C. L. (2004). *Phase I UK tidal. stream energy resource assessment*.

Badano, N., Valdés, R. E., & Álvarez, E. Á. (2018). Tidal current energy potential of Nalón river estuary assessment using a high precision flow model. *Open Engineering, 8*(1), 118-123. https://doi.org/doi:10.1515/eng-2018-0015

Bahaj, A., Myers, L., Thomson, M., & Jorge, N. (2007, 01/01). Characterising the wake of horizontal axis marine current turbines.

Bahaj, A. S. (2011). Generating electricity from the oceans. *Renewable and Sustainable Energy Reviews, 15*, 3399-3416.

Bahaj, A. S., & Myers, L. (2004). Analytical estimates of the energy yield potential from the Alderney Race (Channel Islands) using marine current energy converters. *Renewable Energy, 29*(12), 1931-1945. https://doi.org/https://doi.org/10.1016/j.renene.2004.02.013

Bai, G., Li, J., Fan, P., & Li, G. (2013). Numerical investigations of the effects of different arrays on power extractions of horizontal axis tidal current turbines. *Renewable Energy, 53*, 180-186. https://doi.org/https://doi.org/10.1016/j.renene.2012.10.048

Ball, I. (2002). *Turning the tide: Power from the sea and protection for nature* (World wide fund for nature report, Issue.

Batten, W., & Bahaj, A. (2006). CFD Simulation of a Small Farm of Horizontal Axis Marine Current Turbines. *Conference: 9th World Renewable Energy Congress (WREC-IX)At: Florence, Italy*.

Batten, W., Bahaj, A., Molland, A. F., & Chaplin, J. R. (2008). The Prediction of the Hydrodynamic Performance of Marine Current Turbines. *Renewable Energy, 33*, 1085-1096. https://doi.org/10.1016/j.renene.2007.05.043

Batten, W., Harrison, M., & Bahaj, A. (2013). Accuracy of the actuator disc-RANS approach for predicting the performance and wake of tidal turbines. *Philosophical transactions. Series A, Mathematical, physical, and engineering sciences, 371*, 20120293. https://doi.org/10.1098/rsta.2012.0293

Batten, W. M. J., Bahaj, A. S., Molland, A. F., & Chaplin, J. R. (2007). Experimentally validated numerical method for the hydrodynamic design of horizontal axis tidal turbines. *Ocean Engineering, 34*(7), 1013-1020. https://doi.org/http://dx.doi.org/10.1016/j.oceaneng.2006.04.008

Black and Veatch Consulting Ltd, B. V. (2011). *UK Tidal Current Resource & Economics* (Technical Report. Project Number 121393, Issue June 2016). C. Trust.

Blunden, L., & Bahaj, A. (2007). Tidal energy resource assessment for tidal stream generators. *Proceedings of The Institution of Mechanical Engineers Part A-journal of Power and Energy - PROC INST MECH ENG A-J POWER, 221*. https://doi.org/10.1243/09576509JPE332

Blunden, L. S., & Bahaj, A. S. (2006, 2006/02/01/). Initial evaluation of tidal stream energy resources at Portland Bill, UK. *Renewable Energy, 31*(2), 121-132. https://doi.org/https://doi.org/10.1016/j.renene.2005.08.016

Bonar, P. A. J., Schnabl, A. M., Lee, W.-K., & Adcock, T. A. A. (2018). Assessment of the Malaysian tidal stream energy resource using an upper bound approach. *Journal of Ocean Engineering and Marine Energy, 4*(2), 99-109. https://doi.org/10.1007/s40722-018-0110-5

Boyle, G. (2004). Renewable Energy,Power for a Sustainable Future. *Oxford University Press, Oxford*.

Boyle, G., Everett, R., & Ramage, J. (Eds.). (2003). *Energy Systems and Sustainability*. Oxford University Press. http://oro.open.ac.uk/3121/.

Bryden, I., Couch, S., Owen, A., & Melville, G. (2007). Tidal current resource assessment. *Proceedings of The Institution of Mechanical Engineers Part A-journal of Power and Energy - PROC INST MECH ENG A-J POWER, 221*. https://doi.org/10.1243/09576509JPE238

Bryden, I. G. (2006). The marine energy resource, constraints and opportunities. *Maritime Engineering, Vol. 159(MA2)*, 55-65.

Bryden, I. G., & Couch, S. J. (2006). Marine energy extraction: tidal resource analysis. *Journal of Renewable Energy, Vol. 32(1)*, 133-139.

Bryden, I. G., & Couch, S. J. (2006). ME1-marine energy extraction: tidal resource analysis.
. *Renew Energ 2006, 31*, 133-139.

Buigues, I. G., S. Naik, & Bullen, C. R. (1998). Matching tidal current plants to local flow conditions. *Energy (Oxford), vol. 23*, pp. 699-709.

Burton, T., Sharpe, D., Jenkind, N. a., & Bossanyi, E. (2001). *Wind Energy Handbook*. John Wiley & Sons, Ltd.

Carballo, R., Iglesias, G., & Castro, A. (2009). Numerical model evaluation of tidal stream energy resources in the Ría de Muros (NW Spain). *Renewable Energy, 34*(6), 1517-1524. https://doi.org/https://doi.org/10.1016/j.renene.2008.10.028

Cartwright, D. E., Spencer, R., Vassie, J. M., & Woodworth, P. L. (1988). The tides of the Atlantic Ocean, 60° N to 30° S. *Philosophical Transactions of the Royal Society of London. Series A, Mathematical and Physical Sciences, 324*(1581), 513-563. https://doi.org/10.1098/rsta.1988.0037

Cave, P. R., Evans, E. M., & George, K. J. (1987). *Assessment of tidal streams as an energy resource* International conference on energy options: the role of alternatives in the world energy scene. 5 (1987),

Chamorro, L. P., Hill, C., Morton, S., Ellis, C., Arndt, R. E. A., & Sotiropoulos, F. (2013). On the interaction between a turbulent open channel flow and an axial-flow turbine. *Journal of Fluid Mechanics, 716*, 658-670. https://doi.org/10.1017/jfm.2012.571

Chatzirodou, A., & Karunarathna, H. (2014). IMPACTS OF TIDAL ENERGY EXTRACTION ON SEA BED MORPHOLOGY. *Coastal Engineering Proceedings; No 34 (2014): Proceedings of 34th Conference on Coastal Engineering, Seoul, Korea, 2014*. https://doi.org/10.9753/icce.v34.sediment.33

Chatzirodou, A., Karunarathna, H., & Reeve, D. (2015). *Modelling the Response of Sandbank Dynamics to Tidal Energy Extraction* 6th IAHR World Congress, Hague, the Netherlands.

Chatzirodou, A., Karunarathna, H., & Reeve, D. E. (2019). 3D modelling of the impacts of in-stream horizontal-axis Tidal Energy Converters (TECs) on offshore sandbank dynamics. *Applied Ocean Research, 91*, 101882. https://doi.org/https://doi.org/10.1016/j.apor.2019.101882

Chen, W.-B., Liu, W.-C., & Hsu, M.-H. (2013). Modeling Evaluation of Tidal Stream Energy and the Impacts of Energy Extraction on Hydrodynamics in the Taiwan Strait. *Energies, 6*(4). https://doi.org/10.3390/en6042191

Chen, Y., Lin, B., Lin, J., & Wang, S. (2015). Effects of stream turbine array configuration on tidal current energy extraction near an island. *Computers & Geosciences, 77*, 20-28. https://doi.org/http://dx.doi.org/10.1016/j.cageo.2015.01.008

Chua, T., Gorre, I., Ross, S., Bernad, S., Gervacio, B., & Ebarvia, M. (2000). The Malacca Straits. Marine Pollution Bulletin. *4*(1-6), 160-178.

Churchfield, M. J., Li, Y., & Moriarty, P. J. (2013). A large-eddy simulation study of wake propagation and power production in an array of tidal-current turbines. *Philosophical Transactions of the Royal Society A: Mathematical, Physical and Engineering Sciences, 371*(1985), 20120421. https://doi.org/10.1098/rsta.2012.0421

Courant, R., Friedrichs, K., & Lewy, H. (1928). Über die partiellen Differenzengleichungen der mathematischen Physik. *Mathematische Annalen, 100*(1), 32-74. https://doi.org/10.1007/BF01448839

Davide Magagna, A. M., Henry Jeffrey, Clare Hanmer, Alex Raventos, Abbie Badcock-Broe and Evangelos Tzimas (2014). *Wave and Tidal Energy Strategic Technology Agenda*. S. Ocean.

Defne, Z., Haas, K. A., & Fritz, H. M. (2011). Numerical modeling of tidal currents and the effects of power extraction on estuarine hydrodynamics along the Georgia coast, USA. *Renewable Energy, 36*(12), 3461-3471. https://doi.org/https://doi.org/10.1016/j.renene.2011.05.027

Deltares. (2021). *Delft3D-FLOW, User Manual* (Delft3D-FLOW Simulation of multi-dimensional hydrodynamic flows and transport phenomena, including sediments, Issue.

Department of Irrigation and Drainage Malaysia, D. (2008). *The Integrated Shoreline Management Plan for the Coastline of Negeri Sembilan*.

Department of Trade and Industry DTI. (2002). *Research and development of a 150 kW tidal stream generator*.

Department of Trade and Industry DTI. (2003). Stingray tidal stream energy device - Phase 2. . *Rep No. 03/1433*, 67p.

Divett, T., Vennell, R., & Stevens, C. (2013). Optimisation of multiple turbine arrays in a channel with tidally reversing flow by numerical modeling with adaptive

mesh. *Philosophical transactions. Series A, Mathematical, physical, and engineering sciences, 371*, 20120251. https://doi.org/10.1098/rsta.2012.0251

Doodson, A. T., & Warburg, H. D. (1941). *Admiralty manual of tides*. H.M.S.O.

Draper, S., Adcock, T. a. a., Borthwick, A. G. L., & Houlsby, G. T. (2014). A note on the power potential of tidal currents in channels. *International Journal of Marine Energy, Vol. 6*(No. 1), pp. 1-17.

Draper, S., Borthwick, A. G. L., & Houlsby, G. T. (2013). Energy potential of a tidal fence deployed near a coastal headland [10.1098/rsta.2012.0176]. *Philosophical Transactions of the Royal Society A: Mathematical, Physical and Engineering Sciences, 371*(1985). http://rsta.royalsocietypublishing.org/content/371/1985/20120176.abstract

Draper, S., Houlsby, G., Oldfield, M. L. G., & Borthwick, A. (2010). Modelling tidal energy extraction in a depth-averaged coastal domain. *Renewable Power Generation, IET, 4*, 545-554. https://doi.org/10.1049/iet-rpg.2009.0196

Easton, M. C., Woolf, D. K., & Bowyer, P. A. (2012). The dynamics of an energetic tidal channel, the Pentland Firth, Scotland. *Continental Shelf Research, 48*, 50-60. https://doi.org/https://doi.org/10.1016/j.csr.2012.08.009

Egbert, G. D., Bennett, A. F., & Foreman, M. G. G. (1994). TOPEX/POSEIDON tides estimated using a global inverse model. *Journal of Geophysical Research: Oceans, 99*(C12), 24821-24852. https://doi.org/10.1029/94JC01894

Egbert, G. D., & Erofeeva, S. Y. (2002). Efficient Inverse Modeling of Barotropic Ocean Tides. *Journal of Atmospheric and Oceanic Technology, 19*(2), 183-204. https://doi.org/10.1175/1520-0426(2002)019<0183:EIMOBO>2.0.CO;2

El-Shahat, S. A., Li, G., & Fu, L. (2021, 2021/07/15/). Investigation of wave–current interaction for a tidal current turbine. *Energy, 227*, 120377. https://doi.org/https://doi.org/10.1016/j.energy.2021.120377

EMEC. (2020). *Tidal Devices*. The European Marine Energy Centre Ltd. Retrieved 8.11.2020 from http://www.emec.org.uk/marine-energy/tidal-devices/

Emmel, F. J., & Curray, J. R. (1982). A submerged late pleistocene delta and other features related to sea level changes in the Malacca Strait. . *Marine Geology, 47*, 197 - 216.

Engineering Business Ltd. (2003). *STINGRAY TIDAL STREAM ENERGY DEVICE – PHASE 2* https://archive.uea.ac.uk/~e680/energy/energy_links/renewables/stingray_part1.pdf

Faez Hassan, H., El-Shafie, A., & Karim, O. A. (2012, 10//). Tidal current turbines glance at the past and look into future prospects in Malaysia. *Renewable and Sustainable Energy Reviews, 16*(8), 5707-5717. https://doi.org/http://dx.doi.org/10.1016/j.rser.2012.06.016

Fallon, D. (2012). *Numerical Modelling of the Far-field Impacts of Tidal Turbines* National University of Ireland, Galway]. National University of Ireland, Galway.

Fallon, D., Hartnett, M., Olbert, A., & Nash, S. (2014). The effects of array configuration on the hydro-environmental impacts of tidal turbines. *Renewable Energy 64* 10-25. www.elsevier.com/locate/renene

Finkl, C. W., & Charlier, R. (2009). Electrical power generation from ocean currents in the Straits of Florida: Some environmental considerations. *Renewable and Sustainable Energy Reviews, 13*(9), 2597-2604. https://doi.org/https://doi.org/10.1016/j.rser.2009.03.005

Fitri, A., Hashim, R., Abolfathi, S., & Maulud, K. (2019). Dynamics of Sediment Transport and Erosion-Deposition Patterns in the Locality of a Detached Low-Crested Breakwater on a Cohesive Coast. *Water, 11*, 1721. https://doi.org/10.3390/w11081721

Fraenkel, P. (2007). Marine current turbines: pioneering tidal stream technology. Proc. IMechE

Fraenkel, P. L. (2002). Power from marine currents. *Proc IMechE, 216 Part A*(Special Issue Paper 1), 1-14. https://doi.org/doi:10.1243/095765002760024782

Fraenkel, P. L. (2004). Marine Current Turbines: an emerging technology. *Paper for Scottish Hydraulic Study Group Seminar in Glasgow: Renewable Energy-Hydraulic Applications-Theory and Practice*.

Fraenkel, P. L., & Musgrove, P. J. (1979). Tidal and river current energy systems.

Frau, J. P. (1993). Tidal Energy: promising projects: La Rance, a successfuly industrial-scale experiment. *IEEE Transactions on ENergy Conversion, 8*, 552-558.

Funke, S. W., Farrell, P. E., & Piggott, M. D. (2014). Tidal turbine array optimisation using the adjoint approach. *Renewable Energy, 63*, 658-673. https://doi.org/https://doi.org/10.1016/j.renene.2013.09.031

Funke, S. W., Kramer, S. C., & Piggott, M. D. (2016). Design optimisation and resource assessment for tidal-stream renewable energy farms using a new continuous turbine approach. *Renewable Energy, 99*(C), 1046-1061. https://doi.org/10.1016/j.renene.2016.07. (Renewable Energy)

Gan, S. W. (2014). *HYDRODYNAMIC MODELLING FOR MANGROVE REFORESTATION AT TANJUNG PIAI, WEST COAST PENINSULAR MALAYSIA* National University of Singapore (NUS)]. Singapore.

Gao, P., Zheng, J., Zhang, J., & Zhang, T. (2015). Potential Assessment of Tidal Stream Energy Around Hulu Island, China. *Procedia Engineering, 116*, 871-879. https://doi.org/10.1016/j.proeng.2015.08.376

Garrett, C., & Cummins, P. (2007). The efficiency of a turbine in a tidal channel. *Journal of Fluid Mechanics, 588*, 243-251. https://doi.org/10.1017/S0022112007007781

Garrett, C., & Cummins, P. (2008, 2008/11/01/). Limits to tidal current power. *Renewable Energy, 33*(11), 2485-2490. https://doi.org/https://doi.org/10.1016/j.renene.2008.02.009

Garrett, C., & Greenberg, D. (1977). Predicting Changes in Tidal Regime: The Open Boundary Problem. *Journal of Physical Oceanography, 7*(2), 171-181. https://doi.org/10.1175/1520-0485(1977)007<0171:PCITRT>2.0.CO;2

GasMalaysia. (2019). GasMalaysia. https://www.gasmalaysia.com/

Gillibrand, P. A., Walters, R. A., & McIlvenny, J. (2016). Numerical Simulations of the Effects of a Tidal Turbine Array on Near-Bed Velocity and Local Bed Shear Stress. *Energies, 9*(10). https://doi.org/10.3390/en9100852

González-Gorbeña, E., Rosman, P. C. C., & Qassim, R. Y. (2015). Assessment of the tidal current energy resource in São Marcos Bay, Brazil. *Journal of Ocean Engineering and Marine Energy, 1*(4), 421-433. https://doi.org/10.1007/s40722-015-0031-5

Gorban, A. N., Gorlov, A. M., & Silantyev, V. M. (2001). Limits of the Turbine Efficiency for Free Fluid Flow. *Journal of Energy Resources Technology, 123*(4), 311-317. https://doi.org/10.1115/1.1414137

Gorji-bandpy, M. (2013). Tidal Energy and MainResources In the Persian Gulf. *Distributed Generation & Alternative Energy Journal, Vol. 28*(No. 2), pp. 61-77.

Gorlov, A. M. (2001). Tidal energy. *Academic London*, pp. 2955–2960.

Grabbe, M., Lalander, E., Lundin, S., & Leijon, M. (2009). A review of the tidal current energy resource in Norway. *Renewable and Sustainable Energy Reviews, 13*(8), 1898-1909. https://doi.org/https://doi.org/10.1016/j.rser.2009.01.026

Guillou, N., & Chapalain, G. (2017). Assessing the impact of tidal stream energy extraction on the Lagrangian circulation. *Applied Energy, 203*(Supplement C), 321-332. https://doi.org/https://doi.org/10.1016/j.apenergy.2017.06.022

Hammons, T. J. (1993). Tidal Power. Proceedings of the IEEE,

Hannan, M. A., Begum, R. A., Abdolrasol, M. G., Hossain Lipu, M. S., Mohamed, A., & Rashid, M. M. (2018, 2018/10/01/). Review of baseline studies on energy policies and indicators in Malaysia for future sustainable energy development. *Renewable and Sustainable Energy Reviews, 94*, 551-564. https://doi.org/https://doi.org/10.1016/j.rser.2018.06.041

Harding, S., & Bryden, I. (2012). Generating controllable velocity fluctuations using twin oscillating hydrofoils. *Journal of Fluid Mechanics, 750*, 150-158. https://doi.org/10.1017/jfm.2012.442

Harrison, M. E., Batten, W., Myers, L., & Bahaj, A. (2010). Comparison between CFD simulations and experiments for predicting the far wake of horizontal axis tidal turbines. *Renewable Power Generation, IET, 4*, 613-627. https://doi.org/10.1049/iet-rpg.2009.0193

Hasegawa, D., Sheng, J., Greenberg, D. A., & Thompson, K. R. (2011). Far-field effects of tidal energy extraction in the Minas Passage on tidal circulation in the Bay of Fundy and Gulf of Maine using a nested-grid coastal circulation model. *Ocean Dynamics, 61*(11), 1845-1868. https://doi.org/10.1007/s10236-011-0481-9

Hassanzadeh, R., Yaakob, O. b., & Ahmed, Y. M. (2017). An innovative configuration for new marine current turbine. *Renewable Energy*. https://doi.org/https://doi.org/10.1016/j.renene.2017.11.095

Haverson, D., Bacon, J., Smith, H. C. M., Venugopal, V., & Xiao, Q. (2017). Cumulative impact assessment of tidal stream energy extraction in the Irish Sea. *Ocean Engineering, 137*, 417-428. https://doi.org/https://doi.org/10.1016/j.oceaneng.2017.04.003

Haverson, D., Bacon, J., Smith, H. C. M., Venugopal, V., & Xiao, Q. (2018). Modelling the hydrodynamic and morphological impacts of a tidal stream development in Ramsey Sound. *Renewable Energy, 126*, 876-887. https://doi.org/https://doi.org/10.1016/j.renene.2018.03.084

Healy, T., Wang, Y., & Healy, J. A. (2002). Muddy Coasts of the World: Processes, Deposits and Functions. *Elsevier Amsterdam*, pp: 61 - 81.

Hicks, S. D. (2006). *Understanding Tides*

Houlsby, G. T., Draper, S., & Oldfield, M. L. G. (2008). *Application of Linear Momentum Actuator Disc Theory to Open Channel Flow* [Other output](Department of Engineering Science, University of Oxford, Issue 1).

Jeffcoate, P., Starzmann, R., Elsaesser, B., Scholl, S., & Bischoff, S. (2015). Field Measurements of a Full Scale Tidal Device [Article]. *International Journal of Marine Energy, 12*, 3-20. https://doi.org/10.1016/j.ijome.2015.04.002

Jiang, C. B., Kang, Y. T., Qu, K., Kraatz, S., Deng, B., Zhao, E. J., Wu, Z. Y., & Chen, J. (2021, 2021/09/15/). High-resolution numerical survey of potential sites for tidal energy extraction along coastline of China under sea-level-rise condition. *Ocean Engineering, 236*, 109492. https://doi.org/https://doi.org/10.1016/j.oceaneng.2021.109492

JPS, J. P. d. S. M. (2008). Integrated Shoreline Management Plan Negeri Sembilan. *Coastal Zone Mangement Division, Ministry of Environment and Water, Malaysia*.

Kanniah, K. D., Sheikhi, A., Cracknell, A. P., Goh, H. C., Tan, K. P., Ho, C. S., & Rasli, F. N. (2015). Satellite Images for Monitoring Mangrove Cover Changes in a Fast Growing Economic Region in Southern Peninsular Malaysia. *Remote Sensing, 7*(11). https://doi.org/10.3390/rs71114360

Karsten, R. H., McMillan, J. M., Lickley, M. J., & Haynes, R. D. (2008). Assessment of tidal current energy in the Minas Passage, Bay of Fundy. *Proceedings of the Institution of Mechanical Engineers, Part A: Journal of Power and Energy, 222*(5), 493-507. https://doi.org/10.1243/09576509JPE555

Keenan, G., Sparling, C., William, H., & Fortune, F. (2011). *SeaGen Environmental Monitoring Programme*. Haskoning UK LTD.

Kenyon, N. H., & Cooper, B. (2005). Sand banks, sand transport and offshore windfarms.

Kim, K.-P., Ahmed, M. R., & Lee, Y.-H. (2012, 2012/12/01/). Efficiency improvement of a tidal current turbine utilizing a larger area of channel. *Renewable Energy, 48*, 557-564. https://doi.org/https://doi.org/10.1016/j.renene.2012.06.018

Koh, S. L., & Lim, Y. S. (2008). Preliminary investigation of the potential of harnessing tidal energy for electricity generation in Malaysia. 2008 IEEE/PES Transmission and Distribution Conference and Exposition,

Lee, K. S., & Seng, L. Y. (2009). Simulation Studies on the Electrical Power Potential Harnessed by Tidal Current Turbines. . *Journal of Energy and Environment, Vol. 1* (No. 1), pp. 18-23.

Legrand, C. (2009). *Assessment of Tidal Energy Resource* (Marine Renewable Energy Guides, Issue 2009). T. E. M. E. C. Ltd.

Lesser, G. R., Roelvink, J. A., van Kester, J. A. T. M., & Stelling, G. S. (2004). Development and validation of a three-dimensional morphological model. *Coastal Engineering, 51*(8–9), 883-915. https://doi.org/http://dx.doi.org/10.1016/j.coastaleng.2004.07.014

Lewis, M., McNaughton, J., Márquez-Dominguez, C., Todeschini, G., Togneri, M., Masters, I., Allmark, M., Stallard, T., Neill, S., Goward Brown, A., & Robins, P. (2019). Power variability of tidal-stream energy and implications for electricity supply. *Energy, 183*. https://doi.org/10.1016/j.energy.2019.06.181

Lewis, M., Neill, S., Robins, P., & Hashemi, M. R. (2015, 03/11). Resource assessment for future generations of tidal-stream energy arrays. *Energy, 83*, 403-415. https://doi.org/10.1016/j.energy.2015.02.038

Li, X., Li, M., Jordan, L.-B., McLelland, S., Parsons, D. R., Amoudry, L. O., Song, Q., & Comerford, L. (2019). Modelling impacts of tidal stream turbines on surface waves. *Renewable Energy, 130*, 725-734. https://doi.org/https://doi.org/10.1016/j.renene.2018.05.098

Lim, X.-L., Lam, W.-H., & Hashim, R. (2015). Feasibility of marine renewable energy to the Feed-in Tariff system in Malaysia. *Renewable and Sustainable Energy Reviews, 49*, 708-719. https://doi.org/http://dx.doi.org/10.1016/j.rser.2015.04.074

Lim, Y. S., & Koh, S. L. (2010). Analytical assessments on the potential of harnessing tidal currents for electricity generation in Malaysia. *Renewable Energy, 35*(5), 1024-1032. https://doi.org/https://doi.org/10.1016/j.renene.2009.10.016

Liu, F.-y., Zhang, Z.-h., Xu, H.-r., Meng, J., & Zhang, R. (2007). Evaluation method of fuzzy integrated estimate for potential impacts on the environment of tide power stations. *Ocean Technology, 26*(3), 110-113.

Lo Brutto, O. A., Guillou, S. S., Thiébot, J., & Gualous, H. (2017). Assessing the effectiveness of a global optimum strategy within a tidal farm for power maximization. *Applied Energy, 204*(Supplement C), 653-666. https://doi.org/https://doi.org/10.1016/j.apenergy.2017.07.090

Logan, M. A., Ryan, P. M., & Brent, A. L. (2016). Variability in suspended sediment concentration in the Minas Basin, Bay of Fundy, and implications for changes due to tidal power extraction. *Coastal Engineering, 107*, 102-115. www.elsevier.com/locate/coastaleng

MacLeod, A. J., Barnes, S., Rados, K. G., & Bryden, I. (2002). Wake effects in tidal current turbine farms. *MAREC 2002, International Conference on Marine Renewable Energy - Conference Proceedings*, 49-53.

Mann, K. H., & Lazier, J. R. (2013). *Dynamics of Marine Ecosystems: Biological–Physical Interactions in the Oceans*. John Wiley and Sons.

Marine Energy. (2020, 19.7.2020). OES: Wave and Tidal Energy from 5GWh to 45GWh in 10 Years.

Martin-Short, R., Hill, J., Kramer, S. C., Avdis, A., Allison, P. A., & Piggott, M. D. (2015). Tidal resource extraction in the Pentland Firth, UK: Potential impacts on flow regime and sediment transport in the Inner Sound of Stroma. *Renewable Energy, 76*, 596-607. https://doi.org/10.1016/j.renene.2014.11.079

Mason, K. (2005). *A Composite tidal turbine to harness ocean energy*

Masters, I., Williams, A., Croft, N., Togneri, M., Edmunds, M., Zangiabadi, E., Fairley, I., & Karunarathna, H. (2015). A Comparison of Numerical Modelling Techniques for Tidal Stream Turbine Analysis. *Energies, 2015*, 7833-7853. https://doi.org/10.3390/en8087833

Mastura, S. (1992). *The coastal zone of Peninsular Malaysia*. Penerbit Universiti Kengangsaan Malaysia.

McNaughton, J., Harper, S., Sinclair, R., & Sellar, B. (2015). *Measuring and modelling the power curve of a Commercial-Scale tidal turbine*.

Mejia-Olivares, C. J., Haigh, I. D., Wells, N. C., Coles, D. S., Lewis, M. J., & Neill, S. P. (2018). Tidal-stream energy resource characterization for the Gulf of California, México. *Energy, 156*, 481-491. https://doi.org/https://doi.org/10.1016/j.energy.2018.04.074

Melo, A. B. e. V., José Luis. (2014). *2014 Annual Report: Implementing Agreement on Ocean Energy Systems*. T. E. C. o. O. E. Systems.

Mestres, M., Cerralbo, P., Grifoll, M., Sierra, J. P., & Espino, M. (2019, 2019/02/01/). Modelling assessment of the tidal stream resource in the Ria of Ferrol (NW Spain) using a year-long simulation. *Renewable Energy, 131*, 811-817. https://doi.org/https://doi.org/10.1016/j.renene.2018.07.105

MeyGen. (2012). *MeyGen Tidal Enery Project - Phase 1: Environmental Statement*. Retrieved 20.10.2020 from https://simecatlantis.com/projects/meygen/

Mohamed, N. A. M. Y. N. L. R. M. R. (2015). Investigation of the Potential Tidal Energy in Malaysia *ARPN Journal of Engineering and Applied Sciences, 10*(21), 9835 - 9841.

Mozafari, J., & Teymour, A. (2010). *Numerical Modeling of Tidal Turbines: Methodology Development and Potential Physical Environmental Effects*

Mozafari, J., Teymour, A., Stelzenmuller, N., & Aliseda, A. (2017). Experimental and numerical analysis of the performance and wake of a scale–model horizontal axis marine hydrokinetic turbine. *Journal of Renewable and Sustainable Energy, 9*, 044504. https://doi.org/10.1063/1.4999600

Myers, L., & Bahaj, A. S. (2005). Simulated electrical power potential harnessed by marine current turbine arrays in the Alderney Race. *Renewable Energy, 30*(11), 1713-1731. https://doi.org/https://doi.org/10.1016/j.renene.2005.02.008

Myers, L. E., & Bahaj, A. S. (2010). Experimental analysis of the flow field around horizontal axis tidal turbines by use of scale mesh disk rotor simulators. *Ocean Engineering, 37*(2), 218-227. https://doi.org/https://doi.org/10.1016/j.oceaneng.2009.11.004

Myers, L. E., & Bahaj, A. S. (2012). An experimental investigation simulating flow effects in first generation marine current energy converter arrays. *Renewable Energy, 37*(1), 28-36. https://doi.org/https://doi.org/10.1016/j.renene.2011.03.043

Nash, S., O'Brien, N., Olbert, A., & Hartnett, M. (2014). Modelling the far field hydro-environmental impacts of tidal farms – A focus on tidal regime,inter-tidal zones and flushing. *Computers & Geosciences 71* 20-27. https://doi.org/https://doi.org/http://dx.doi.org/10.1016/j.cageo.2014.02.001

National Geospatial-Intelligence Agency. (2016). *Strait of Malacca and Sumatera*.

Naval Postgraduate School of Department of Oceanography. (2015). *Tidal constituents.PNG* https://upload.wikimedia.org/wikipedia/commons/d/d9/Tidal_constituents.PNG

Neill, S. P., & Hashemi, M. R. (2018). Chapter 3 - Tidal Energy. In S. P. Neill & M. R. Hashemi (Eds.), *Fundamentals of Ocean Renewable Energy* (pp. 47-81). Academic Press. https://doi.org/https://doi.org/10.1016/B978-0-12-810448-4.00003-3

Neill, S. P., Jordan, J. R., & Couch, S. J. (2012). Impact of tidal energy converter (TEC) arrays on the dynamics of headland sand banks. *Renewable Energy, 37*(1), 387-397. https://doi.org/10.1016/j.renene.2011.07.003

Neill, S. P., Litt, E. J., Couch, S. J., & Davies, A. G. (2009). The impact of tidal stream turbines on large-scale sediment dynamics. *Renewable Energy, vol. 34*, pp. 2803-2812.

Orhan, K., & Mayerle, R. (2020). Potential Hydrodynamic Impacts and Performances of Commercial-Scale Turbine Arrays in the Strait of Larantuka, Indonesia. *Journal of Marine Science and Engineering, 8*(3). https://doi.org/10.3390/jmse8030223

Ouro, P., Harrold, M., Stoesser, T., & Bromley, P. (2017, 2017/05/01/). Hydrodynamic loadings on a horizontal axis tidal turbine prototype. *Journal of Fluids and Structures, 71*, 78-95. https://doi.org/https://doi.org/10.1016/j.jfluidstructs.2017.03.009

Pacheco, A., & Ferreira, Ó. (2016). Hydrodynamic changes imposed by tidal energy converters on extracting energy on a real case scenario. *Applied Energy, 180*(Supplement C), 369-385. https://doi.org/https://doi.org/10.1016/j.apenergy.2016.07.132

Paduan, J., & Shulman, I. (2004). HF radar data assimilation in the Monterey Bay area. *J. Geophys. Res, 109*. https://doi.org/10.1029/2003JC001949

Partheniades, E. (1965). Erosion and Deposition of Cohesive Soils. *Journal of the Hydraulics Division, Vol. 91,*(Issue 1), Pg. 105-139.

Pelc, R., & Fujita, R. M. (2002). Renewable energy from the ocean. *Marine Policy, 26*, 471-479.

Phillips, R. P. (1985). Longshore transport of sediment during August and September on the Terengganu coast. *Pertanika, 8*(2), 273-279.

Phoenix, A. (2017). *Development of a tidal flow model for optimisation of tidal turbine arrays* National University of Ireland, Galway]. https://aran.library.nuigalway.ie/handle/10379/7145?show=full

Plew, D., & Stevens, C. (2013). Numerical modelling of the effect of turbines on currents in a tidal channel – Tory Channel, New Zealand. *Renewable Energy, 57*, 269–282. https://doi.org/10.1016/j.renene.2013.02.001

Polagye, B., Van Cleve, B., Copping, A., & Kirkendall, K. (2011). *Environmental Effects of Tidal Energy Development* [Technical Report].

Rahman, N., Kamaruzzaman, S. N., & Akashah, F. W. (2019). Scenario and Strategy towards Energy Efficiency in Malaysia: A Review. *MATEC Web of Conferences, 266*, 02012. https://doi.org/10.1051/matecconf/201926602012

Ramos, V., Carballo, R., Álvarez, M., Sánchez, M., & Iglesias, G. (2013). Assessment of the impacts of tidal stream energy through high-resolution numerical modeling. *Energy, 61* 541-554. www.elsevier.com/locate/energy

Ramos, V., Carballo, R., & Ringwood, J. V. (2019). Application of the actuator disc theory of Delft3D-FLOW to model far-field hydrodynamic impacts of tidal turbines. *Renewable Energy, 139*, 1320-1335. https://doi.org/https://doi.org/10.1016/j.renene.2019.02.094

Ramos, V., Carballo, R., Sanchez, M., Veigas, M., & Iglesias, G. (2014). Tidal stream energy impacts on estuarine circulation. *Energy Conversion and Management, 80*, 137-149.

Ramos, V., & Iglesias, G. (2013). Performance assessment of Tidal Stream Turbines: A parametric approach. *Energy Conversion and Management, 69*(Supplement C), 49-57. https://doi.org/https://doi.org/10.1016/j.enconman.2013.01.008

Ramos, V., Iglesias, G., Carballo, R., Álvarez, M., & Sánchez, M. (2013). Assessment of the impacts of tidal stream energy through high-resolution numerical modeling. *Energy, 61* 541-554. www.elsevier.com/locate/energy

RGU, R. G. U. (2002). *A scoping study for an environmental impact field programme in tidal current energy* D. Publication.

Robins, P. E., Neill, S. P., & Lewis, M. J. (2014). Impacts of tidal-stream energy converter TEC arraysin realtion to the natural variability of sedimentary processes. 9th European Wave and Tidal Energy Conference (EWTEC), Stornoway, Scotland.

Robins, P. E., Neill, S. P., Lewis, M. J., & Ward, S. L. (2015). Characterising the spatial and temporal variability of the tidal-stream energy resource over the northwest European shelf seas. *Applied Energy, 147*(Supplement C), 510-522. https://doi.org/https://doi.org/10.1016/j.apenergy.2015.03.045

Roc, T., Conley, D. C., & Greaves, D. (2013). Methodology for tidal turbine representation in ocean circulation model. *Renewable Energy, 51*(Supplement C), 448-464. https://doi.org/https://doi.org/10.1016/j.renene.2012.09.039

Roshanmanesh, S., Hayati, F., & Papaelias, M. (2020). Chapter 10 - Tidal turbines. In M. Papaelias, F. P. G. Márquez, & A. Karyotakis (Eds.), *Non-Destructive Testing and Condition Monitoring Techniques for Renewable Energy Industrial Assets* (pp. 143-158). Butterworth-Heinemann. https://doi.org/https://doi.org/10.1016/B978-0-08-101094-5.00010-1

Rourke, F. O., Boyle, F., & Reynolds, A. (2010). Marine current energy devices: Current status and possible future applications in Ireland. *Renewable and Sustainable Energy Reviews, 14*(3), 1026-1036. https://doi.org/https://doi.org/10.1016/j.rser.2009.11.012

Royal Malaysian Navy, R. (2019). *Malaysia Tide Table* (Tide Table, Issue 2019). Royal Malaysian Navy.

Sakmani, A. S., Lam, W.-H., Hashim, R., & Chong, H.-Y. (2013). Site selection for tidal turbine installation in the Strait of Malacca. *Renewable and Sustainable Energy Reviews, 21*, 590-602. https://doi.org/http://dx.doi.org/10.1016/j.rser.2012.12.050

Sanchez, M., Carballo, R., Ramos, V., & Iglesias, G. (2014). Floating vs. bottom-fixed turbines for tidal stream energy: A comparative impact assessment. *Energy 72* 691-701.

Satrio, D., & Utama, I. K. A. P. (2021, 2021/11/01/). Experimental investigation into the improvement of self-starting capability of vertical-axis tidal current turbine. *Energy Reports, 7*, 4587-4594. https://doi.org/https://doi.org/10.1016/j.egyr.2021.07.027

Schlezinger, D. R., Taylor, C. D., & Howes, B. L. (2013, July - Aug 2013). Assessment of Zooplankton Injury and Mortality Associated With Underwater Turbines for Tidal Energy Production. *MarineTechnology Society Journal, 47*, 142-150.

Schmitt, P., Elsaesser, B., Bischof, S., & Starzmann, R. (2015). Field testing a full-scale tidal turbine Part 2: In-line Wake Effects.

Seng, L. Y., Lalchand, G., Lin, S., & Mak, G. (2008). Economical, environmental and technical analysis of building integrated photovoltaic systems in Malaysia. *Energy Policy, 36*(6), 2130-2142. https://doi.org/https://doi.org/10.1016/j.enpol.2008.02.016

Shaharudin, I., Mohd Lokman, H., Sulong, I., & Persad, V. J. (2001). Current status of Malaysian mangroves. In B. Nizam (Ed.), *State of the Malaysian Marine Resources (in press)*.

Shapiro, G. (2011). Effect Of Tidal Stream Power Generation On The Region-wide Circulation In A Shallow Sea. *Ocean Science Discussion, 7*(5), 165-174.

Sheng, J., Thompson, K., Greenberg, D., & Hill, P. (2012). Assessing the Far Field Effects of Tidal Power Extraction on the Bay of Fundy, Gulf of Maine and Scotian Shelf. *Report by Bedford Institute of Oceanography.*

Shukri, M. P. N. I., Ramli, N. L., Ghani, S. A., & Sharif, M. S. A. (2013). *Study of tides prediction for Malaysia electricity generation purposes using Matlab Simulink* Conference: 2nd International Conference on Sustainable Cities, Urban Sustainability and Transportation (SCUST13), Baltimore, MD, USA

Stallard, T., Collings, R., Feng, T., & Whelan, J. (2013). *Interactions between tidal turbine wakes: Experimental study of a group of three-bladed rotors* (Vol. 371). https://doi.org/10.1098/rsta.2012.0159

Sun, X., Chick, J. P., & Bryden, I. G. (2008). Laboratory-scale simulation of energy extraction from tidal currents. *Renewable Energy, 33*(6), 1267-1274. https://doi.org/https://doi.org/10.1016/j.renene.2007.06.018

Sutherland, W. J. (2007). Future directions in disturbance research. *Ibis, 149*(s1), 120-124. https://doi.org/https://doi.org/10.1111/j.1474-919X.2007.00673.x

Tao, S., Xu, Q., Feijóo-Lorenzo, A. E., Zheng, G., & Zhou, J. (2021, 2021/08/01/). Optimal layout of a Co-Located wind/tidal current farm considering forbidden zones. *Energy, 228*, 120570. https://doi.org/https://doi.org/10.1016/j.energy.2021.120570

Thiébaut, M., Sentchev, A., & du Bois, P. B. (2019). Merging velocity measurements and modeling to improve understanding of tidal stream resource in Alderney Race. *Energy, 178*, 460-470. https://doi.org/https://doi.org/10.1016/j.energy.2019.04.171

Thompson, L. (2007). *Tides Intro, Lecture Notes*. University of Washington. Retrieved 26.7.2020 from http://faculty.washington.edu/luanne/pages/ocean420/notes

Thyng, K. M., & Riley, J. J. (2010, 20-23 Sept. 2010). Idealized headland simulation for tidal hydrokinetic turbine siting metrics. OCEANS 2010 MTS/IEEE SEATTLE,

Turner, N. E., & Owen, A. (2007, 18-21 June 2007). The Development of a Tidal Turbine for Deployment in Areas with Slow Moving Tidal Flows. OCEANS 2007 - Europe,

Turnock, S. R., Phillips, A. B., Banks, J., & Nicholls-Lee, R. (2011). Modelling tidal current turbine wakes using a coupled RANS-BEMT approach as a tool for analysing power capture of arrays of turbines. *Ocean Engineering, 38*(11), 1300-1307. https://doi.org/https://doi.org/10.1016/j.oceaneng.2011.05.018

Uihlein, A., & Magagna, D. (2016). Wave and tidal current energy – A review of the current state of research beyond technology. *Renewable and Sustainable Energy Reviews, 58*, 1070-1081. https://doi.org/http://dx.doi.org/10.1016/j.rser.2015.12.284

Van Koningsveld, M., De Boer, G. J., Baart, F., Damsma, T., Den Heijer, C., Van Geer, P., & De Sonnevile, B. (2010). OpenEarth-inter-company management of: data, models, tools & knowledge.

Vennell, R. (2010). Tuning turbines in a tidal channel. *Journal of Fluid Mechanics, 663*, 253-267. https://doi.org/10.1017/S0022112010003502

Vennell, R., Funke, S. W., Draper, S., Stevens, C., & Divett, T. (2015). Designing large arrays of tidal turbines: A synthesis and review. *Renewable and Sustainable Energy Reviews, 41*, 454-472. https://doi.org/https://doi.org/10.1016/j.rser.2014.08.022

Waggitt, J. J., & Scott, B. E. (2014). Using a spatial overlap approach to estimate the risk of collisions between deep diving seabirds and tidal stream turbines: A review of potential methods and approaches. *Marine Policy, vol. 44*, pp. 90-97.

Walters, R. A., Tarbotton, M. R., & Hiles, C. E. (2013). Estimation of tidal power potential. *Renewable Energy, 51*, 255-262. https://doi.org/https://doi.org/10.1016/j.renene.2012.09.027

Wang, T., & Yang, Z. (2017). A modeling study of tidal energy extraction and the associated impact on tidal circulation in a multi-inlet bay system of Puget Sound. *Renewable Energy, 114*(Part A), 204-214. https://doi.org/https://doi.org/10.1016/j.renene.2017.03.049

Wang, Y., Sun, X., Huang, D., & Zheng, Z. (2016, 2016/10/01/). Numerical investigation on energy extraction of flapping hydrofoils with different series foil shapes. *Energy, 112*, 1153-1168. https://doi.org/https://doi.org/10.1016/j.energy.2016.06.092

Weatherall, P., Marks, K. M., Jakobsson, M., Schmitt, T., Tani, S., Arndt, J. E., Rovere, M., Chayes, D., Ferrini, V., & Wigley, R. (2015). A new digital bathymetric model of the world's oceans. *Earth and Space Science, 2*(8), 331-345. https://doi.org/10.1002/2015EA000107

Westwood, A. (2004). Ocean power: Wave and tidal energy review. *Refocus, 5*(5), 50-55. https://doi.org/http://dx.doi.org/10.1016/S1471-0846(04)00226-4

Westwood, A. (2007). Wave and tidal – project review. *Renewable Energy Focus, 8*(4), 30-33. https://doi.org/http://dx.doi.org/10.1016/S1471-0846(07)70103-8

Wyman, P. R., & Peachey, C. J. (1979, January 01, 1979). Tidal current energy conversion.

Yang, Z., Wang, T., & Copping, A. E. (2013). Modeling tidal stream energy extraction and its effects on transport processes in a tidal channel and bay system using a three-dimensional coastal ocean model. *Renewable Energy, 50*(Supplement C), 605-613. https://doi.org/https://doi.org/10.1016/j.renene.2012.07.024

Yusoff, N. A. M., Ramli, N. L., & Mohamed, M. R. (2015). Investigation of the Potential Harnessing Tidal Energy in Malaysia *ARPN Journal of Engineering and Applied Sciences, VOL. 10*(NO. 21).

Zitti, G., Fattore, F., Brunori, A., Brunori, B., & Brocchini, M. (2020, 2020/02/01/). Efficiency evaluation of a ductless Archimedes turbine: Laboratory experiments and numerical simulations. *Renewable Energy, 146*, 867-879. https://doi.org/https://doi.org/10.1016/j.renene.2019.06.174